



363

A STUDY OF THE WIND PRESSURE FORCES
ACTING ON GROUPS OF BUILDINGS

Baher Fathy Soliman,
B. Arch.

Thesis submitted to fulfil the
requirements for the degree of

Doctor of Philosophy

at the

Department of Building Science,
University of Sheffield.

October 1976

To My Wife

AESHA

With Love

V

LIST OF CONTENTS

List of Figures

List of Tables

Acknowledgement

Summary

Nomenclature

<u>CHAPTER</u>		<u>Page</u>
1	INTRODUCTION	1
1.1	Natural Ventilation of Buildings	1
1.2	Natural Ventilation Calculation	4
1.3	The Factors Affecting the Pressure Difference Across Buildings.	6
1.4	Formulation of the Problem and the Pattern of Investigation.	9
2	THE PROPERTIES OF THE WIND AND THEIR INFLUENCE ON THE PRESSURES ON BLUFF BODIES.	13
2.1	The Structure and Behaviour of the Natural Wind.	13
2.2	Effect of Flow Parameters on the Mean Pressure Difference Across Buildings.	24
3	A REVIEW ON PREVIOUS WORK RELEVANT TO NATURAL VENTILATION OF BUILDING GROUPS.	32
3.1	Introduction	32
3.2	Previous Work on Natural Ventilation of Building Groups	33
3.3	Previous Work on Wind Loading on Building Groups.	40
3.4	Previous Work on Flow Round Groups of Buildings	49
3.5	Conclusions	52

<u>CHAPTER</u>		<u>Page</u>
4	DENSITY AND FORM	54
4.1	Introduction	54
4.2	Density of Residential Areas	55
4.3	The Geometrical Parameters	
	Defining Group Density and Form	67
4.4	Limits of the Parameters	78
4.5	Conclusions	82
5	FLOW OVER ROUGH SURFACES	84
5.1	Introduction	84
5.2	Flow Over Smooth Surfaces	85
5.3	Flow Over Rough Surfaces	89
5.4	Effect of Roughness Geometry on the Velocity Profile Parameters	95
5.5	The Effect of a Step Change in Surface Roughness	106
5.6	Effect of Roughness Geometry on the Mean Pressures and Their Distribution.	108
6	EXPERIMENTAL ARRANGEMENT AND TECHNIQUES	119
6.1	Introduction	119
6.2	Details of Wind Tunnel, Model and Incident Flow Modification	126
6.3	Measurement Technique and Accuracy Level	128
6.4	Flow Visualization Technique	137
7	EXPERIMENTAL RESULTS AND DISCUSSION: Pressure Measurements	140
7.1	The Effect of Fetch on the Central Model Drag	140
7.2	The Size of Influence Area Around the Central Model	142
7.3	The Effect of Density on the Pressure Forces	149
7.4	The Effect of Pattern and Orientation on the Pressure Difference Between Two Opposite Faces, ΔC_p	172
7.5	Conclusions	177

<u>CHAPTER</u>		<u>Page</u>
8	EXPERIMENTAL RESULTS AND DISCUSSION. Velocity Profile Measurements.	182
8.1	Introduction	182
8.2	Velocity Profile Analysis: the Two Incident Flows	183
8.3	Velocity Profile Analysis: Flow Within the Group Layout	189
8.4	Discussion of the Velocity Profile Parameters	208
8.5	Correlations Between Group Geometry, Flow Properties and the Resulting Pressure Forces	216
8.6	Conclusions	223
9	EXPERIMENTAL RESULTS AND DISCUSSION: Surface Flow Visualization.	226
9.1	Introduction	226
9.2	Discussion of the Isolated Cube Case	226
9.3	Discussion of the Isolated Flow Regime Results	232
9.4	Discussion of the Wake Interference Flow Regime Results	237
9.5	Discussion of the Skimming Flow Regime Results	241
9.6	Conclusions	251
10	GENERAL APPLICATION FOR BUILDINGS	253
10.1	Introduction	253
10.2	The Three Flow Regimes and Their Generalized Parameters	253
10.3	The Relationship Between the Building Form, Its Relative Height and the Downstream Eddy Size	258
10.4	The Suggested Method for Determining the Natural Ventilation Potential, ΔC_p	263
10.5	Conclusions	273
11	CONCLUSIONS	274
	References	280

LIST OF FIGURES

<u>Figure</u>	<u>Title</u>	<u>Page</u>
2.1	Spectrum of the horizontal wind component.	16
2.2	Wind rose diagram for Sheffield	18
2.3	Mean wind velocity profiles for surfaces of different roughness	20
2.4	A model for air flow in urban areas	23
2.5	Variation of C_{D1} with H/δ and u_*/U_1	27
2.6	Variation of C_{DH} with Hu_*/ν and u_*/U_1	28
2.7	Variation of C_{DH} with H/Z_0	29
2.8	The pressure distribution of a model house for different values of H/Z_0	30
3.1	Effect of distance of separation on the resulting ventilation using Weston's data	34
3.2	Vincent and Bailey's results	43 - 45
4.1	Graphical presentation of Gropius's model	61
4.2	Building arrangement studied by Beckett	63
4.3	Graphical presentation of Beckett's mathematical model	64

<u>Figure</u>	<u>Title</u>	<u>Page</u>
4.4	Effect of incomplete definition of form determining parameters	66
4.5	General grouping form and its geometrical parameters	69
4.6(a)	Variation of F.S.I. with λ_p for different No. of storeys.	71
4.6(b)	Variation of F.S.I. with open space between buildings for different values of O.S.I.	71
4.7	Graphical presentation of the relationships between the planning parameters.	73
4.8	Transformation of Figure 4.7 into log-log form.	74
4.9	Variation of λ_p , λ_f and A_s with $\tan \gamma_x$ for two-dimensional building forms.	76
4.10	Variation of λ_p , λ_f and A_s with $\tan \gamma_x$ for square plan building forms.	77
4.11	Examples of housing schemes for various values of F.S.I, O.S.I. and λ_p .	79-80
4.12	Distribution of λ_p for 110 housing schemes.	81
5.1	The general structure of turbulent boundary layer flows.	86
5.2	Definition of the roughness length and the three zones of flow in the inner layer for smooth walls	88

<u>Figure</u>	<u>Title</u>	<u>Page</u>
5.3	Definition of the roughness function.	91
5.4	Variation of $\Delta u/u_*$ with Hu_*/ν in the three conditions of flow.	93
5.5	Variation of k_s/H with λ_f for different element forms.	98
5.6	Graphical presentation of the variation of $\Delta u/u_*$ with $k_s u_*/\nu$ and the roughness element density, λ for any one roughness element form in the fully rough flow.	101
5.7	The flow structure for: (a) The wake interference flow regime. (b) The skimming flow regime.	103
5.8	Checking the validity of Perry et. al. suggested scheme on the isolated roughness flow regime.	105
5.9	Variation of C_{D*} with Hu_*/ν	112
5.10(a)	The pressure distribution on an isolated body.	113
5.10(b)	The pressure distribution on an element in the wake interference flow regime.	116
5.10(c)	The pressure distribution on an element in the skimming flow regime.	117
6.1	The parameters considered in the present study.	121
6.2	Details of wind tunnel and model used	124

<u>Figure</u>	<u>Title</u>	<u>Page</u>
6.3	Details of model mounting system and set-up of equipments.	129
6.4	Definition of hot-wire orientation and effective angles.	133
6.5	Calibration at each angle of yaw.	136
6.6	Cross wire yaw calibration.	138
7.1	Variation of C_{D1} with group layout size R/H^1 ($\theta = 0, \phi = 0$).	141
7.2	Variation of the model drag with the group angle ϕ at the extreme values of fetch.	143
7.3	Variation of C_{D1} with group layout size, R/H , ($\theta = 0, -90 < \phi < +90$).	144
7.4	Variation of the influence area with the angle of the surrounding blocks, ϕ .	147
7.5	Limits of the influence area round the model.	148
7.6	Pressure coefficient distribution on the isolated model.	150
7.7	Pressure coefficient distribution on the model centre line at various densities, (normal pattern, rough flow).	151
7.8	Pressure coefficient distribution on the model centre line at various densities, (staggered pattern, rough flow).	152
7.9	Pressure coefficient distribution on the model centre line at various densities, (normal pattern smooth flow).	153

<u>Figure</u>	<u>Title</u>	<u>Page</u>
7.10	Pressure coefficient distribution on the model centre line at various densities, (staggered pattern, smooth flow).	154
7.11	Variation of the wall pressure and the drag force with the cube spacing, (normal pattern, rough flow).	156
7.12	Variation of the wall pressure and the drag force with the cube spacing (staggered pattern, rough flow).	157
7.13	Variation of the wall pressure and the drag force with the cube spacing (normal pattern, smooth flow).	158
7.14	Variation of the wall pressure and the drag force with the cube spacing (staggered pattern, smooth flow).	159
7.15	Surface flow visualization of the isolated cube, (smooth flow).	163
7.16	Surface flow visualization of the isolated cube, (rough flow).	164
7.17	A replot of the results of Tani et. al. (1961) for the leeward groove-wall pressure C_{p_1} .	165
7.18	Variation of the effective skin friction coefficient with density, (rough flow).	167
7.19	Variation of the effective skin friction coefficient with density, (smooth flow).	168

<u>Figure</u>	<u>Title</u>	<u>Page</u>
7.20	Grouping of the windward and leeward pressure distributions according to the different flow regimes.	171
7.21	Normalized windward pressure profiles with respect to the maximum pressure, (rough flow).	173
7.22	Normalized windward pressure profiles with respect to the maximum pressure, (smooth flow).	174
7.23	Variation of ΔC_p with the orientation angle, θ , for various densities.	175
7.24	Variation of the pressure difference coefficient with incident flow direction for regular patterns compared with the random pattern.	178
8.1	Location of the velocity profiles measured at different densities.	184
8.2	Incident flow profiles, power law form.	185
8.3	Incident flow profiles, log-law form.	186
8.4	Incident flow profiles in the form u/u_* versus $y u_*/\nu$.	188
8.5	The effect of the surface roughness changes on the incident rough flow profile.	191
8.6	Comparison between different profiles at cube centre lines showing the effect of the subsequent changes of surface roughness.	192

<u>Figure</u>	<u>Title</u>	<u>Page</u>
8.7	Comparison between cube centre line profiles and street centre line profiles at $\lambda = 4\%$, 12.5% and 32% .	194
8.8	Variation of velocity profiles with fetch, street centre line profiles, $\lambda = 4\%$.	195
8.9	Variation of velocity profiles with fetch, cube centre line profiles, $\lambda = 4\%$.	196
8.10	Street centre line profiles at different densities.	197
8.11	Cube centre line profiles at various densities.	198
8.12	The graphical method for determining the zero plane displacement, d , ($\lambda = 4\%$).	200
8.13	The graphical method for determining the zero plane displacement, d , ($\lambda = 8\%$).	201
8.14	The graphical method for determining the zero plane displacement, d , ($\lambda = 12.5\%$).	202
8.15	The graphical method for determining the zero plane displacement, d , ($\lambda = 25\%$).	203
8.16	The graphical method for determining the zero plane displacement, d , ($\lambda = 32\%$).	204
8.17	Velocity profiles in the form u/u_* versus $y u_*/\nu$.	206
8.18	Variation of the roughness function with the roughness Reynolds number, Hu_*/ν	209

<u>Figure</u>	<u>Title</u>	<u>Page</u>
8.19	Variation of the roughness function with the roughness Reynolds number, $\epsilon u_* / \nu$.	210
8.20	Variation of the zero plane displacement with density.	212
8.21	Variation of Z_0/H with λ_f .	213
8.22	Variation of k_s/H with λ_f .	215
8.23	Comparison of experimental growth of internal layer with theory and present results.	217
8.24	Variation of $\frac{u_H}{U_1}$ with S_c/H .	219
8.25	Variation of C_{D*} with ϵ/Z_0 .	220
8.26	Normalized pressure profiles for the three flow regimes.	222
9.1	The isolated cube (Smooth flow)	227
9.2	The isolated cube (Rough flow)	228
9.3	The flow pattern round an isolated cube.	229
9.4	Suggested three-dimensional diagram for the flow pattern round the isolated cube.	230
9.5	Isolated roughness flow regime, $\lambda = 4\%$, Normal Pattern, (Rough flow).	233

<u>Figure</u>	<u>Title</u>	<u>Page</u>
9.6	Isolated roughness flow regime, $\lambda = 8\%$, Staggered Pattern, (Rough flow).	234
9.7	Isolated roughness flow regime, $\lambda = 4\%$, Normal Pattern, (Smooth flow).	235
9.8	Isolated roughness flow regime, $\lambda = 8\%$, Staggered Pattern, (Smooth flow).	236
9.9	Wake interference flow regime, $\lambda = 16\%$, Normal Pattern, (Smooth flow).	238
9.10	Flow pattern in the wake interference flow regime.	239
9.11	Wake interference flow regime, $\lambda = 16\%$, Normal Pattern, (Rough flow).	240
9.12	Wake interference flow regime, $\lambda = 32\%$, Staggered Pattern, (Smooth flow).	242
9.13	Wake interference flow regime $\lambda = 32\%$, Staggered Pattern, (Smooth flow).	243
9.14	Wake interference flow regime, $\lambda = 32\%$, Staggered Pattern, (Rough flow).	244
9.15	Skimming flow regime, $\lambda = 50\%$, Staggered Pattern, (Smooth flow).	245
9.16	Skimming flow regime, $\lambda = 50\%$, Staggered Pattern, (Rough flow).	246
9.17	Flow pattern in the skimming flow regime.	247

<u>Figure</u>	<u>Title</u>	<u>Page</u>
9.18	Skimming flow regime, $\lambda = 50\%$, Normal Pattern, (Smooth flow).	248
9.19	Skimming flow regime, $\lambda = 50\%$, Normal Pattern, (Rough flow)	249
9.20	Skimming flow regime, $\lambda = 50\%$, Normal Pattern, (Rough flow).	250
10.1	The IHVE Guide infiltration chart.	254
10.2	The governing conditions for the three flow regimes.	256
10.3	Examples showing that the three flow regimes are not a sole function of λ_p , λ_f or A_f .	259
10.4	Variation of E_d/H with L/H .	261
10.5	Analysis of Evans's results.	263
10.6	Identification of the three flow regimes from the layout pattern.	264
10.7	Variation of C_{D_H} with S_c/H .	266
10.8	Suggested variation of C_{D_H} with S_c/H for different building Forms.	267
10.9	Suggested variation of C_{D_H} with fetch in the three flow regimes.	269
10.10	Variation of the normalized pressure difference with the building angle of orientation θ .	270

<u>Figure</u>	<u>Title</u>	<u>Page</u>
10.11	The suggested chart for the prediction of ΔC_{p_H} .	272

LIST OF TABLES

<u>Table</u>	<u>Title</u>	<u>Page</u>
3.1	Dimensions of the buildings used by Weston, E. T.	33
3.2	Values of C_{p_f} for different surrounding buildings and distances of separation.	39
3.3	Description of the models used by Vincent and Bailey.	41
3.4	Dimension of the models used by Wise et. al. (1965) in terms of the low rise building height.	49
4.1	Density and space parameters proposed by Svennar (1972).	57
6.1	The variables considered in the two stages of the investigation.	122
6.2	The combination of the parameters considered for pressure measurements made in the first stage.	123
6.3	The combination of the parameters considered and the measurements made in the second stage.	125
6.4	Variation of the constants E^2 , T and m/m_Δ with small yaw angles $\pm \Delta\psi$.	135
8.1	Velocity profile parameters determined from pressure measurement results	199
8.2	Velocity profile parameters at four various densities.	205
8.3	Roughness function parameters at various densities.	207

ACKNOWLEDGEMENT

I would like to thank Dr. B. E. Lee, my Supervisor for his invaluable guidance, advice and assistance throughout every stage of the experimental work and the writing of the thesis.

I would also like to thank Dr. F. R. Fricke, who was my supervisor in the initial period of the research.

I want also to gratefully acknowledge the assistance of the Department of Building Science and Professor J. K. Page.

Special thanks are due to the members of the technical staff of the Department of Building Science, Mr. R. Webster, Mr. A. Shale, Mr. C. Hardwick, Mr. K. Holdsworth (who designed and built the electronics), Mr. R. Skelton, Mr. P. Williams, Mr. M. Broady and Mr. T. Thomas for their assistance in constructing the models used in this study.

Mrs. B. M. Wilson typed this thesis and I would like to thank her for her care and diligence with which she carried out her work.

The financial support provided by the Egyptian Government is also acknowledged.

Finally, I would like to thank my wife for her help and encouragement during the period of my research and in particular for her assistance in the writing of the thesis.

SUMMARY

A STUDY OF THE WIND PRESSURE FORCES ACTING ON GROUPS OF BUILDINGS

BAHER F. SOLIMAN

In urban areas, where buildings are mostly in groups, wind pressure forces are expected to depend on the natural wind properties as well as on the building group form. A reliable estimate of these pressure forces on buildings is necessary not only for the prediction of wind loading, but also for an accurate prediction of natural ventilation.

In an attempt to gain an understanding of the wind flow properties and the pressure forces on low rise buildings in urban areas, a detailed investigation on the interaction between the group geometry, flow properties and the resulting pressure forces has been carried out. From the review of previous work on natural ventilation, wind loading and air flow round groups of buildings, it has been concluded that no general relationship exists at present which defines this interaction. However, the similarity between boundary layer flow over rough surfaces and the natural wind on the earth's surface served to provide useful information. Considering buildings as roughness elements on the earth's surface, the geometrical and the planning parameters were investigated in order to arrive at a complete definition and the practical limits of building group forms.

In the present study, a series of model scale experiments have been performed which considered a wide range of group forms subject to two different incident flow conditions. The detailed measurements of the pressure forces on the faces of a model building situated within a variety of groups of similar form and size indicated three different trends in the behaviour of these forces. The hypothesis made, that these trends would correspond to the three flow regimes known to exist for flow over general roughness elements was substantiated by velocity profile measurements as well as by surface flow visualization tests.

Finally, the case of generalized application on buildings was investigated on the basis of the relationships obtained between group geometry, flow properties and the resulting pressure forces. Here, an alternative method for the prediction of natural ventilation in low rise buildings is presented in which the geometrical parameters defining the building group form is taken into account. It is suggested that this approach will lead to an improvement in the present methods of natural ventilation calculation.

NOMENCLATURE

A list of the nomenclature used in the thesis is given below. The list covers the nomenclature used in all Chapters apart from Chapter 4. In this Chapter the nomenclature is given within.

List of Nomenclature

Symbol

A	Area of the intervening smooth surface/roughness element, also site area/building.
A_f	Frontal aspect ratio (L/H).
A_s	Side aspect ratio (W/H).
a_f	Frontal area of roughness element.
B	Constant in equation (5.2).
B_1	Constant in equation (5.23).
B_2	Constant in equation (5.24).
B_3	Constant in equation (5.25).
b	The groove breadth in the flow direction.
C	Constant in equation (5.7).
C_1	Constant in equation (2.4).
C_{D1}	Drag coefficient based on the free stream dynamic head.
C_{DH}	Drag coefficient based on the dynamic head at the building (or roughness element) height, H .

Symbol

C_{D_m}	Drag coefficient based on the maximum pressure difference across the element.
C_{D_*}	Drag coefficient based on the friction velocity, u_* .
C_f	Local skin friction coefficient.
C_{f_e}	Effective local skin friction coefficient, C_{D_l}/A .
C_i	Infiltration coefficient of the opening
C_{p_f}	Pressure correction factor in equation (3.1).
C_{p_l}	Leeward wall mean pressure coefficient.
C_{p_w}	Windward wall mean pressure coefficient.
C_{-p_l}	Pressure coefficient based on U_l .
ΔC_p	Mean pressure difference coefficient across two opposite faces of the model or a building, (based on U_l).
ΔC_{p_H}	Mean pressure difference coefficient across two opposite faces of the model or a building, (based on u_H).
D	Drag force on a building or roughness element.
d	Ground level displacement, zero plane displacement.
\bar{d}	Mean value of d .
E	Constant in equation (5.8).

Symbol

E	Mean bridge voltage of the anemometer.
E_d	The reattachment distance downstream the building or any roughness element.
E_o	Mean bridge voltage of the anemometer at zero velocity.
E_t	The sum of the separation and reattachment distances E_u and E_d around the building or any roughness element.
E_u	The separation distance upstream the building or any roughness element.
E_v	Dimension of the stable vortex in the flow direction.
F	Constant in equation (5.18).
F_1	Functional dependence of the inner layer.
F_2	Functional dependence of the outer layer.
F_3	Functional dependence of the windward pressure profile.
F_4	Functional dependence of the leeward pressure profile.
f	Coriolis parameter.
H	Building height, roughness element height.
\bar{H}	Average value of H .
H_o	Height of obstructing building.
h	Low building height.

Symbol

K	Constant in equation (3.2)
K_o	Correction factor to allow for variation of pressure with orientation of building.
k_s	The equivalent sand grain roughness size.
L	Building or roughness element dimension across flow direction.
L_c	Length of the opening (crack).
L_x	Distance of separation between buildings also site length, in the wind direction.
M_3	The simple model used in the first stage of the investigation.
M_{24}	The detailed model used in the second stage of the investigation.
m	Constant in equation (6.1).
m_1	Constant in equation (5.23).
m_3	Constant in equation (5.25).
n	Exponent.
p	Wind pressure on the building surface.
p_l	Leeward wall pressure.
p_{max}	Maximum wind pressure on the building, (or roughness element).
p_{min}	Minimum wind pressure on the building, (or roughness element).

Symbol

p_o	The static pressure at the reference point.
p_y	Wind pressure on the building at any height, y.
Δp	Pressure difference across the building.
Δp_o	Pressure difference across any opening.
q_1	The free stream dynamic head.
R	Group layout radius, also the central model fetch.
S	The cube spacing in the flow direction.
\bar{S}	The mean spacing of the cubes in the flow direction.
S_c	The clear spacing between the cubes or buildings in the flow direction.
T	Slope of the hot-wire calibration lines.
u	Mean velocity in the wind direction.
U_1	Mean velocity in the free stream.
u_{10}	Mean velocity at 10m above the ground.
u_*	Friction velocity.
u_{eff}	Effective velocity acting on the hot-wire.
u_G	Gradient velocity.
u_H	Mean velocity at height H.
u_y	Mean velocity at any height y.

Symbol

$\frac{\Delta u}{u_*}$	Roughness function.
V	Volume flow rate.
v	Velocity component in the vertical direction.
W	Building (or roughness element) dimension along flow direction.
x	Distance along wind direction, also representing building group fetch.
y	Height above the ground.
y_G	Gradient height at the top of the boundary layer.
z_o	Roughness length.
$\overline{z_o}$	Mean value of z_o .
α	Exponent in the power law.
α_I, α_{II}	Orientation angles of the hot wires (I and II) with respect to the x axis.
γ	Angle of obstruction between buildings.
δ	Boundary layer thickness.
δ_i	Internal layer thickness.
δ_l	Laminar sublayer thickness.
δ_r	Rough flow boundary layer thickness.
δ_s	Smooth flow boundary layer thickness.

Symbol

ϵ	Error in origin for measuring y , ($H = \epsilon + d$).
θ	The building or central model orientation angle with respect to wind direction.
κ	Universal constant (≈ 0.4).
λ	Density of building (or roughness element) groups.
λ_f	Frontal area density.
λ_p	Plan area density
ν	Kinematic viscosity of air.
ρ	Density of air.
τ_o	Surface shear stress
τ_{oe}	Effective surface shear stress.
ϕ	The surrounding group angle of orientation with respect to wind direction.
ψ	Effective angle between the flow direction and the plane normal to the wire axis.
ψ_x	Ratio between building width, W and the site length, L_x .
ψ_y	Ratio between building length, L and the site lateral dimension, L_y .
I, II	Subscript denoting hot wire no.
Δ	Subscript denoting values corresponding to small change in the hot wire effective angle, ψ .

CHAPTER 1

INTRODUCTION .

1. INTRODUCTION

1.1 Natural Ventilation of buildings

1.1.1 Ventilation in terms of supplying fresh outside air into building interiors is one of several means by which the indoor climate of a building could be controlled. Introducing outside air internally may be achieved by means of natural ventilation, mechanical ventilation or air-conditioning. The choice of either method not only has its consequence on the architectural design principles, but also on the building cost and the resulting indoor environment; for example, the building depth and in turn its form is directly affected by this choice. Mechanical ventilation will involve additional initial expenditure and increased running costs which might in some buildings be necessary and may be compensated for economically. The artificial control of ventilation will enable the provision of conditions very close to the required internal environment, in contrast with the natural methods of ventilation which rely on highly variable external climatic conditions. However, in most cases, where the external climatic impacts are not too severe to produce balanced conditions by natural means and when minimum building cost is of prime importance, natural ventilation becomes the only available alternative for the designer. It may also be noted that housing consumption of energy for heating purposes in many countries represents a large proportion of the national energy budget, a considerable part of which is wasted by uncontrolled excessive ventilation.

Therefore a proper estimate of the natural ventilation rates in buildings is necessary if buildings are to meet their environmental and economic requirements.

1.1.2 Natural ventilation occurs in virtually all buildings through the openings in their envelope.

Intentional air flow through openings provided in the building, such as windows or ducts is usually referred to as ventilation. On the other hand, unintentional flow may occur through gaps and cracks in the building such as those round windows or doors. This type of flow is known as infiltration. Where ventilation may be allowed or prevented through controlling the ventilation openings, infiltration is usually out of control and subject to variability of the natural forces created in the ambient climatic conditions. However, infiltration rates may be put to minimum if the gaps and cracks round ventilation openings and doors are minimized.

1.1.3 The main principle that operates to produce natural ventilation in buildings is the existence of a pressure difference between the inside and the outside of the building. The magnitude of the pressure difference and the flow resistance will determine the rate of air flow through the openings. The size, shape and location of openings determine the speed and pattern of internal flow. The two forces that produce pressure differences across building elements are the wind force and the thermal force, known as "stack effect". Due to air flow around a building, different pressures are exerted on its external surfaces. For an isolated building of simple

rectangular form with a flat roof, if the wind is normal to one of its sides, positive pressures develop on the windward wall and negative pressures on the roof and the rest of the walls. The pattern of the pressure distribution as well as its magnitude will depend mainly on the properties of the oncoming flow, the building form and other parameters relating the building to the flow. This point is discussed in detail in Chapter 2.

1.1.4 Ventilation may also occur, though to a lesser extent, either due to pressure fluctuations on the walls, an action related to the turbulent nature of the wind, or due to turbulence diffusion. Although the magnitude of ventilation provided by these two mechanisms is normally negligible, it could be of considerable weight in situations where only one opening is provided to the space or during the absence of both wind and thermal forces.

1.1.5 Natural ventilation principles have been established through the extensive studies made either on full scale buildings or on scale models. However, a detailed accurate description of the natural ventilation occurring in any building of moderate complexity appears to be very difficult, Bilsborrow (1973). This is partly due to the lack of an accurate practical measure of the effectiveness of ventilation, but probably mainly due to the complex interaction of the factors affecting the ventilation potential in any circumstances. At present the accepted measure is the rate of air flow, m^3/hr , sometimes expressed in terms of the number of a certain volume (usually taken as the room volume or the total building volume) per

unit time, air change/hr.

1.2 Natural ventilation calculation

1.2.1 The two common methods currently in use for natural ventilation calculations are the air change method and the crack method. Both methods are described in the IHVE Guide (1970) and the ASHRAE Guide (1972). The air change method which is entirely empirical is based on the assumption that similar building types of typical construction and normal use in winter would have similar infiltration rates. Therefore, tabulated values of infiltration rates are given for different building types assuming normal exposure and an average ratio (25%) of openable areas (windows and doors) to external wall area. Allowance of 25-50% is given for higher ratios of openable areas in the external walls as well as for different degrees of building exposure. The latter being 50% increase for severely exposed sites and 33% decrease for sheltered sites. The three degrees of building exposure are classified as follows:

Sheltered:	Up to third floor of buildings in city centres.
Normal:	Most suburban and country premises: fourth to eighth floors of buildings in city centres.
Severely Exposed:	Buildings on the coast or exposed on hill sites: floors above the fifth of buildings in suburban or country districts: floors above the ninth of buildings in city centres.

In the air change method quoted in the ASHRAE Guide, allowance is made for opening distribution in the external wall and weather stripping. A reduction of 33% is made in the latter case.

1.2.2 The crack method for infiltration calculation is based in principle on the following equation which relates the ventilation rate, V , to the pressure difference, Δp_o , acting across any opening,

$$V = C_i \cdot L_c (\Delta p_o)^{1/n} \quad \dots\dots (1.1)$$

For a particular building, the infiltration coefficient, C_i , and the crack length, L_c , are dependent on the type and the area of the openings respectively. From the work on air flow through openings, a relationship is shown to exist between C_i and the exponent n , Bilsborrow (1973). Therefore, it remains to determine Δp_o in equation (1.1) in order to obtain the ventilation rate, V . From the work on air flow round building models an estimate of the mean pressure difference across the building Δp , may be obtained, half of which is assumed to act across each of the windward and the leeward faces of the building, giving Δp_o . The main assumption made in the IHVE Guide to estimate the mean pressure difference across any building, Δp , (hence Δp_o) is that the velocity pressure of the wind at the roof top level is approximately equal to Δp . Therefore, for one design wind speed and three velocity profiles assumed to occur on three different sites (open country, suburban areas and city centres) the corresponding velocity pressure profiles are plotted. These velocity pressure profiles are then used to obtain Δp for buildings

of any given height in the three site conditions. It seems that the main assumption made in the IHVE Guide to estimate Δp may result in considerable error since important factors affecting Δp such as the building form and the properties of the oncoming flow are neglected. The effect of these factors is well documented (see for example the Code of Practice CP3, Chapter V, part 2 (1972) and the work of Jensen and Franck (1965)). The conclusions that can be made from the above discussion is that the accuracy level of the ventilation rate using the crack method depends on the accuracy of determining the pressure difference across the building, Δp , in different sites. Therefore it is important to consider the factors affecting Δp if any reliable estimate of the ventilation rate is to be made.

1.3 The factors affecting the pressure difference across buildings

1.3.1 There are a large number of variables affecting the pressure difference across buildings in the natural wind. The complexity of interaction between these variables and the difficulty of controlling them in nature called for the dependence on the scale model experimental work as a main source of information. In particular the work done on the drag (hence Δp) of bluff bodies immersed in turbulent boundary layers provide the basic information required, see for example the work of Good and Jourbet (1968), Jensen and Franck (1965), Morris (1955), Joubert, Perry and Stevens (1971) and Wooding, Bradley and Marshall (1973).

From this work the similarity of wind flow over the earth's surfaces to the turbulent boundary layer flow over rough surfaces is established. Hence, buildings on the earth's surface may be considered as elements on a rough surface over which a turbulent boundary layer flows.

1.3.2 By definition, the drag exerted on any bluff body in boundary layer flow is the difference between the integral of the windward and the leeward pressures. These pressures are determined by the process of separation and reattachment of air flow round the body. Although the factors affecting separation are not necessarily the same as those affecting reattachment, it seems logical to classify all the factors involved into the following two groups:

- (a) factors related to the building form, and
- (b) factors related to the properties of the wind.

The main properties of form known to affect the drag of buildings in urban areas are:

- (a) individual form, and
- (b) group form.

Individual building form is the only form factor affecting the drag of isolated buildings and may be broken down to:

- (i) building shape, (ii) building size and
- (iii) building permeability.

1.3.3 The effect of varying rectangular building shape on the drag coefficient, C_{D_H} , is well documented in the Code of Practice CP3 (1972). The method of determining

the wind pressures on buildings, used in CP3, utilizes a design wind speed and a drag coefficient C_{DH} . For a particular case, the height of the building is taken into account since the reference dynamic head is that appropriate to the top of the building. The value of C_{DH} used simply takes account of the building geometry. However, the extensive work of Good and Joubert (1968) and Jensen and Franck (1965) has demonstrated that for buildings in the turbulent boundary layer, the size of the building alone in a particular flow situation will influence C_{DH} . The third property of individual form that affect the drag coefficient, is the building permeability, though relatively less information is available in the literature to illustrate its effect. The full scale measurement on Royex House reported by Newberry, Eaton and Mayne (1973) indicate that permeability reduced the pressure difference across the building by a factor of about 30%.

1.3.4 In the case of low building density where buildings are wide apart i.e. in open country, the individual building form is the only form that the wind can "see". As the density increases, i.e. in suburban and urban areas, buildings are close to each other so that each building form becomes a detail in the group form as a whole. In this case the group form becomes more important than the individual building form in influencing the drag forces experienced by each building. Recent experimental work (see for example Joubert, Perry and Stevenson (1971)) shows how the group geometry of roughness elements simulating buildings immersed in turbulent boundary layer flow affect the drag force on each element.

1.4 Formulation of the problem and the pattern of investigation

1.4.1 In the discussion so far, the problem of estimating a reliable value of Δp for natural ventilation calculation is shown to depend on two main groups of factors, i.e. form-related factors and flow-related factors. Thus, in urban areas where buildings are mostly in groups, it is expected that the two main factors affecting Δp are (i) the group form and (ii) the properties of the natural wind. Therefore, in an attempt to gain further understanding of the wind flow and more important the pressure forces in urban areas, it is intended to carry out a detailed investigation on the interaction between group geometry, properties of air flow and the resulting pressures. It is hoped that a relationship may be obtained between the group geometry, and the resulting pressure forces and also between the group geometry and the interacting flow. If this is the case, then a relationship must exist between the pressure forces and the flow properties. Such relationships may well exist since similar relationships between the flow properties, the element form and the resulting pressures are reported by Good and Joubert (1968) for the simple case of a two dimensional isolated element in smooth surface flow.

1.4.2 In order to cover the different aspects of form and flow in urban areas in the present investigation, and because of its implications on planning decisions, it was necessary for the investigation to meet the theoretical aspects as well as the practical aspects of different fields.

For example the investigation of air flow is to meet both the practical aspects of air flow in the natural wind as well as the theoretical aspects of turbulent boundary layer flow over idealized rough surfaces. The geometry of building groups must also consider the practical aspects of the planning parameters as well as the theoretical aspects of form description. Consequently, the following pattern of investigation emerged, to meet these diverse requirements.

1.4.3 Since the properties of flow in the natural wind are important factors in determining the pressure forces on buildings, they are first considered in Chapter 2.

A review on the previous work on the wind pressure and flow over groups of buildings is made in Chapter 3 so that relevant information may be obtained. In Chapter 4 the different aspects of density and form are investigated in an attempt to link the planning parameters in urban areas to the geometrical parameters describing various arrays of rectilinear elements simulating building groups. Since buildings may be considered as roughness elements on the earth's surface over which the atmospheric boundary layer flows, the idealized case of flow over rough surfaces is discussed in Chapter 5. From this Chapter an understanding of the interaction between the flow, the roughness geometry and the resulting pressures is achieved. At the end of Chapter 5 it is shown that further investigation is needed to close the gap between the idealized theoretical case and the practical case of buildings in the natural wind.

1.4.4 In Chapters 6 - 8 the results of the experimental investigation carried out in the present work using cubes as a simplified building form are explained and discussed. The main variables considered are:

- (a) the properties of the oncoming flow: two different flow conditions,
- (b) the group form: including a wide range of group density and pattern and
- (c) the resulting pressure forces: detailed pressure measurements on two opposite faces of the cube.

Pressure measurements were made from a pressure tapped model within the group. Velocity profile measurements were also made for the flow over the different groups considered. The measurement techniques, the accuracy level and the set up of the models and equipment is given in Chapter 6. Following in Chapter 7, the discussion on the pressure measurement results is given and a hypothesis concerning the flow behaviour is made. The flow measurement results given in Chapter 8 enabled a check to be made on the hypothesis outlined in Chapter 7 as well as providing information about relevant velocity profile parameters. This information enabled a comparison to be made between the results obtained and the established work on flow over roughness. In addition it enabled correlations to be made between the different parameters considered. The flow visualization experiments are presented in Chapter 9 and a discussion is given on the way in which these results can be used to substantiate

the hypothesis for the existence of different flow regimes formulated in Chapters 7 and 8.

1.4.5 In Chapter 10 a more general discussion is presented on the application of this study to the building designers problems. The guide lines of an alternative method for the prediction of the pressure differences across buildings is given in an attempt to improve the current IHVE Guide method for the calculation of infiltration rates. Finally in Chapter 11 the general conclusions reached in the thesis are summarized.

CHAPTER 2

THE PROPERTIES OF THE WIND AND THEIR INFLUENCE
ON THE PRESSURES ON BLUFF BODIES.

2. THE PROPERTIES OF THE WIND AND THEIR INFLUENCE ON THE PRESSURES ON BLUFF BODIES

2.1 The structure and behaviour of the natural wind

2.1.1 The main flow variables in the natural wind that affect the drag of buildings are the velocity profile of the wind, wind turbulence and wind direction. Before discussing their effect on the drag of buildings some background information about the structure and behaviour of the natural wind is given.

2.1.2 The structure of the atmospheric boundary layer is highly complicated. This may explain the fact that although many experiments are being and have been made of the atmospheric boundary layer, much more information is needed concerning its detailed flow structure and flow patterns, Counihan (1975). In the atmospheric boundary layer, wind properties are dependent on both the upper boundary conditions which are the Gradient wind speed and its direction, and more important the lower boundary conditions the topography, surface roughness and surface temperature at the earth's surface. This boundary layer may be regarded as the layer from which momentum is directly extracted and transferred downward to overcome the aerodynamic friction arising from the motion of the air relative to the earth's surface, Pasquill (1970). Within the boundary layer, regions of different properties can be identified. Close to the surface, the shear stress is approximately constant and independent of height. Wind direction is also independent of height. This defines the

"roughness layer" or "surface layer" which extends from the ground up to about 30 metres in open country and 100m in urban areas, after which this approximation breaks down, Counihan (1975). On top of the roughness layer and occupying the rest of the boundary layer is "Ekman layer". In this layer the shear stress decreases with height from its maximum value at the roughness layer to zero at the Gradient wind, a height of some 300-600 meters. Another characteristic of this layer is that wind direction also changes with height in a clockwise rotation known as "Ekman spiral". Within large surface roughness, such as in urban areas, we may define an "interfacial layer" in which the downward flux of momentum is transferred to pressure forces acting on the surface roughness elements themselves, Pasquill (1970). This layer is characterized by wake flows and large variations of static pressure.

2.1.3 Over land, the earth's boundary layer is always adapting to changes of surface roughness. It is observed that an internal layer grows from the surface at a roughness change and develops until it displaces the old layer, Elliott (1958), Munn (1966). In nature the normal fetches of towns are not sufficient for the boundary layer to adapt fully, (i.e. the velocity profile does not change with fetch), before the surface roughness changes again. However, in the lower layers close to the surface, adaptation to roughness change takes place very rapidly and relatively short fetches (\approx 100-500 meters) may be required for these layers to adapt completely, BRE Digest 119 (1970).

2.1.4 The structure of atmospheric turbulence is usually described by the existence of eddies of different sizes and highly irregular shape in the atmospheric boundary layer. In general the eddy size increases with distance above the ground as there will be more room for larger eddies to grow. It is postulated that eddies comparable with the boundary layer height exist in the earth's boundary layer, Townsend (1951). As a result of this eddy cascade, the wind speed changes continuously with time, and the mean value of the wind speed is then dependent on the period taken for averaging. The energy contained in the eddies can be analysed for different frequencies to yield a spectrum similar to that shown in Figure 2.1, Van der Hoven (1957). From the discussion on this spectrum made by Davenport (1963) the following may be quoted:

"One of the most important distinctions that it appears can be made is between the fluctuations of a macrometeorological kind such as the movement of large-scale pressure systems, seasonal variations etc. and those which are of a local, micrometeorological kind and associated with the flow characteristics of the boundary layer itself" "It appears that these two types of fluctuations are separated by a gap extending from roughly five minutes to five hours. This gap is important to our evaluation of wind loads for several reasons. It enables a clear cut distinction to be made between gusts and weather-map disturbances and furthermore their causes: in another sense this distinction can be

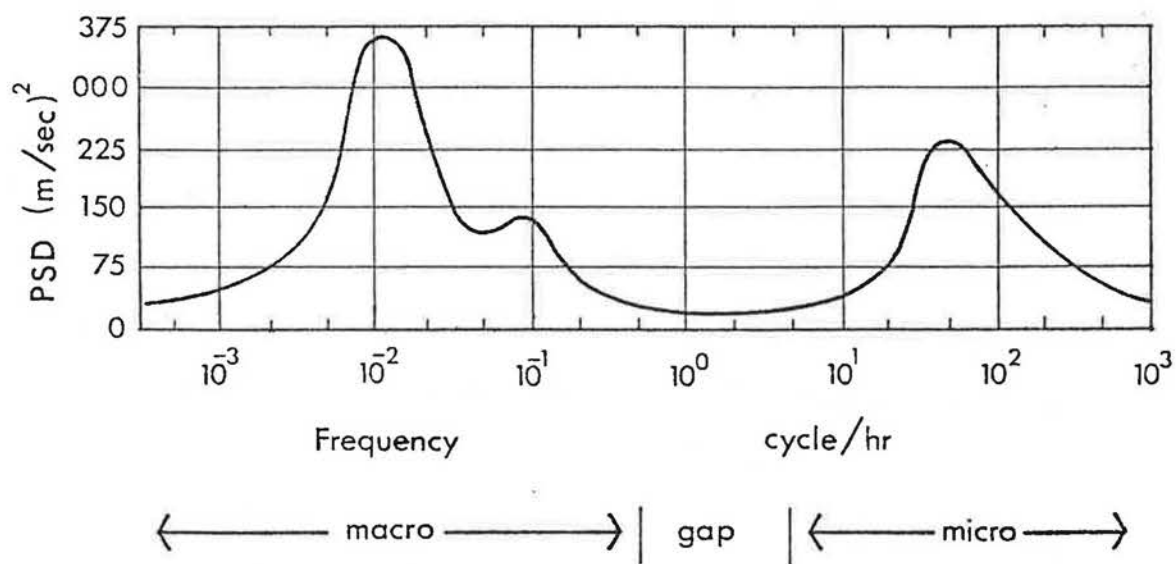


Figure 2.1 SPECTRUM OF THE HORIZONTAL WIND COMPONENT,
(after Van der Hoven, 1957).

regarded as between gusts and the mean wind where the mean wind is characterized by the average velocity over some period within the spectral gap".

2.1.5 In the discussion so far, the wind direction has been considered constant.

As this is not the case in natural wind where these variables are constantly changing, wind may blow from different directions throughout the year for various periods of time. The statistical analysis and presentation of wind speed in terms of percentage of time and direction is known as a wind rose (see Figure 2.2) and is necessary for each site due to climatic variations and the local effect of topography or large obstruction on the prevailing wind direction. A change in wind direction for a building on a site may result in completely different flow conditions due to the corresponding change in the surface roughness up wind.

2.1.6 It is well known that in boundary layer flow over flat surfaces the flow speed changes with the distance from the surface. For the earth's boundary layer, several empirical forms have been suggested to describe the velocity profile of the wind. The two "laws" in common use are the "power law" and the "log law". The power law takes the simple form of:

$$\frac{u}{u_G} = \left(\frac{y}{y_G}\right)^\alpha \quad \dots \quad (2.1)$$

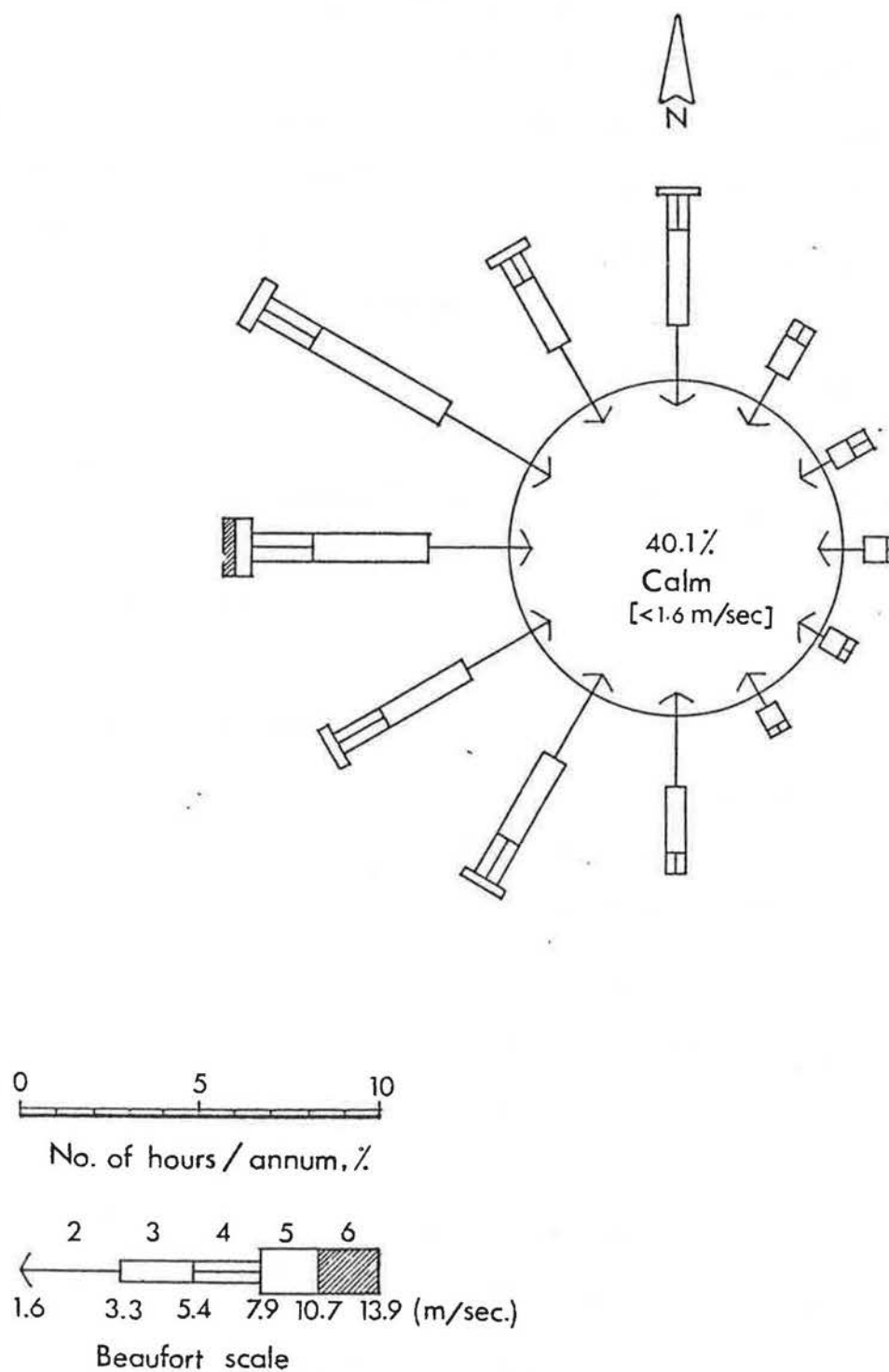


Figure 2.2 WIND ROSE DIAGRAM FOR SHEFFIELD,
(replotted from Lee, E., 1975,C)

where u_G is the Gradient wind speed and y_G is the Gradient height (the boundary layer height). Davenport (1963) collected together mean wind speed profile data for a wide range of countries and terrains. He showed that the index of the power law, α , and the Gradient height, y_{G*} , varied with the nature of the terrain and suggested the representative values shown in table 2.1 and Figure 2.3.

Table 2.1 Variation of the exponent α with type of terrain

(After Harris, 1972)

Type of terrain	Exponent α	Gradient height y_G (m)
Grassland	0.16	280
Woodlands, Suburbia	0.28	400
Urban Centres	0.40	430

The extensive amount of available data for lakes and mud flats through to suburban terrain confirms that the exponent α could take the value of 0.11 up to 0.3 respectively. However, the values for urban terrain are less well established, Harris (1972), Caton (1975).

2.1.7 As an alternative approach, the application of boundary layer theories based on experiment to the earth's natural boundary layer was preferred by meteorologists due to the empirical nature of the "power law". In strong winds and neutral stability the wind flow on the earth's surface is completely turbulent. Therefore a logarithmic law of the form:

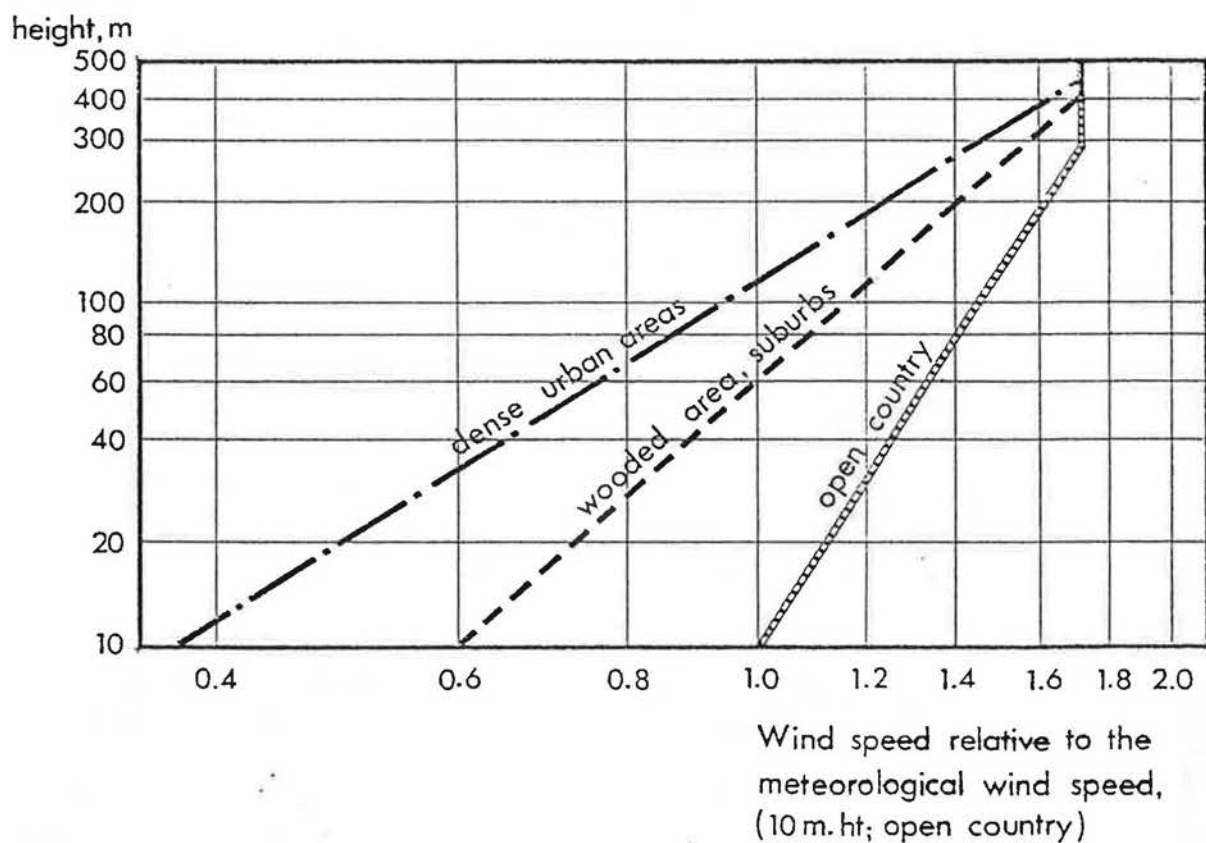


Figure 2.3 MEAN WIND VELOCITY PROFILES FOR SURFACES OF DIFFERENT ROUGHNESS, (after Davenport, 1965).

$$\frac{u}{u_*} = \frac{1}{\kappa} \ln \frac{y}{z_o} \quad \dots\dots (2.2)$$

where $y \geq z_o$, was proposed, Sutton (1953)
 This equation is meaningless for $y < z_o$. To satisfy the
 condition $u = 0$ on $y = 0$, the above equation may be written
 as,

$$\frac{u}{u_*} = \frac{1}{\kappa} \ln \frac{y+z_o}{z_o} \quad \dots\dots (2.3)$$

This equation is approximately the same as equation (2.2)
 for small values of z_o and large values of y . Typical
 values of the roughness length, z_o , for different types
 of terrain are given in table 2.2.

Table 2.2 Values of z_o for various types of terrain

Type of terrain	z_o (m)	Reference
Very smooth (mud flats, ice)	0.00001	Sutton (1953)
Lawn, grass up to 0.01m	0.001	Sutton (1953)
Downland, thin grass, up to 0.1m	0.007	Sutton (1953)
Thick grass, up to 0.1m	0.023	Sutton (1953)
Thin grass, up to 0.5m	0.050	Sutton (1953)
Thick grass, up to 0.5m	0.09	Sutton (1953)
Rural terrain	0.10	Counihan (1972)
Suburban terrain	1.0	Counihan (1972)
Urban terrain	2.50	Counihan (1972)

It may be noted that the form of the logarithmic law as in equation (2.2) applies only to the constant shear stress layer, i.e. the roughness layer. To extend the validity of the logarithmic law to Ekman layer where the shear stress is no longer constant, a linear term should be added and equation (2.3) takes the form, Harris (1972).

$$\frac{u}{u_*} = \frac{1}{\kappa} \ln \frac{y + z_o}{z_o} + C_1 f y \quad \dots\dots (2.4)$$

where f is the Coriolis parameter, and C_1 is a function of u_* , z_o , f and the gradient velocity and wind deviation between ground level and Gradient height.

2.1.8 In the case of flow over urban areas, the flow assumes a ground level displacement, d , therefore equations (2.2) and (2.3) should be modified to read:

$$\frac{u}{u_*} = \frac{1}{\kappa} \ln \frac{y - d}{z_o} \quad \dots\dots (2.5)$$

$$\text{and} \quad \frac{u}{u_*} = \frac{1}{\kappa} \ln \frac{y - d + z_o}{z_o} \quad \dots\dots (2.6)$$

The model for flow in urban areas proposed by Harris (1972) shown in Figure 2.4 and based on equation (2.6) assumes three zones of flow, "A", "B" and "C". Region "A" represents that part of the flow described by a logarithmic profile similar to equation (2.6). While in region "C", i.e. within the displacement height, apart from the fact that wind speed is zero at zero height no general law is applicable and the flow is determined by the adjacent buildings. Finally region "B" is simply a transition from region "A" to region "C". More important is the assumption that,

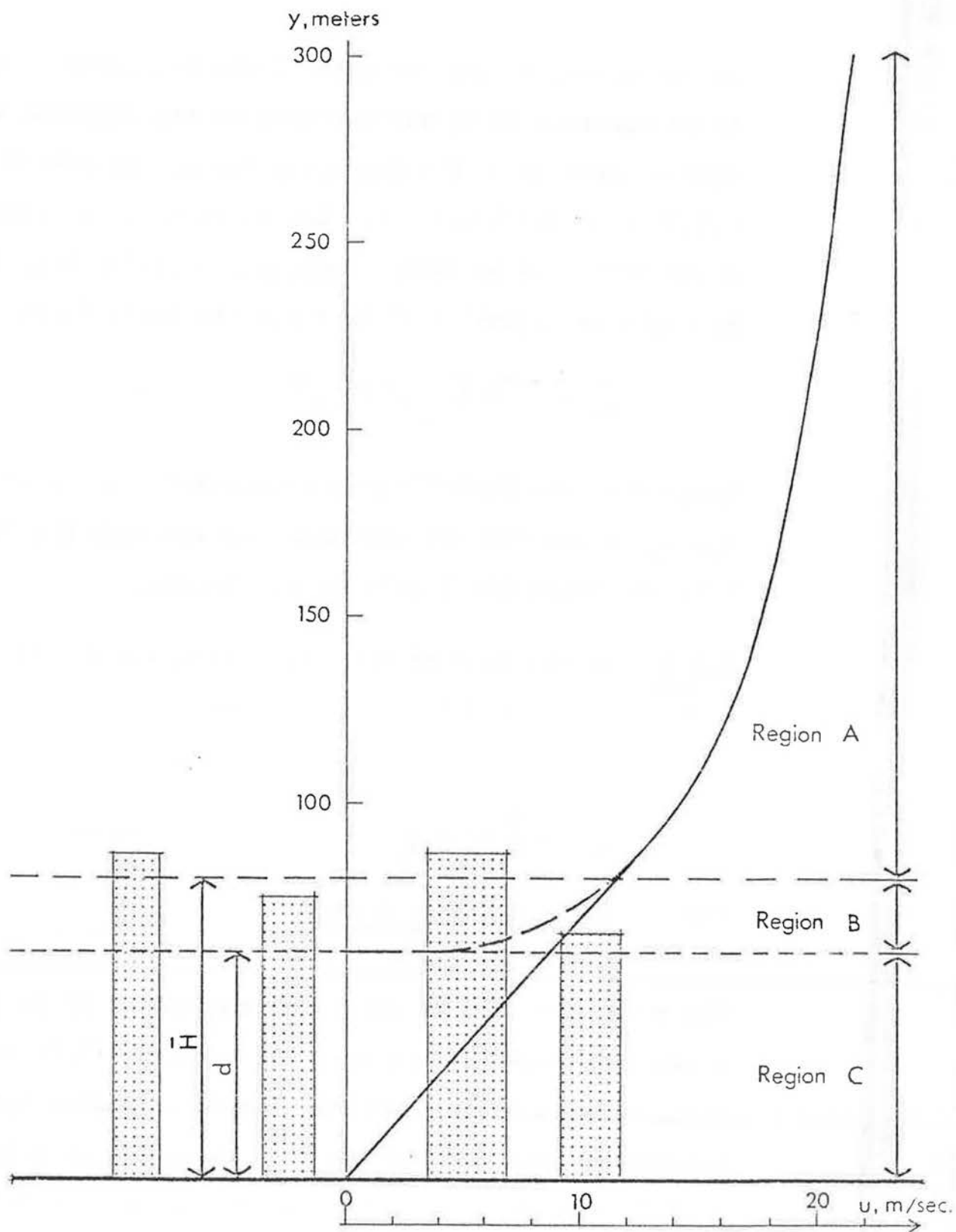


Figure 2.4 A MODEL FOR AIR FLOW IN URBAN AREAS, (after Harris, 1972).

d , is of the same order of the average building height \bar{H} and no profile law can be expected to fit data above an urban terrain below a height of about $1.5d$. In the present study these assumptions are examined.

2.2 Effect of flow parameters on the mean pressure difference across buildings

2.2.1 From wind tunnel experiments, the effect of wind direction, turbulence and the velocity profile parameters on the mean pressure difference across buildings is established. However, the comparison between full scale and model results provide some basic information, see for example Jensen and Franck (1965). The effect of varying wind direction on the pressure difference, Δp , has two-fold effect. First, variation of wind direction might imply completely different flow conditions due to variation of upstream surface roughness, hence different turbulence characteristics and velocity profiles. Second, varying wind direction might change Δp across two opposite faces of a building. Dick (1949) noted in his full scale studies on natural ventilation of houses, that wind direction is of negligible effect. However, this might not be the case for:

- (i) buildings of long plan shapes
- (ii) buildings grouped at large spacings and
- (iii) where ventilation openings are only supplied on two opposite faces of the building.

Under these conditions, the driving force for ventilation is the mean pressure difference, Δp , across the faces, rather

than the drag force, D , in the flow direction. The drag force may show little variation due to the change in wind direction, hence ventilation is expected to reflect the same trend of, D , for buildings not satisfying conditions (i) and (iii). On the other hand if conditions (i), (ii) and (iii) are satisfied, the mean pressure difference across two opposite faces may range from a maximum equal to the drag force, at normal incidence to a minimum for the wind at right angles. Therefore, information about wind directions in nature is necessary if any estimate of Δp is required.

2.2.2 It is known that turbulent scale and intensity affect the drag coefficient of rectangular body forms through its effect on the separated flow region, Lee (1975 (a)), Lee (1975 (b)). On three dimensional rectangular forms, very little work exists, apart from that by Cook (1972) where only the effects of turbulence scale or intensity were investigated independently. Jensen and Franck (1965) conducted wind tunnel experimental work in which the flow structure was varied using different surface roughness upstream the model, on which the boundary layer naturally developed. Although no attempt was made to measure the associated turbulence characteristics or to reproduce the atmospheric turbulence structure, it was implied that modelling the correct ratio of H/Z_0 in natural wind was closely related to modelling the turbulence properties.

In general it appears that higher turbulence intensities reduce the pressure difference by increasing the negative leeward pressure. On the other hand, effects of turbulence scale would appear to be dependent on the ratio of eddy size to building dimensions. Dominant effects would occur at values of this ratio ranging between 0.5 - 10, Cook (1972), Armitt (1974).

2.2.3 The main parameters of the boundary layer velocity profile known to affect the flow mechanism, hence the pressures and the drag force on bluff bodies, are the boundary layer thickness, δ , the roughness length, Z_0 , the zero plane (ground plane) displacement, d and the friction velocity u_* . The effect of increasing the ratio $\frac{H}{\delta}$ and u_l/\bar{u}_* on the drag of a two dimensional plate normal to the flow on a smooth surface was investigated by Good and Joubert (1968). In this study, Good et. al. showed how C_{D_L} as well as C_{D_H} are dependent on H/δ and $\frac{H}{v/u_*}$, hence H/Z_0 , since v/u_* is a length scale proportional to Z_0 for smooth surface flow. Their results may be seen in Figures 2.5 and 2.6

2.2.4 The work of Jensen and Franck (1965) not only shows the effect of the ratio H/Z_0 , for various rough surfaces, on the pressure difference (see Figure 2.7) but also on the pressure distribution as can be seen in Figure 2.8. In this work although no allowance seems to have been made for d in determining the values of Z_0 , the effect of variations of Z_0 as a parameter of value was demonstrated. Due to the dependence of Z_0 or d in the cases where high roughness elements were used, large values

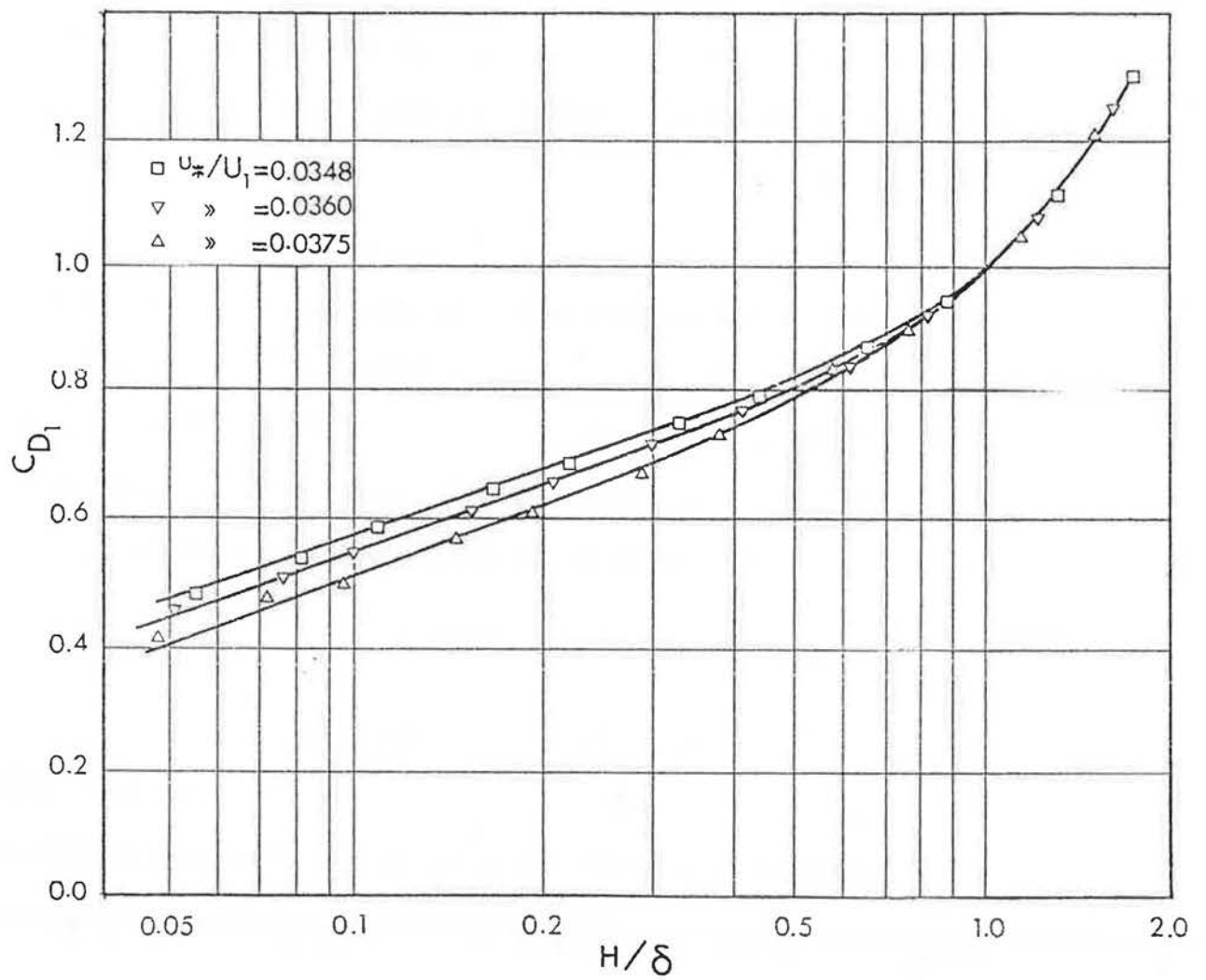


Figure 2.5 VARIATION OF C_{D1} WITH H/δ and u_*/U_1 ,
(after Good and Joubert, 1968).

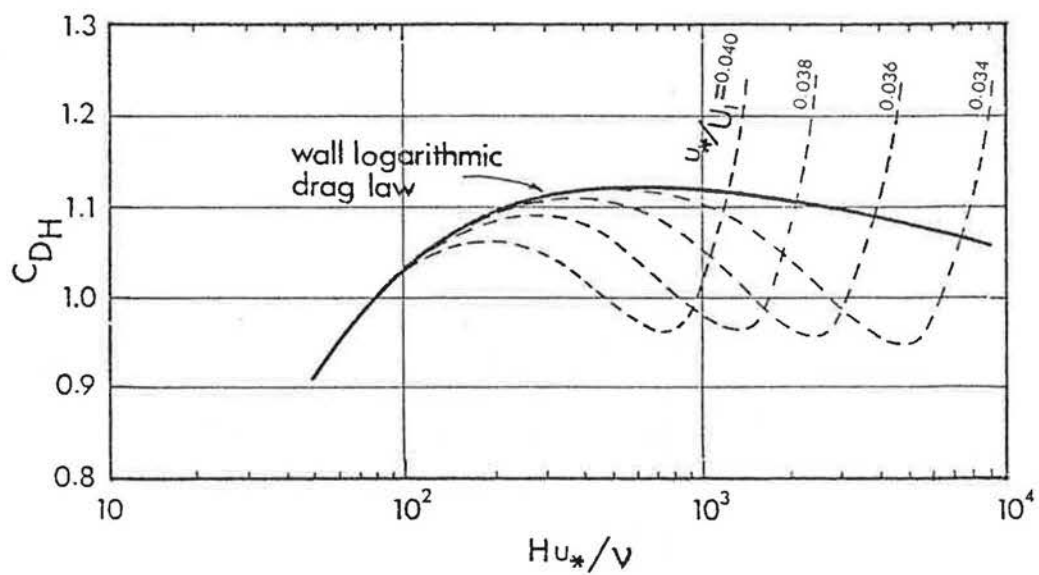
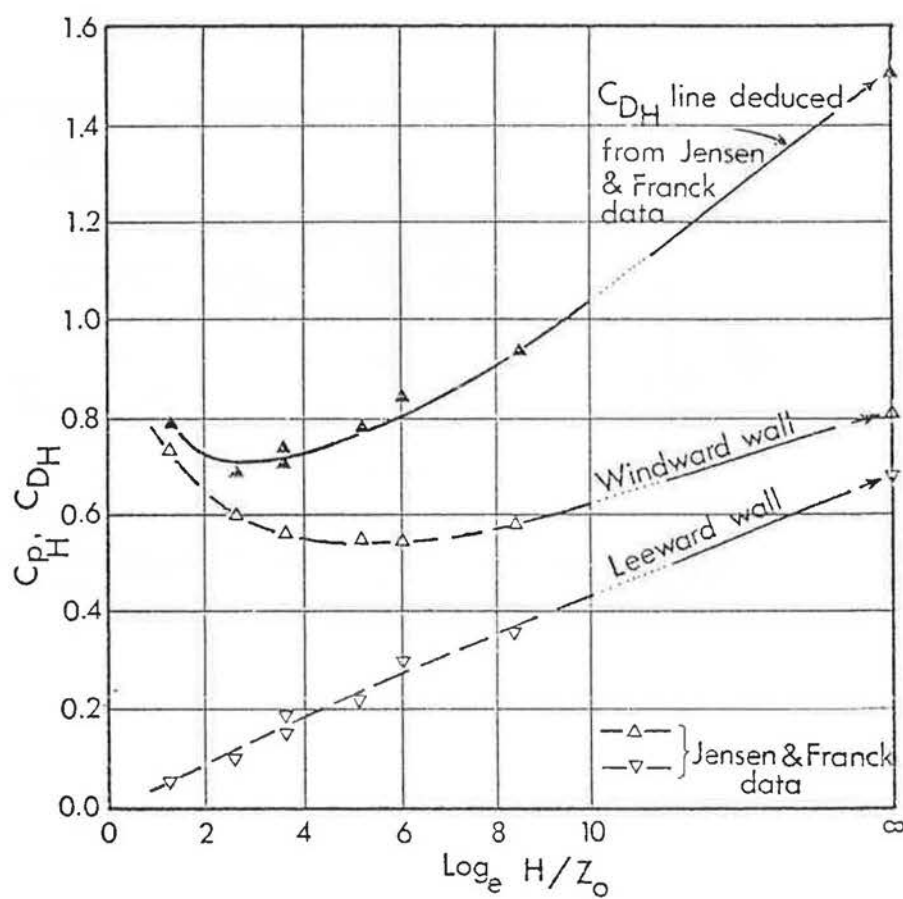
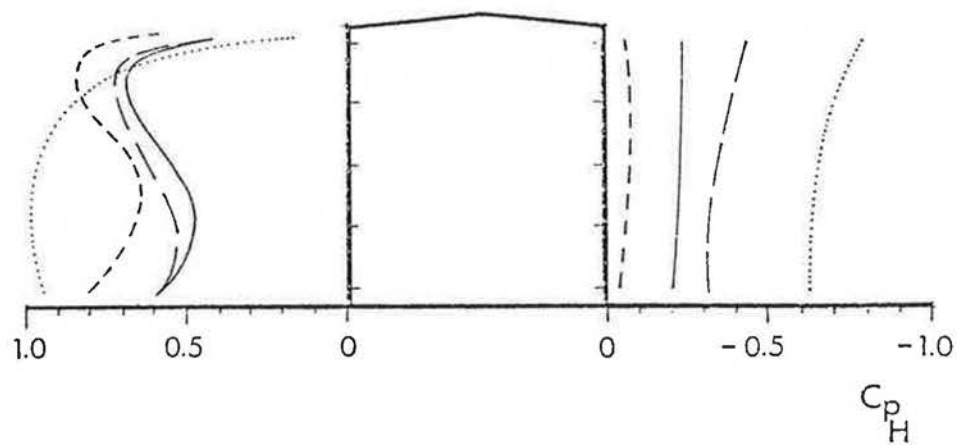
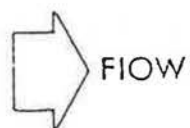


Figure 2.6 VARIATION OF C_{DH} WITH Hu_*/ν AND u_*/U_1 ,
(after Good and Joubert, 1968).





$H/Z_o = 3.6$ -----
 180 —————
 4600 - - - - -
 ∞

Figure 2.8 THE PRESSURE DISTRIBUTION OF A MODEL HOUSE FOR DIFFERENT VALUES OF H/Z_o , (after Jensen and Franck, 1965).

of d are to be expected. Hence the corresponding values of Z_0 are possibly an overestimate.

2.2.5 It may also be noted that due to the disturbance of the flow and the growth of an internal layer (referred to in 2.1.3) at a change of surface roughness, the shear stress at the surface, hence u_* , experience a sudden change followed by gradual change until the value of the new shear stress is attained, Blom and Wartena (1969). Consequently, the drag force on large groups of bluff bodies reflects the same disturbance experienced by u_* at the leading part of the group as well as the trailing part of the group, Antonia and Luxton (1971), Antonia and Luxton (1972). In between these two parts, adaptation takes place. However, for very small groups of bluff bodies, the drag force may not reach stability before the disturbance of the trailing part is experienced. The detailed discussion on the behaviour of the flow parameters is given in Chapter 5.

CHAPTER 3

A REVIEW ON PREVIOUS WORK RELEVANT TO
NATURAL VENTILATION OF BUILDING GROUPS.

3. A REVIEW ON PREVIOUS WORK RELEVANT TO NATURAL VENTILATION OF BUILDING GROUPS

3.1 Introduction

3.1.1 Over the years a considerable amount of work has been done in the investigation of wind effects on buildings for various purposes, which might be broadly categorized as wind loading, wind environment and the natural ventilation of buildings. Most of the work has concentrated on isolated buildings, while groups of buildings have received comparatively very little attention. Hence, because of the interrelationship between building form, wind flow and the resulting pressure forces, the findings of any particular investigation will be useful not only for its original purpose but also may help with the solution to other problems in related categories. With the factors affecting the pressure difference across buildings in mind, it is intended in this section to give a review of the previous work on building groups. It will include the relevant work made on:

1. Natural ventiation of building groups, by Weston (1956), Givoni (1968) and Nelson (1971).
2. Wind loading on building groups, by Vincent and Bailey (1943) and
3. Air flow round groups of buildings, by Wise, Sexton and Lillywhite (1965), Wise (1970), Olgyay and Olgyay (1963) and Koenigsberger, Ingersoll, Mayhew and Szokolay (1973).

3.2 Previous work on natural ventilation of building groups

3.2.1 In the work reported by Weston (1956), the effect of obstructing a simple industrial building by other different building forms placed at different upstream distances was investigated. Measurements of average internal air speeds were made in a 1/16 scale model, for different obstruction cases, the results being presented in the form of the percentage of the mean internal air speed obtained for the same building when unobstructed. For ease of comparison, all dimensions which were given in the report, in full scale equivalent, are given here normalized by the windward wall height, H , of the experimental building (4.57m in full scale). Table 3.1 gives the dimensions of the experimental building together with average and extreme values of the 18 different obstructing buildings used.

Table 3.1 Dimensions of the buildings used by Weston, E.T.

Dimension	Experimental Building	Obstructing Buildings		
		min	avg	max
Building length (across wind)	4H	3.07H	4.04H	6.67H
Building depth (along wind)	12H	1H	2.71H	4H
Building height	1H	0.67H	1.82H	2.73H

From the information given by Weston, the results obtained from the different obstructing buildings were averaged and the standard deviation was calculated. This form of presentation is shown in Figure 3.1 which shows the effect

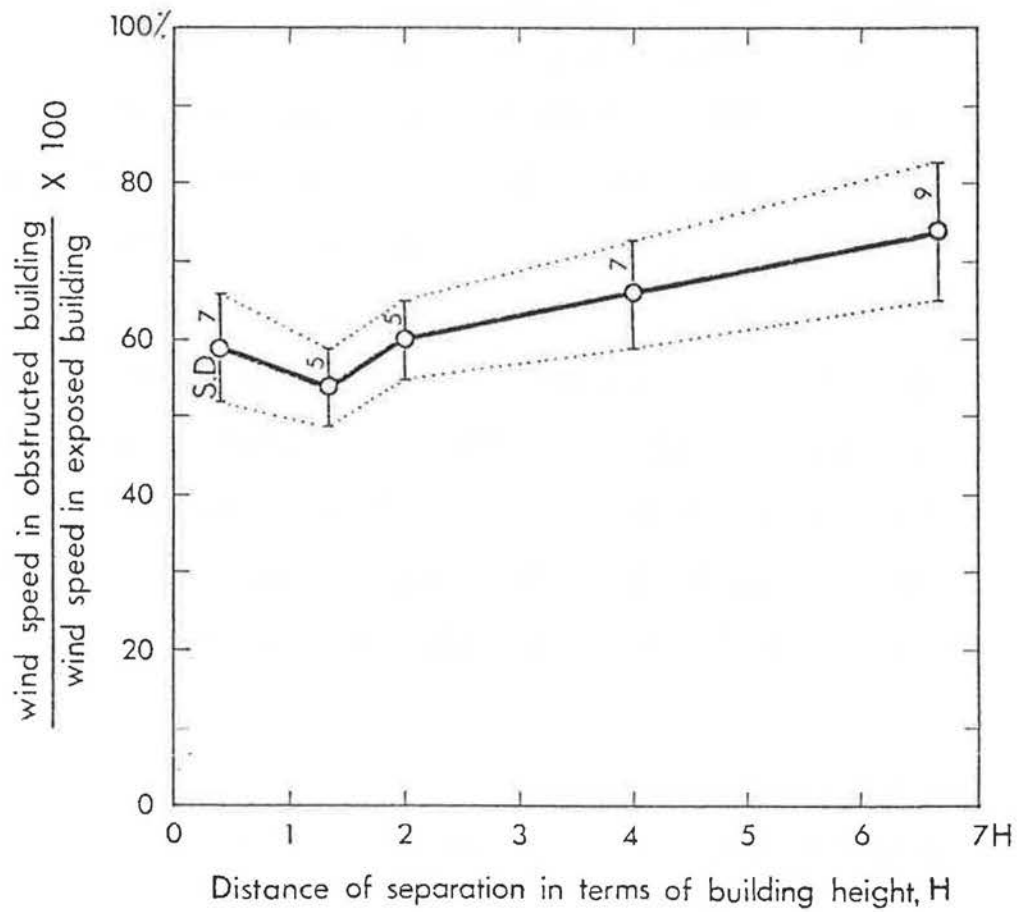


Figure 3.1 EFFECT OF DISTANCE OF SEPARATION ON THE RESULTING VENTILATION USING WESTON'S DATA (1965).

of the distance of separation on the internal air velocity. From this work Weston drew the following conclusions:

- (i) As a general rule, increasing the distance of separation between the building and its obstruction improves the natural ventilation.
- (ii) There is a certain distance of separation at which a change of flow conditions appears to occur, in that, ventilation conditions are found to be at a minimum and to improve by any increase or decrease in the distance of separation. For most of the cases tested this distance was found to be $1.33H$ (see Figure 3.1).
- (iii) At small distances of separation natural ventilation improved by increasing the height of the obstructing building. The reverse occurred if the distance of separation is increased beyond $2H$.
- (iv) A similar effect was obtained, though to a lesser extent, by increasing the length of the obstructing building normal to the wind.

The explanations given in the report of these phenomena were assisted by the use of smoke flow visualization techniques and may be summarized as follows. Ventilation conditions improve if the pressure difference across the building increases. At small distances of separation (i.e. less than $1.33H$) the windward building wall is in the reduced pressure zone of the obstructing building and becomes subject to a lower pressure than that at the leeward wall.

In this case reversed flow was noted in the test building. Decreasing the distance of separation intensified these conditions, hence improving natural ventilation. At larger distances of separation i.e. greater than $1.33H$, the reduced pressure zone of the obstructing building no longer appeared to affect the windward wall and in the general ventilation conditions were found to be proportional to the distance of separation. The decreased pressure to the leeward of the obstructing building was also found to be intensified by either increasing its height or its length normal to the wind. From the work of Weston shown above, the following additional comments may be made.

- (i) The values of the standard deviations of the internal flow rates shown in Figure 3.1, indicate that the variation in natural ventilation conditions due to the various obstructions investigated were small (order of 5 - 10%) for any particular distance.
- (ii) It is not possible to establish any meaningful relationship between the ventilation conditions and the geometry of the obstruction owing to the limited test range (see table 3.1)

3.2.2 In a series of wind tunnel experiments reported by Givoni (1968), the effect of building group geometry on natural ventilation and air flow round building blocks was investigated. In this study measurements of average air speed were made both inside and outside the models, and expressed as a percentage of the wind speed at the same height upstream of the group. As no mention was made

of the mean velocity gradient in the incident flow, it is reasonable to assume that the flow was uniform. The blocks which measured 600 x 200mm in plan by 400 mm high were arranged in either two or three rows normal to the wind. In the former arrangement in which only two blocks were used one block in each row, the longitudinal distance of separation was varied from 0.75 to 3.25H at 0.25H intervals, where H is the block height. In the latter arrangement where three rows were considered, longitudinal distances of separation took the values of 0.75H, 1H and 1.25H, while the lateral distance of separation between blocks in the same row varied from 0 to 1.25H at intervals of 0.25H. In this latter arrangement the case of a single block in each row was also studied as an extreme where the lateral distance of separation is ∞ . The main conclusions obtained by Givoni, from this work were:

- (i) The effect of increasing the longitudinal distance of separation between blocks in two rows was to increase the air speed between the blocks whilst the internal air speed in the leeward block reflected an initial decrease followed by an increase.
- (ii) The effect of increasing the lateral distance of separation between blocks in the same row was to initially increase both internal and external air speeds then to reach a maximum followed by gradual decrease to a value approximately equal to the initial value where the lateral distance was zero.

Despite the usefulness of these results it is difficult to extend their applicability to other situations, since the values of internal air speeds given is dependent largely on the block proportions and the wall opening details, as well as the flow properties.

3.2.3 Nelson (1971) reported an algorithm for the computerized calculation of natural ventilation rates in which an equation similar in form to the equation

$$V = C_i \cdot L_c \cdot (\Delta p)^{1/n} \quad \text{.....(1.1)}$$

was adopted. The effect of the surrounding buildings as well as the building orientation was taken into consideration for assessing wind pressure. In principle, it is assumed that the pressure, P_y , acting at any height, y , on the building facade may be obtained using the following formula:-

$$P_y = K_o (C_{p_f} \cdot \frac{1}{2} \rho u_y^2) \quad \text{.....(3.1)}$$

where C_{p_f} is a correction factor for the effect of surroundings and K_o is a correction factor dependent on the facade orientation. The pressure correction factor C_{p_f} is given for three types of surrounding buildings at different distances of separation, which are given in table 3.2.

Table 3.2 Values of C_{Pf} for different surrounding buildings
and distances of separation

Separation distance	Lower building Upstream			Equally high or higher building Upstream			Taller building downstream		
Subject building thickness	Wind-ward wall	Lee-ward wall	Side wall	Wind-ward wall	Lee-ward wall	Side wall	Wind-ward wall	Lee-ward wall	Side wall
0.5	0.10	-0.30	-0.80	-0.50	-0.25	-0.45	0.50	0.45	0.45
1.0	-0.10	-0.25	-0.50	-0.50	-0.20	-0.30	0.45	0.30	0.30
2.0	0.10	-0.25	-0.40	0.00	-0.20	-0.30	0.45	0.10	0.10
3.0	0.10	-0.25	-0.40	0.10	-0.20	-0.35	0.45	0.00	0.00
5.0	0.25	-0.35	-0.60	0.25	-0.25	-0.45	0.50	-0.10	-0.10
∞	0.60	-0.35	-0.70	0.60	-0.35	-0.70	0.60	-0.35	-0.70

The dynamic head $\frac{1}{2}\rho u_y^2$ was determined from a velocity profile formula similar to that used by Vincent and Bailey (equation 3.2) given in the next section. The correction factor K_o , which allowed for the variation of pressure with orientation, is assumed to be equal to -1.0 for the leeward walls, whilst for the windward walls $K_o = \cos \theta$ and for the side walls $K_o = -\cos \theta$, where θ is the angle between the wind and a normal to the building face. The following ranges of θ are given for each wall:

Windward wall	$315^\circ < \theta < 45^\circ$
Side Wall	$\begin{cases} 45^\circ < \theta < 90^\circ \\ 270^\circ < \theta < 315^\circ \end{cases}$
Leeward Wall	$90^\circ < \theta < 270^\circ$

3.2.4 The following remarks may be noted on the method suggested by Nelson.

- (i) The basic concept of using the dynamic head of the flow to describe the pressure on the building suggests a similarity to the concept employed in the Crack Method of the IHVE Guide. The main criticism in such a concept is that the pressure coefficient used is independent on both the building shape and the properties of the incident flow.
- (ii) A closer look on the correction factor for the surrounding buildings, C_{p_f} , shows that it is actually a different way of presenting the results of Vincent and Bailey (1943) which will be commented on in the next section
- (iii) The variation of the pressure correction factor, K_o , with the angle of incidence θ shows an abrupt change of sign for the same magnitude at $\theta = 45^\circ$ and 315° , the angle at which the facade changes from windward to sideward. Though there will be a gradual change of sign it will not be as abrupt as this method indicates.

3.3 Previous work on wind loading on building groups

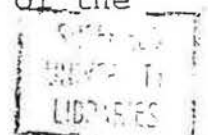
3.3.1 Vincent and Bailey (1943) carried out a series of wind tunnel experiments to investigate proximity effects on the wind loading of buildings. The cases considered were mainly for two buildings, one downstream of the other,

though some additional results are given for the isolated building case and for an array of three identical buildings. All of the cases of building proximity investigated showed the effect of the obstruction by an upstream building apart from one case in which the effect of a downstream high building on a low building upstream was investigated. The geometrical variables considered in this study were the building shape, the group form and the distance of separation between buildings. In the seven shapes of buildings considered, (see table 3.3) variations were made in the height and roof shapes while the length and thickness remained approximately constant.

Table 3.3 Description of the models used by Vincent and Bailey

Model	Height to eaves (mm)	Overall height (mm)	Length normal to Wind (mm)	Thickness along wind (mm)	Type of Roof
A	30.5	42.7	127	53.8	Sloped at 23.5°
B	30.5	58.7	127	53.8	Sloped at 45°
C	63.5	91.7	127	53.8	Sloped at 45°
D	30.5	46.7	127	53.8	Sloped at 30°
E	30.5	31.2	127	53.8	Flat
F	63.5	64.3	127	53.8	Flat
G	-	132.1	203.2	50.8	Stepped

The distance of separation was varied in units of the building thickness, from a minimum of zero to a maximum which varied from 3 to 20 for different models. Despite the early date of this report, consideration was given to the simulation of the

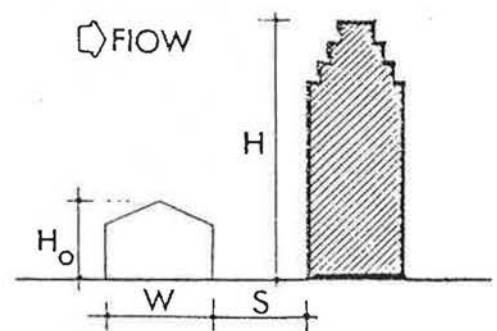
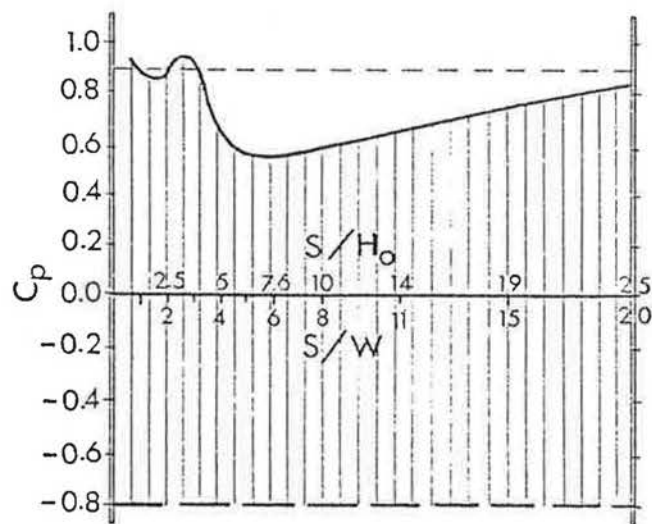


natural wind profile at least in terms of velocity gradient. The profile simulated was that appropriate to flow in open country with a boundary layer thickness, δ , of 203mm. The profile shape was a close approximation to the following formula, suggested by the Meteorological Office at the time.

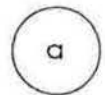
$$\frac{u_y}{u_{10}} = K \{1.00 + 2.81 \log (y + 4.75)\} \dots\dots (3.2)$$

No mention was made of the method by which the velocity profile was simulated. In the course of this investigation pressure measurements were obtained from a centre line row of tapings of the windward wall and the roof. The leeward wall pressure was obtained from only one tapping near the top of the wall. The pressures were given in the form of coefficients non-dimensionalized with respect to the dynamic head at a height of 50.8mm from the tunnel wall. From the results obtained, those concerning the wall pressures are considered most relevant and are shown in Figure 3.2 (a) - (j). For convenience of comparison and analysis, the variation of mean pressure on both walls with distance of separation have been replotted together with the corresponding values for the isolated test building in each case. The main conclusions drawn by Vincent and Bailey from this study were:

- (i) The effect of a small building on the pressure difference across a heigh building downstream, case (a), is small. The maximum reduction at any distance was about 20% of the isolated case.
- (ii) In the case of two high buildings, case (b), a considerable effect on the wall pressures was found



$$\frac{H}{H_o} = 3.1$$




- Isolated model
- Windward wall
- - - Leeward wall
-  Instrumented model

Figure 3.2 VINCENT AND BAILEY'S RESULTS,
(adapted from Vincent and Bailey, 1943).

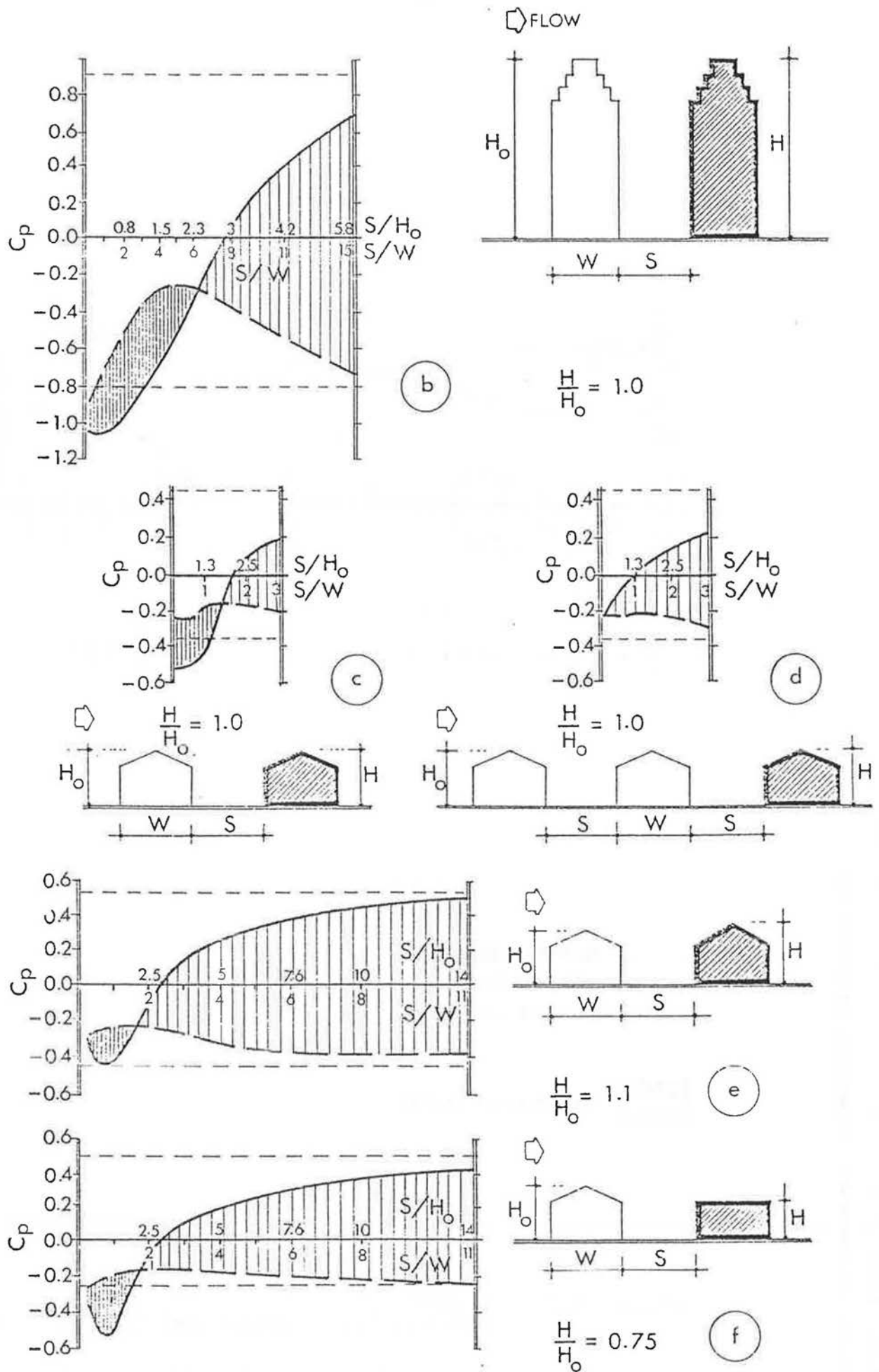


Figure 3.2 VINCENT AND BAILEY'S RESULTS, (adapted from Vincent and Bailey, 1943).

For legend, see Figure 3.2(a)

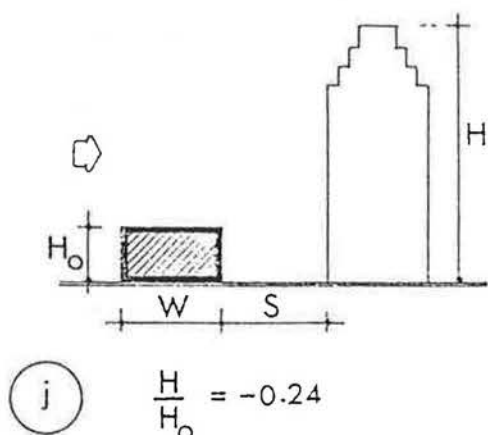
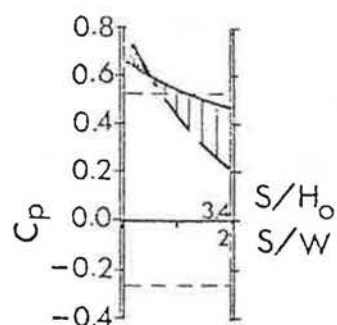
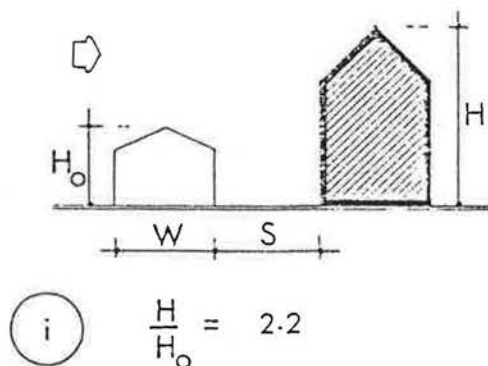
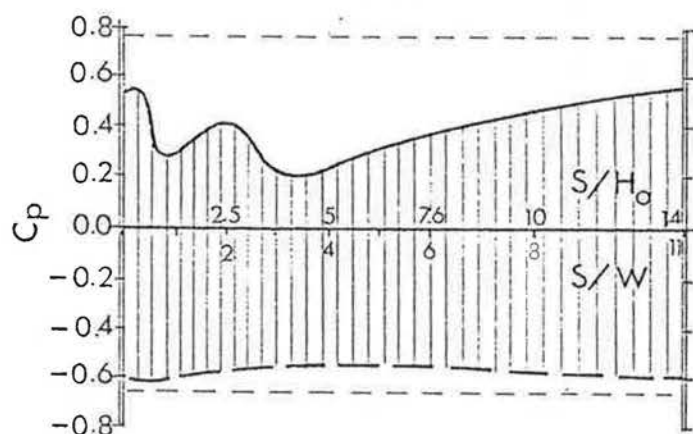
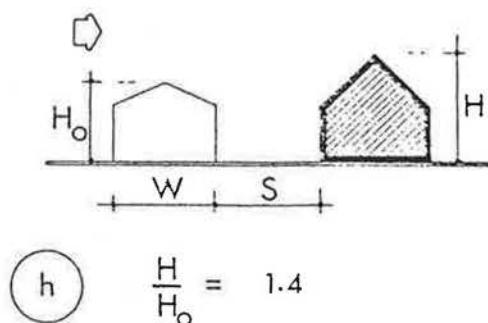
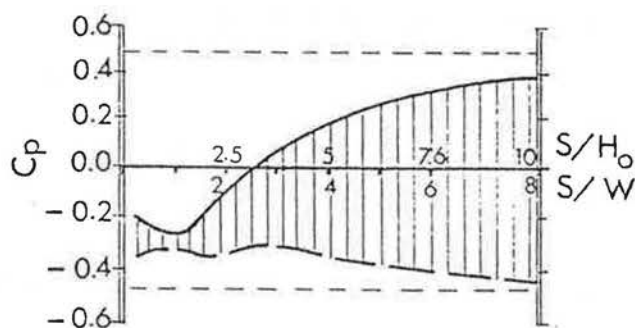
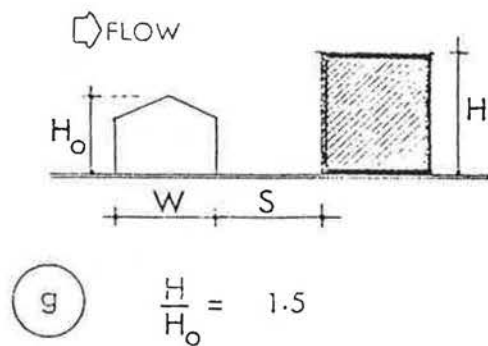
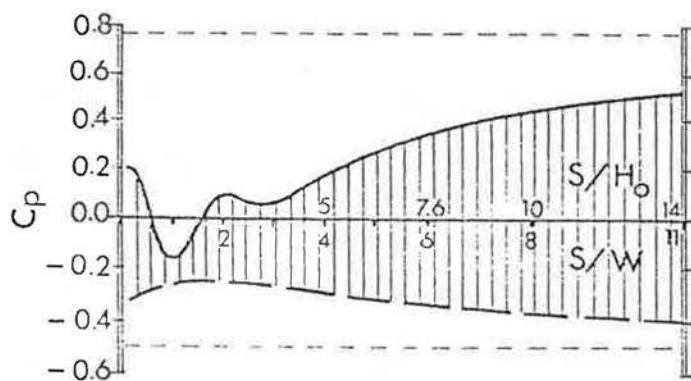


Figure 3.2 VINCENT AND BAILEY'S RESULTS, (adapted from Vincent and Bailey, 1943).

For legend see Figure 3.2(a)

to occur as the distance of separation decreased. The pressure difference between the windward and leeward walls was zero at a distance of separation 6 times the building thickness. Furthermore, thrust forces, where the windward wall pressures were more negative than those on the leeward wall, were experienced at smaller separation distances.

- (iii) The effect of the number of models upstream, cases (c) and (d), was found to be small, therefore, the results would be expected to be representative of built up areas.
- (iv) Due to the downwind shelter effect present in most cases even at large separation distances, allowance should be made to reduce the fully exposed values for the lower part of a building up to some specific height.

3.3.2 From a further consideration of the results obtained by Vincent and Bailey the following points emerged:-

- (1) For the two building cases it can be shown that the variation of wall pressure with distance of separation in the different cases depends on group form. Suggesting H/H_0 as a parameter roughly describing group form, (where H is the height of the building under investigation and H_0 is the height of the obstructing building) different group forms regardless of roof shape may be written as:-

- (i) $H/H_0 < 1$, high building upstream
- (ii) $H/H_0 = 1$, two equal buildings
- (iii) $H/H_0 > 1$, low building upstream

A negative sign may be given to this parameter to indicate a reverse situation when the building under consideration is upstream of the obstructing building. An example of this case was included in the study and the result is shown in case (j).

2. In case of more than two buildings additional geometrical parameters are needed to describe the group form, where variations in individual building dimensions will add complexity to these parameters. Here only one simple case has been considered, case (d) where the three buildings tested were identical.
3. A zone of negative pressure difference at certain distances of separation can be seen as a common feature in the cases of Figure 3.2 (b), (c), (e) and (f). The significance of this observation is that these are the only cases where $H/H_0 \leq 1$. Furthermore, the distance at which the pressure difference changes its sign appears to be approximately the same in all those cases apart from case (b). However, normalizing the distance of separation with respect to H_0 rather than the building thickness, is not only more appropriate because of the sensitivity of flow to variation in height but also makes the separation distance at which zero pressure difference occurs approximately equal in all cases.
4. In the cases where $H/H_0 > 1$ i.e. cases (a), (g), (h), and (i), the pressure difference between the windward and leeward faces was positive at all distances, and the shelter effect decreased as H/H_0 increased.

5. Finally, a relevant point may be made concerning the case of more than two buildings shown in case (d). Here, contrary to the conclusion given in the paper which implies a negligible effect for the number of models, it can be seen by comparing cases (c) and (d) that two major differences occur. First, the zone of negative pressure difference which was dominant in the two building case, (c), disappeared in the three building case, (d); and secondly, the point at which the pressure difference is zero occurs approximately at zero distance of separation.

3.3.3 The general conclusions which could be obtained from Vincent and Bailey's work are:

1. The parameters governing the flow and pressures in groups of two buildings are not the same as those for an array of more than two.
2. For pairs of buildings subject to the same incident flow conditions, the pressure difference between the windward and leeward faces was affected both by the building form and the distance of separation. Better correlation of the results was obtained when the group form parameter H/H_0 was used and when the distance of separation was normalized with respect to H_0 rather than the building thickness.

3.4 Previous work on air flow round groups of buildings

3.4.1 Wise, Sexton and Lillywhite (1965) have reported some measurements of the flow round buildings on the basis of wind tunnel experiments. The building types under investigation consisted of a low rise building, a tower building and a slab building. The dimensions of these models in terms of the low rise building height are given in table 3.4.

Table 3.4 Dimension of the models used by Wise et. al (1965)
in terms of the low rise building height

Model	Height, H	Length	Thickness
Tower	4	1	1
Slab	3	4	1
Low building	1	4	1

where the length is the dimension normal to the flow and the thickness is the in-wind dimension. The incident flow simulated a suburban velocity profile artificially generated using vertical array of horizontal slats. The buildings were relatively large in size compared with the boundary layer thickness, δ , i.e. $H/\delta = 0.22, 0.67, 0.89$ for the low building, the slab and the tower respectively. Three forms of building groups were studied in addition to the isolated building cases, in which the air velocity was measured at discrete points round the blocks. The groups considered were: (i) two low buildings, (ii) three low buildings and (iii) a slab with a low building upstream. In all cases the distance of separation was kept constant

at double the low building height. The results showed that a vortex existed between the buildings in all cases. However, the wind speed at any point between the buildings compared with that at the same height far upstream is shown to be reduced in between the buildings in cases (i) and (ii) whilst in case (iii) it increased by about 30% in the region close to the ground. Furthermore, it was noted that the effect of adding the third building, case (ii), on the relative speeds observed in the two building group, case (i), was negligible. An examination of the data presented here does not, however, yield the information that the relative speed between building 1 and 2 (the upstream pair) is 30% less than that between buildings 2 and 3 (the downstream pair) in case (ii). The particular geometric parameters considered in the work of Wise et.al coupled with the relaxation of simulating size parameters, i.e. H/δ or H/Z_0 will tend to limit the general applicability of the results. In addition, the flow speed measurement at discrete points makes it difficult to obtain any relation between the flow parameters and the group form parameters.

3.4.2 In order to relate the flow speed at one point to the geometrical parameters describing a group of two buildings, Wise (1970), in a later investigation, carried out a more detailed study of case (iii), the combination of a slab with an upstream low rise building. The geometrical parameters varied were: the distance of separation, L_x , the slab building thickness, W , and the slab building height H . The main conclusion reached was

that the velocity at one point between the two buildings and close to the ground, u_A is a complex function of the wind speed at the top of the slab building, u_H ; the height of the point above the ground, a ; the slab building length, L , height, H and thickness, W ; as well as the low building height h . The following expression was obtained for u_A .

$$\frac{u_A}{u_H} = 0.24 \left\{ \left(\frac{a}{H} \right)^{0.28} + \left(\frac{L}{H} \right)^{0.4} \left(\frac{W}{H} \right)^{0.4} \left(\frac{H}{h} \right)^{0.8} \right\} \dots\dots (3.3)$$

This equation was found to be applicable within the following limits only $\frac{H}{a} > 33$, $\frac{W}{H} > 1$, $\frac{L}{H} > 1$ and $\frac{H}{h} > 8$.

3.4.3 In a study, whose purpose was to improve the natural ventilation rates of low rise housing in different layout patterns, Olgyay (1963) presents a series of useful flow visualization photographs. The group model consisted of six blocks, arranged in three rows at different spacing in each layout pattern. The main conclusion resulting from this study was that the gridiron pattern (where buildings are aligned in the wind direction) causes more shelter to subsequent rows of buildings, while the staggered pattern (where buildings are shifted laterally every other row) gives better ventilation. It was recommended that a spacing of seven times the building height should secure satisfactory ventilation for each unit. Similar comments are given in the book by Koenigsberger, Ingersoll, Mayhew and Szokolay, (1973) in a series of sketches which were based on studies carried out in the A.A. school of Architecture. Here, a distance of six times the building height is given as the satisfactory limit for

an adequate natural ventilation.

3.4.4 In the studies of Olgyay and Koenigsberger, et. al. the measure of satisfactory ventilation was not defined, nor was the form of the individual buildings considered to be an important parameter. The effect of the latter is expected to play an important role and such recommendations as they give should be treated with caution.

3.5 Conclusions

3.5.1 From the above review, the following conclusions may be drawn:

1. The flow and the pressure forces on groups of buildings are dependent on both the individual building form, i.e. size and shape and the building group form, i.e. the relative size of individual buildings and the layout pattern.
2. The simulation of the natural boundary layer properties in terms of the velocity profile shape was considered by some workers. However the effect of building size in terms of H/δ or H/Z_0 was not considered at all.
3. The effect of fetch on either the flow or the drag forces was not considered at all.
4. Despite the useful information obtained from the work on natural ventilation, wind loading and wind flow round groups of buildings, no general relationship was obtained between the group geometry, the resulting flow and the pressure forces. This

conclusion is natural as the number of variables involved is prohibitively large and any general relationship would be a complex one.

5. It is evident that the pressure forces on a group of two similar buildings, hence the flow, does not represent the flow round a group of more than two buildings, the case of urban areas.

3.5.2 The complexity of the problem indicated by the above conclusions suggest that in order to obtain any relationship between individual building form, building group form and the resulting pressure forces, great limitations ought to be put to the variables involved, and in particular those concerning the building and group form. A more appropriate approach may then include the effect of building size, (H/δ) , as well as the size of the building group (in terms of fetch) required to give representative results of the corresponding conditions in urban areas.

CHAPTER 4

DENSITY AND FORM.

4. DENSITY AND FORM

4.1 Introduction

4.1.1 The design and planning of residential areas often refers to housing density as an indicator of environmental quality. This follows from the hypothesis that the geometry of urban form will largely determine its environmental conditions. Since the density of built form is a function of its geometry it is important to determine the relation between the geometrical parameters needed to define group form and its density.

4.1.2 Several studies have been made in which the density of residential areas were considered in relation to planning parameters as well as geometrical parameters for different environmental criteria. A review on these studies is made in order to see how accurately group form can be defined in terms of the parameters considered, as well as to determine the practical limits of these parameters. A theoretical analysis is also presented to enable a complete definition of group form to be made, in terms of a proposed set of geometrical parameters and group density.

4.1.3 Due to the complex interaction between the parameters involved, a method of graphical presentation has been evolved to show the interaction between these parameters, as well as the commonly accepted zones confined within their limits. If flow conditions are dependent on group form then the suggested graphical

presentation would help in identifying zones of similar flow conditions. Such an identification procedure will not only help the planner in recognizing the consequences of form variation on the resulting flow, but also would guide the aerodynamicist to design meaningful experiments within the practical limits of urban form.

4.2 Density of Residential Areas

4.2.1 The density of residential areas has been investigated from many different aspects and for various criteria, Gropius (1956), Stevens (1960), Segal (1965) and Martin and March (1972). The large number of the variables involved coupled with the interrelationship existing between them, make it necessary to clarify the concept of density. It is of particular importance to identify the relevant parameters linking the planning and aerodynamic aspects of urban building density.

4.2.2 For provision of sunlighting, Gropius considered the problem as a two dimensional building array and investigated the following variables:

site area/building	A
angle of sunlighting	γ
number of beds	N
number of storeys	F

His conclusions were reported by Martin et.al. (1972) in which the following relationships were suggested:

- (i) N increases as F increases when A and γ are constant.
- (ii) A decreases as F increases when N and γ are constant.
- (iii) γ decreases as F increases when A and N are constant.

Although these relationships considered descriptions of form, they are neither conclusive nor do they recommend the limit of each variable. Moreover, the relations are not presented in a manner which quantifies the extent to which these variables are inter-dependent.

4.2.3 In his study, Stevens (1960) was concerned with the aspect of population density in residential areas. Although some of the parameters he considered affect the group form (e.g. number of storeys and plot coverage), the way in which the charts and tables supplied are presented does not convey how different geometrical forms are utilised for the same population density. Furthermore the range of these parameters is limited, i.e. the numbers of storeys considered were 1, 2, 4, 8 and 12.

4.2.4 The analytical approach taken by Segal (1965) considered the following variables:

1. Floor space rate (unit area/person)
2. Floor space/dwelling (dwelling area)
3. Angle of obstruction
4. Open space area/dwelling
5. Storey height
6. Site area
7. Number of storeys
8. Ground coverage (area density)
9. Number of dwellings

He noted that if the first five variables are kept constant then by increasing the number of storeys the resulting changes to the remaining variables were as follows:

- (i) The site area/dwelling decreased,

- (ii) the site coverage/dwelling decreased,
- (iii) the number of dwellings/acre increased.

However, the rate of decrease or increase is negligible as the number of storeys increases reaching an optimum value between 10 - 15 storeys. These results are helpful in determining the geometrical configuration of a group of houses, However, some of the parameters which were maintained as constants, i.e. the angle of obstruction and the open space area/unit floor area, are of considerable influence on the grouping form; thus restricting the scope of Segal's conclusions.

4.2.5 Svennar (1972) discussed the viability of 14 parameters used in studying the density of residential areas, and proposed a standard set of parameters (Table 4.1), differentiating between those related to density and those related to space. Either group of parameters could be expressed in terms of floor area, dwelling units or population.

Table 4.1 Density and space parameters proposed by Svennar (1972)

	Density	Space	
		Indoors	Outdoors
Floor area	Floor Space Index = $\frac{\text{gross floor area}}{\text{gross site area}}$	Open Space Index = $\frac{\text{free site area}}{\text{gross floor area}}$	
Dwelling Units	Housing density = dwelling units/dekare	Unit size = gross floor/unit	Free area/unit
Population	Population density = persons/dekare	Floor space rate = gross floor/person	Free area/unit

In these parameters four independent variables were considered:

λ_p = fraction of site area used for building; %
(plan area density)

F = average number of floors

Z = average dwelling unit size

G = average number of people per unit

For a given building site area, A, the following functions were derived:

$$\text{Floor Space Index (F.S.I)} = \frac{\frac{\lambda_p}{100} \cdot A \cdot F}{A}$$

$$= \frac{\lambda_p \cdot F}{100}$$

$$\text{Open Space Index (O.S.I)} = \frac{A - \frac{\lambda_p \cdot A}{100}}{\frac{\lambda_p}{100} \cdot A \cdot F}$$

$$= \frac{100 - \lambda_p}{\lambda_p \cdot F}$$

$$\text{Housing Density} = \frac{\frac{\lambda_p}{100} \cdot A \cdot F \cdot \frac{1}{Z}}{A}$$

$$= \frac{\lambda_p \cdot F}{100 \cdot Z}$$

$$\text{Free Area per unit} = \frac{A - \frac{\lambda_p \cdot A}{100}}{\frac{\lambda_p}{100} \cdot \frac{A \cdot F}{Z}}$$

$$= \left(\frac{100 - \lambda_p}{\lambda_p \cdot F} \right) \cdot Z/\text{unit}$$

$$\text{Population Density} = \frac{\lambda_p \cdot F \cdot G}{100 \cdot Z}$$

$$\text{Floor Space Rate} = \frac{Z}{G}/\text{person}$$

$$\text{Free Area per Person} = \left(\frac{100 - \lambda_p}{\lambda_p \cdot F} \right) \frac{Z}{G}/\text{person}$$

From a geometrical approach it appears that the expression of both the density and the space parameters are more relevant in terms of floor area. For each function a table was supplied for different values of the four independent variables. These values ranged between:

$$5\% - 40\% \text{ for } \lambda_p$$

$$1 - 12 \text{ for } F$$

$$0.05 - 4.8 \text{ for F.S.I.}$$

$$0.1 - 19 \text{ for O.S.I.}$$

Although the requirement for sunlighting and its dependence on site latitude was noted, the variation of density with the angle of obstruction was not considered. The final part of Svennar's work dealt with an analysis of 19 residential developments of different types from which measurements of density parameters have been taken.

4.2.6 Martin and March (1972) analysed two mathematical models, the first based on Gropius's hypothesis (1956) and the second based on the work of Beckett (1942). In Gropius's model the dependent variables are:

$$N = \text{number of beds}$$

$$A = \text{area of site}$$

$$T = \text{tangent of the angle of sunlight, } \gamma.$$

In each of the following equations one of these variables is the dependent variable while the others are assumed constant. The remaining parameters are (see Figure 4.1(a)):

$$\begin{aligned}
 L &= \text{length of block} \\
 W &= \text{width of block} \quad (\text{assumed to be constant}) \\
 S_x &= \text{width of site} \\
 S_y &= \text{length of site} \\
 (S_x - W) &= \text{space between blocks} \\
 h &= \text{storey height} \quad (\text{assumed to be constant}) \\
 g &= \text{parapet height} \quad (\text{assumed to be constant}) \\
 b &= \text{number of beds per unit floor area (assumed} \\
 &\quad \text{to be constant)}
 \end{aligned}$$

The principal independent variable is:

$$F = \text{number of storeys}$$

The three expressions derived from Gropius's model are

$$\begin{aligned}
 N &= \phi_1 F = bWAT \cdot \frac{F}{hF + WT + g} \\
 A &= \phi_2 F = \frac{N}{bWT} \cdot \frac{hF + WT + g}{F} \\
 T &= \phi_3 F = \frac{N}{W} \cdot \frac{hF + g}{bAF - N}
 \end{aligned}$$

The first derivatives $\frac{d\phi_n}{dF}$ were obtained and are shown graphically in Figure 4.1(b), (c) and (d). It can also be shown that:

$$hN - bWAT = 0 \quad \text{when } F \rightarrow \infty$$

The second derivative of $\phi_1 F$ which shows the rate of increase of N decreased very rapidly (i.e. $\frac{d^2 N}{dF^2} \propto \frac{1}{F^3}$)

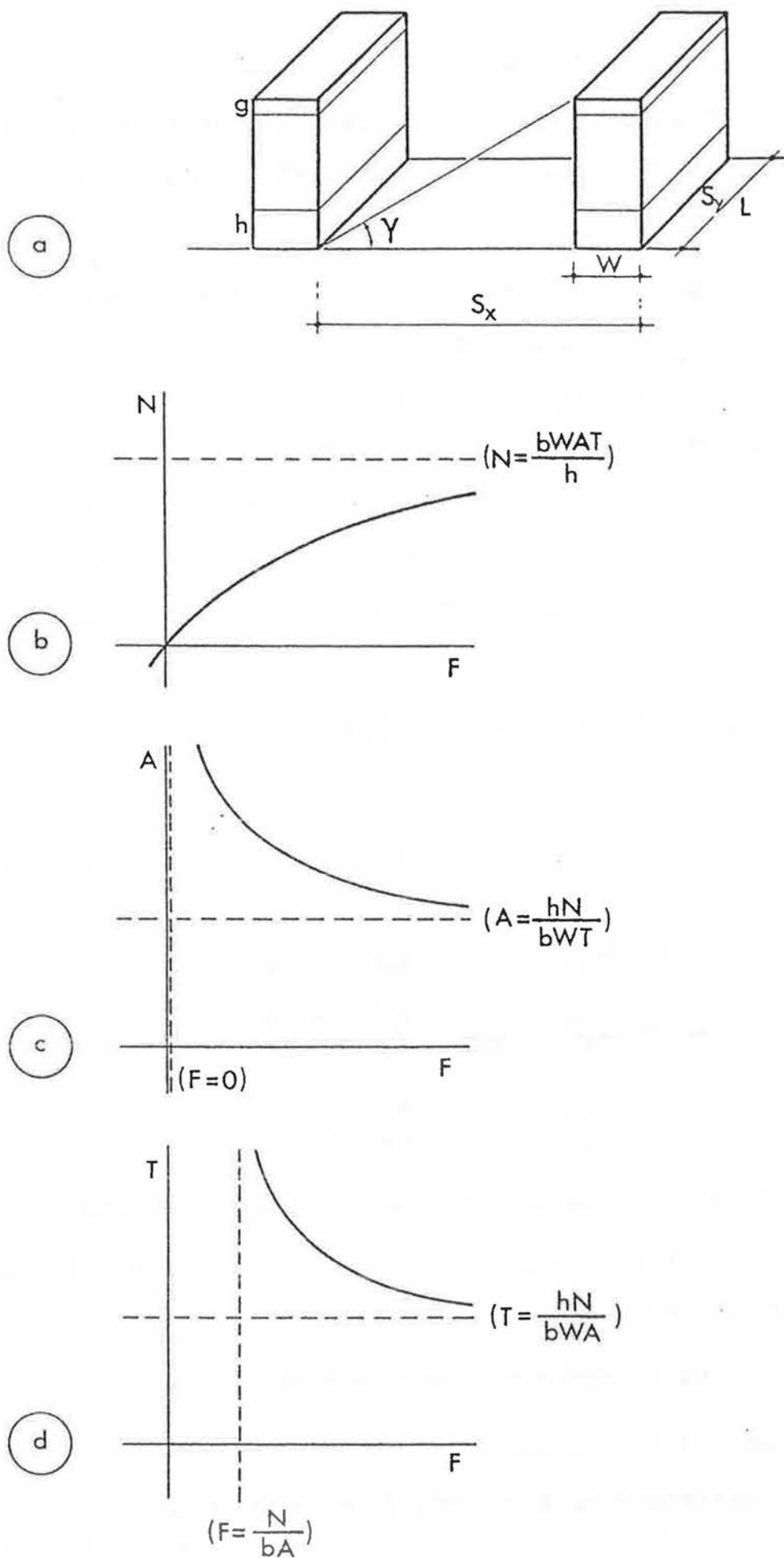


Figure 4.1 GRAPHICAL PRESENTATION OF GROPIUS'S MODEL, (after Martin and March, 1972).

4.2.7 The mathematical model of Beckett is more elaborate and refine form of Gropius's model, and differs in the following respects:

- (i) The blocks were arranged in parallel rows with intersecting streets.
- (ii) The angle of obstruction is read from a point above the ground on the window sill of the first floor, see Figure 4.2.

The same notation as Gropius's model is used here with the following additions:

i = height at which the angle of obstruction intersects the facade ($0 < i < h$)

$$\psi_y = \frac{L}{S_y}$$

O = area of open space

The principal dependent variables studies by Beckett were:

$G_1 = N/A$ = bed space (population, etc.) density
in relation to site area

$$G_2 = O/A = (1 - \lambda_p)$$

$$G_3 = G_1/G_2 = \frac{1}{\text{Open Space Index}}$$

Figure 4.3 shows the variation of G_1 , G_2 and G_3 with F , for different values of T for $b = 1$, $\psi_y = 0.75$, $i = 0.6 h$, $g = 0.3h$. Here it should be noted that Beckett actually studied G_2/G_1 which is the Open Space Index. For small number of floors G_1 and G_3 change their behaviour for small and large values of T respectively. This contradicts Gropius's model and is mainly due to changing the point at which the angle of obstruction is measured. Martin and March conclude that for practical purposes Gropius's

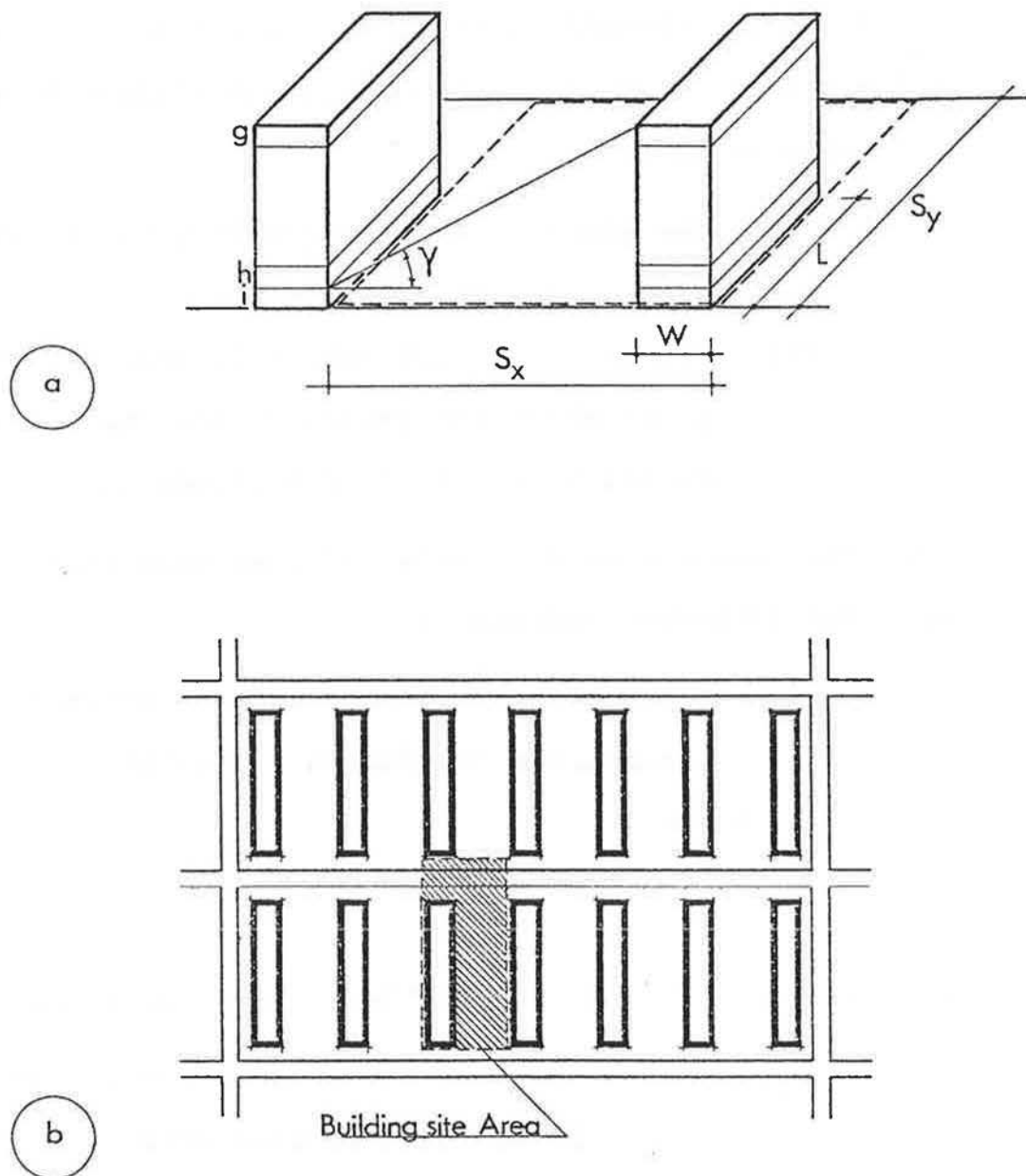


Figure 4.2 BUILDING ARRANGEMENT STUDIED BY BECKETT, (after Martin and March 1972).

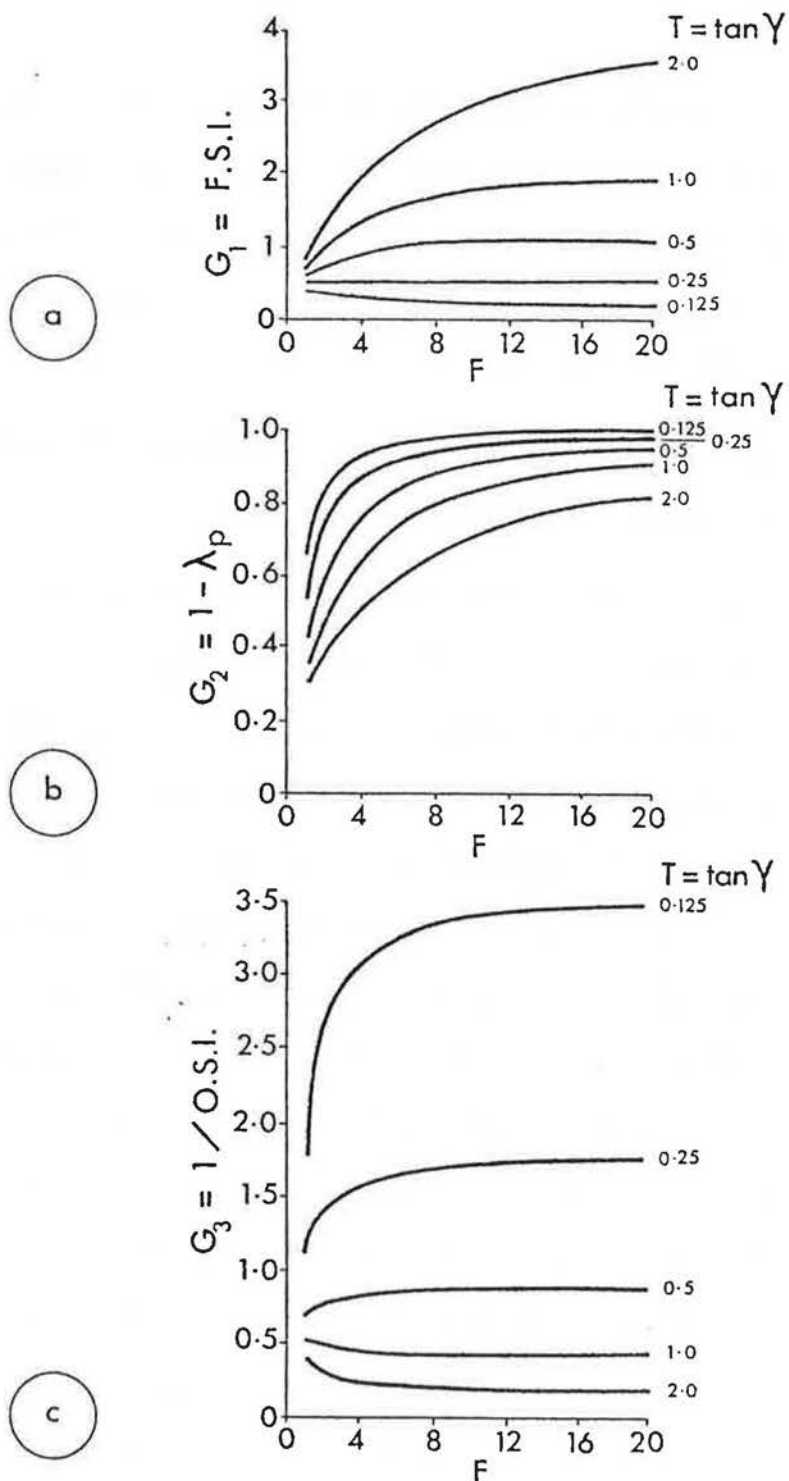


Figure 4.3 GRAPHICAL PRESENTATION OF BECKETT'S MATHEMATICAL MODEL, (after Martin and March, 1972).

model is probably as good as Beckett's and is simpler to use. Recent investigations on daylighting suggests that the choice of reference point makes very little difference to the value of the external daylight factor and thus the angle of obstruction.

4.2.8 This review of the various methods of defining housing densities suggests the following:

- (i) For a given site area, A , and constant storey height, h , the F.S.I. determines the total volume of building(s), see Figure 4.4(a). Further knowledge of the O.S.I. helps in determining number of storeys, F , and the plan Area Density, λ_p , see Figure 4.4(b). Although a complete definition of density and space is achieved in terms of floor area, further information is needed to determine the building group form.
- (ii) The angle of obstruction, γ , (on the assumption of a regular array of uniform buildings on a grid) together with the F.S.I. and the O.S.I. might be sufficient for the assessment of some urban environmental conditions, i.e. daylighting or sunlighting. However, different forms which fulfil these conditions would behave differently in aerodynamic terms, see Figure 4.4(c).
- (iii) Most of the investigations considered the number of storeys as the main independent variable while other parameters relevant to air flow were either not considered in depth (i.e. the plan area density;

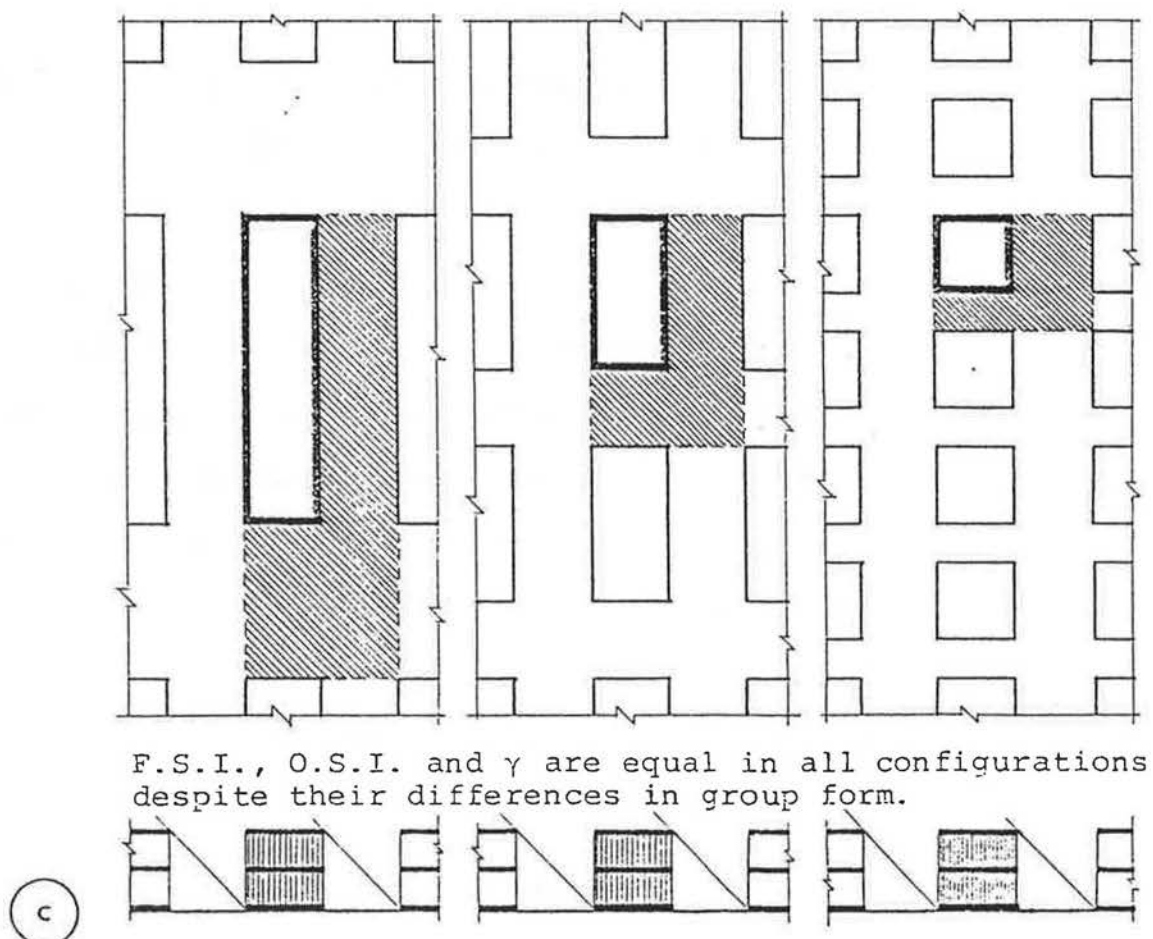
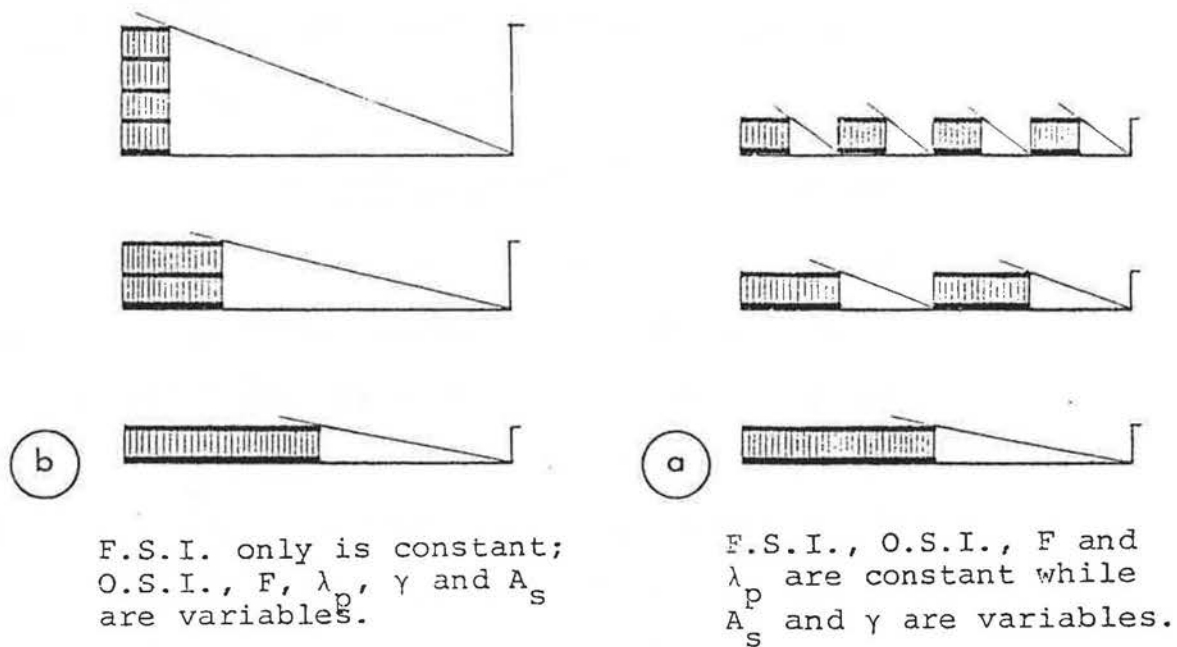


Figure 4.4 EFFECT OF INCOMPLETE DEFINITION OF FORM DETERMINING PARAMETERS.

$\frac{\text{Building plan area}}{\text{Building site area}}$) or not considered at all.

(i.e. the Frontal Area Density, $\frac{\text{Building facade area}}{\text{Building site area}}$,
Side Aspect Ratio, $\frac{\text{Building thickness}}{\text{Building height}}$, and Frontal
Aspect Ratio, $\frac{\text{Building length}}{\text{Building height}}$).

- (iv) As the parameters are interdependent a representation more suitable than tables (Svennar), and more compact than several graphs (Martin and March), on which the range and limits of all the relevant variables could be seen, is desirable. Furthermore it is apparent that density limits depend on the criterion considered. This criteria in turn selects or may sometimes introduce its own governing parameters. For example the form determining parameters for daylighting would not consider orientation while for sunlighting, orientation and latitude would be important. Considering boundary layer flow over urban areas, the group form determining parameters may be selected so as to be more oriented towards flow criteria. No such attempt has been previously undertaken.

4.3 The geometrical parameters defining group density and form

4.3.1 An attempt is made here to analyse the density of urban building form which overcomes some of the criticisms of previous work reported in the preceding section. With

particular reference to air flow over building groups, it is expected that a complete definition of group form would include the geometrical parameters of the individual buildings as well as those of the group. For rectangular building forms, uniformly distributed on a grid pattern, see Figure 4.5, the following parameters are chosen.

(i) Individual form parameters

h = storey height

F = number of storeys

H = building height (= $F.h$)

L = building length (across flow direction)

W = building thickness (along flow direction)

a_p = building plan area (= $L.W$)

a_f = building facade area (= $L.H$)

A_f = frontal aspect ratio = $\frac{L}{H}$

A_s = side aspect ratio = $\frac{W}{H}$

W_r = floor width ratio = $\frac{W}{h}$

(ii) Group form parameters

S_x = building site length (in the flow direction)

S_y = building site width (across flow direction)

A = building site area (= $S_x.S_y$)

γ_x = angle of obstruction (in the flow direction)

γ_y = angle of obstruction (across flow direction)

$\tan \gamma_x = \frac{\text{building height}}{\text{longitudinal space between buildings}}$

$$= \frac{H}{S_x - W}$$

$\tan \gamma_y = \frac{\text{building height}}{\text{lateral space between buildings}}$

$$= \frac{H}{S_y - L}$$

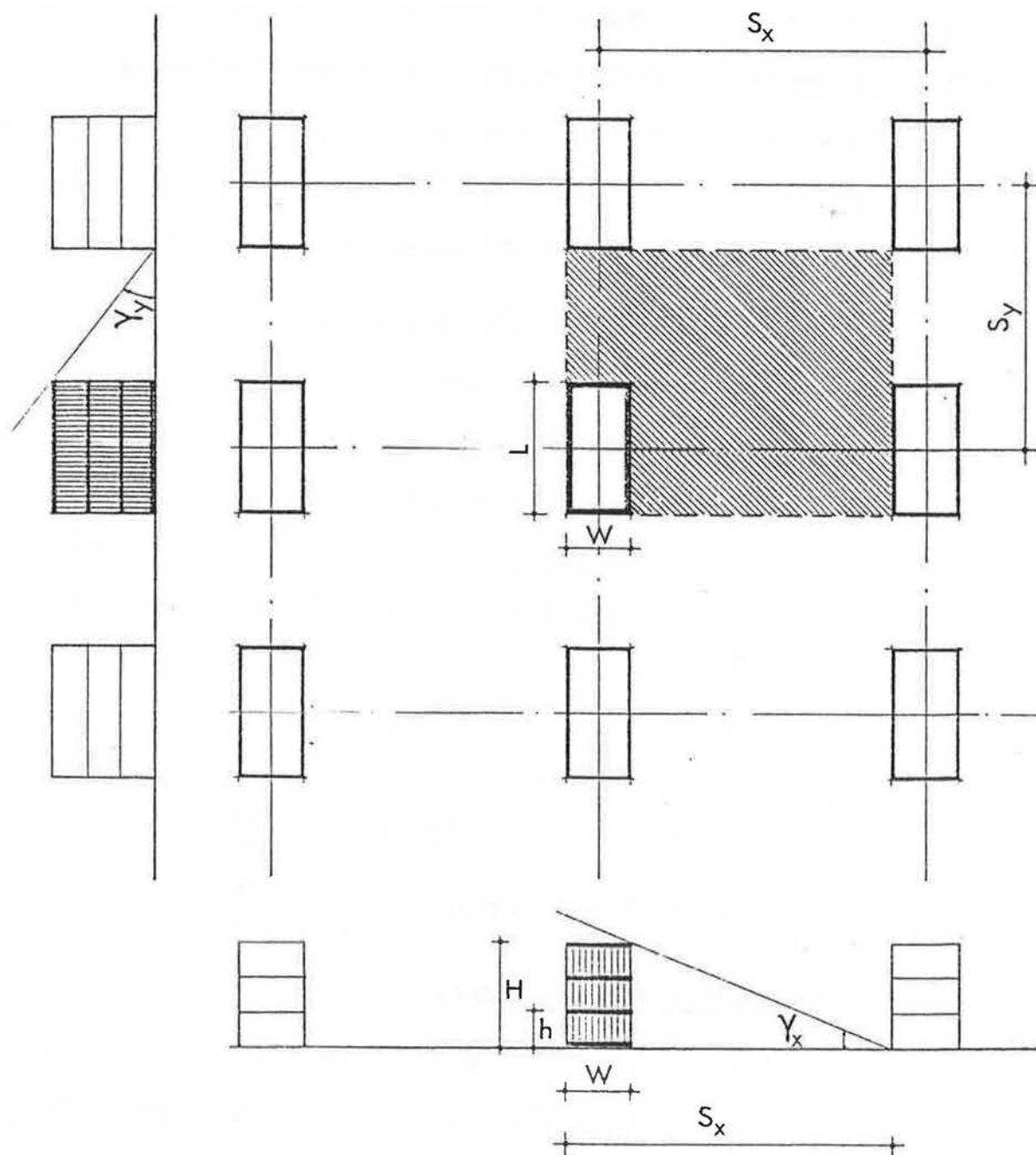


Figure 4.5 GENERAL GROUPING FORM AND ITS GEOMETRICAL PARAMETERS.

$$\psi_x = \frac{\text{building thickness}}{\text{building site length}} = \frac{W}{S_x}$$

$$\psi_y = \frac{\text{building length}}{\text{building site width}} = \frac{L}{S_y}$$

$$\lambda_p = \text{plan area density} = \frac{\text{building plan area}}{\text{building site area}} = \frac{a_p}{A}$$

$$\lambda_f = \text{frontal area density} = \frac{\text{building facade area}}{\text{building site area}} = \frac{a_f}{A}$$

$$\therefore \lambda_p = \lambda_f \cdot A_s$$

4.3.2 It is shown in paragraph 4.2.8(i) how the planning parameters (F, F.S.I and O.S.I) are not sufficient to define a particular group form. However, they may be expressed in terms of the geometrical parameters as follows:-

$$\text{F.S.I} = \text{Floor Space Index} = \frac{\text{total floor area}}{\text{building site area}} = \frac{a_p F}{A}$$

$$\text{O.S.I.} = \text{Open Space Index} = \frac{\text{open space area}}{\text{total floor area}} = \frac{A - a_p}{a_p F}$$

Similarly, these planning parameters are related to the plan area density as follows:

$$\text{F.S.I} = F \cdot \lambda_p \quad \dots\dots (4.1)$$

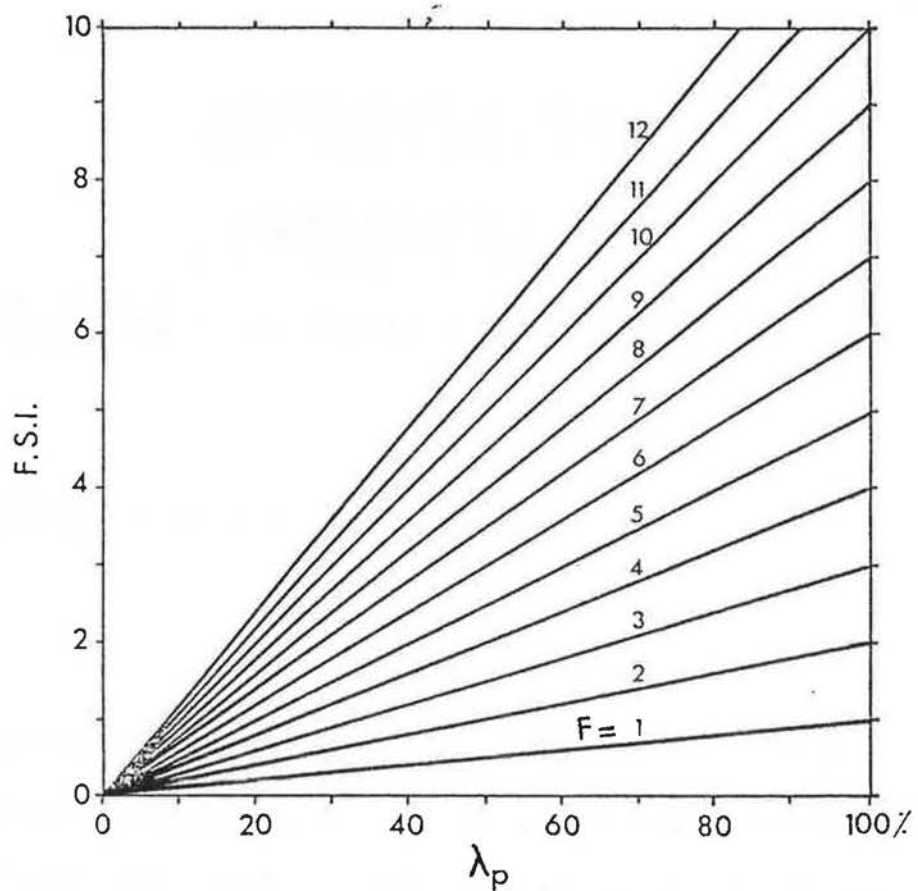
$$\text{and } \text{O.S.I} = \frac{1}{\text{F.S.I}} (1 - \lambda_p)$$

This may be re-arranged into:

$$\text{F.S.I} = \frac{1}{\text{O.S.I}} (1 - \lambda_p) \quad \dots\dots (4.2)$$

A graphical presentation of equation (4.1), Figure 4.6(a), gives a family of straight lines, the slope of each line would correspond to the number of storeys. In the same way, a graphical presentation of equation (4.2), Figure 4.6(b), gives a family of straight lines, the slope of each line would correspond to the reciprocal of O.S.I.

(a)



(b)

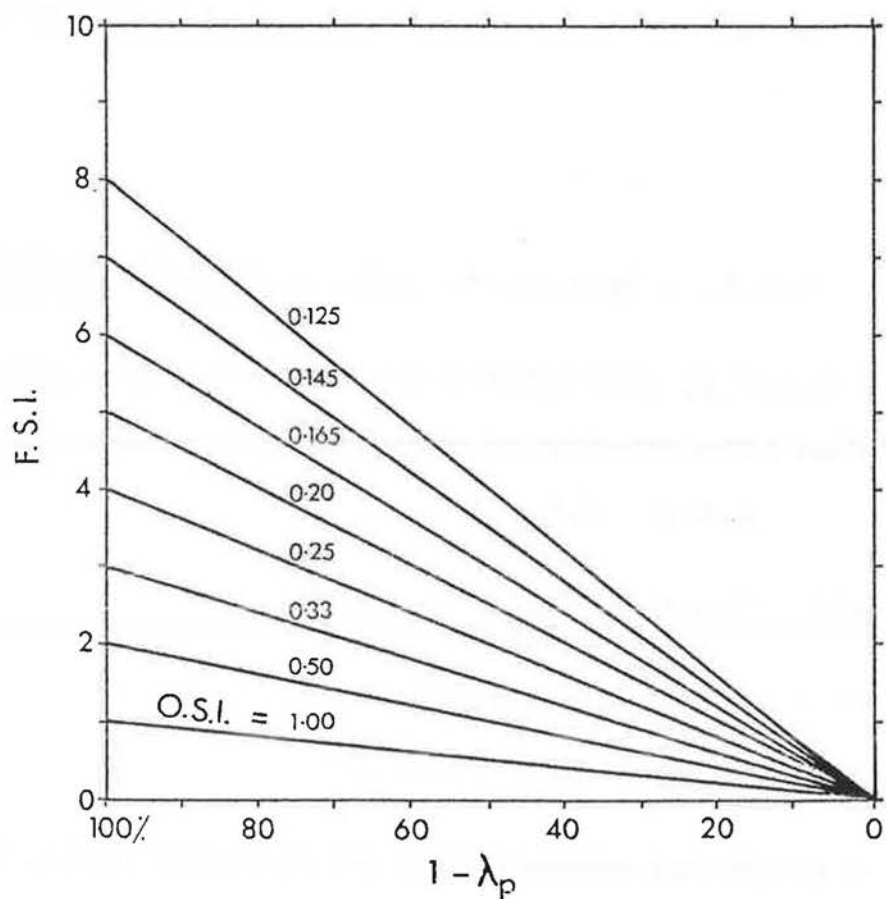


Figure 4.6 (a) VARIATION OF F.S.I. WITH λ_p FOR DIFFERENT NO. OF STOREYS.
(b) VARIATION OF F.S.I. WITH OPEN SPACE BETWEEN BUILDINGS FOR DIFFERENT VALUES OF O.S.I.

A combined graphical presentation of equations (4.1) and (4.2) is shown in Figure 4.7. For convenience and ease of reading, particularly at low values of λ_p , Figure 4.7 is redrawn in log-log form as shown in Figure 4.8.

4.3.3 From the geometry of the group it can be seen that, for the longitudinal direction

$$\begin{aligned} \cotan \gamma_x &= \frac{S_x - W}{H} \\ \text{but since } \lambda_p &= \frac{W L}{S_x \cdot S_y} \\ \therefore \cotan \gamma_x &= \left\{ \frac{W}{\lambda_p} \left(\frac{L}{S_y} \right) - W \right\} / H \\ &= \left(\frac{A_s}{\lambda_p} \right) \psi_y - A_s \\ \therefore \lambda_p &= \frac{A_s \cdot \psi_y}{\cotan \gamma_x + A_s} \end{aligned} \quad \dots\dots (4.3)$$

Considering the lateral direction and following the same procedure gives:

$$\lambda_p = \frac{A_f \cdot \psi_x}{\cotan \gamma_y + A_f} \quad \dots\dots (4.4)$$

Adding (4.3) and (4.4) yields the general form:

$$\lambda_p = \frac{1}{2} \left\{ \frac{A_s \cdot \psi_y}{\cotan \gamma_x + A_s} + \frac{A_f \cdot \psi_x}{\cotan \gamma_y + A_f} \right\} \quad \dots\dots (4.5)$$

It was also previously shown how the plan area density is related to the frontal area density, i.e.

$$\lambda_p = \lambda_f \cdot A_s \quad \dots\dots (4.6)$$

Equation (4.6) will be used later on in Chapter 5.

It can be seen that equation (4.5) is the general form in which the plan area density is presented in terms of all the geometrical parameters needed to completely define

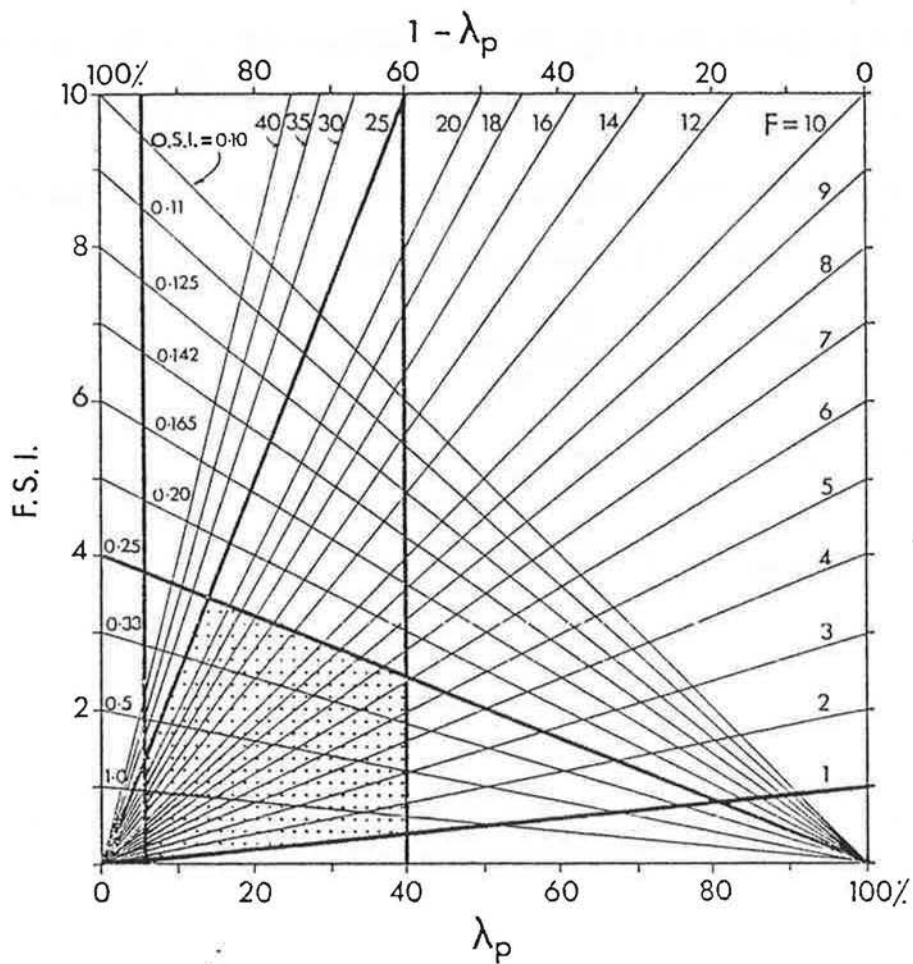


Figure 4.7 GRAPHICAL PRESENTATION OF THE RELATIONSHIPS BETWEEN THE PLANNING PARAMETERS. (Heavy lines indicate the suggested limits).

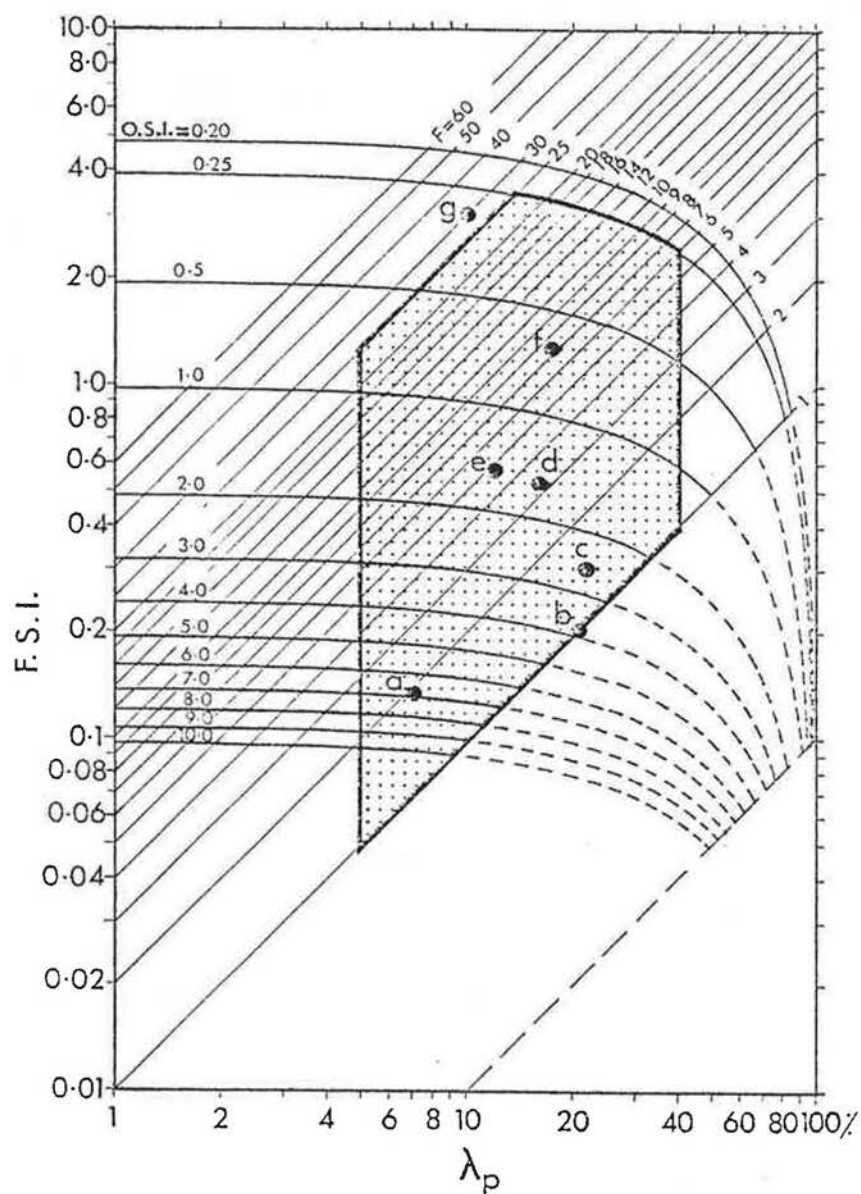


Figure 4.8 TRANSFORMATION OF FIGURE 4.7 INTO LOG-LOG FORM (Examples a - g given by Svennar are also plotted).

both the individual and the group geometry.

4.3.4 It can also be seen that the geometry of surface roughness investigated in the literature of flow over rough surfaces are only special cases of equation (4.5). For example, in the case of two dimensional roughness elements, i.e. when the building covers the site length, $\psi_y = 1$, and $\gamma_y = 0$. Then equation (4.5) will take the form:

$$\lambda_p = \frac{1}{2} \left\{ \frac{A_s}{\cotan \gamma_x + A_s} + \psi_y \right\}$$

$$\text{i.e. } \lambda_p = \frac{A_s}{\cotan \gamma_x + A_s} \quad \dots\dots (4.7)$$

When the building or roughness element is square in plan, and $S_x = S_y$ it follows that, the variables in the x direction will be identical to the variables in the y direction, i.e. $A_s = A_f$, $\psi_x = \psi_y$ and $\gamma_x = \gamma_y$. It also follows that $\lambda_p = \psi_{x,y}^2$. Therefore equation (3.5) will take the form:

$$\lambda_p = \frac{A_s \sqrt{\lambda_p}}{\cotan \gamma_x + A_s}$$

$$\text{i.e. } \sqrt{\lambda_p} = \frac{A_s}{\cotan \gamma_x + A_s} \quad \dots\dots (4.8)$$

Figures 4.9 and 4.10 show $\cotan \gamma_x$ plotted against λ_p and give families of curves for values of A_s in equations (4.7) and (4.8) respectively together with families of curves representing the variations in λ_f .

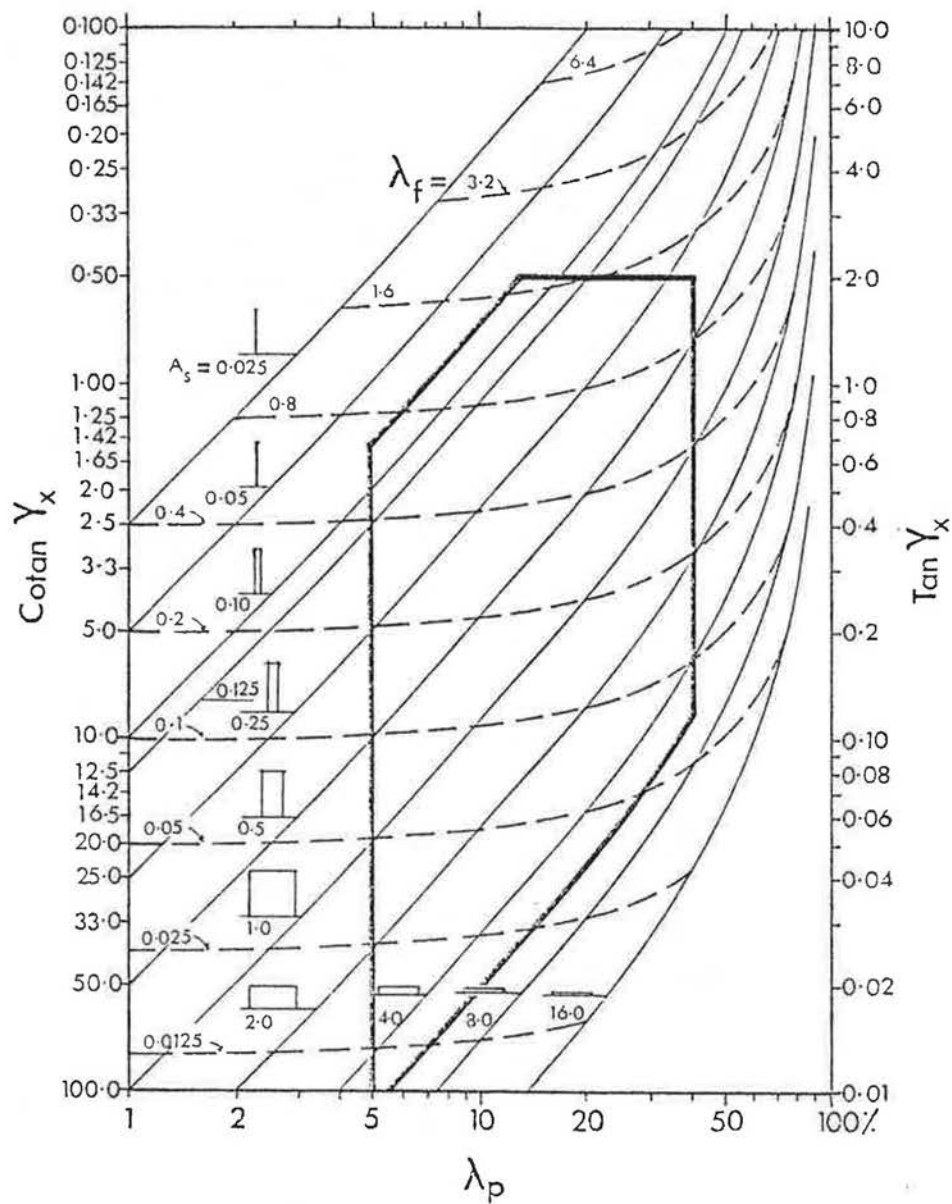


Figure 4.9 VARIATION OF λ_p , λ_f AND A_s WITH $\text{TAN } \gamma_x$ FOR TWO-DIMENSIONAL BUILDING FORMS.

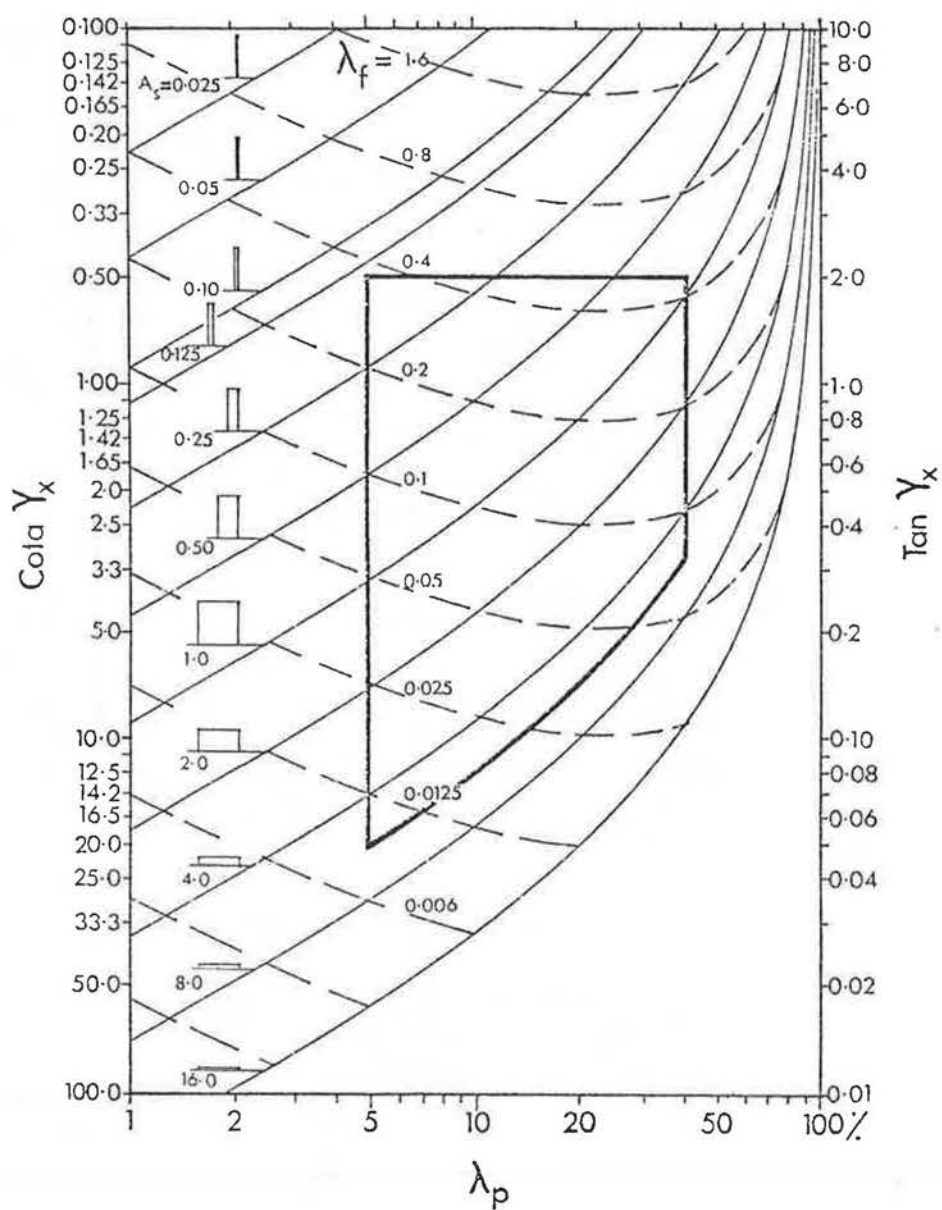


Figure 4.10 VARIATION OF λ_p , λ_f AND A_s WITH $\tan \gamma_x$ FOR SQUARE PLAN BUILDING FORMS.

4.3.5 In order to give some meaning to the interpretation of the chart given in Figure 4.8, examples from the housing schemes reported by Svennar (1969) are shown in Figure 4.11 (a) to (g). The values of F.S.I., O.S.I. and λ_p given with each scheme enabled plotting corresponding points on the chart of Figure 4.8. It may be noted that the resulting number of floors, F, on the chart is an average value for the whole site. Therefore, an integer value of F will only appear where uniform buildings were used throughout the site.

4.4. Limits of the Parameters

4.4.1 The purpose of this chapter has been to achieve the following objectives:

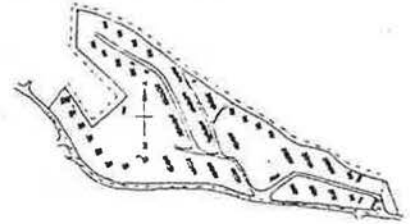
- (i) to investigate the parameters governing the geometrical configuration of housing groups
- (ii) to define the range and limits of these parameters.

The first of these objectives has been fulfilled by equations (4.1), (4.2) and (4.5). So far as the second objective is concerned the survey and statistical analysis of 110 housing schemes made by the Department of the Environment (Turner, 1973), together with the examples quoted by Svennar (1972) give some of the required information.

Figure 4.1 shows the F.S.I. plotted against λ_p for all the 110 schemes. It is clear that the majority of the schemes, 108 out of 110, lie on the scale of λ_p between 5% and 40% while the average is in the region 10 - 20% λ_p . Although the maximum value of F (number of storeys) was 30, it would

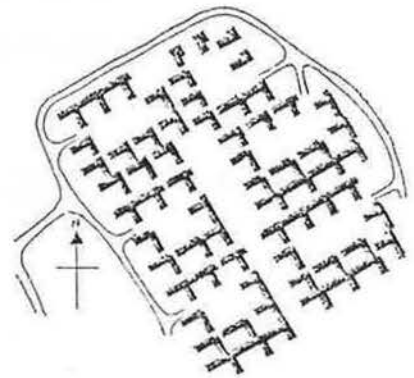
- (a) Husebygrenda Borettslag,
Makrellbekken Bjarne Lous
Mohr and Helge Hoel

Scale 1:7500
F.S.I. 0.13
O.S.I. 7.00
 λ_p 7.10 %



- (b) Solvangen Skedsmo Mari
and Gullik Kollandstrud

Scale 1:3000
F.S.I. 0.20
O.S.I. 3.90
 λ_p 20.90 %



- (c) Albertslund Syd,
Herstedene, Copenhagen
Kund Svensson,
Viggo Moller-Jensen,
Ole Norgard and others

Scale 1:14,000
F.S.I. 0.30
O.S.I. 2.50
 λ_p 22.00 %

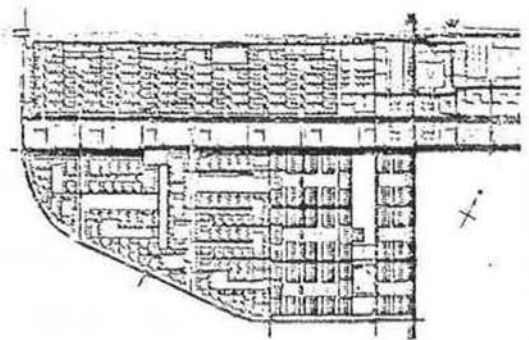


Figure 4.11 EXAMPLES OF HOUSING SCHEMES FOR
VARIOUS VALUES OF F.S.I., O.S.I.,
AND λ_p (after Svennar, 1972).

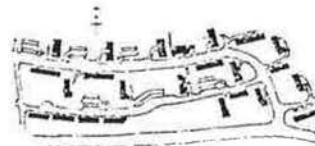
- (d) Blafjellet Borettslag, Lambertseter
Knut Knutsen

Scale 1:7500
F.S.I. 0.51
O.S.I. 1.70
 λ_p 15.30 %



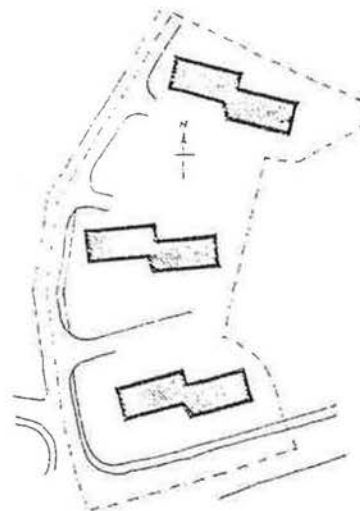
- (e) Lillo Terrasse, Grefsen
Alex Christiansen and Nils Rosland

Scale 1:7500
F.S.I. 0.58
O.S.I. 1.50
 λ_p 12.20 %



- (f) Frognerstranda, Skoyen
Jan Lie-Nielsen

Scale 1:3000
F.S.I. 1.33
O.S.I. 0.60
 λ_p 17.40 %



- (g) High Blocks in Manhattan
I. M. Pei and Partners

Scale 1:3000
F.S.I. 3.14
O.S.I. 0.30
 λ_p 10.50 %

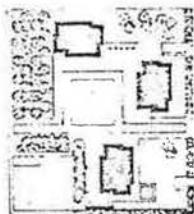


Figure 4.11 EXAMPLES OF HOUSING SCHEMES
FOR VARIOUS VALUES OF F.S.I.,
O.S.I., and λ_p (after Svennar,
1972).

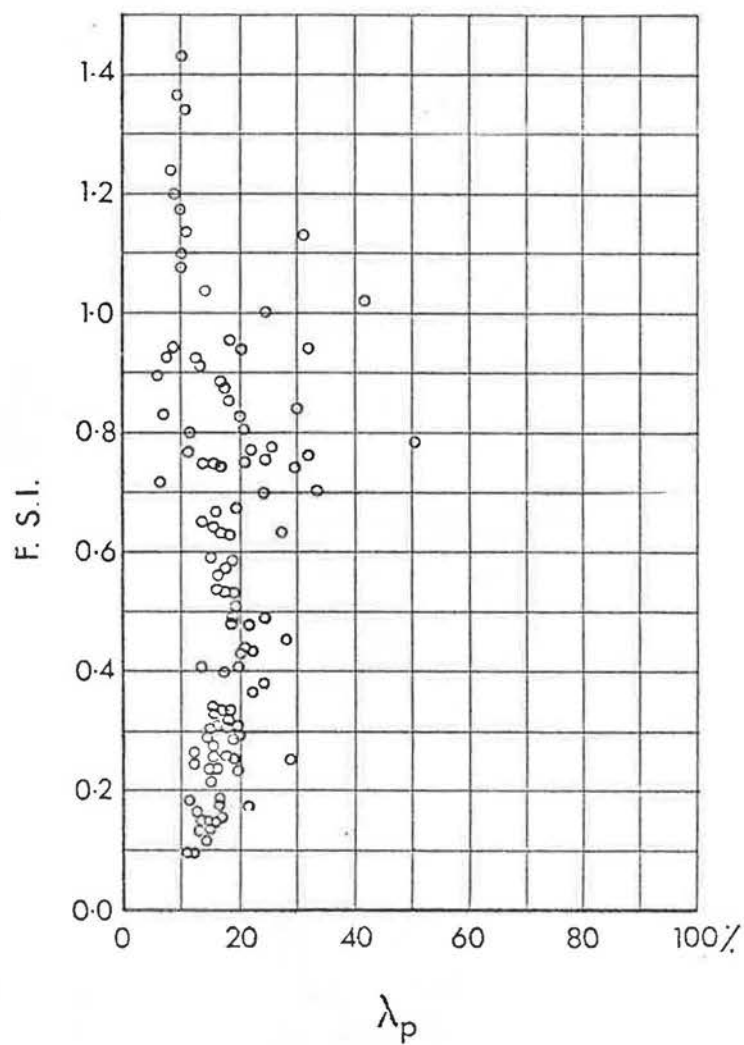


Figure 4.12 DISTRIBUTION OF λ_p FOR 110 HOUSING SCHEMES (after Turner, 1973).

be reasonable to assume that 90% of the housing blocks are less than 25 floors. In addition, from the examples given in Svennar's report (1972) it is seen that the open space index is not likely to be less than 0.25. These limits have been shown in Figure 4.7 as heavy lines indicating the limited area in which most of the schemes are built. The side aspect ratio, $\frac{W}{H}$ is limited by the floor width ratio, $\frac{W}{h}$. If we assume a constant storey height, h , the range of $\frac{W}{h}$ is likely to be from 2 to 6. This is equal to 6 to 18 metres for a 3 metre storey height. Accordingly, as the range of F is from 1 - 25 storeys, the range of A_s , ($= \frac{W}{F \cdot h}$), lies between 0.08 and 6. The upper limit of $\cotan \gamma_x$ may well be more than 10 for very low densities but it is hardly acceptable at less than 0.5 for any density. These limits have been shown in Figures 4.9 and 4.10 as heavy lines indicating the limited area in which building group forms in urban areas may occur.

4.5 Conclusions

4.5.1 For a matrix of similar buildings, the planning parameters, i.e. Floor Space Index, Open Space Index and consequently number of storeys together with the plan area density are not sufficient to give a particular form.

4.5.2 Specifying the angle of obstruction normal to the building facade may help to quantify environmental conditions such as daylighting or sunlighting, but does not give complete definition of form, an essential requirement for air flow.

4.5.3 In order to achieve complete definition of group geometry, the frontal and side aspect ratios together with the ratio of building length to site length in both directions are required as well as the cotan of the angle of obstruction in both directions. Equations are given for the general relation between these parameters in terms of the plan area density or the frontal area density.

4.5.4 Different grouping forms of buildings have been presented graphically. In those cases in which flow investigations have been undertaken, it would be possible to plot the limits of the different known flow regimes on the graph. This would enable the planner or the architect, when sufficient data are collected, to recognize the different flow conditions, hence to properly choose the grouping form.

4.5.5 Although group geometry could be completely specified, different scales can be given to the same geometry. The required scale can be obtained by linking the geometrical parameters to the planning parameters through the plan area density. For this reason the plan area density was deliberately chosen as an abscissa for the planning parameters presented in Figure (4.8), similar to the abscissa for the geometrical parameters presented in Figures 4.9 and 4.10.

CHAPTER 5

FLOW OVER ROUGH SURFACES.

5. FLOW OVER ROUGH SURFACES

5.1 Introduction

5.1.1 In previous chapters the practical problem has been explained. This can be stated briefly as the definition of the forces on arrays of similar buildings caused by the wind flow. Leaving aside the practical details for a moment, this problem can be re-stated as the definition of the forces on the roughness elements of a surface over which a turbulent boundary layer flow occurs. The application of the boundary layer theory to the flow over the earth's surface has been shown to be valid in the study of micro-meteorology and to be helpful in providing a flow model for wind tunnel simulation of the natural wind. Thus the solution to the practical problem may be considerably eased if some consideration is given to the way in which the idealized problem has been tackled in the past.

5.1.2 In this brief consideration of the general properties of flow over idealized smooth and rough surfaces, the case of flow over large roughness elements will be reviewed and in particular the effect of roughness geometry on the properties of flow. The investigation will extend to consider possible relationships between the roughness geometry, the resulting flow and the external pressure forces. It should be noted that these idealized considerations are normally limited to an infinitely extending uniformly roughened surface. Such situations rarely exist

in nature, particularly for large roughness elements. Therefore, the effect of a step change in surface roughness will also be considered.

5.2 Flow over smooth surfaces

5.2.1 The general structure of turbulent boundary layer flow over smooth surfaces may be divided into two main layers.

- (i) an inner layer, usually called the wall layer, in which the velocity is a function of a Reynolds number based on the friction velocity and the distance from the wall, i.e.

$$\frac{u}{u_*} = F_1 \left(\frac{yu_*}{\nu} \right)$$

and (ii) an outer layer in which the velocity defect law applies, i.e.

$$\frac{u-U_1}{u_*} = F_2 (y/\delta)$$

The entire velocity profile (Figure 5.1) may then be expressed as:

$$\frac{u}{u_*} = F_1 \left(\frac{yu_*}{\nu} \right) + F_2 (y/\delta)$$

A zone of overlap exists in which both F_1 and F_2 are valid, consequently the logarithmic velocity distribution is obtained, Clauser (1956). While the flow in the outer layer is insensitive to the conditions at the surface and is mainly affected by pressure gradients, the reverse applies to the inner layer in which the flow is entirely dependent on the turbulent friction generated at the wall. Therefore, the inner layer is the more relevant part of the

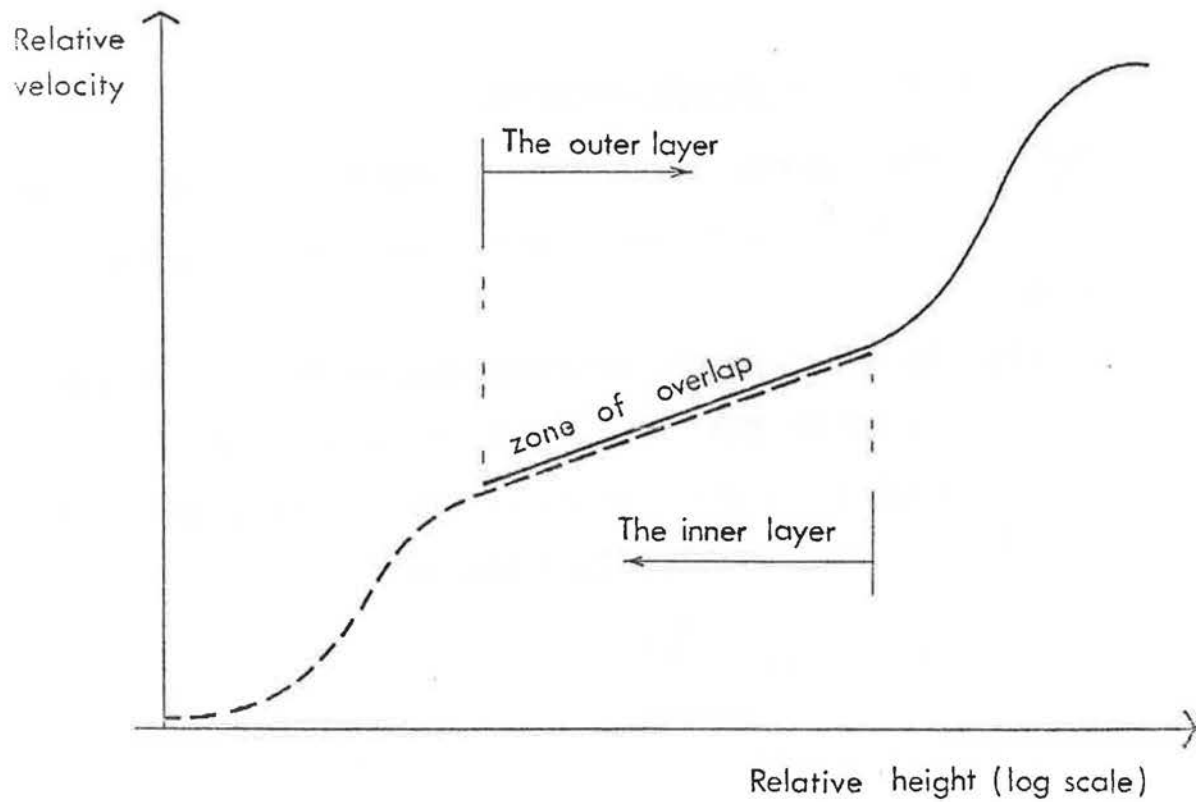


Figure 5.1 THE GENERAL STRUCTURE OF TURBULENT BOUNDARY LAYER FLOWS.

turbulent boundary layer in the present study and will be more closely examined.

5.2.2 In the inner layer, three regions of flow may be identified. Very close to the wall, a very thin laminar sublayer exists in which the velocity is linearly related to the distance from the wall, i.e.

$$\frac{u}{u_*} = \frac{yu_*}{\nu} \quad \dots\dots (5.1)$$

The thickness of the laminar sublayer, δ_1 , corresponds to a value of $\frac{yu_*}{\nu} = 5$. At the top end of the inner layer, fully turbulent flow prevails in which the well known logarithmic velocity distribution may be written as:

$$\frac{u}{u_*} = \frac{1}{\kappa} \ln \frac{yu_*}{\nu} + B \quad \dots\dots (5.2)$$

Fully turbulent flow is usually found at values of

$\frac{yu_*}{\nu} > 70$. In between the laminar sublayer and the logarithmic layer, at $5 < \frac{yu_*}{\nu} < 70$, a transition zone is present. For smooth walls, the constant B in equation (5.2) takes a value of approximately 5.1, different values being obtained from different sources, 4.9, Clauser (1956), 5.5, Schlichting (1968). Graphical presentation of equation (5.2) is shown in Figure 5.2.

5.2.3 The extension of the logarithmic line down to the surface gives a finite height, known as the roughness length, z_0 , at which the velocity is theoretically zero, Figure 5.2. Using this roughness length, equation (5.2) may be written in the form:

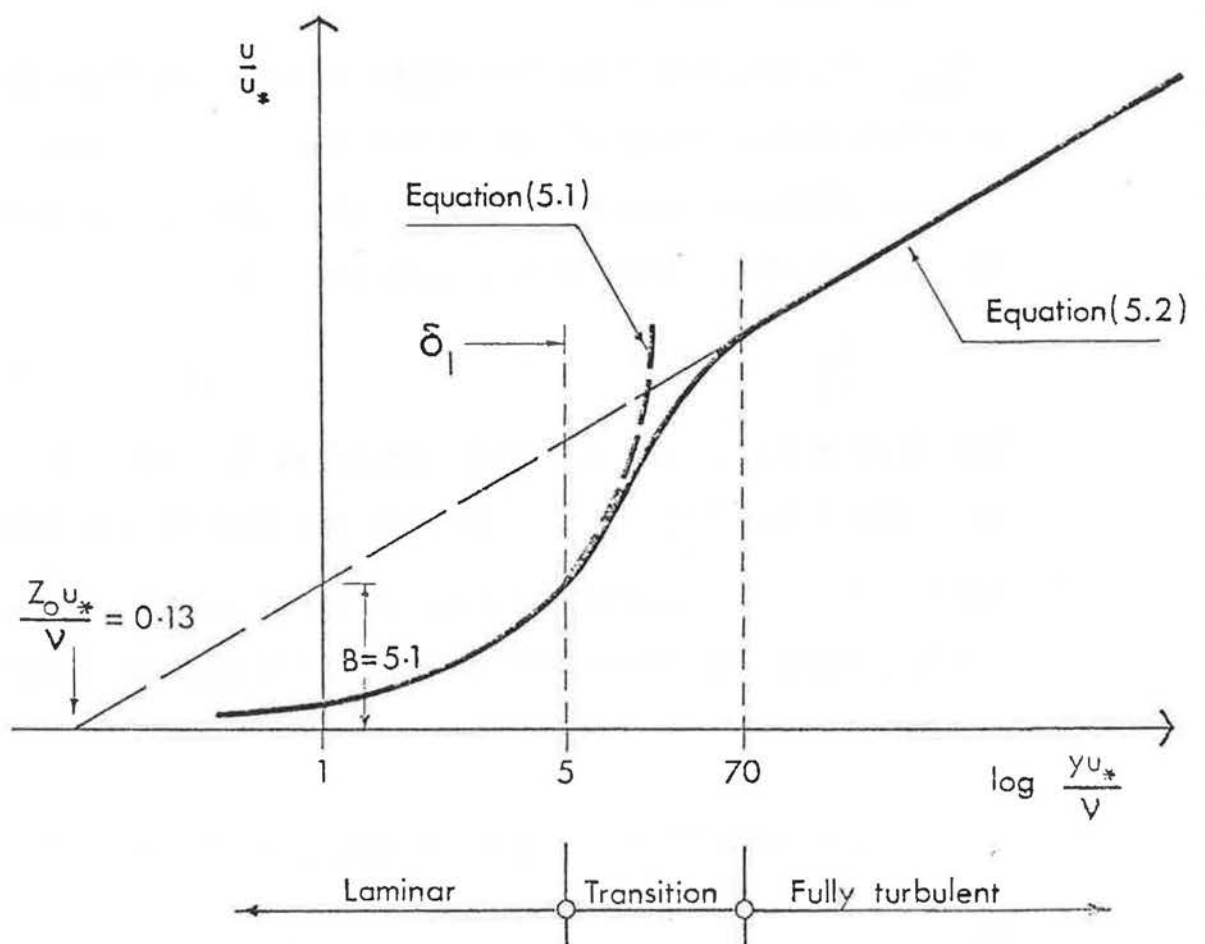


Figure 5.2 DEFINITION OF THE ROUGHNESS LENGTH, z_0 , AND THE THREE REGIONS OF FLOW IN THE INNER LAYER OF SMOOTH WALLS.

$$\frac{u}{u_*} = \frac{1}{\kappa} \ln \frac{yu_*}{\nu} - \frac{1}{\kappa} \ln \frac{z_0 u_*}{\nu}$$

$$\text{where } B = - \frac{1}{\kappa} \ln \frac{z_0 u_*}{\nu}$$

$$\text{thus } \frac{u}{u_*} = \frac{1}{\kappa} \ln \frac{y}{z_0} \quad \dots\dots (5.3)$$

$$\text{where } z_0 = \frac{\nu}{u_*} \exp. (-\kappa B) \quad \dots\dots (5.4)$$

The universal constants κ and B are commonly given the values of 0.4 and 5.1 respectively. Hence

$$\frac{z_0 u_*}{\nu} = 0.13 \quad \dots\dots (5.5)$$

Equation (5.5) implies that z_0 is not constant for smooth surfaces and that its value is determined by the friction velocity, u_* .

5.3 Flow over rough surfaces

5.3.1 From the fundamental work of Nikuradse on the effect of sand grain roughness on pipe flow three flow conditions were established. These are as follows:

- (i) The completely smooth flow where the roughness size is small and contained within the laminar sublayer.
- (ii) The completely rough flow where the roughness extend completely outside the laminar sublayer.
- (iii) The intermediate roughness or transitional flow where the roughness extend partially outside the laminar sublayer.

Nikuradse used sand grains as his roughness elements glued to the surface in the maximum possible concentration.

His results for the three flow conditions may be expressed in terms of a Reynolds number based on the sand grain roughness height, K_s , as follows:

$$\begin{array}{ll} \frac{K_s u_*}{\nu} < 5 & \text{Completely smooth flow} \\ 5 < \frac{K_s u_*}{\nu} < 70 & \text{transitional flow} \\ \frac{K_s u_*}{\nu} > 70 & \text{completely rough flow} \end{array}$$

5.3.2 In the case of turbulent boundary layer flow over rough surfaces the flow structure still retains an inner and outer layer analogous to the smooth surface flow. The logarithmic distribution of velocity in the zone of overlap between the inner and outer layers imply that a similar logarithmic distribution should also exist in the inner layer, Clauser (1956). Since the addition of roughness always increases turbulent skin friction, and hence u_* , the logarithmic line of the inner layer represented by equation (5.2) must shift to the right and downward because of the way u_* occurs in both the abscissa and ordinate. Hence, for rough wall flows, equation (5.2) takes the form:

$$\frac{u}{u_*} = \frac{1}{\kappa} \ln \frac{yu_*}{\nu} + B - \frac{\Delta u}{u_*} \quad \dots\dots (5.6)$$

where $\frac{\Delta u}{u_*}$ represents the vertical shift of the logarithmic line caused by roughness and is known as the roughness function, (see Figure 5.3). It has been found that for flow

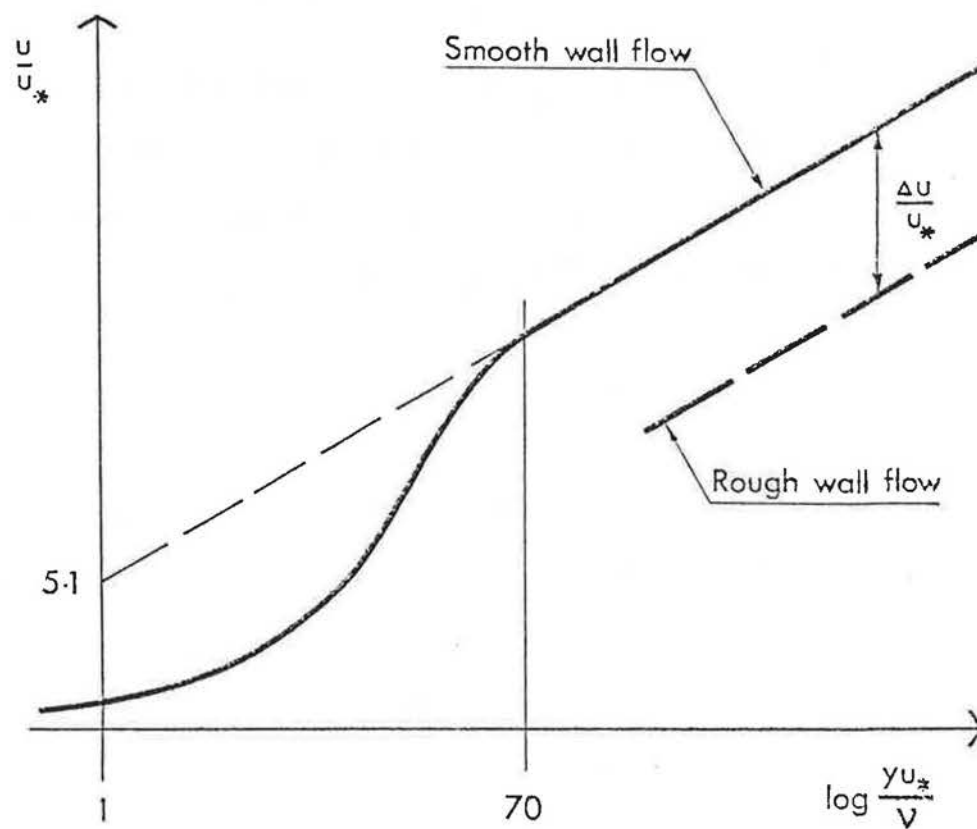


Figure 5.3 DEFINITION OF THE ROUGHNESS FUNCTION.

over rough surfaces $\frac{\Delta u}{u_*}$ depends on the size, shape and distribution of the roughness elements. Following from this the dependence of $\frac{\Delta u}{u_*}$ on the roughness Reynolds number $\frac{Hu_*}{\nu}$ has been established, where H is the roughness element height. This analysis made by Clauser (1956) and Hama (1954), showed that in the fully rough flow, the dependence of $\frac{\Delta u}{u_*}$ on $\frac{Hu_*}{\nu}$ can be expressed as:

$$\frac{\Delta u}{u_*} = \frac{1}{\kappa} \ln \frac{Hu_*}{\nu} + C \quad \dots\dots (5.7)$$

In the intermediate roughness flow, $\frac{\Delta u}{u_*}$ behaves differently in that smaller values are obtained than are indicated by equation (5.7) until it reaches zero, a condition of the smooth flow as shown in Figure 5.4. Due to variations in roughness element form, size and pattern of distribution, different lines can be obtained for equation (5.7) corresponding to different values of C. This point will be considered in detail in section 5.4. In the analysis reported by Clauser (1956), it was pointed out that if a suitable roughness dimension replaced the roughness height H, the different lines obtained for equation (5.7) would collapse on a single line with a universal constant. In the next paragraph it will be shown that such a collapse could be obtained if the equivalent sand grain roughness K_s is used in place of the roughness height H.

5.3.3 In the fully rough flow, Schlichting (1968) shows that:

$$\frac{u}{u_*} = \frac{1}{\kappa} \ln \frac{Y}{K_s} + E \quad \dots\dots (5.8)$$

where E is a universal constant = 8.5.

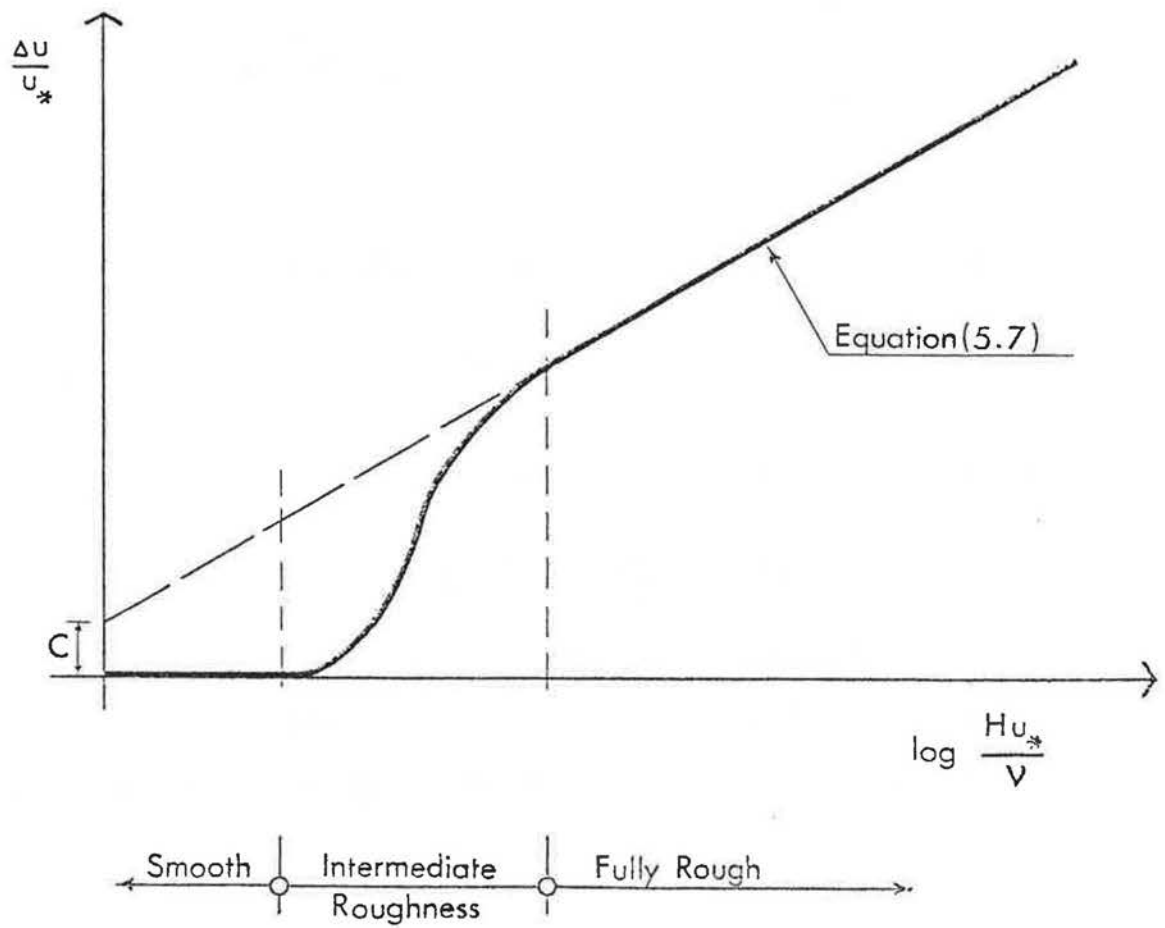


Figure 5.4 VARIATION OF $\Delta u/u_*$ WITH Hu_*/ν IN THE THREE FLOW CONDITIONS.

Equation (5.8) may be re-written as:

$$\frac{u}{u_*} = \frac{1}{\kappa} \ln \frac{yu_*}{v} - \frac{1}{\kappa} \ln \frac{k_s u_*}{v} + 8.5$$

i.e.
$$\frac{u}{u_*} = \frac{1}{\kappa} \ln \frac{yu_*}{v} + B - \left\{ \frac{1}{\kappa} \ln \frac{k_s u_*}{v} - 3.4 \right\} \dots\dots (5.9)$$

where $B = 5.1$

Comparing equations (5.6) and (5.9) gives

$$\frac{\Delta u}{u_*} = \frac{1}{\kappa} \ln \frac{k_s u_*}{v} - 3.4 \dots\dots (5.10)$$

This may also be written as:

$$\frac{\Delta u}{u_*} = \frac{1}{\kappa} \ln \frac{Hu_*}{v} + \frac{1}{\kappa} \ln \frac{k_s}{H} - 3.4 \dots\dots (5.11)$$

Equation (5.11) will be used later on. Comparing equation (5.8) with equation (5.3), which is still valid for rough surfaces provided y is measured from the correct origin, gives in the fully rough flow:

$$\frac{k_s}{Z_o} = 30 \dots\dots (5.12)$$

Therefore the condition of completely rough flow expressed previously as $\frac{k_s u_*}{v} > 70$ may now be written as $\frac{Z_o u_*}{v} > 2.33$.

An approximately similar value was noted by Jensen and Franck (1965).

5.3.4 Due to the irregularity of rough surfaces, the question will arise as to which origin should be taken for the measurement of y , whether it is more appropriate to choose the crest of roughness or the lowest point on the surface. However, if y is shifted by a constant amount, curvature will appear in the straight line logarithmic part

of the velocity profile. Therefore the experimental points measured from the wall may be shifted upward assuming a zero plane displacement, d , until a straight line is obtained, Clauser, (1956). On the other hand, if y was taken from the crest of the roughness elements, a downward shift will be necessary to bring the origin of y at a distance ϵ below the crests such that (Perry & Jourbert, 1963).

$$H = \epsilon + d \quad \dots\dots (5.13)$$

5.4 Effect of roughness geometry on the velocity profile parameters

5.4.1 A considerable amount of work has been done on the investigation of fully rough flows over rough surfaces consisting of regular arrays of geometrical roughness elements in different regimes. The classification of the flow over roughness elements into three regimes was first introduced by Morris (1955). These flow regimes which are applicable to pipe flow, open channel flow and flat plate boundary layers are denoted as isolated roughness flow, wake interference flow and skimming flow. In the isolated roughness flow, the roughness elements are sufficiently far apart that each element acts in isolation and behind which the wake and the separation bubble develop completely, reattachment occurring before the next element is reached. In the second regime the roughness elements are close enough to each other so that the separation bubble associated with each element does not have room to develop fully. In the third regime, the roughness elements are closer still

so that stable vortices are created in the spaces between the elements. The flow here appears to skim on the crests of the elements.

5.4.2 Considerable work has been done on the investigation of the effect of roughness geometry and distribution on the resulting flow. Due to the complexity of the problem and the great number of parameters which can be considered to fully specify the element shape and distribution on the surface, the majority of the work has been done on the simple case of two dimensional roughness elements. An excellent review on this case is given by Liu, Kline & Johnston (1966). In regular arrays of three dimensional elements, the parameters required to fully describe the roughness geometry (i.e. element shape and distribution) may also be simplified to depend on either the frontal area density, λ_f , or the plan area density, λ_p . This simplification can be made if the frontal aspect ratio, A_f , the side aspect ratio, A_s , as well as ψ_x/ψ_y , which define the pattern of distribution are kept constant. This may explain why in most of the investigations, the correlations are made with the roughness density, neglecting the other variables. However, in the analytical review made by Wooding, Bradley and Marshall (1973) the inclusion of an aspect ratio factor $\phi(A_f, A_s)$ was suggested.

5.4.3 The effect of changing roughness density on the velocity profile parameters has been investigated by Koloseus and Davidian (1966) and Wooding, Bradley and Marshall (1973) and was found to influence the value of $\frac{K_s}{H}$. Furthermore,

the work reported by Dvorak (1969) and Simpson (1973) indicate that the effect of changing roughness density is to vary the constant C in equation (5.7), such an effect was also reported by Clauser (1956). From equations (5.7) and (5.11) it can be shown that a relationship between C and $\frac{k_s}{H}$ does exist. This may be written as:

$$C = \frac{1}{\kappa} \ln \frac{k_s}{H} - 3.4 \quad \dots\dots (5.14)$$

Wooding, Bradley and Marshall (1973) explained the results and analysis of Koloseus et. al. (1966) on the grounds of the three flow regimes of Morris. The results showed how the parameter $\frac{k_s}{H}$ increases linearly with the density, λ_f , in the isolated roughness regime reaching a maximum value in the transition to the wake interference regime and subsequently decreases. It may be noted however that the distinction between the wake interference and the skimming flow regime is not clear. From the comparison between roughness elements of different geometrical form it is evident that the behaviour of each of them is characterized by a particular line on a plot of k_s/H against λ_f . Although all the lines showed the same trend, they all showed variations in the location of the maxima, as can be seen in Figure 5.5.

5.4.4 In the paper by Dvorak it was suggested that the constant C of equation (5.7) was a function of the roughness density defined as $1/\lambda_p$ in the present notation. The variation of C obtained from the experimental results of different workers was represented by the following equations:

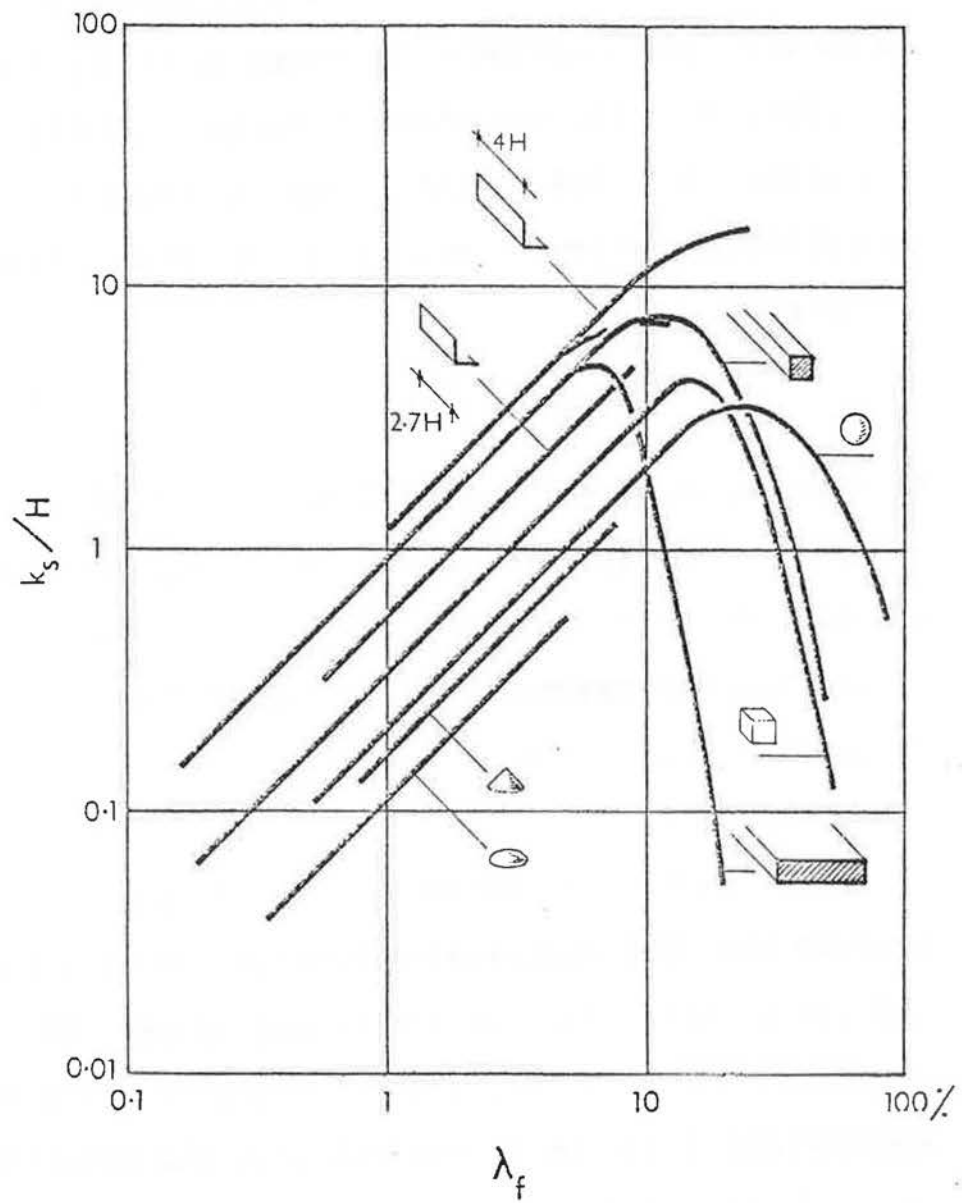


Figure 5.5 VARIATION OF k_s/H with λ_f FOR DIFFERENT ELEMENT FORMS.

$$\text{for } \lambda_p < 20\% \quad C = 5.95 (1.103 \log \lambda_p - 1) \quad \dots\dots (5.15)$$

$$\text{and for } \lambda_p > 20\% \quad C = 17.35 (1.625 \log \lambda_p - 1) \quad \dots\dots (5.16)$$

The experimental points given supporting equation (5.15) ranged from 1% $< \lambda < 13\%$ approximately, while those supporting equation (5.16) ranged from 24% $< \lambda_p < 50\%$. In a later paper by Simpson (1973), C was termed $f(\lambda_H)$ and an improved correlation was suggested by using the frontal area density (defined in terms of the present notations by $1/\lambda_f$) in place of the plan area density used by Dvorak (1969). However, the scatter of the extra experimental results quoted by Simpson from other workers indicate that equation (5.15) is better represented as a family of parallel lines. This was independently shown from the work of Koloseus and Davidian (1966) in the isolated roughness flow. Comparing equations (5.14) and (5.15) shows that λ_f can be related to $\frac{k_s}{H}$ as follows:

$$\begin{aligned} \frac{1}{K} \ln \frac{k_s}{H} - 3.4 &= 5.95 (1.103 \log \lambda_f - 1) \\ \text{i.e. } \log \frac{k_s}{H} &= 1.14 \log \lambda - 0.426 \quad \dots\dots (5.17) \end{aligned}$$

The slope of the logarithmic line of 1.14 from equation (5.17) is in good agreement with the corresponding value of 1.0 obtained from the results of Koloseus and Davidian (1966) in the isolated roughness regime.

5.4.5 In the previous sections the multiple relationships between $\frac{k_s u_*}{v}$, $\frac{Hu_*}{v}$, $\frac{k_s}{H}$ and $\frac{\Delta u}{u_*}$ are given by equations

(5.10 and (5.11) (see Figure 5.6 (a)). Further relationships between $\frac{\Delta u}{u_*}$, C and λ are also given by

equations (5.7), (5.15) and (5.16) (see Figure 5.6(a) and 5.6(b)). From the above relationships the three dimensional diagram shown in Figure 5.6(d) was constructed to illustrate the effect of the roughness density λ on $\frac{\Delta u}{u_*}$, $\frac{Hu_*}{v}$ and $\frac{k_s}{H}$ for any one particular roughness element form in the fully rough flow .

5.4.6 From their extensive work on two dimensional square sectioned roughness elements, Perry and Joubert (1963) and Perry, Schofield and Joubert (1969) reported two types of roughness geometry, "k type" and "d type" roughness corresponding to the wake interference and skimming flow regimes respectively. The error in origin ϵ in the wake interference flow was shown to be proportional to the roughness height H , while in the skimming flow regime, ϵ is not proportional to H but to the boundary layer thickness δ . They also found that the correlation scheme for $\frac{\Delta u}{u_*}$ versus $\frac{Hu_*}{v}$ suggested by Clauser is only valid in the wake interference flow. No such correlation was obtained in the skimming flow regime.

5.4.7 From their work on the flow structure for both the wake interference flow and the skimming flow regimes Perry et.al. (1969) were able to offer the following explanation of the flow mechanism :

- (i) In the wake interference flow, eddies with a length scale proportional to the roughness height H are assumed to be shed into the flow, forming a sublayer structure having a thickness of some factor times H . Further away from the

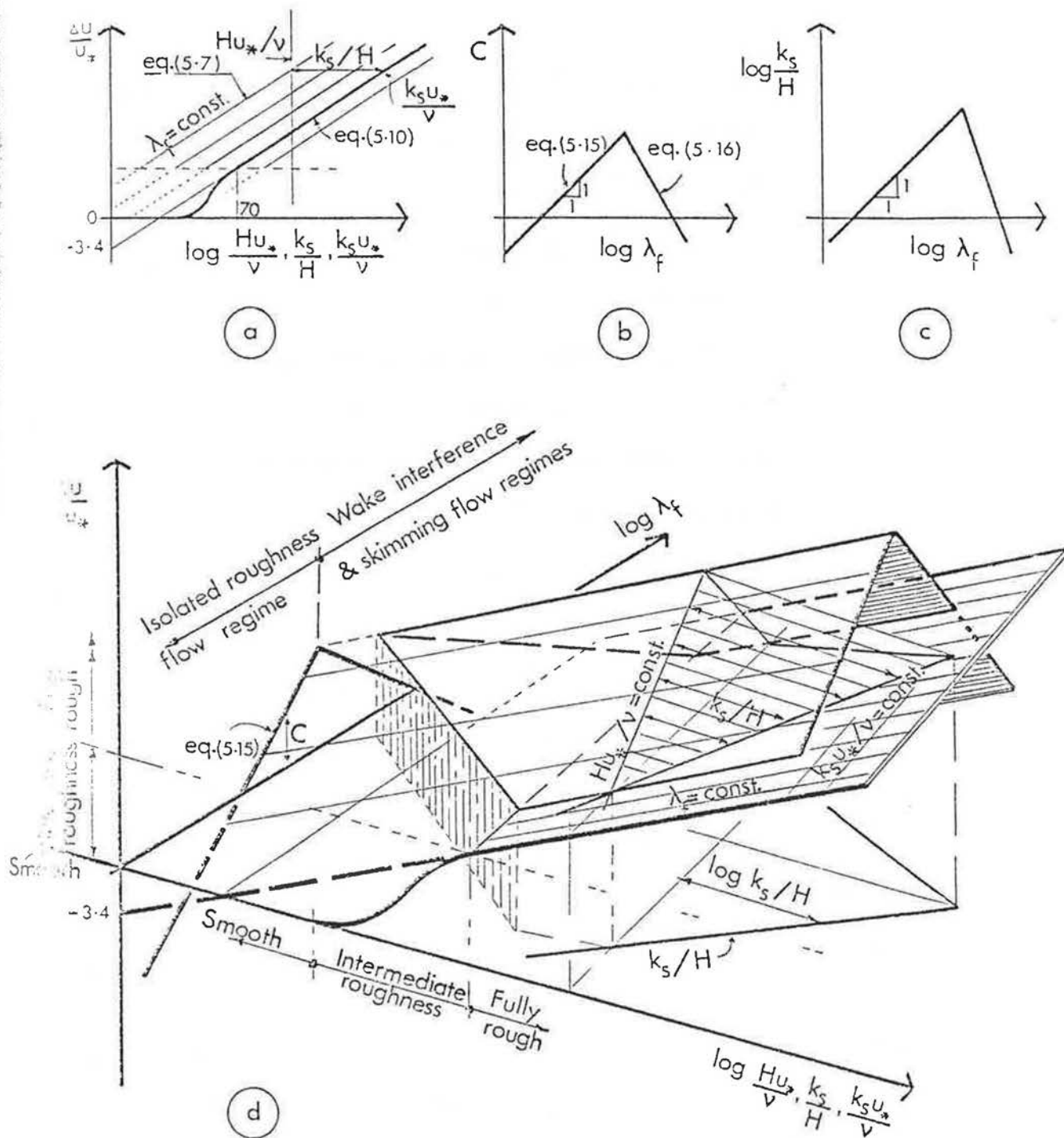


Figure 5.6

GRAPHICAL PRESENTATION OF THE VARIATION OF $\Delta u/u_*$ WITH $k_s u_*/v$ AND THE ROUGHNESS ELEMENT DENSITY, λ , FOR ANY ONE ROUGHNESS ELEMENT FORM IN THE FULLY ROUGH FLOW.

crests, this sublayer structure blends smoothly into the flow described by the logarithmic law, see Figure 5.7(a).

- (ii) In the skimming flow regime, the stability of the vortices between the elements result in negligible eddy shedding from the elements into the flow. The outer flow rides over the elements relatively undisturbed and the sublayer structure forming on top of the elements approaches zero, (see Figure 5.7(b)).

5.4.8 As an alternative scheme to that proposed by Clauser, Perry et. al. (1969) suggested the use of a roughness Reynolds number based on the error in origin ϵ and the friction velocity, i.e. $\frac{\epsilon u_*}{\nu}$ for the correlation of the data. The roughness function is then expressed as follows:

$$\frac{\Delta u}{u_*} = \frac{1}{K} \ln \frac{\epsilon u_*}{\nu} + F \quad \dots \quad (5.18)$$

where F is a universal constant and was found to have the value of -0.4 . This scheme is superior to that by Clauser in that its validity is extended to cover the wake interference flow, the skimming flow regime and also flows with adverse pressure gradients, Perry and Joubert (1963), Perry, et. al. (1969) and Schofield (1975). A recent paper by Wood and Antonia (1975) has shown that this correlation extends also to the intermediate roughness flow where $\frac{\Delta u}{u_*}$ is as low as 3 and $\frac{H u_*}{\nu} = 60$.

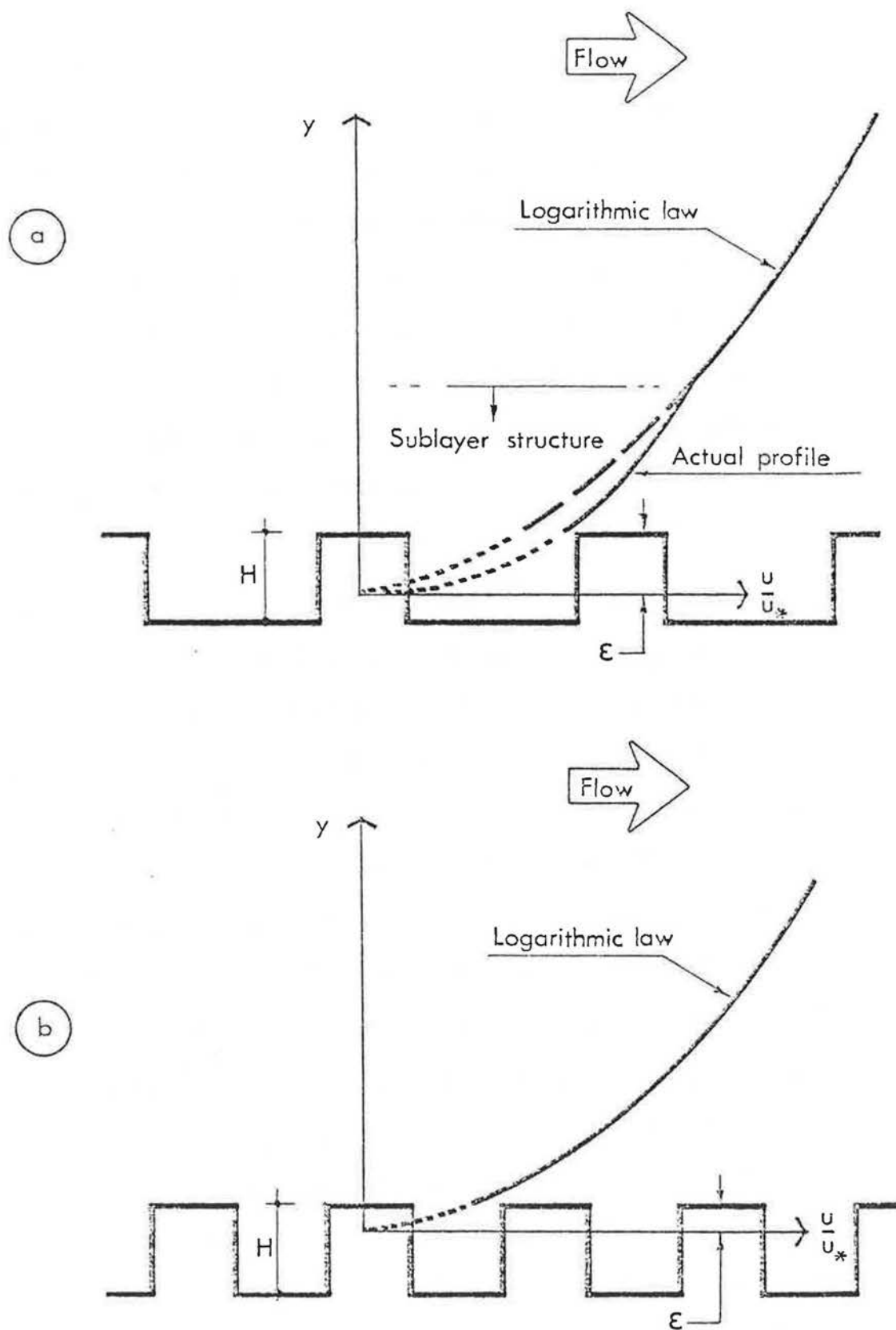


Figure 5.7 THE FLOW STRUCTURE FOR
 (a) THE WAKE INTERFERENCE FLOW REGIME,
 (b) THE SKIMMING FLOW REGIME.
 (after Perry et. al. 1969).

5.4.9 In order to check the validity of this scheme on the isolated roughness flow regime, the data of Liu, Kline and Johnston (1966), obtained for two dimensional square roughness elements in the 3 flow regimes are plotted in Figure 5.8 and compared with the results of both Perry et. al. (1969) and Wood et. al. (1975). The satisfactory correlation indicates that the validity of this scheme may well extend to include the isolated roughness flow regime.

5.4.10 The variation of \bar{d}/H and \bar{Z}_O/H with roughness density, λ_p , was investigated by Counihan (1971). For approximately cubical roughness elements (the elements were square in plan with 15.9 mm side length and 9.5 mm high), Counihan found that $\frac{\bar{d}}{H}$ increased linearly with λ_p and suggested that beyond a value of λ_p approximately 50% $\frac{\bar{d}}{H}$ will follow an asymptotic line to reach a maximum value of 1.0 at $\lambda_p = 100\%$. The variation of $\frac{\bar{Z}_O}{H}$ with λ_p was different in that it increased linearly with λ_p to reach a maximum value and then decreased with increasing λ_p . Here it may be noted that this variation is expected to be similar to that of $\frac{k_s}{H}$ with density due to the proportionality between k_s and Z_O in the fully rough flow (see Equation (5.12)). The maximum in $\frac{\bar{Z}_O}{H}$ was at $\lambda_p = 25\%$ for Counihan's results compared with $\lambda_f = 15\%$ for the cubical roughness elements reported by Koloseus and Davidian (1966). This discrepancy is thought to be attributed to the difference in the definition of density used in each case. Transforming λ_p used by

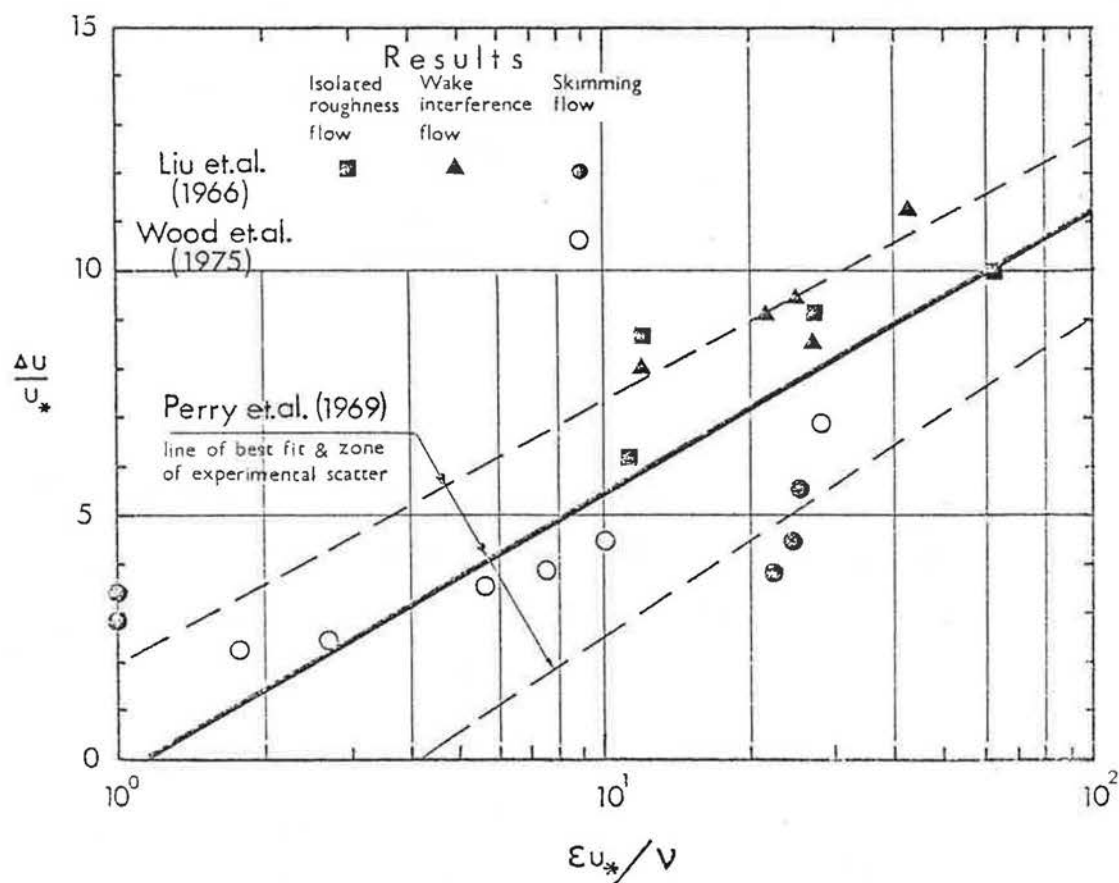


Figure 5.8 A CHECK ON THE VALIDITY OF THE CORRELATION SCHEME SUGGESTED BY PERRY et. al. (1969) ON THE ISOLATED ROUGHNESS FLOW REGIME.

used by Counihan to λ_f using the previously given relation:

$$\lambda_f = \frac{\lambda_p}{A_s} \dots\dots (4.6)$$

and knowing that A_s for Counihan's roughness elements was 1.67, gives a correction factor of 0.597 to be multiplied by his values of λ_p . Therefore λ_p at 25% will be corresponding to λ_f at 14.9% which is only 0.1% different from that noted by Koloseus et. al. (1966) of 15%.

5.5 The effect of a step change in surface roughness

5.5.1 The discussion so far has been limited to an idealized surface of uniform roughness elements extending for very long fetches, so that flow stability is assumed to have been achieved. However, in situations where a step change in surface roughness occurs, an internal layer grows on the new roughness surface and develops in the flow direction to replace the older layer as the fetch increases. This problem is of great interest to the studies of air flow in the atmosphere as such surface changes are frequently met on the earth's surface, see for example Elliott (1958), Bradley (1968), Panofsky and Townsend (1964) and Blom and Wartena (1969). The main conclusion from the results of these investigations is that the adaptation of the surface shear stress to the new boundary condition takes place fairly rapidly, therefore reliable values of the drag forces on an element may be obtained at a relatively short fetch compared with that required for the whole boundary

layer to adapt.

5.5.2 The effect of fetch on velocity profile parameters has been reported to be different for different flow regimes. From the work of Perry, Schofield and Joubert (1969), Antonia and Wood (1975), Schofield (1975) and Wood and Antonia (1975) on the skimming flow regime, the following behaviour of velocity profile parameters was confirmed:

1. Z_0 is proportional to the internal layer thickness δ_i and both of them increase linearly as a function of fetch. The same applies to ϵ although it grows very slowly with fetch.
2. The local skin friction coefficient C'_f and hence the element drag coefficient, C_{D1} , for a particular density is constant and does not vary with fetch, a characteristic of a self preserving flow.

5.5.3 From the work of Perry et. al. (1969), Antonia and Luxton (1971) and Joubert, Perry and Stevens (1971) on the wake interference flow regime the effect of fetch on the same parameters was noted as follows:

1. Both Z_0 and ϵ are constant and instead of being dependent on fetch, they are dependent on the roughness element height H .
2. The internal layer thickness δ_i increases logarithmically with fetch.
3. Unlike the flow in the skimming flow regime the local skin friction coefficient C'_f decreases with fetch.

5.5.4 As relatively less work has been reported on flow in the isolated roughness flow regime compared with the other two regimes, the effect of fetch on the profile parameters is not well established. However, from the work of Liu, Kline and Johnston (1966) and Counihan (1971) the following behaviour may be noted:

1. Z_o , C'_f and ϵ show a similar behaviour of decreasing by increasing the fetch.
2. As usual, the internal layer thickness, δ_i , increases with fetch.

As an extreme, when the roughness density reaches zero, i.e. smooth wall turbulent flow, the effect of fetch will be to increase Z_o and decrease C'_f and hence u_* , since $\frac{Z_o u_*}{\nu} = \text{constant}$.

5.6 Effect of roughness geometry on the mean pressures and their distribution

5.6.1 It was shown in the last sections that the main effect of roughness geometry, characterized by its density, is to change the flow from one regime to the other. In the present section, the attention will be given to the resulting drag forces on the roughness elements as well as to their pressure distribution in each of the three flow regimes. In the case of a rough surface with the roughness density so low that the total drag on the surface is approximately equal to the frictional drag on the smooth intervening boundary, the total drag will be a function of only the Reynolds number based on the

free stream velocity and the fetch. If the total drag is chiefly due to the form drag on the roughness elements and if the zones of separation round the elements do not change, then the total drag on the surface will be a function of only the geometry of the roughness and independent on the Reynolds number. In between these extremes a transition region exists where the total drag is dependent on both the Reynolds number and the roughness geometry. Hence in the isolated roughness flow regime where the density is low, these three cases will exist. The total drag will be independent of the Reynolds number in the higher density range of this regime. In the wake interference regime, the total drag is only due to the form drag on the elements. As the density increases the flow changes to the skimming flow regime. For identical roughness elements with flat top surface the flow may once again experience a transition region and ultimately a smooth surface flow on top of the elements as the density λ_p reaches 100.

5.6.2 For simplicity in the present work, the only case that will be considered is that the total surface drag force is dependent only on the roughness geometry and that the frictional drag on the wall between roughness elements is negligible. In this case the element drag coefficient may be written as:

$$C_{D1} = \frac{D}{q_1 a_f} \quad \dots\dots (5.19)$$

and the effective shear on the surface τ_{oe} may be written as:

$$\tau_{oe} = \frac{D}{A} \quad \dots\dots (5.20)$$

Hence, the effective local skin friction coefficient may be written as:

$$C'_{fe} = \frac{\tau_{oe}}{q_1} \quad \dots\dots (5.21)$$

substituting from equation (5.19) and (5.20) into (5.21) gives:

$$C'_{fe} = \frac{C_{D1} \cdot a_f}{A} = C_{D1} \cdot \lambda_f \quad \dots\dots (5.22)$$

5.6.3 Due to the scarcity of data on the drag of regular arrays of roughness elements in the isolated roughness flow regime, we will have to rely on the analogy between this flow and the smooth wall flow round a single element being reasonably correct. However, some difference may occur due to the different properties of incident flow in each case. For example, the value of d which will be zero for the smooth flow incident on a single roughness element, is only approaching zero at very low densities. From the work of Good and Joubert (1968) on two dimensional bluff plate in smooth wall flow, the main conclusions may be summarized as follows:-

1. The drag coefficient C_{D1} is dependent on the outer flow variables H/δ and $\frac{u_*}{U_1}$ up to $H/\delta \approx 0.8$ after which it is dependent on H/δ alone, see Figure 2.5.
2. A drag coefficient based on the friction velocity, C_{D*} , is dependent only on the roughness Reynolds number $\frac{Hu_*}{\nu}$ if the roughness is within the inner

layer of the incident velocity profile (see Figure 5.9). The relationship quoted is of the form:

$$C_{D*} = m_1 \log \frac{Hu_*}{v} + B_1 \quad \dots\dots (5.23)$$

3. A linear relationship was found to exist between the windward and the leeward pressure coefficients provided that the element height is within the inner layer of the incident velocity profile. The same result was also noted by Plate (1964).
4. A drag coefficient, C_{D_m} , based on the maximum pressure difference over the bluff-plate was approximately constant, i.e.

$$C_{D_{max}} = \left(\frac{D}{P_{max} - P_l} \right) H \approx 0.945$$

which agrees well with the value of 0.95 obtained by Plate.

5. Normalized pressure distributions with respect to the maximum pressure were obtained as a function of the relative height on the plate face y/H . The pressure distribution was of an "S" form with the peak pressure occurring at $y/H \approx 0.6$, (see Figure 5.10(a)). Such pressure distribution form is usually obtained for isolated buildings.
6. The dependence of C_{D_H} on $\frac{Hu_*}{v}$ was also shown in this work. This implies a dependence of C_{D_H} on H/Z_o following from equation (5.5). The same dependence on H/Z_o was also reported by Jensen and Franck (1965) for completely rough flows.

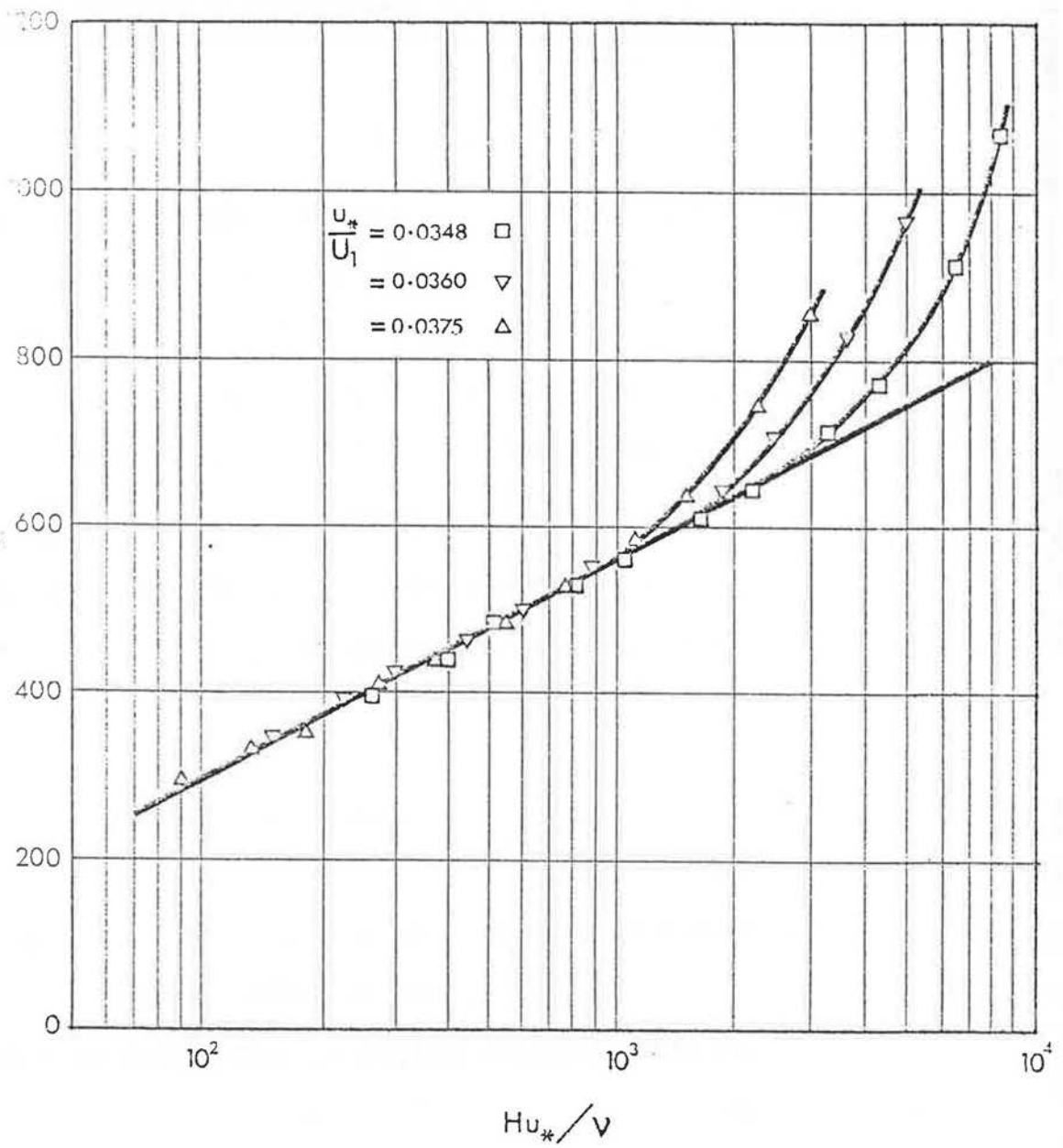


Figure 5.9 VARIATION OF C_{D*} WITH Hu_*/v
(after Good and Joubert, 1968).

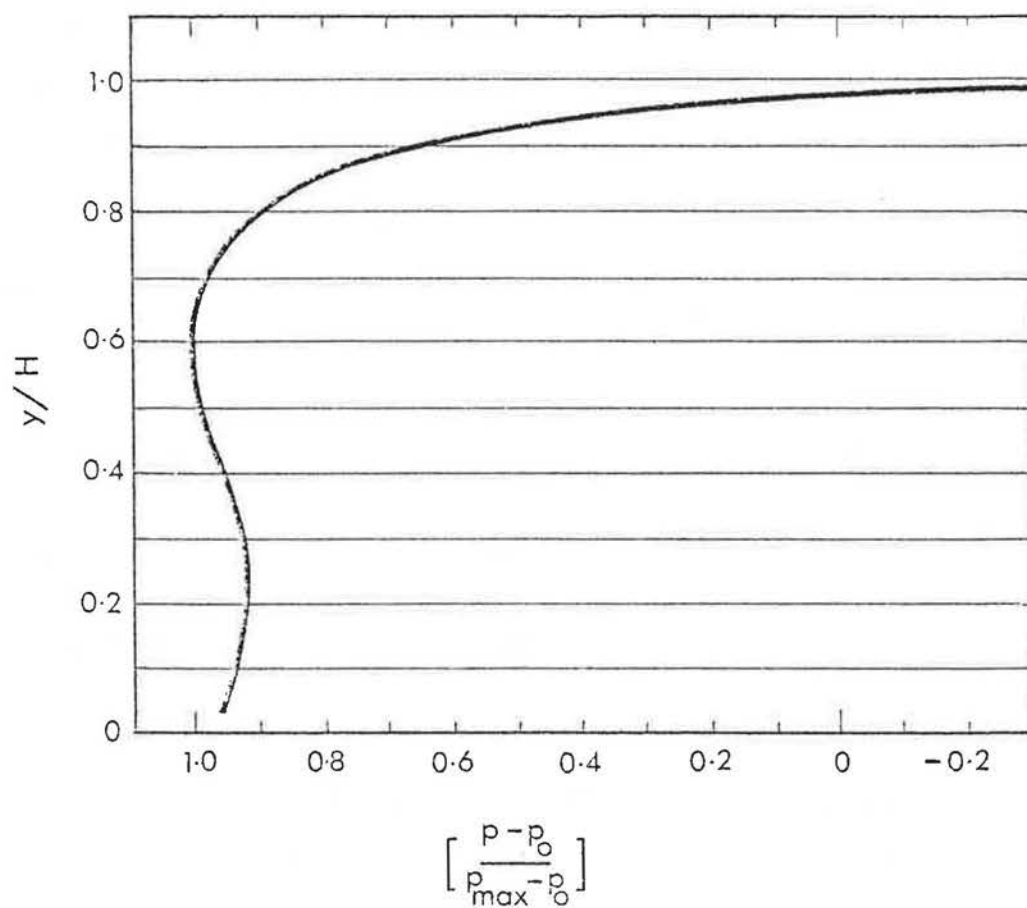


Figure 5.10 (a) THE PRESSURE DISTRIBUTION ON
AN ISOLATED BODY.
(after Good and Joubert, 1968).

Since the above work was conducted in smooth wall flow, one would expect that the differences that would occur on fully rough surface would be due to the introduction of the zero plane displacement d and the variation of z_o with roughness density. Therefore, equation (5.23) may be altered to read, for smooth flow:

$$C_{D*} = m_1 \log \frac{H}{z_o} + B_2 \quad \dots\dots (5.24)$$

where $B_2 = m_1 \log \frac{z_o u_*}{\nu} + B_1$

and for rough surfaces

$$C_{D*} = m_3 \log \frac{\epsilon}{z_o} + B_3 \quad \dots\dots (5.25)$$

where B_3 and m_3 are constants to be determined for rough surfaces.

5.6.4 In the wake interference flow regime, owing to the increase of the zero plane displacement, the drag coefficient C_{D1} is expected to decrease as the density increases. It is also expected that equation (5.25) will be valid. The pressure distribution on the face of the elements is different from that of the isolated roughness flow regime in that the "S" form is slightly distorted and would be better represented by a reversed "C" over 95% of the element height, Schofield, Perry and Joubert (1974), Figure 5.10(b)). Similar results though less accurate at the lower and upper parts on the element were obtained from the work of Antonia and Luxton (1971). On the leeward face, the pressure distribution is approximately uniform. These distributions are obtained from two dimensional square roughness elements in zero pressure

gradients. Unfortunately, no similar data are available on three dimensional roughness elements.

5.6.5 In the skimming flow regime, the rate of change of the zero plane displacement with density is less than the corresponding rate in the other two regimes, (see Counihan (1971)). This would imply that the drag coefficient C_{D1} is less sensitive to variations in density. However, significant effects on C_{D1} were observed due to the vertical misalignment of the element crests, Perry, Schofield and Joubert (1969). From these observations it seems that in the skimming flow regime, where ϵ is very small, a small fraction of the element height could be very large relative to the value of ϵ . The pressure distributions on the front face of a two dimensional square element are rather similar to those corresponding to the wake interference regime, where the reversed "C" form of the pressure profile now covers up to 98% of the element height (Figure 5.10(c)). The pressures on the upper part have higher values than those on the lower part of the face. On the leeward face, the pressure profile becomes non-uniform and similar to the windward face pressure in the lower half of the face with minimum pressure occurring at mid-height, Schofield, Perry and Joubert (1974). Such variation on the leeward face is characteristic of the stable vortex created in the space between elements, Roshko (1955).

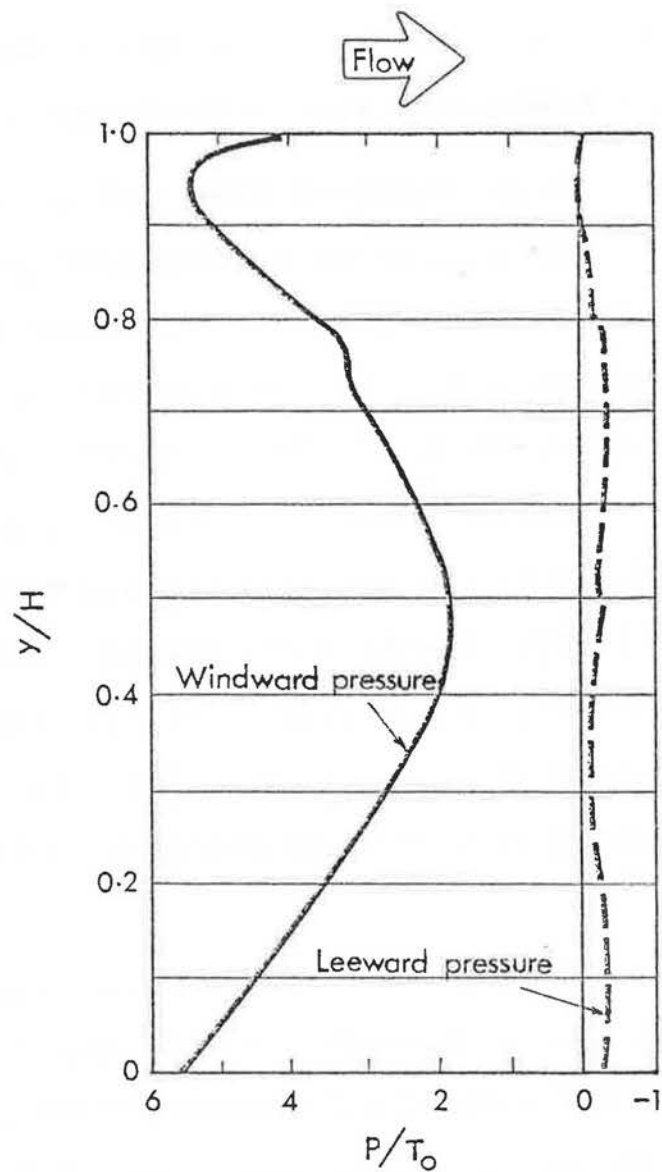


Figure 5.10 (b) THE PRESSURE DISTRIBUTION ON AN ELEMENT IN THE WAKE INTERFERENCE FLOW REGIME. (after Schofield et. al. 1974).

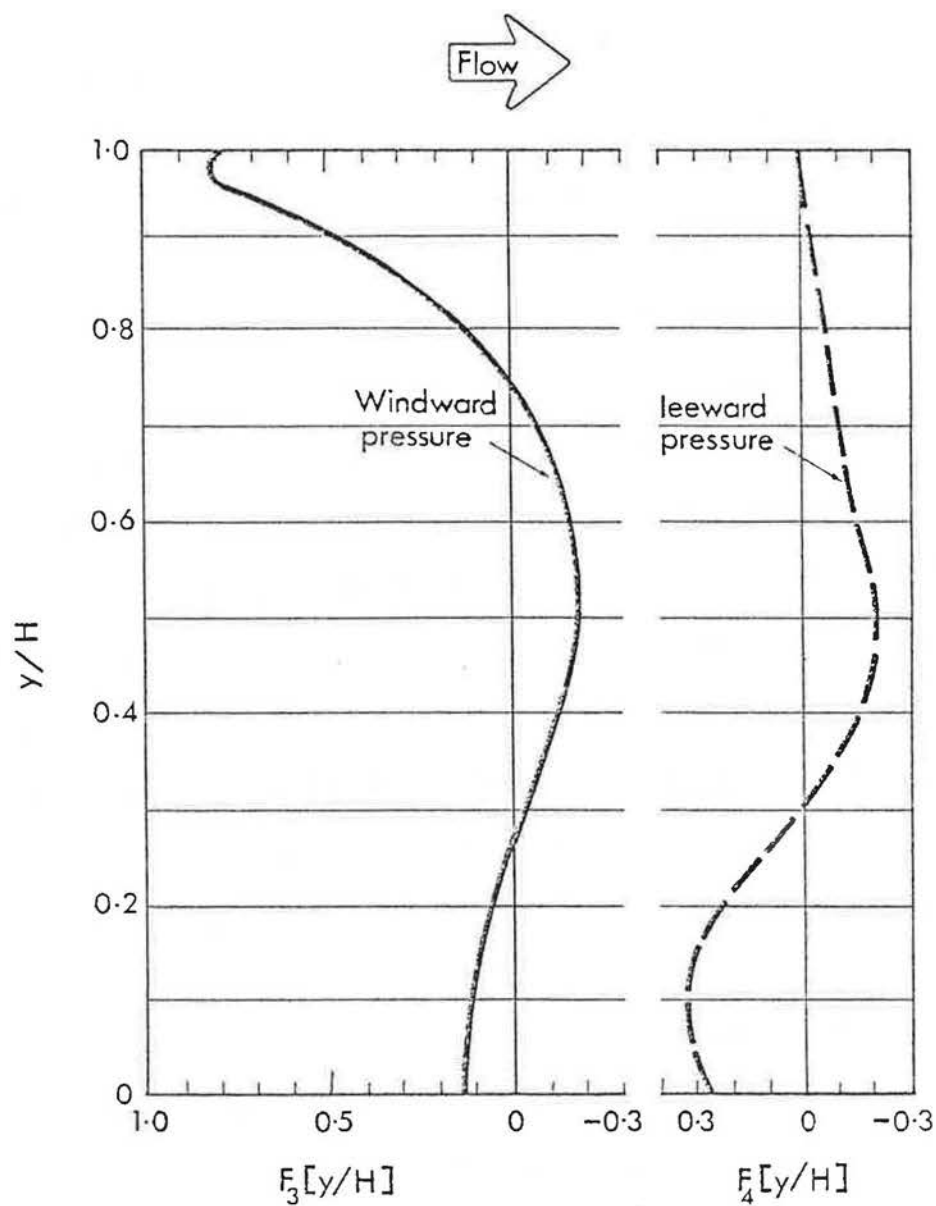


Figure 5.10 (c) THE PRESSURE DISTRIBUTION ON AN ELEMENT IN THE SKIMMING FLOW REGIME. (after Schofield et. al. 1974).

5.6.6 In this chapter it is shown that the main effect of changing the roughness geometry and pattern of distribution is to produce different flow regimes. It is also shown that the velocity profile parameters i.e. Z_0 and d as well as the resulting drag forces (hence u_*) are dependent on the flow regime hence the roughness geometry. Since air flow in urban areas in strong winds is completely rough, it is considered that the results obtained for the different regimes may well extend to include arrays of similar buildings in full scale conditions. However, as most of the work reported has been for idealized conditions of 2 dimensional roughness elements and single step change in surface roughness, further work on three dimensional rectilinear roughness elements in semi idealized conditions (i.e. multiple changes of surface roughness) and covering wider range of densities and patterns is required. Such work is not only useful in closing the gap between the idealized and the natural random conditions, but also in providing relevant information on the behaviour of the element drag, hence the natural ventilation potential, in the different flow regimes.

CHAPTER 6

EXPERIMENTAL ARRANGEMENT AND TECHNIQUES.

6. EXPERIMENTAL ARRANGEMENT AND TECHNIQUES

6.1 Introduction

6.1.1. In order to carry out a detailed investigation of the effect of building group geometry and the properties of wind flow on the resulting pressure forces, a series of wind tunnel model studies were made. To obtain any general relationship between the pressure forces and the geometry of the group, it was necessary to limit the great number of the geometrical parameters involved. Since the cube is the only three-dimensional rectangular body form that is characterized by a single dimension, it was chosen as the individual building form. The group form was also limited by considering buildings of uniform size, though in different configurations. Contrary to these limitations on form, the incident flow properties were varied, since they were shown in Chapter 5 to have an effect on the resulting drag forces. Consequently two incident flows were chosen as part of this study,

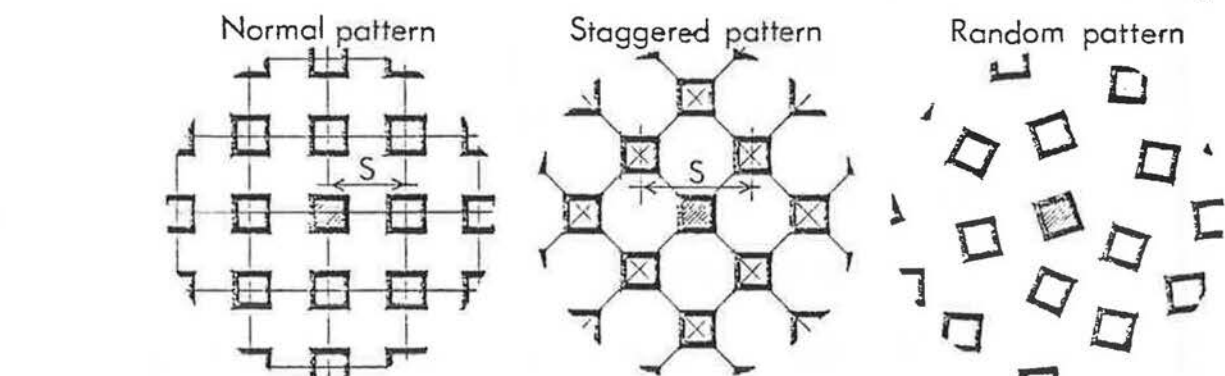
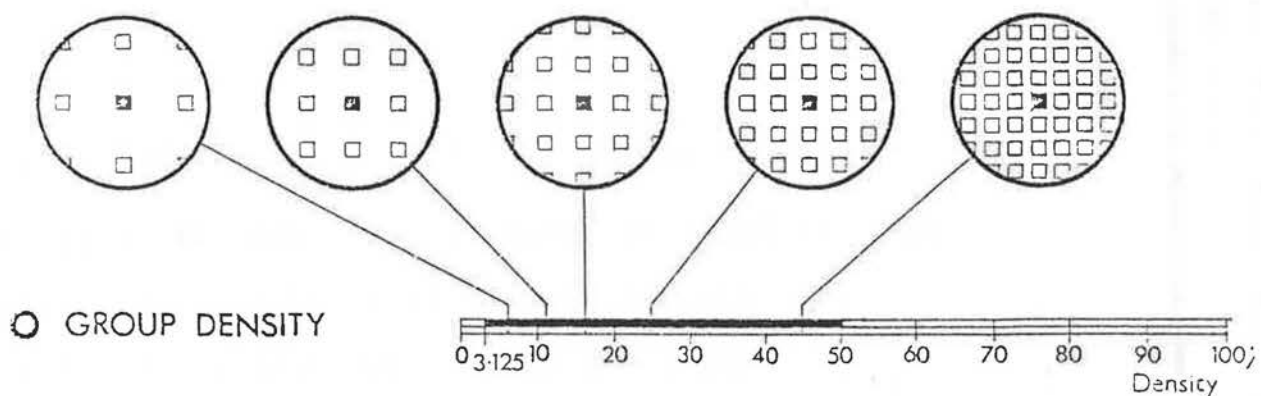
- (a) a relatively thin boundary layer, resulting from the flow on the smooth wind tunnel floor (smooth flow) and
- (b) a relatively deep boundary layer, resulting from the boundary layer growth over a rough sheet placed on the tunnel floor upstream the group (rough flow). Details of both flows will be given subsequently.

6.1.2 Considering the model as the centre of the group in this parametric study, the following variations of

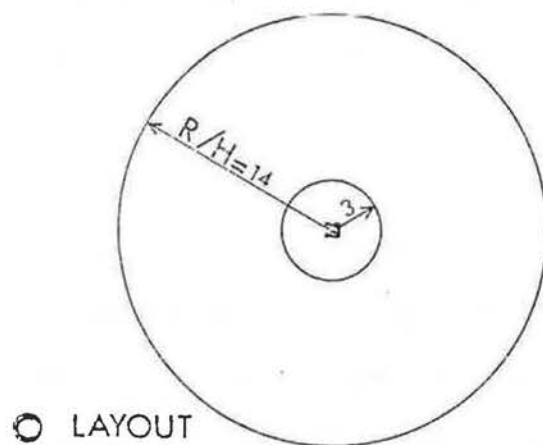
the descriptive parameters were involved, see Figure 6.1.

- (i) The building group density, defined by either plan area or frontal area, as both are equal for cubes, was varied from $3.125\% < \lambda < 50\%$.
- (ii) The building group pattern, (a) normal, (b) staggered, and (c) random.
- (iii) The building group layout size, R/H , where this varies from $3 < R/H < 14$.
- (iv) The incident flow, (a) rough flow, and (b) smooth flow.
- (v) The incident flow direction. Tests have been performed with the group layout rotated at 15° intervals in the range $-90^\circ < \phi < +90^\circ$ for each value of θ , the orientation of the central model. In the random pattern this range was extended to $-180^\circ < \phi < +180^\circ$. θ was also varied at 15° intervals in the range $-90^\circ < \theta < +90^\circ$. The definition of ϕ and θ are shown in Figure 6.1.

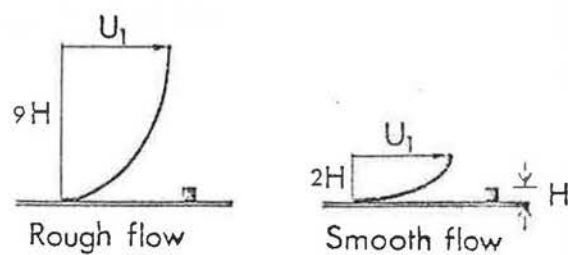
6.1.3 The variations of the above parameters were considered at different levels of detail in two stages of the investigation, the comparison of which is given in table 6.1.



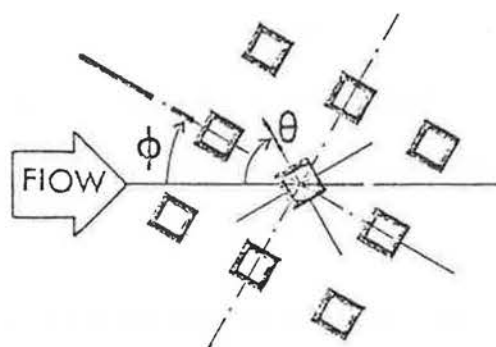
○ GROUP PATTERN



○ LAYOUT SIZE



○ INCIDENT FLOW



○ INCIDENT FLOW DIRECTION

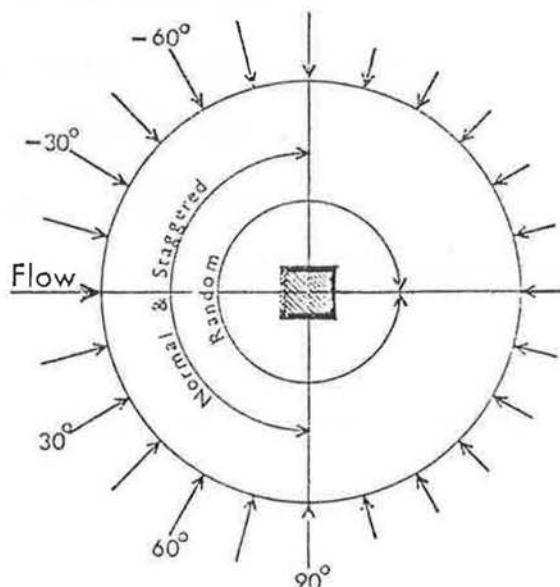


Figure 6.1 THE PARAMETERS CONSIDERED IN THE PRESENT STUDY.

Table 6.1 The variables considered in the two stages
of the investigation.

Variable	1st Stage	2nd Stage
Model	M_3	M_{24}
Density	9.2, 18.9 and 39.1%	14 densities $3.125\% < \lambda < 50\%$
Pattern	Normal, staggered and random.	Normal and staggered
Fetch	$3 < R/H < 14$	Constant at $R/H = 14.$
Incident flow	Smooth and rough	Smooth and rough
Orientation	$-90^\circ < \theta < +90^\circ$ * $-90^\circ < \phi < +90^\circ$ ** $-180^\circ < \phi < +180^\circ$ ***	$\theta = \phi = 0^\circ$
Velocity profiles round the model	Not measured	28 profiles in 6 densities, normal pattern, rough flow
Area of influence round the model.	Investigated for $\lambda =$ 9.2%, normal pattern, rough flow.	Not considered

* all patterns

** normal and staggered patterns

*** random pattern.

In the first stage, only three densities were studied using a simple model, M_3 , with 3 pressure tappings, see Figure 6.2. This limited range allowed detailed studies to be made of the effect of the model orientation, the building group pattern and the building layout size, hence the model fetch. It also enabled a detailed study to be made of "the area of influence" of the building group round the model that is responsible for the pressure forces obtained. This part of the study was performed for one group density, and one layout pattern in the rough flow. The combination of the parameters considered in this stage may be seen in table 6.2.

Table 6.2 The combination of the parameters considered for pressure measurements made in the first stage

Density %	Variable	Normal		Staggered		Random	
		Smooth	Rough	Smooth	Rough	Smooth	Rough
9.2	Fetch Orienta- tion	*	*	*	*	*	*
18.9	Fetch Orienta- tion	*	*	*	*	*	*
39.1	Fetch Orienta- tion	*	*				

In the second stage, a further detailed model, M_{24} , was used having a total of 24 pressure tappings equally

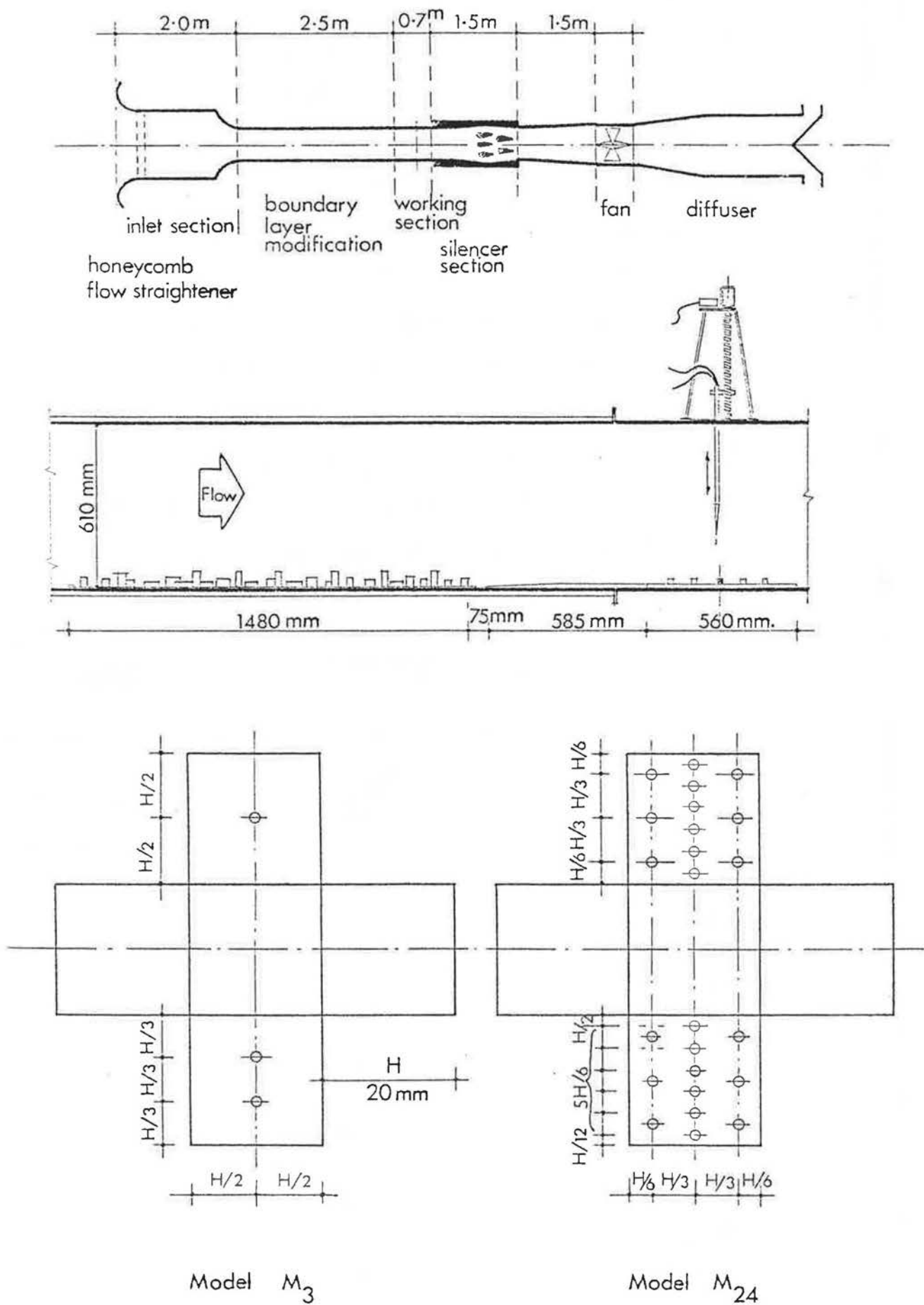


Figure 6.2 DETAILS OF WIND TUNNEL AND MODEL USED.

distributed on two opposite faces, see Figure 6.2. In this stage, both the fetch, R/H , and the incident flow direction, θ were kept constant. Consequently because of the limitations in the variables considered here, it was possible to carry out detailed velocity profile measurements of the flow round the central model at different densities for one pattern. The choice of these densities was based on the analysis and the hypothesis made from the detailed pressure measurement regarding the existence of various flow regimes. The combination of the parameters considered and the measurements made in this stage may be seen in table 6.3.

Table 6.3 The combination of the parameters considered and the measurements made in the second stage

Density %	Normal Pattern Smooth flow	Rough flow	Staggered Pattern Smooth flow	Rough flow
3.125	*	*	*	*
4.0	*	**	*	*
5.0	*	*		
6.25	*	*	*	*
8.0	*	**	*	*
10.0			*	*
12.5	*	**	*	*
16.0	*	*	*	*
20.0	*	*		
25.0	*	**	*	*
32.0	*	**	*	*
40.0			*	*
50.0	*	**	*	*

* Pressure measurements only

** Pressure and velocity profile measurements.

6.1.4 It may be noted that no attempt is made in the present investigation to simulate the properties of the natural wind, i.e. its turbulence structure or the velocity profile shape. Instead, it was considered that an investigation of the effect of changing the boundary layer thickness δ , hence the ratio H/δ , would be of some value since this is a constraint often relaxed in wind tunnel experimental studies (see for example the review made in Chapter 3). It was also considered that the multiple step change of surface roughness caused by placing the rough sheet upstream of the group would extend the scope of the investigation as such multiple changes of surface roughness frequently occur in nature. With regard to the turbulence characteristics of the incident flow, it is assumed that its structure would be determined by the model building group itself, consequently it becomes similar to the turbulence structure created on similar building group geometries in full scale conditions. The validity of this assumption has been substantiated by the work of Jensen and Franck (1965) and is discussed in detail by Sundaram, Ludwig and Skinner (1972).

6.2 Details of wind tunnel, model and incident flow modification

6.2.1 The wind tunnel in which the tests have been carried out is an open circuit tunnel with a closed working section. The lateral dimensions of the working section are 610mm x 610mm, and its length, including the

distance upstream of the model mounting position available for modification of the boundary layer, is 2.98m. A section through the wind tunnel may be seen in Figure 6.2. The wind tunnel speed range was 0-25 m/sec. The tests were carried out at a Reynolds Number of 2.5×10^4 , based on the model height and the free stream velocity. No correction for wind tunnel blockage has been applied since the frontal area blockage ratio was only 3.3% when the model layout extended to the wind tunnel side walls.

6.2.2 The pressure tapped models used in both stages of the investigation were cubes having a side dimension of 20 mm and were made from brass, machined to give sharp edges. All pressure measurements were taken from tappings on two opposite faces of the models. The model used in the first stage, M_3 , had 3 pressure tappings, 1.0 mm in diameter, two on the windward face and one in the leeward face, Figure 6.2. The model used in the second stage, M_{24} had 24 pressure tappings, 0.5 mm in diameter, equally distributed on two opposite faces, Figure 6.2. The surrounding building models used for the arrays were nominally identical to the instrumented model, i.e. 20 mm cubes. Accurately sized plastic cubes were used immediately around the model and less accurate wooden cubes were used for the remainder of the group layout. Double-coated adhesive tape was used to hold the surrounding cubes in position.

6.2.3 The model was mounted on a turntable, 12 mm thick and 560 mm in diameter, in order to vary the flow direction. A special arrangement was made for the

turntable and the model mounting system, Figure 6.3 which enabled roatation of both the model and the turntable independently to any required angle (θ or ϕ), from below the tunnel floor. Care was also taken not to disturb the flow on the smooth tunnel floor due to the turntable thickness. Therefore, a leading plate, the same thickness as the turntable was placed round the upstream half of the latter and extended for 865 mm from the turntable centre, ending with a bevelled edge, Figure 6.3.

6.2.4 The two incident flows used were:

- (a) the boundary layer which resulted from the air flow over the smooth floor of the wind tunnel working section (smooth flow); and
- (b) the flow obtained from the boundary layer growth on a rough sheet placed upstream of the turntable on which the model group layout was positioned (rough flow).

This rough sheet, consisting of a random layout of wooden blocks measuring 50 x 25 x 25 mm, fixed on a hard-board sheet, covered the width of the working section. The rough sheet extended from 2.42 - 0.915 m upstream of the turntable centre.

6.3 Measurement technique and accuracy level

6.3.1 In the first stage of investigation, only pressure measurements were made using the model M_3 . An inclined tube manometer was connected to the stainless steel tubing of the model for pressure measurement.

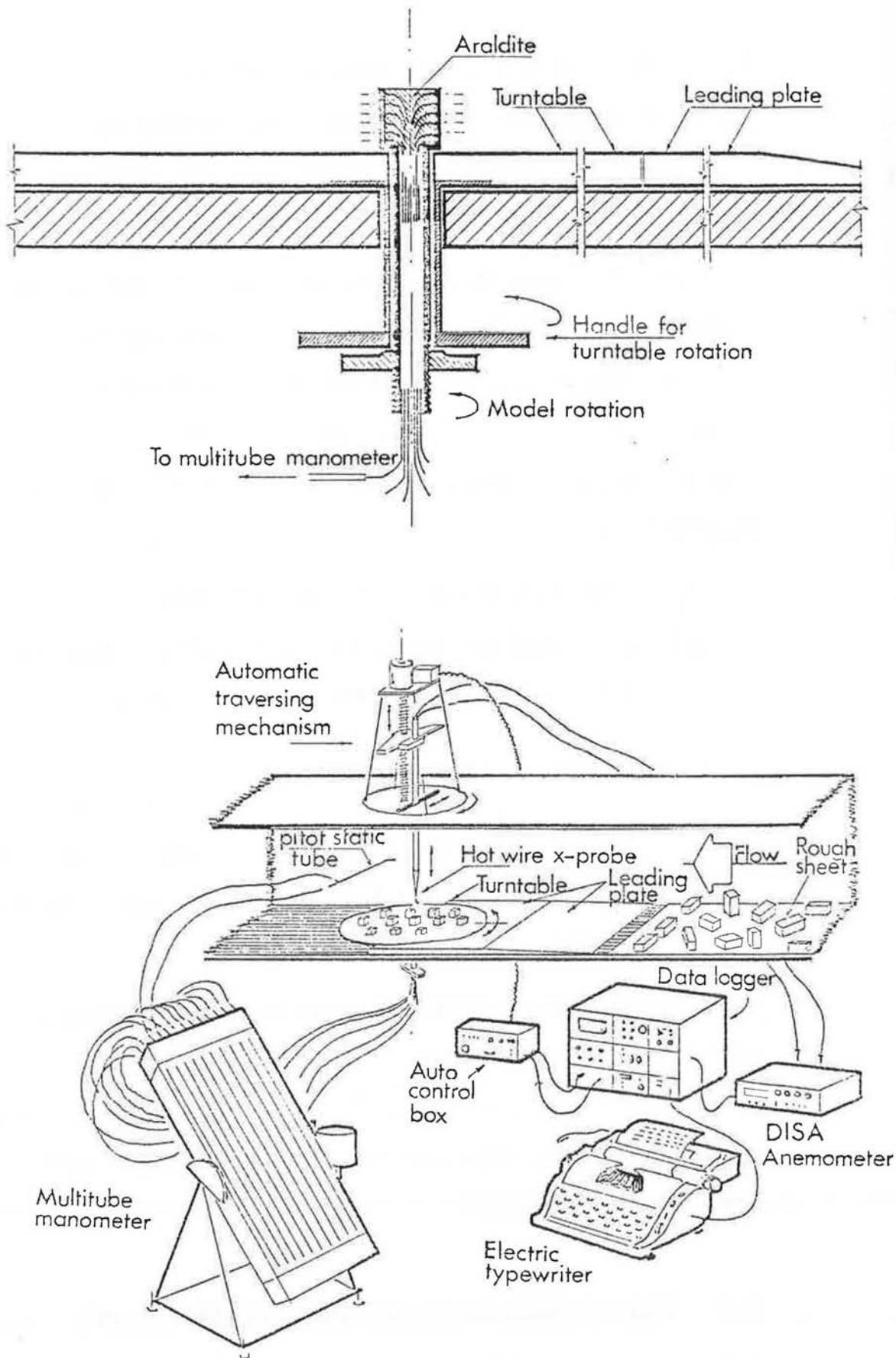


Figure 6.3 DETAILS OF MODEL MOUNTING SYSTEM AND SET-UP OF EQUIPMENTS.

The dynamic head which was used for normalizing the pressure values was that in the free stream at 300 mm above the model position. It was monitored by means of a pitot static tube fixed to the side wall of the tunnel. In the normal and staggered patterns, pressure measurements were made twice at each value of θ , i.e. at $\pm \theta$. An average value was then taken to cancel out any error either due to the positioning of blocks or due to the orientation angle. The same procedure was made when ϕ was varied. In the second stage, the pressure measurements were made using a multitube inclined manometer which enabled a simultaneous reading of the 24 tappings on the model. Direct readings of the pressure coefficient C_{P_1} were taken by tilting the multitube manometer to give a unit length corresponding to the dynamic head.

6.3.2 The accuracy levels of the pressure measurements were not equal in all cases. They were mainly dependent on the fluctuations of the liquid levels in the manometer tubes. Higher accuracy levels ($\pm 2\%$) has been estimated to be obtained for the values of C_{P_1} at the leeward faces, higher densities, rough flows or at large fetches. An accuracy level of $\pm 5\%$ would be anticipated in the other cases.

6.3.3 In the measurement of the velocity profiles a DISA constant temperature hot wire anemometer, Type 55M01, fitted with a miniature X-probe model 55P63 was used. For the purpose of traversing the hot wire probe vertically over the turntable, an automatically controlled traversing mechanism was made which enabled the operator

to control the vertical step of the traverse in the range of 2-30 mm as well as the time delay between steps in the range of 10- ∞ sec. The system was designed so that the signal from the hot-wire was fed to the anemometer there to a Solartron data logger which was used to operate an electric typewriter in order to obtain automatic printout of the output voltage, see Figure 6.3. The operation was further automated by connecting the data logger to the traversing mechanism control box, in order to start the data logger at the end of each vertical step. At each point in the velocity profile, 5 readings of the hot-wire output were taken at 2 second intervals, the average value was then used for the calculation of the mean velocity at that point.

6.3.4 In the calibration of the X-configuration hot-wire probe, a pitot static tube was used in conjunction with the hot wire probe to monitor the flow speed at the wind tunnel centre. Neglecting the fluctuating component of the flow due to turbulence, hence its corresponding fluctuating voltage output, the response of a hot-wire placed normal to the flow may be described by King's Law as follows:

$$E^2 = E_0^2 + m \sqrt{u} \quad \dots\dots (6.1.)$$

where E is the mean bridge voltage of the anemometer and u is the mean velocity. E_0 and m are constants independent of flow velocity. In the case of an inclined wire with respect to flow direction, it may be assumed for simplicity that the hot-wire is cooled only by the effective velocity, u_{eff} , i.e. the velocity component

normal to the wire axis. Hence the cosine law applies:

$$u_{\text{eff}} = u \cos \psi \quad \dots\dots (6.2)$$

where ψ is the effective angle between the flow direction and the plane normal to the wire axis, see Figure 6.4.

Resolving the flow velocity into its two components u and v on the x and y axis gives the following equations for the two wires I and II of the x -probe, Klatt (1969).

$$u_{\text{eff}_I} = u \sin \alpha_I - v \cos \alpha_I \quad \dots\dots (6.3)$$

$$u_{\text{eff}_{II}} = u \sin \alpha_{II} - v \cos \alpha_{II}$$

where α_I and α_{II} are the orientation angles of the wires with respect to the x axis. The effective angles are related to the orientation angles as follows:

$$\alpha_I = (90 + \psi_I) \text{ and } \alpha_{II} = (90 - \psi_{II}) \text{ as}$$

may be seen in Figure 6.4. Assuming that the v component is zero in the free stream, the following relations are then obtained:

$$u_{\text{leff}_I} = U_1 \sin \alpha_I \quad \dots\dots (6.4)$$

$$u_{\text{leff}_{II}} = U_1 \sin \alpha_{II}$$

From equations (6.1), (6.3) and (6.4) and assuming that $\alpha_I \approx 135^\circ$ and $\alpha_{II} \approx 45^\circ$ the relative velocity u/U_1 may be obtained as follows:

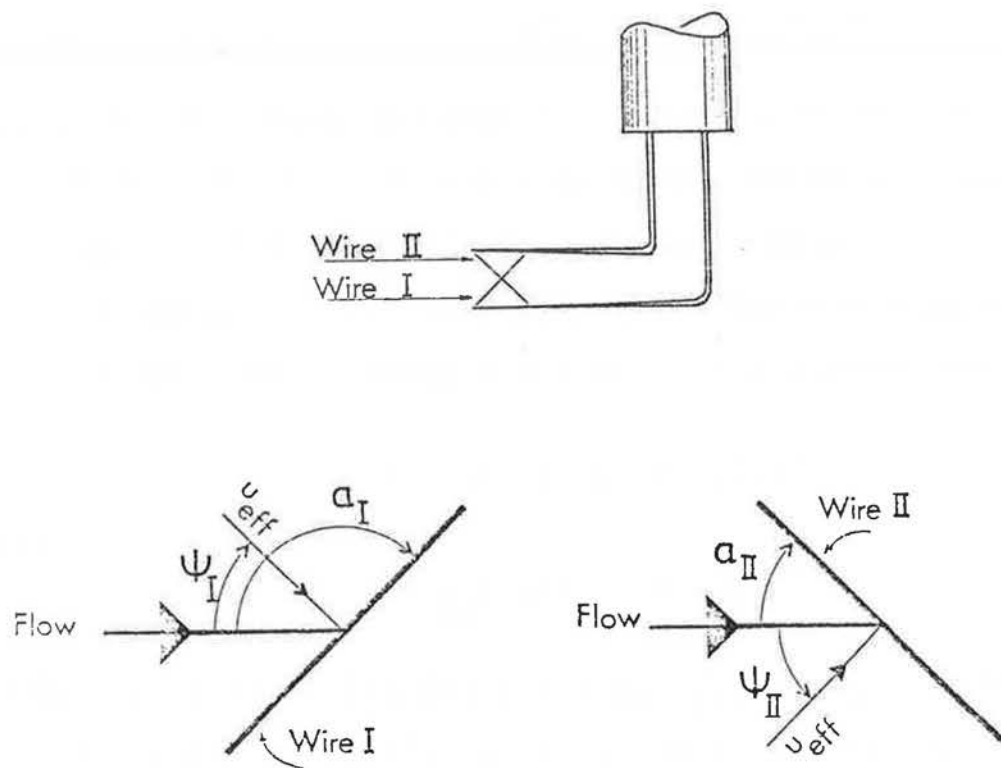


Figure 6.4 DEFINITION OF HOT-WIRE ORIENTATION AND EFFECTIVE ANGLES.

$$\frac{u}{U_1} = 0.5 \left\{ \left(\frac{E_I^2 - E_{OI}^2}{E_{II}^2 - E_{OI}^2} \right) + \left(\frac{E_{II}^2 - E_{OII}^2}{E_{III}^2 - E_{OII}^2} \right) \right\} + \frac{\sin(\alpha_I + \alpha_{II})}{2} \left\{ \left(\frac{E_I^2 - E_{OI}^2}{E_{II}^2 - E_{OI}^2} \right) - \left(\frac{E_{II}^2 - E_{OII}^2}{E_{III}^2 - E_{OII}^2} \right) \right\} \dots\dots (6.5)$$

$$\frac{v}{U_1} = \frac{1 + \cos(\alpha_I - \alpha_{II})}{2} \left\{ \left(\frac{E_I^2 - E_{OI}^2}{E_{II}^2 - E_{OII}^2} \right) - \left(\frac{E_{II}^2 - E_{OII}^2}{E_{III}^2 - E_{OII}^2} \right) \right\} (6.6)$$

If the angles α_I and α_{II} are not 135° and 45° respectively then $\sin(\alpha_I + \alpha_{II}) \neq 0$. Thus the second term in equation (6.5) may be considered as a correction factor for u , dependent on the symmetry of the wires round the x axis. Conversely, the angle between the wires, $(\alpha_I - \alpha_{II})$ determines the accuracy of the v component in equation (6.6).

6.3.5 For the purpose of measuring α_I and α_{II} accurately, the method described by Dean 1974 for measuring the effective angles, $\psi_{I,II}$ hence $\alpha_{I,II}$ was employed. In this method the hot-wire calibration equation (6.1), may be put in the form:

$$E^2 = E_O^2 + m (u \cos \psi)^{0.5} \dots\dots (6.7)$$

If the wire is rotated a further angle $\Delta\psi$ then equation (6.7) may be written as:

$$E_\Delta^2 = E_{O\Delta}^2 + m_\Delta \{u \cos(\psi + \Delta\psi)\}^{0.5} \dots\dots (6.8)$$

where the subscript Δ denotes the values corresponding to the angle $(\psi + \Delta\psi)$. Dividing (6.7) by (6.8), we obtain:

$$\left\{ \frac{(E_\Delta^2 - E_{O\Delta}^2)/m_\Delta}{(E^2 - E_O^2)/m} \right\}^2 = \frac{\cos(\psi + \Delta\psi)}{\cos \psi} \dots\dots (6.9)$$

$$= \cos \Delta\psi - \tan \psi \sin \Delta\psi$$

At $\Delta\psi = 0$,

$$(E^2 - E_O^2) \equiv (E_{\Delta}^2 - E_{O\Delta}^2)$$

Both E_O^2 and m do not vary significantly and the ratio m/m_{Δ} is reasonably constant for small values of $\pm \Delta\psi$ where

$$\frac{m}{m_{\Delta}} = \frac{T}{T_{\Delta}} \left\{ \frac{\cos(\psi + \Delta\psi)}{\cos \psi} \right\}^2$$

and where both T and T_{Δ} are the slopes of the calibration lines given in Figure 6.5, from calibration tests to check this point. The variation of $E_{O\Delta}^2$, T_{Δ} and the ratio m/m_{Δ} with small angles of yaw, up to $\pm 8^\circ$ is given in table 6.4 and may be shown plotted in Figure 6.5.

Table 6.4 Variation of the constants $E_{O\Delta}^2$, T_{Δ} and m/m_{Δ} with small yaw angles $\pm \Delta\psi$

$\Delta\psi$	$E_{O\Delta}^2$	T_{Δ}	m/m_{Δ}
+ 8	6.97	11.55	0.989
+ 6	7.00	11.76	0.993
+ 4	7.01	11.99	0.995
+ 2	7.02	12.18	0.998
0	7.02	12.38	1.000
- 2	7.03	12.54	1.004
- 4	7.07	12.66	1.010
- 6	7.09	12.81	1.013
- 8	7.12	12.91	1.019

$\psi = 45^\circ$

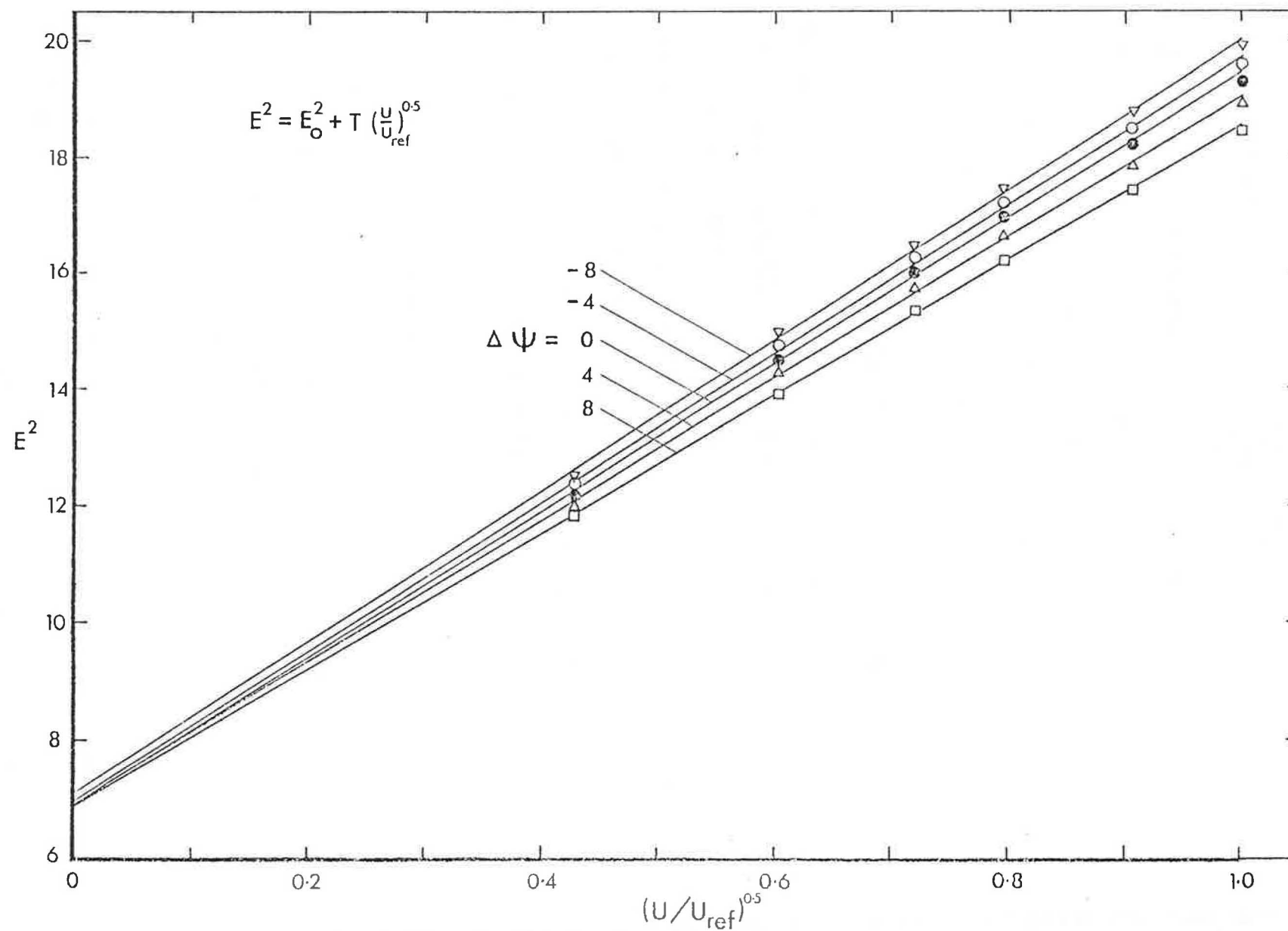


Figure 6.5 CALIBRATION AT EACH ANGLE OF YAW
(a check on the method of finding ψ_{cc}).

Thus equation (6.9) may be simplified to read:

$$\cos \Delta\psi - \left(\frac{E_O^2 - E_{O\Delta}^2}{E^2 - E_O^2} \right)^2 = \tan \psi \sin \Delta\psi \dots\dots (6.10)$$

Plotting the left hand side of equation (6.10) against the right hand side yields $\tan \psi$ as the slope of the straight line. The results are obtained by presenting the data in the manner shown in Figure 6.6, from which ψ_I and ψ_{II} , hence α_I and α_{II} were determined.

6.4 Flow visualization technique

6.4.1 In order to obtain further information about the flow pattern and behaviour in the different flow regimes, a series of flow visualization experiments were undertaken. The wind tunnel used for these experiments was an open circuit tunnel with a closed working section. The working section was 1.20m x 1.20m in cross section and was 6.10 m long. The maximum speed at the tunnel centre was 9 m/sec.

6.4.2 The models used were wooden cubes having 45 mm side dimension, and placed on smooth polished aluminium sheet, measuring 0.91 x 0.91m. Arrays of three densities, one in each flow regime for both the normal and staggered patterns were investigated in addition to the isolated model case.

6.4.3 Two incident flows were also used here, i.e. smooth flow and rough flow, for which the ratios H/δ were 0.5 and 0.05 respectively. In the rough flow, a turbulent boundary layer was grown on a rough sheet covering the wind tunnel width and extended from 6.0 m to 0.6 m upstream of the aluminium sheet on which the

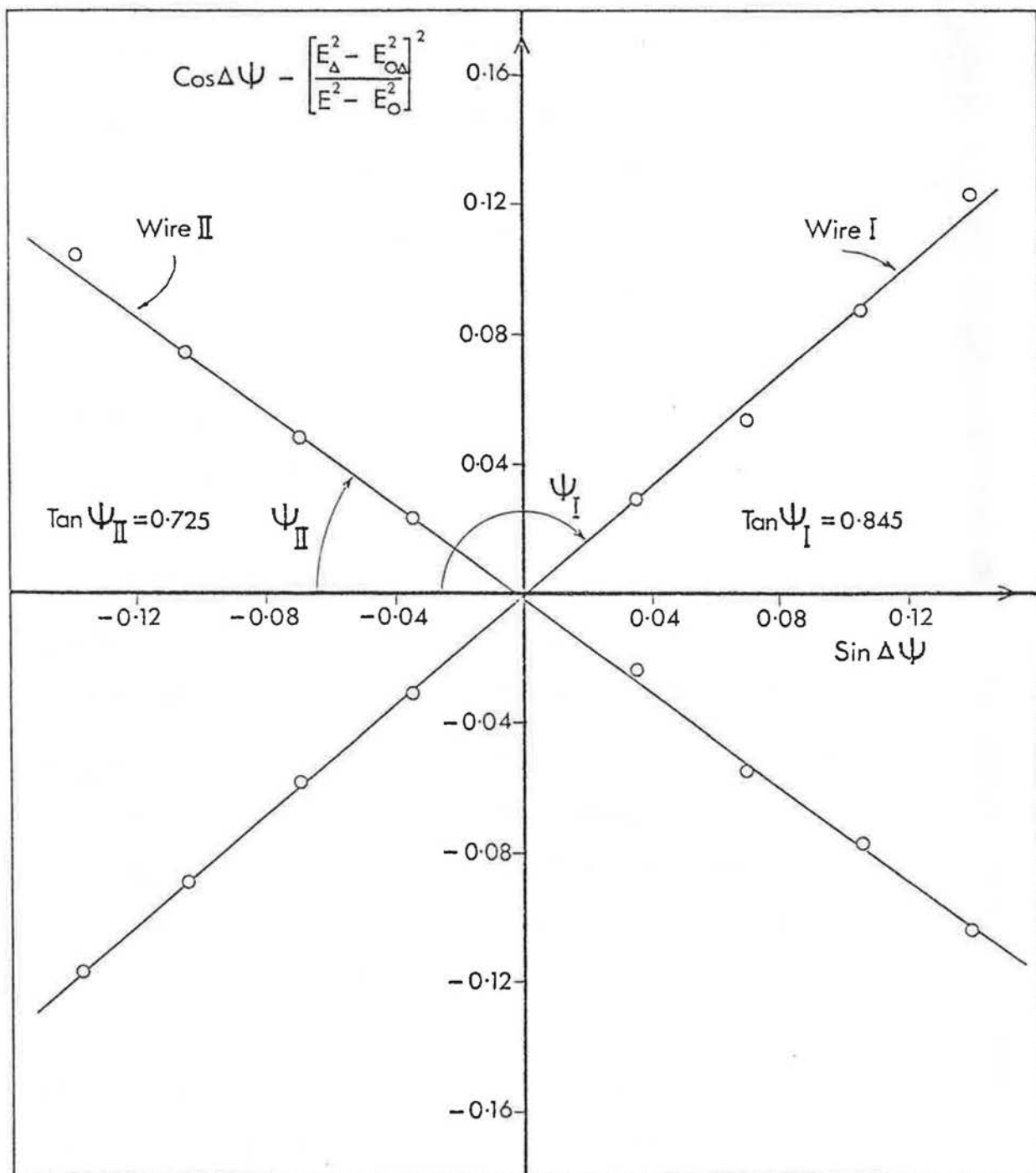


Figure 6.6 CROSS WIRE YAW CALIBRATION.

group layout was placed. Polystyrene blocks measuring 100 x 100 mm and 50 mm high uniformly glued on a hard-board sheet were forming the elements of the rough sheet.

5.4.4 The paint used for visualization was made up as follows, (all parts by volume):

- 1 part Dayglo Saturn yellow pigment,
- 3 parts kerosene
- 7 parts white spirit

from the formula given by Grigg and Sexton (1974). A spray gun was used to cover the aluminium sheet as well as the cubes with a thin uniform layer of paint. The wind tunnel was then turned on maximum speed until the liquid evaporated, in about 30 minutes. The pattern usually developed completely in about 5 minutes.

6.4.5 During the photographing of the high group layout densities, the cubes were so close to each other that the light did not reach the floor areas in between on which the flow pattern was obtained. Therefore, in some cases two photographs were taken, the first with the cubes in position to show the flow pattern made on the top surface of the cubes. Another photograph was then taken after replacing the cubes by thin hard board pieces cut to the same cube size to define the cube position and to show the flow on the floor between the cubes.

CHAPTER 7

EXPERIMENTAL RESULTS AND DISCUSSION:
Pressure Measurements.

7. EXPERIMENTAL RESULTS AND DISCUSSION:

Pressure Measurements.

7.1 The effect of fetch on the central model drag

7.1.1 In this investigation the model group took the form of free standing cubes on a smooth surface, hence the oncoming flow underwent an abrupt change of surface roughness when it reached the group layout. The effect of this disturbance on the incident flow has been investigated to determine the model group layout size required for the surface pressure forces to stabilize.

7.1.2 The variation of C_{D_1} with group layout size R/H (which is also the fetch of the central model) is shown in figure 7.1 where C_{D_1} is defined as the windward and leeward face pressure coefficient difference at $\theta = 0^\circ$. From figure 7.1(a) in which the surrounding group was not rotated, the stability of C_{D_1} is achieved before 6 - 7 R/H in the normal pattern apart from the lowest density in the smooth flow. In this case the fetch required is approximately double the previous value. The staggered pattern behaved differently in that, stability was only achieved for the rough flow cases at $R/H = 12$. The smooth flow in this pattern required fetches longer than $R/H = 13.5$, Figure 7.1(b).

7.1.3 The effect of varying the angle of the surrounding group, ϕ , was also investigated as a step towards the ultimate case of the random pattern. Examples of the effect of varying ϕ on C_{D_1} for the largest and smallest values of R/H examined for the different densities and patterns in the smooth and rough flows are given in

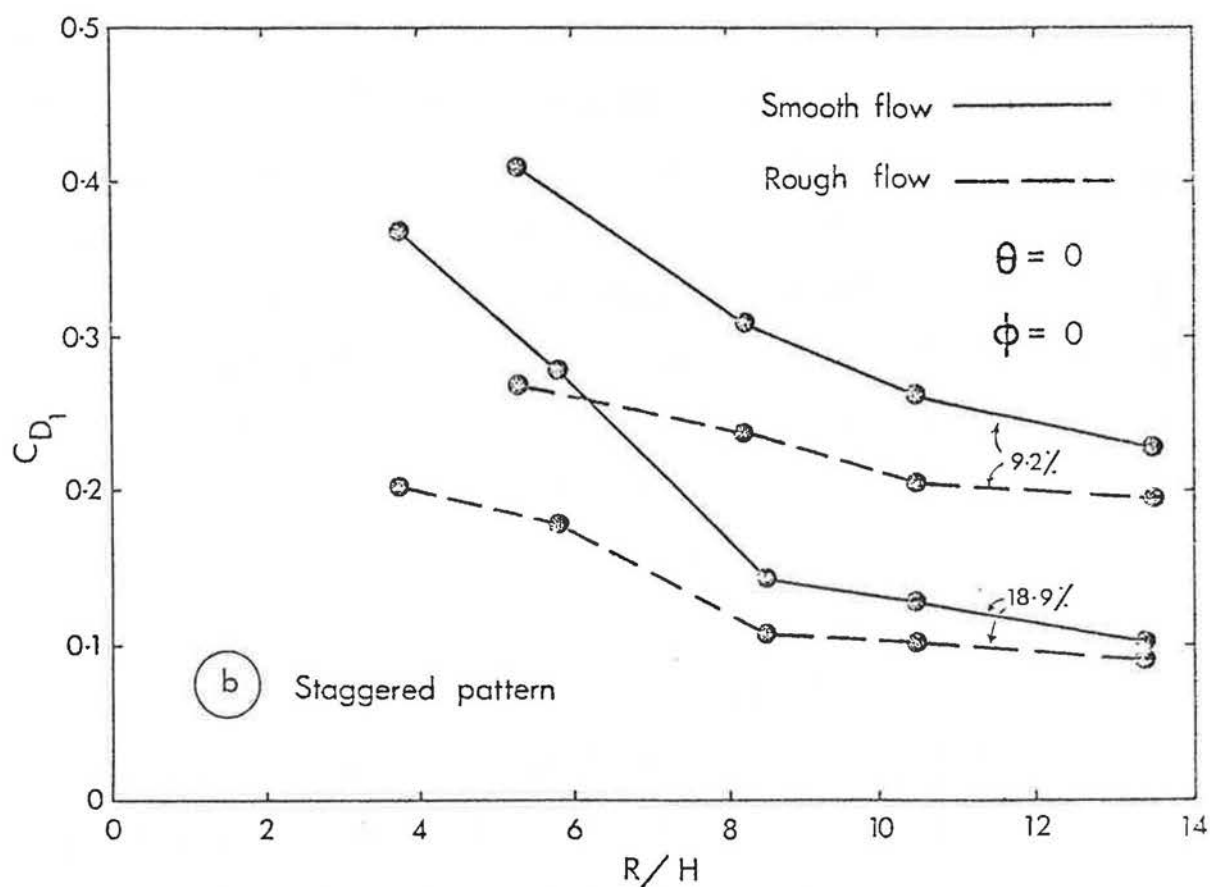
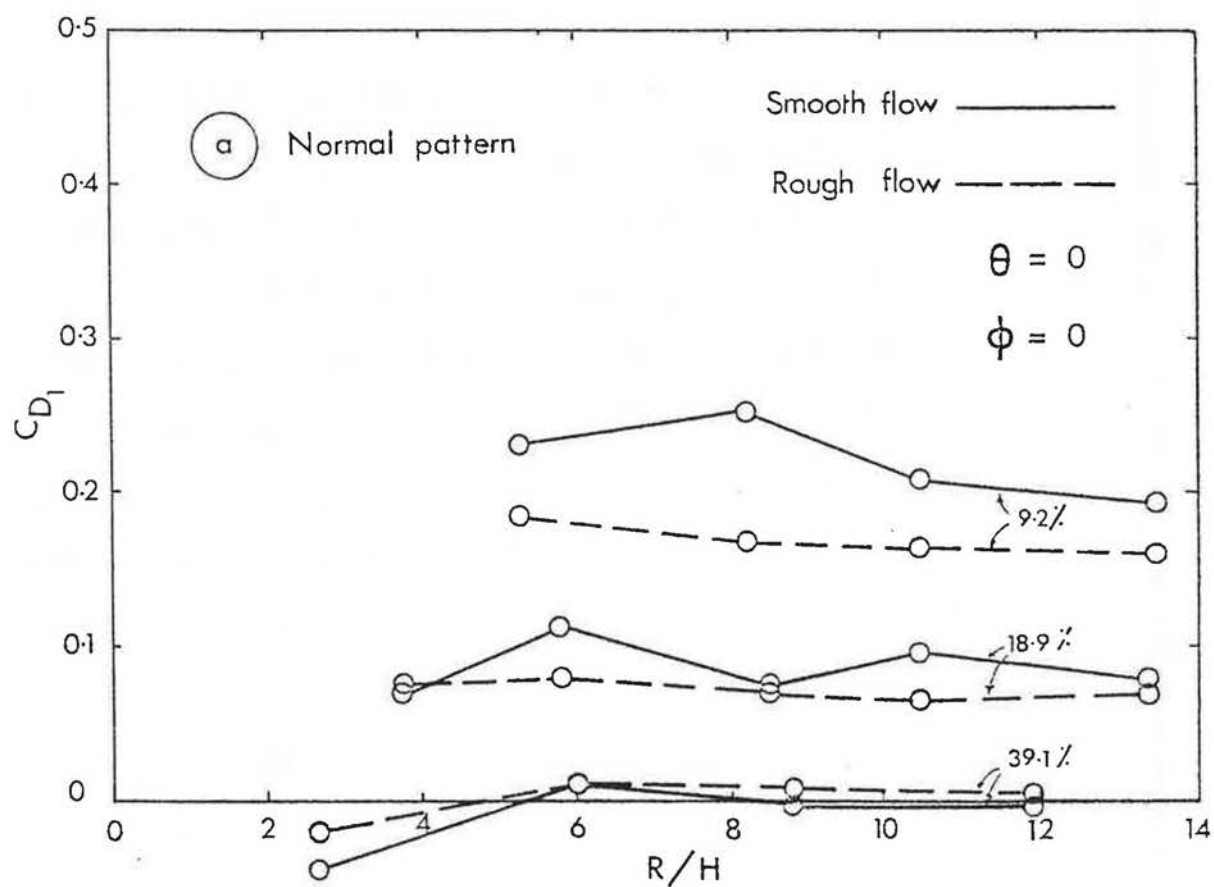


Figure 7.1 VARIATION OF C_{D1} WITH GROUP LAYOUT SIZE, R/H ($\theta = 0, \phi = 0$).

Figure 7.2. Due to the symmetry of layout pattern Figure 7.2 has been plotted for only the range $\phi = \pm 45^\circ$. It is evident from the figure that in the normal pattern, minimum values of C_{D1} are obtained at $\phi = 0$. Conversely, the staggered pattern showed a general trend of decreasing C_{D1} with increasing ϕ particularly at the higher density considered of this pattern, (18.9%). From the way C_{D1} changes with ϕ at the largest fetch in all cases, it may be concluded that the effect of ϕ decreases as the fetch increases.

7.1.4 The different values of C_{D1} obtained from varying ϕ were averaged at each value of R/H to yield the general effect of increasing the fetch on C_{D1} . This effect is shown plotted in Figure 7.3 for the normal and staggered patterns. The effect of varying the incident flow from smooth to rough is also shown. Comparing Figures 7.1 and 7.3 shows that the main effect of varying ϕ is limited only to the small values of R/H . The conclusion to be made from this part of the study is that longer fetches are required for lower densities, staggered patterns or thinner incident boundary layers.

7.2 The size of influence area around the central model

7.2.1 In the case of two dimensional roughness elements, there is only one dimension representing the group layout size, i.e. the length along the wind direction (fetch). The group layout size for three dimensional elements,

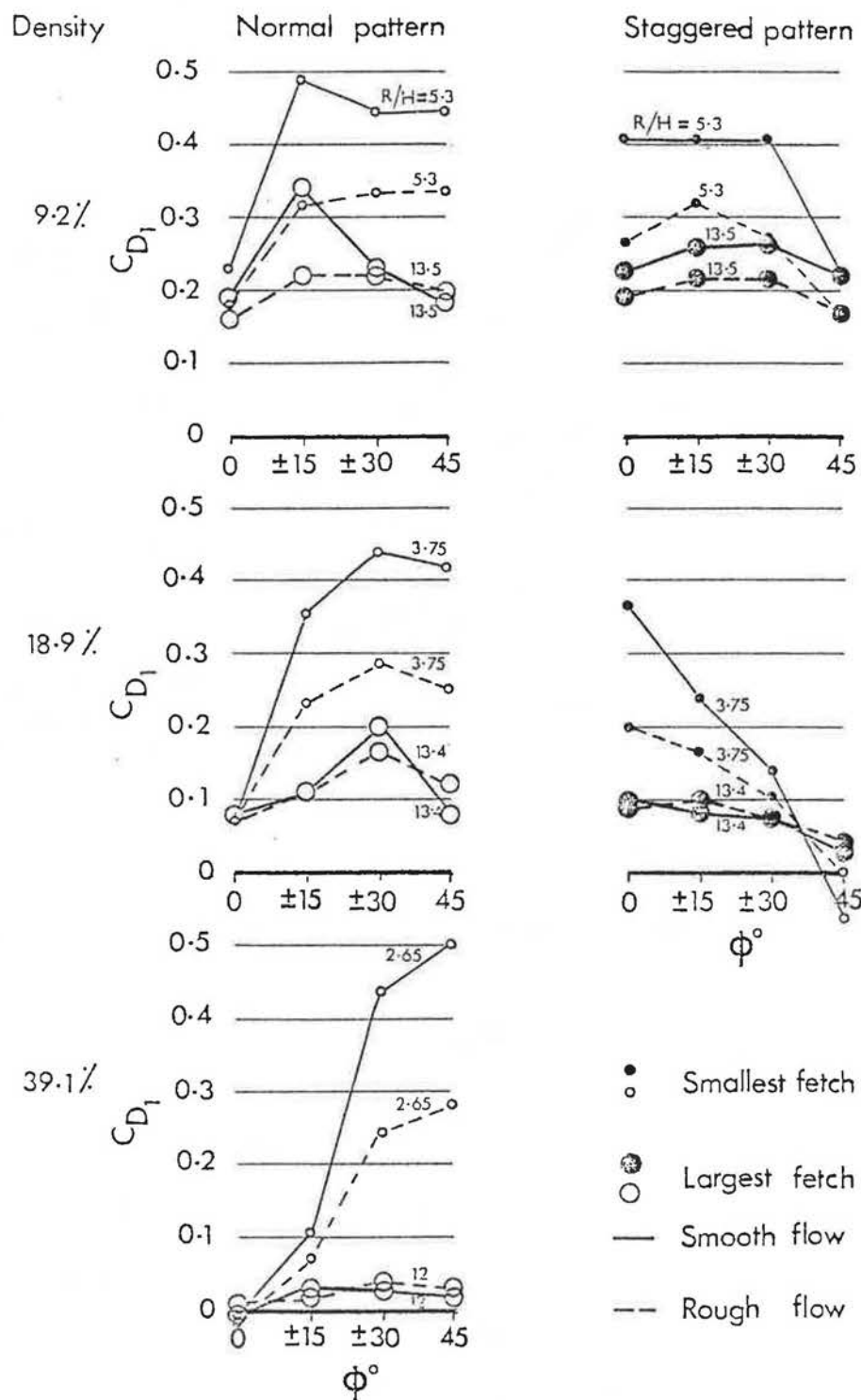


Figure 7.2 VARIATION OF THE MODEL DRAG WITH THE GROUP ANGLE ϕ AT THE EXTREME VALUES OF FETCH.

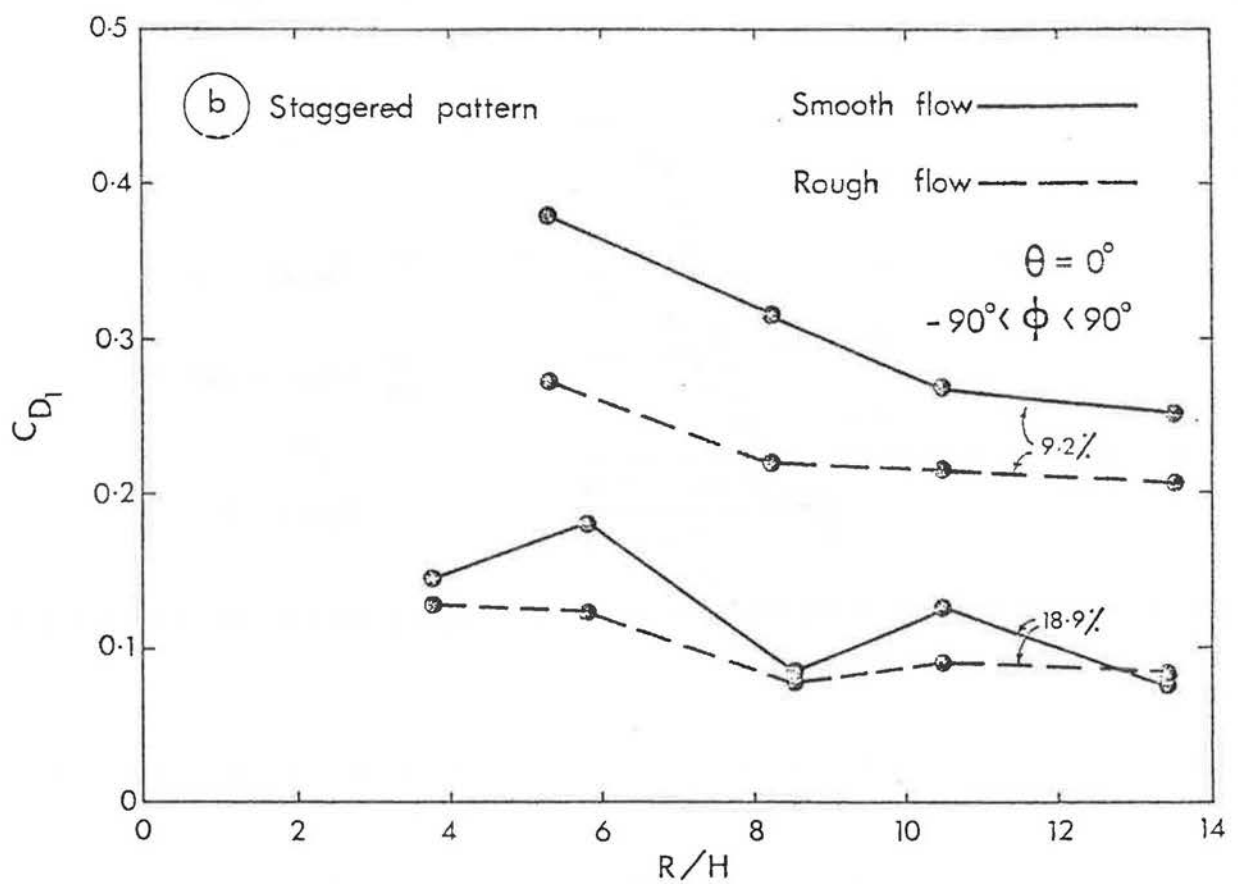
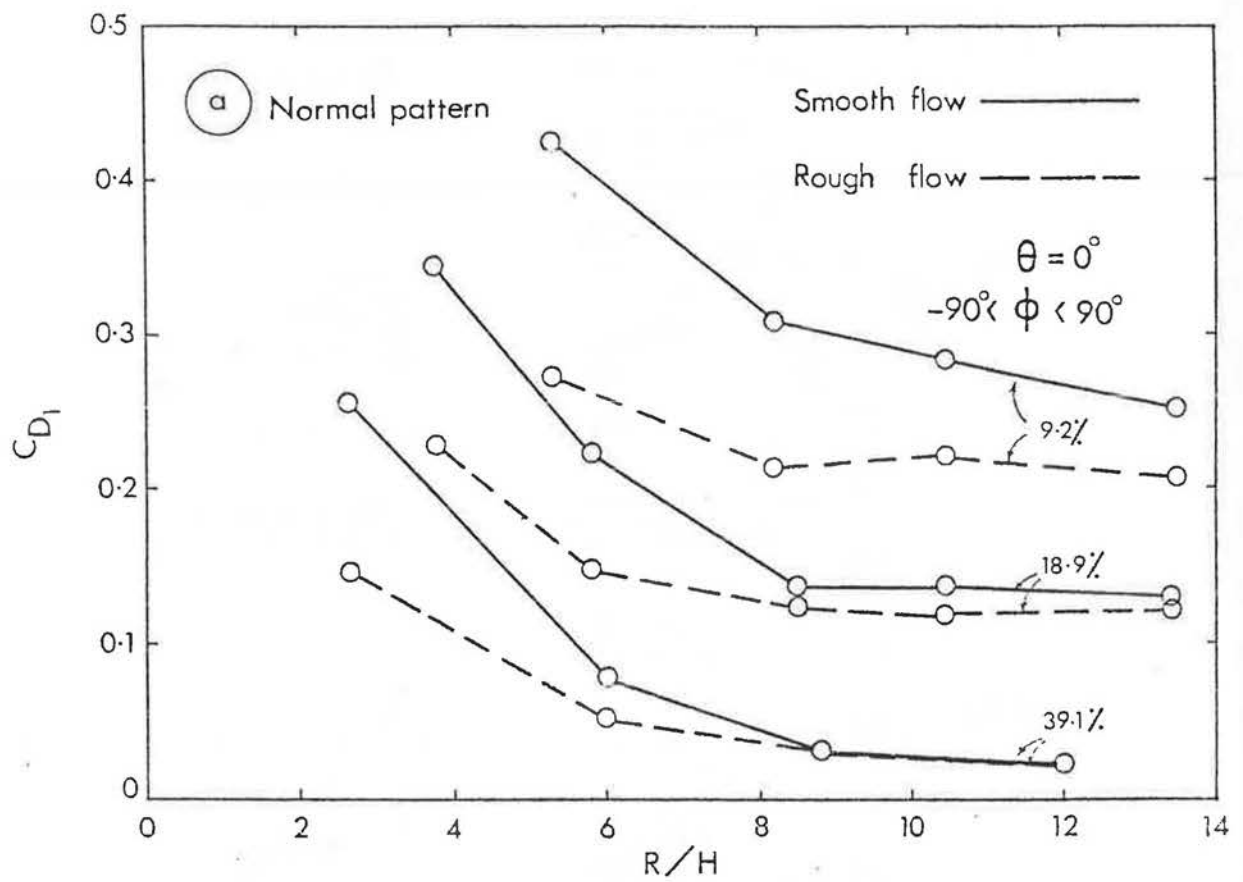


Figure 7.3 VARIATION OF C_{D1} WITH GROUP LAYOUT SIZE, R/H , ($\theta = 0^\circ$; $-90^\circ < \phi < +90^\circ$).

however, may be represented simply by a circle, as has been assumed in the present work. In the following part of the investigation an attempt is made to find out the actual form rather than the assumed circular form of the group layout that produces the stable value of C_{D1} obtained. For this purpose one case only was chosen as an example. This was the normal pattern of 9.2% density in the rough flow. The criterion was to remove all the surrounding model blocks that would produce a change of less than $\pm 5\%$ of the value of C_{D1} obtained for various values of ϕ . This limit was also extended to include a change of less than $\pm 10\%$. On the assumption that the blocks to the leeward of the central model would have the least contribution to the pressure forces on that model, the removal of the blocks started with the leeward-sector blocks of the outer ring ($R/H = 13.5$). The removal of blocks went on to the windward sectors followed in the same way to the inner rings.

7.2.2. During the experiment it was noted that the removal of either the windward or the leeward outer blocks resulted in an increase in the positive windward pressures and negative leeward pressures respectively. Therefore, the values of the pressure difference obtained may also be achieved by balancing the pressures on both faces, i.e. substituting the increase in either pressure by a decrease in the other. A small shift of the instrumented model in the flow direction within the influence zone would result in such balanced conditions. An example of this

case may be seen in Figure 7.4 where $\phi = 45^\circ$.

7.2.3 The results obtained for the layout sizes representing the influence area with $\pm 5\%$ and $\pm 10\%$ limits at $\phi = 0^\circ$, 15° , 30° and 45° are shown in Figure 7.4. It can be seen that the smallest layout size was obtained at $\phi = 0$ and the largest was at $\phi = 15^\circ$. This may be explained as follows. Since the pressure on both windward and leeward faces on the central model is expected to depend on the block spacing in the flow direction, this spacing is a minimum at $\phi = 0$ and maximum at $\phi = 15^\circ$. In between these extremes the influence zone takes an intermediate size.

7.2.4 It can be seen that the influence zone extends to a maximum at the windward side and slightly less to the leeward side. The minimum extension of the influence area at the side sectors normal to the flow suggest that the pressures on the model's windward and leeward wall, are influenced least of all by blocks in these sectors. A superposition of the influence areas obtained at the different values of ϕ has been performed to represent the likely influence area required for a random pattern in the same average density, see Figure 7.5. This figure shows a small difference in the areas representing the limits of $\pm 5\%$ and $\pm 10\%$, indicating that an appreciable difference would occur in the pressure forces if these limits are not taken into account. From this part of the investigation the following points may be concluded for buildings of equal height.

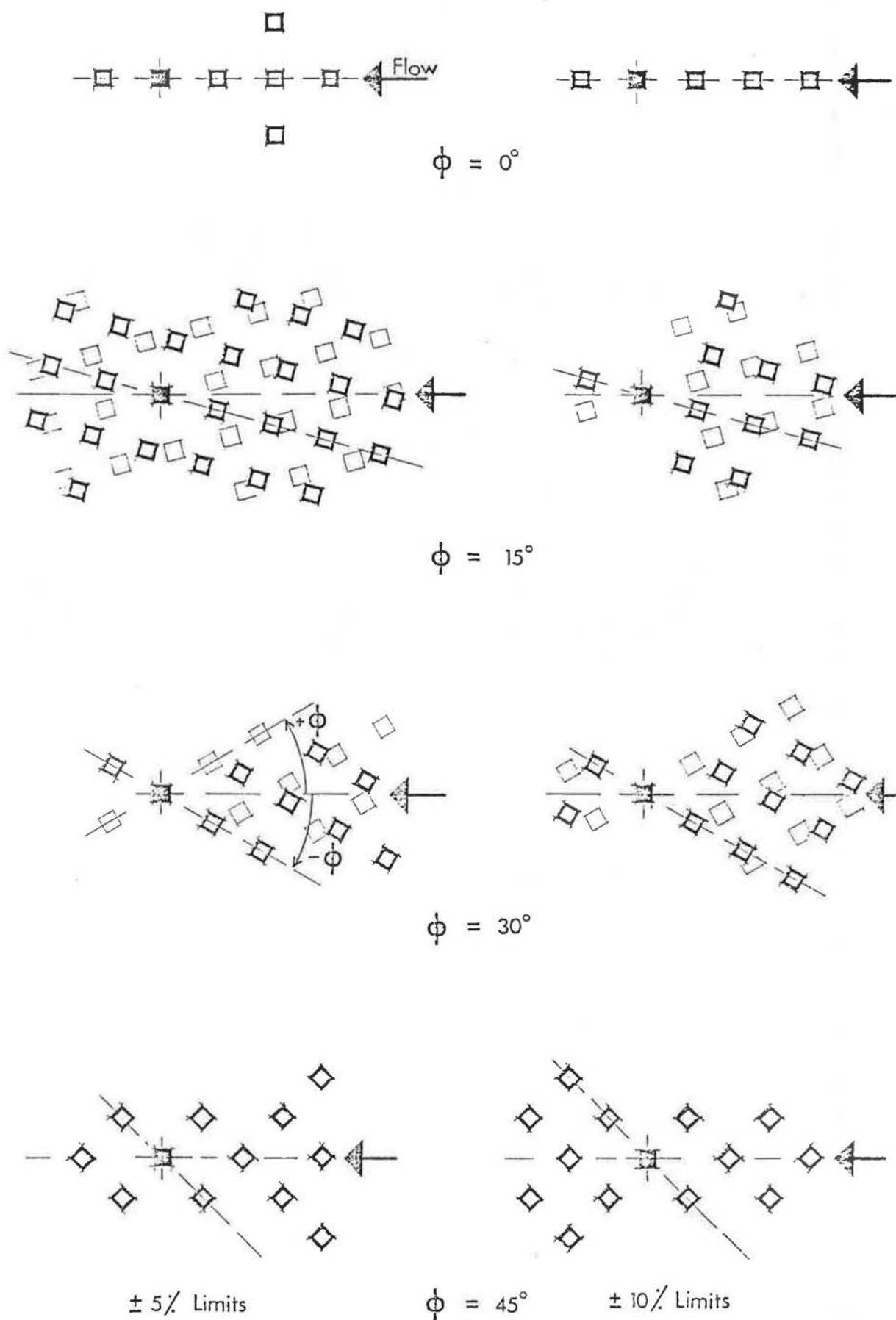


Figure 7.4 VARIATION OF THE INFLUENCE AREA WITH THE ANGLE OF THE SURROUNDING BLOCKS, ϕ .

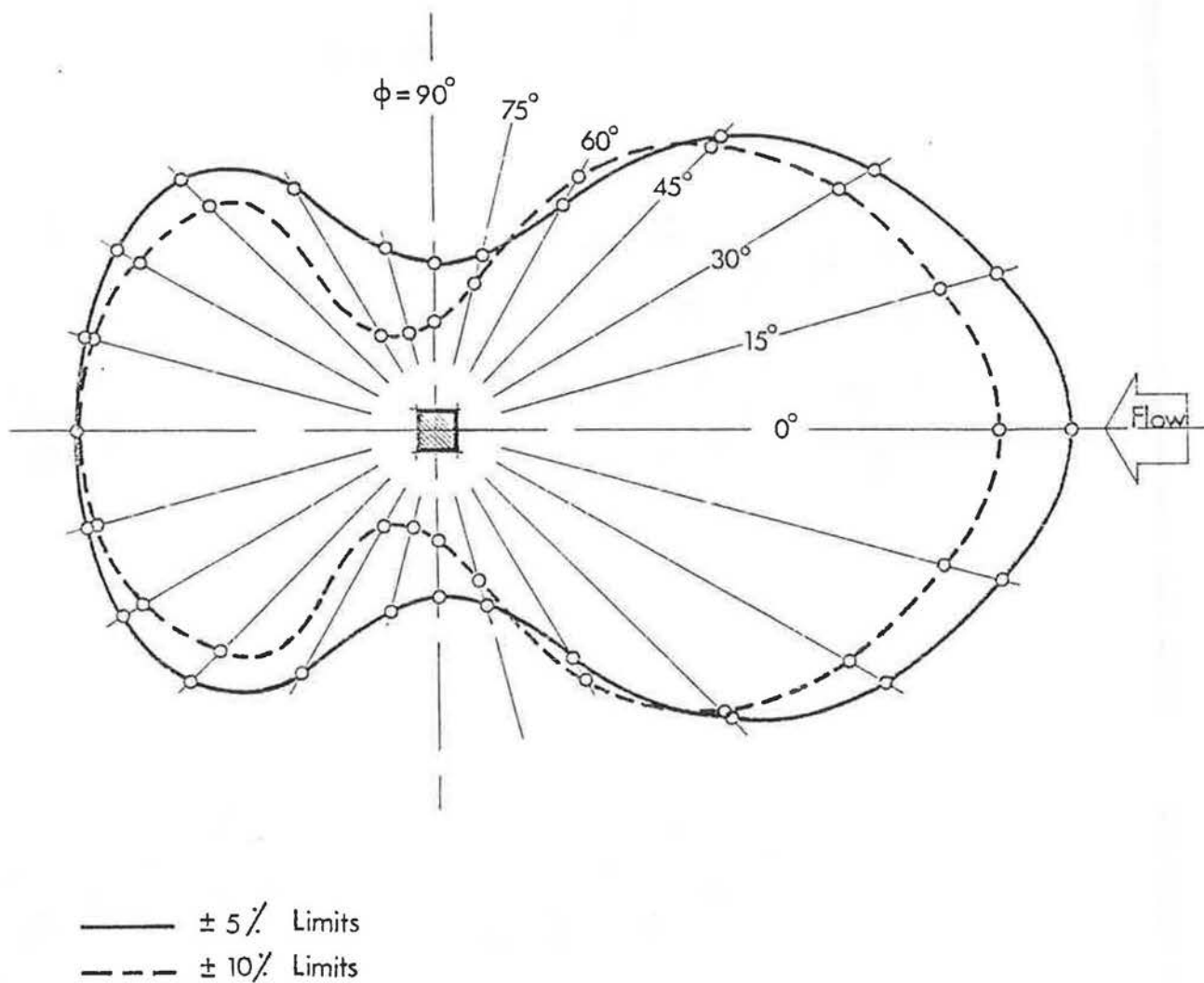


Figure 7.5 LIMITS OF THE INFLUENCE AREA ROUND THE MODEL.

- (i) The size of the influence area depends on the spacing between the buildings in the flow direction.
- (ii) The effect of the blocks at the side sectors, is minimal.
- (iii) The blocks that need modelling are neither a single row nor are they circular in the layout form. Instead they may be approximated to a foot-print shape.
- (iv) As this part of the investigation considered only one density, 9.2%, in the normal pattern and rough flow at $\theta = 0$, it might be expected that other variables will affect the size of influence area.

7.3. The effect of Density on the pressure forces

7.3.1 The pressure coefficient distributions on the windward and leeward faces of the isolated model in the two incident flows are shown in Figure 7.6. In Figures 7.7 to 7.10 pressure coefficient distributions are shown for the model in various layout densities and both patterns, normal and staggered, where $\phi = 0$ and $\theta = 0$. From these pressure distributions, the mean windward and leeward pressure coefficients were calculated, the difference of which yields the drag coefficient, C_{D1} , in each case.

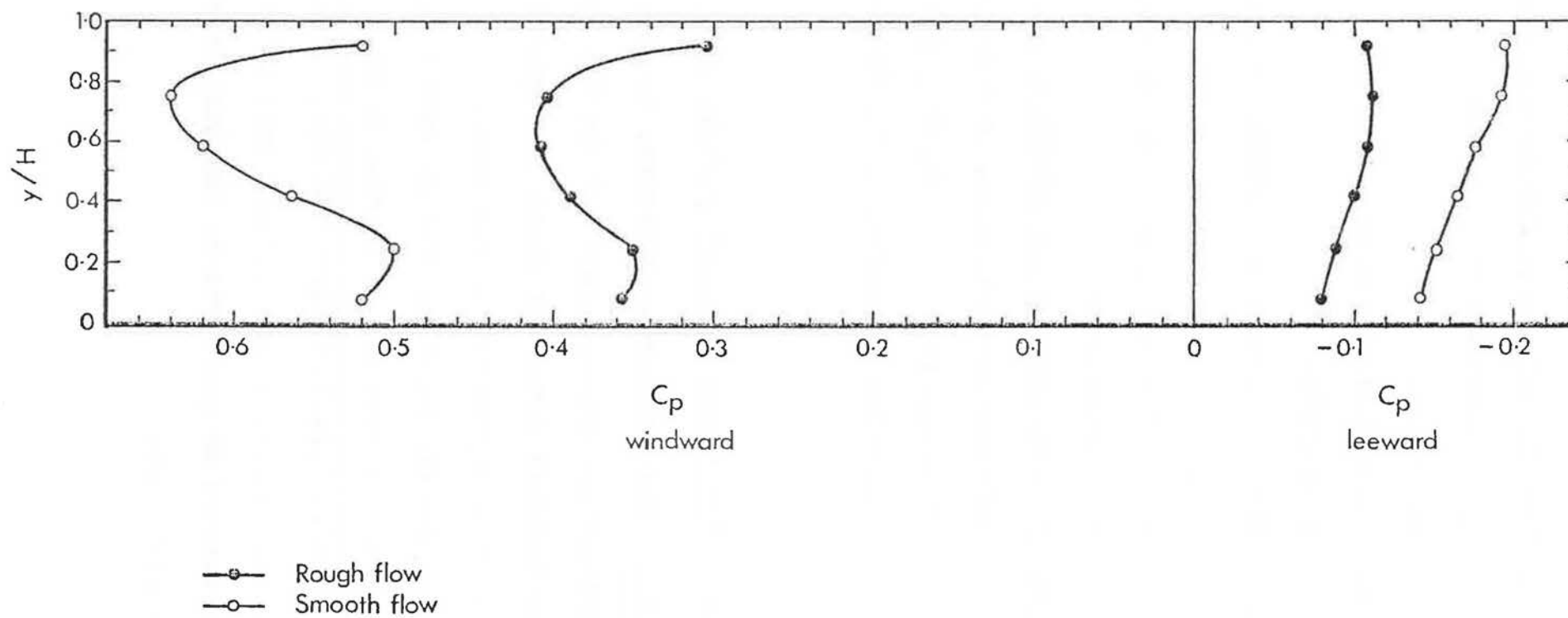


Figure 7.6 PRESSURE DISTRIBUTIONS ON THE ISOLATED MODEL.

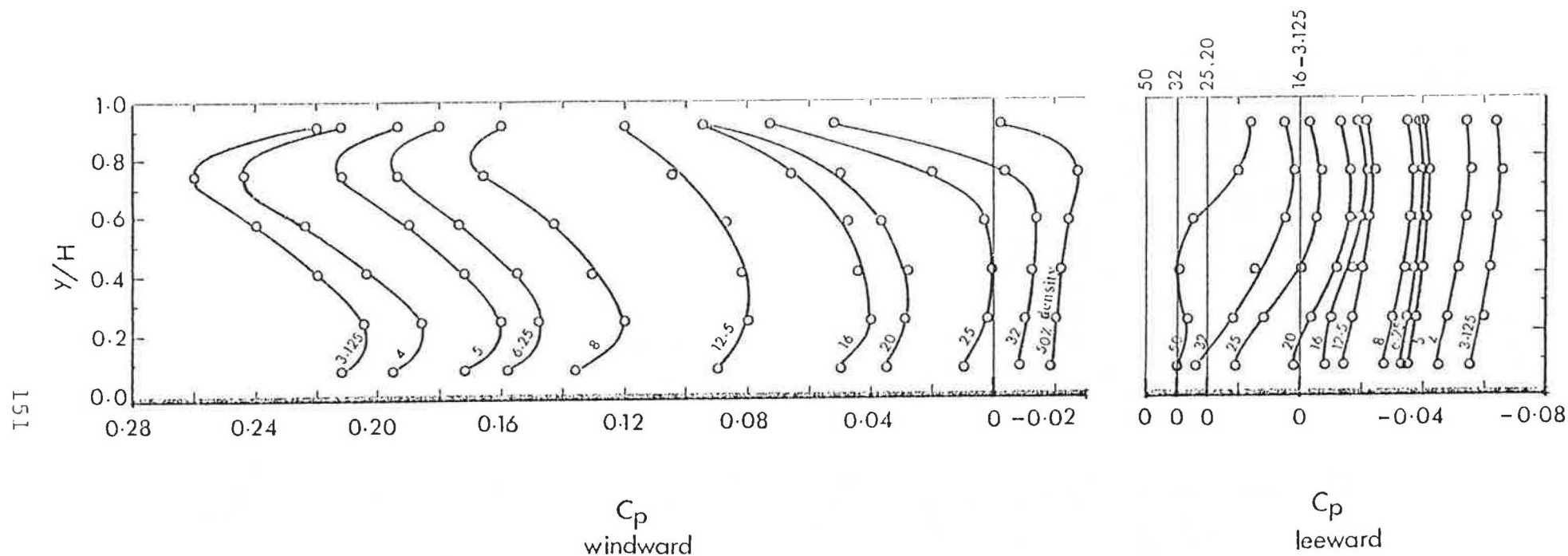


Figure 7.7 PRESSURE COEFFICIENT DISTRIBUTION ON THE MODEL CENTRE LINE AT VARIOUS DENSITIES, (normal pattern, rough flow).

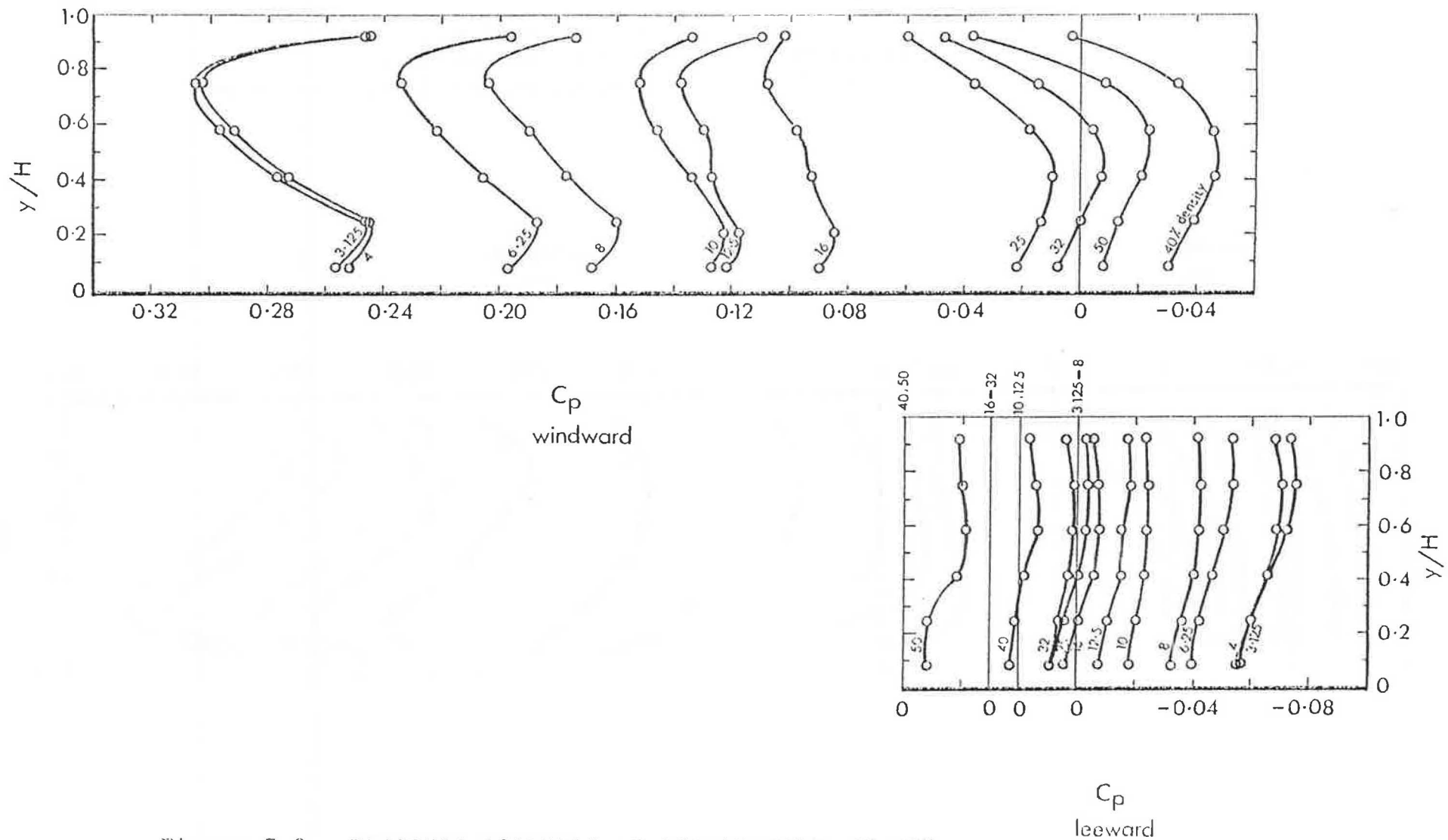


Figure 7.8 PRESSURE COEFFICIENT DISTRIBUTION ON THE MODEL CENTRE LINE AT VARIOUS DENSITIES, (staggered pattern, rough flow).

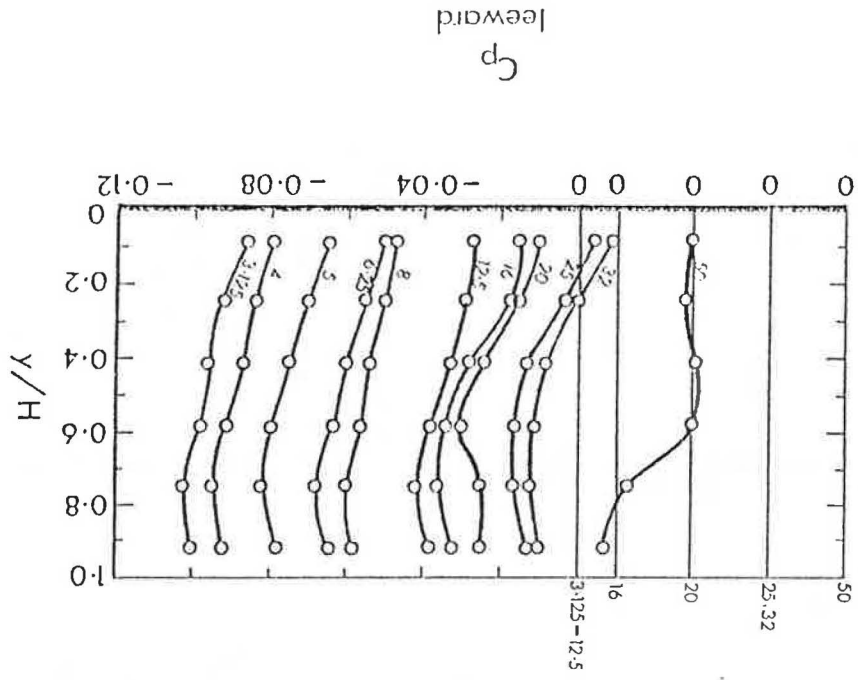
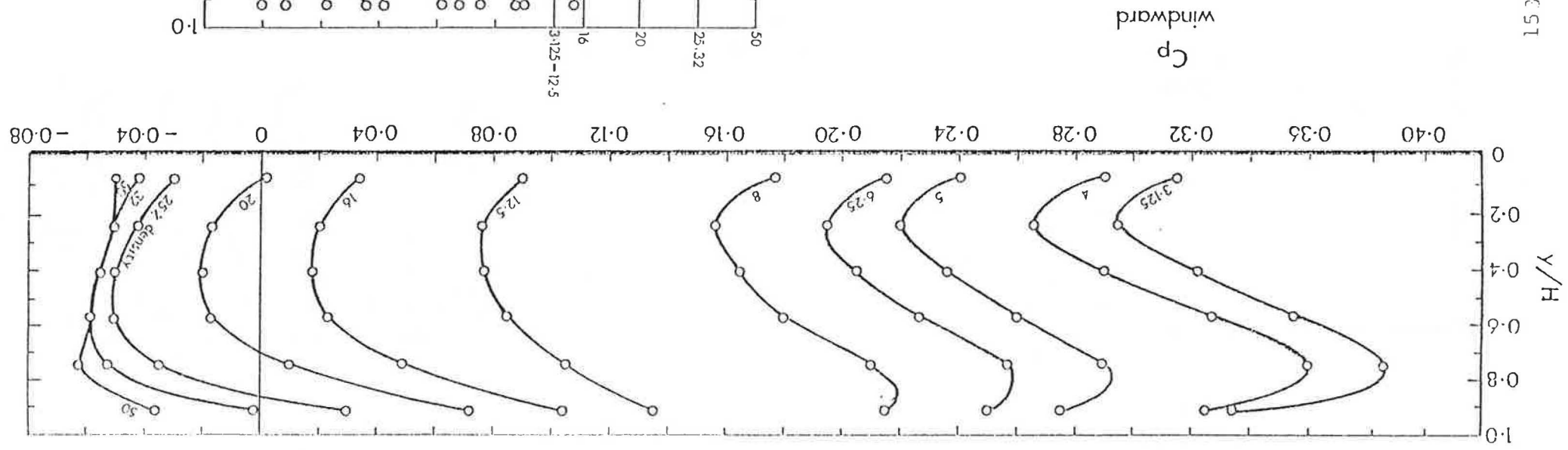


Figure 7.9 PRESSURE COEFFICIENT DISTRIBUTION ON THE MODEL CENTRE LINE AT VARIOUS DENSITIES, (normal pattern, smooth flow)

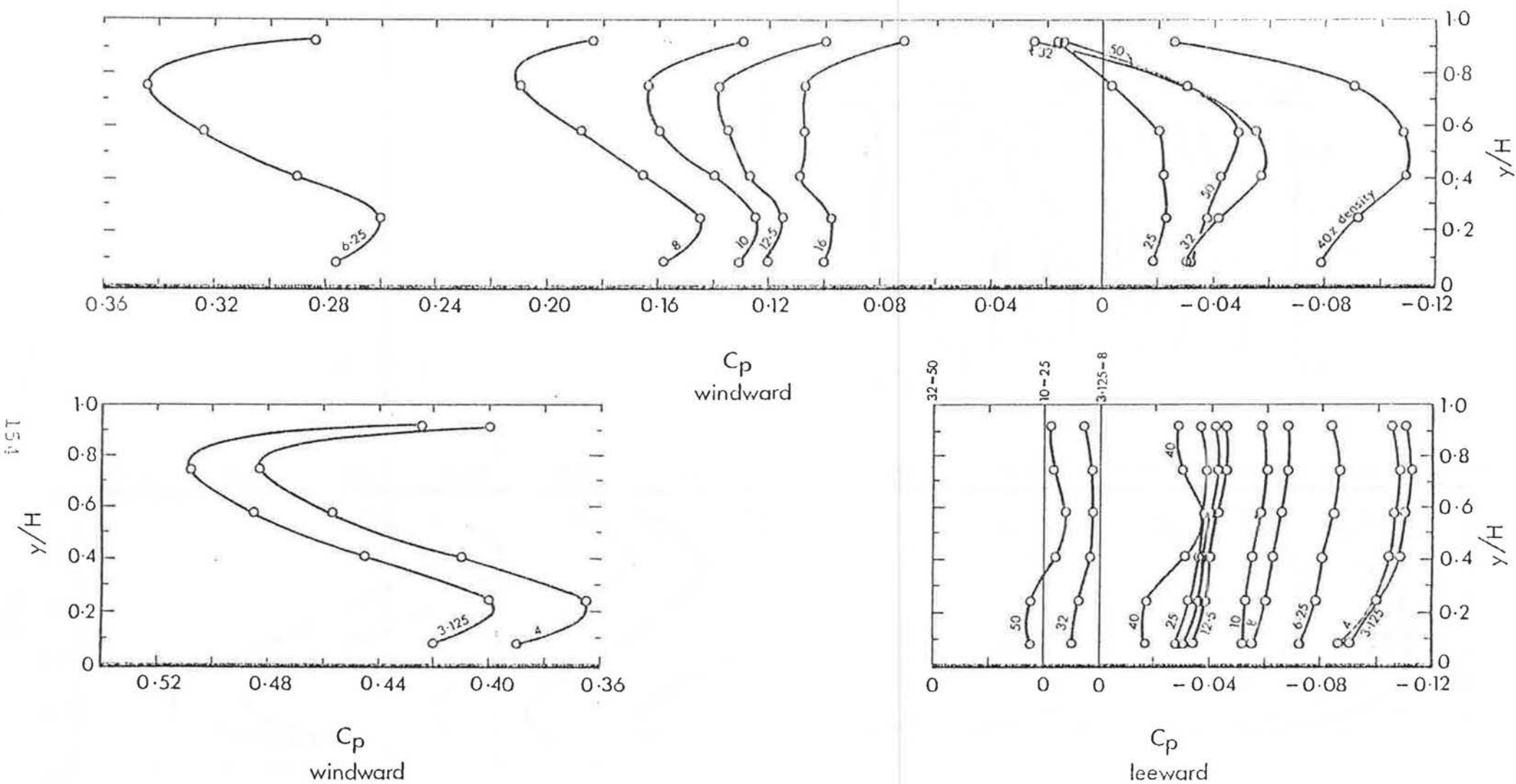


Figure 7.10 PRESSURE COEFFICIENT DISTRIBUTION ON THE MODEL CENTRE LINE AT VARIOUS DENSITIES, (staggered pattern, smooth flow).

7.3.2 In an earlier investigation of the flow over three dimensional cylindrical roughness elements, Marshall (1971) showed that a linear relationship existed between the element drag coefficient, C_{D_1} , and $1/(\lambda_f)^{1/2}$, a function of the element density. Despite the fact that the results quoted by Marshall had a large degree of scatter and that they showed no evidence to support the existence of different flow regimes, the proposal of such a linear relationship is nevertheless of value. In Figure 7.11 the variation of the mean windward and mean leeward pressure coefficients as well as the drag coefficient, C_{D_1} , as a function of S/H in the rough flow case for the normal pattern is shown. The corresponding variation for the staggered pattern is shown in Figure 7.12 while the smooth flow results for both patterns are shown in Figures 7.13 and 7.14. The spacing parameter S/H , is equal to $(\frac{1}{\lambda})^{1/2}$ for the normal layout pattern and $(\frac{2}{\lambda})^{1/2}$ for the staggered layout pattern. In Figure 7.11 the variation of the windward pressure coefficient, C_{p_w} , with S/H shows a broken straight line relationship to exist. The figure also shows another straight line relationship to exist for the variation of the leeward wall pressure coefficient, C_{p_l} , over the range of $S/H > 2.5$. A sudden decrease may be seen in C_{p_l} at $S/H = 2.25$ followed by gradual increase at smaller values of S/H . The variation of C_{D_1} in the same figure reflects these changes in the form of a broken straight line and a jump followed by gradual decrease until the value of C_{D_1} approaches zero.

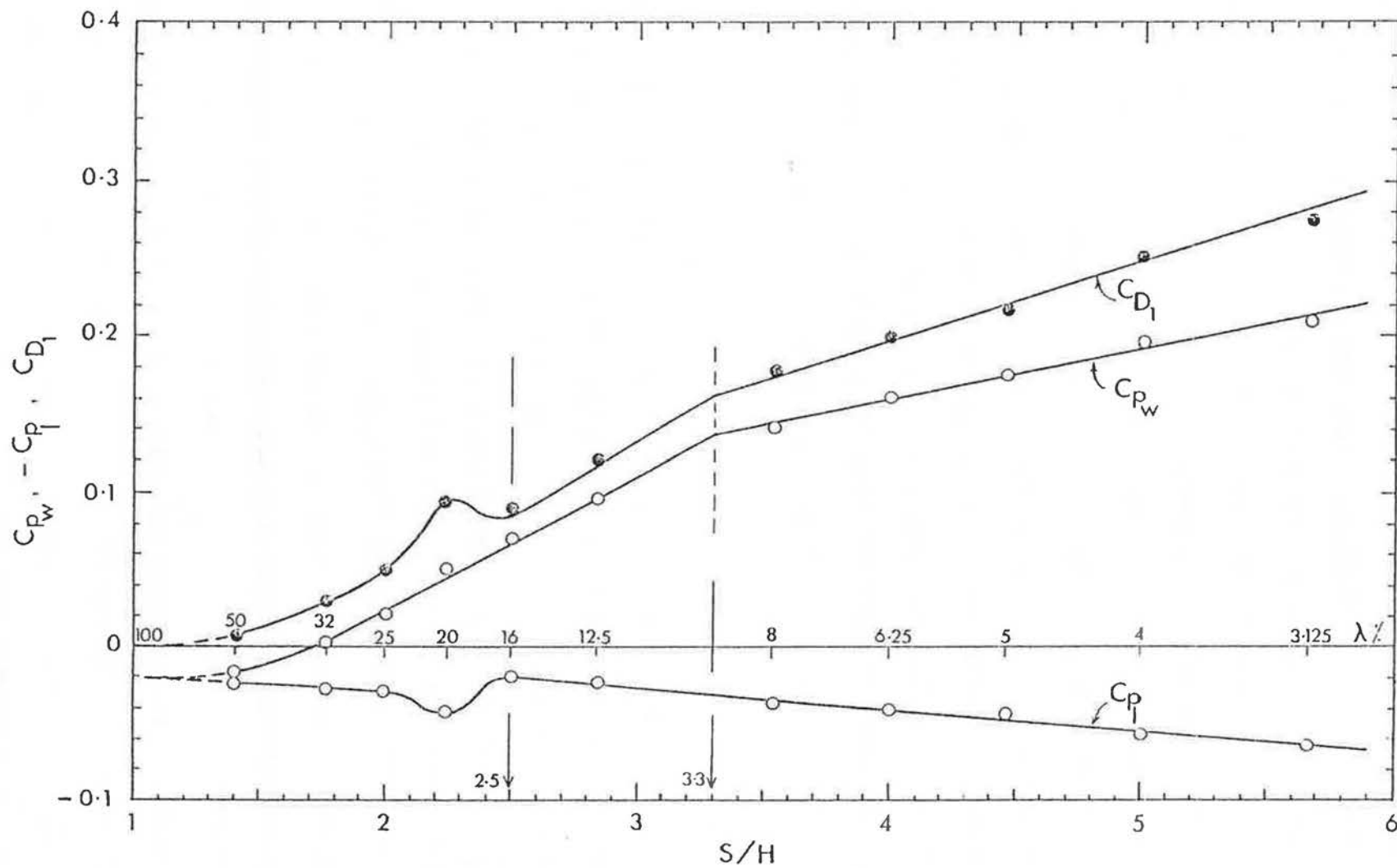


Figure 7.11 VARIATION OF THE WALL PRESSURES AND THE DRAG FORCE WITH THE CUBE SPACING. (normal pattern, rough flow).

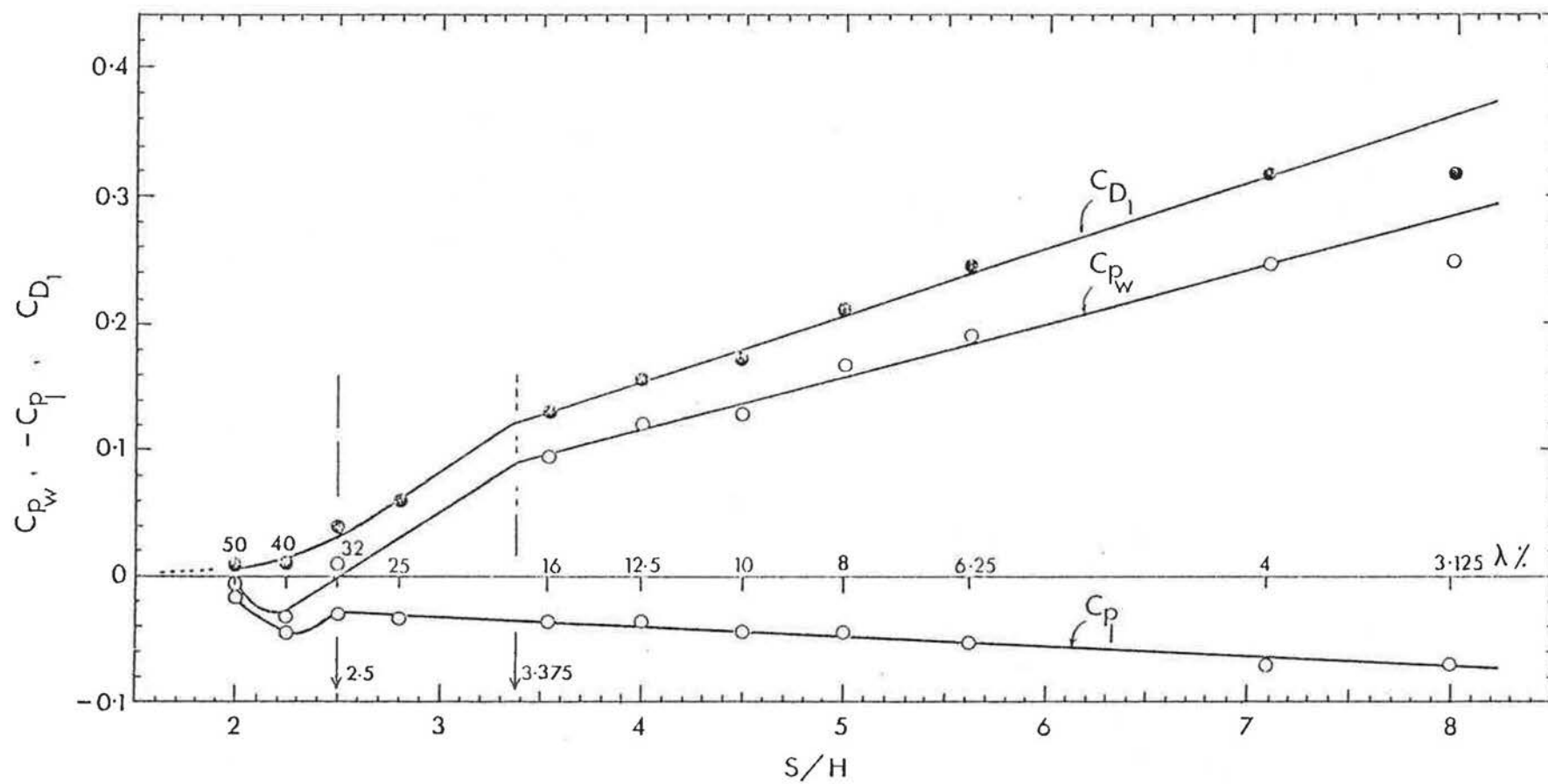


Figure 7.12 VARIATION OF THE WALL PRESSURES AND THE DRAG FORCE WITH THE CUBE SPACING. (staggered pattern, rough flow).

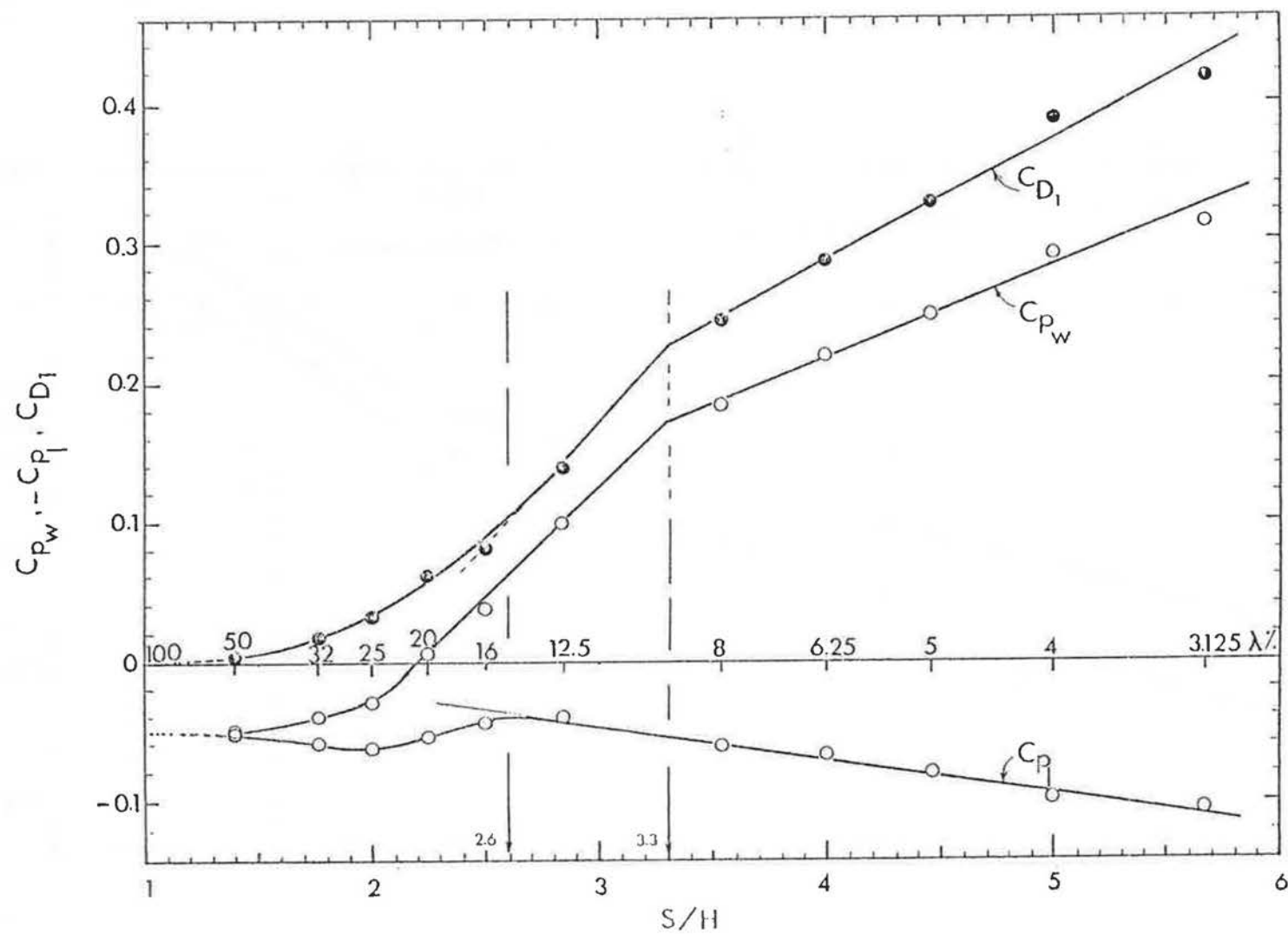


Figure 7.13 VARIATION OF THE WALL PRESSURES AND THE DRAG FORCE WITH THE CUBE SPACING, (normal on flow, smooth flow).

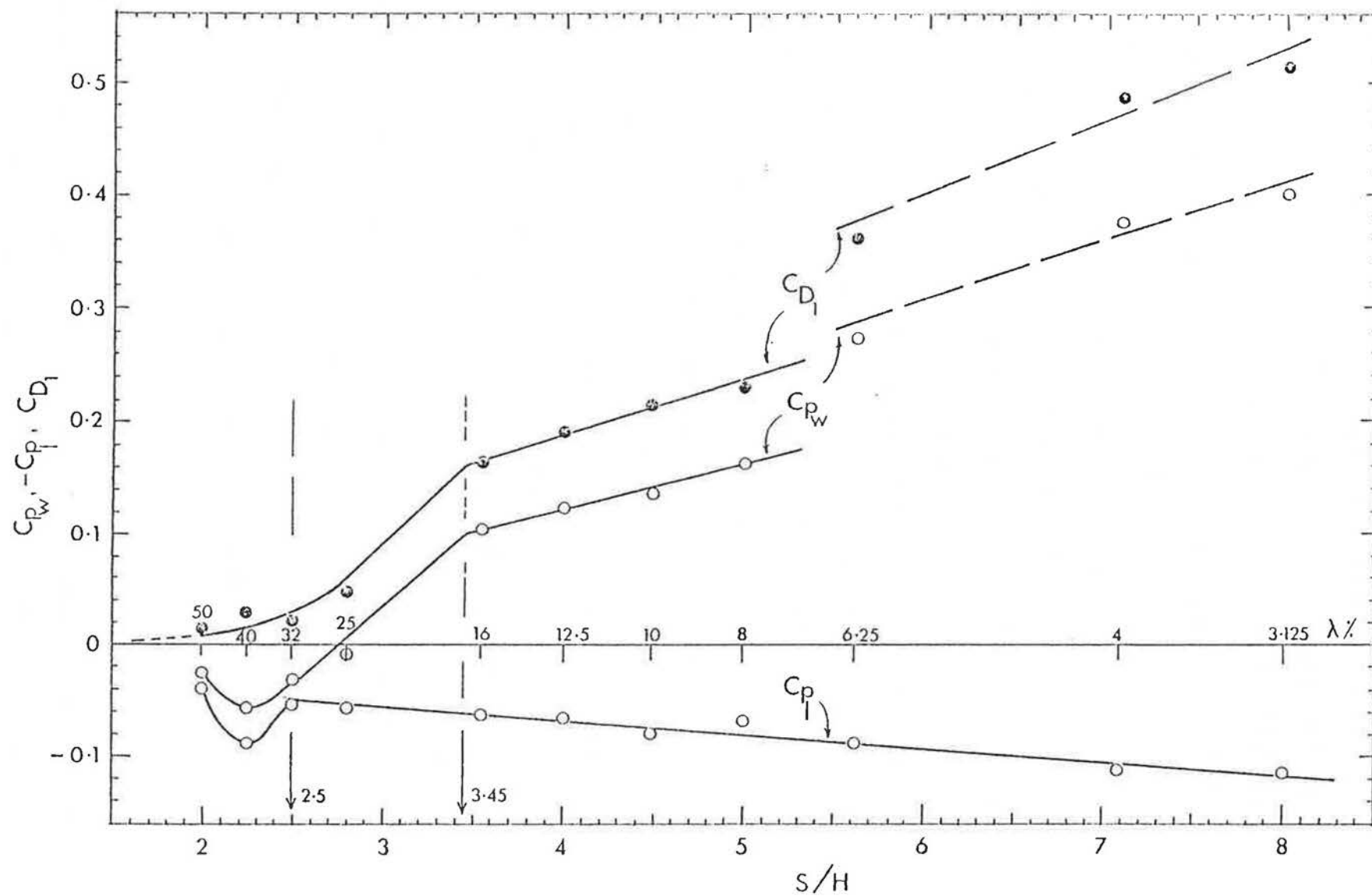


Figure 7.14 VARIATION OF THE WALL PRESSURES AND THE DRAG FORCE WITH THE CUBE SPACING, (staggered pattern, smooth flow).

Comparing the variations of C_{p_w} , C_{p_1} and C_{D_1} with S/H for the normal and staggered patterns in Figures 7.11 and 7.12 prompts two immediate conclusions. First, the behaviour of C_{p_w} and C_{p_1} is similar for the two patterns and second, the break point and the jump occur at the same value of S/H , i.e. $S/H \approx 3.3$ and $S/H \approx 2.25$ respectively. However, it may be noted that the jump of C_{p_1} in the staggered pattern is not reflected in the resulting C_{D_1} line due to the small value of C_{p_w} at that point. The corresponding variation of C_{p_w} , C_{p_1} and C_{D_1} for the two patterns in the smooth incident flow shown in Figures 7.13 and 7.14 indicate that a similar pattern of behaviour also occurs giving the break points at $S/H = 3.3$ and $S/H = 3.45$ for the normal and staggered patterns respectively. The jump in C_{p_1} (which is more gradual for the normal pattern than the staggered pattern in this flow) occurred at $S/H < 2.5$ and $S/H < 2.7$ for the staggered and normal patterns respectively. For the staggered pattern in the smooth incident flow, the high values of C_{p_w} at large spacing ($S/H > 5$) i.e. low densities did not correlate with the linear relationship as can be seen in Figure 7.14. This may be explained by the greater fetch required for stabilization in this particular case indicated to earlier in Figure 7.1.

7.3.3 On the basis by which the different flow regimes are defined in paragraph 5.4.1, it is postulated that with reference to Figures 7.11 - 7.14, the regimes may each be characterised by a different rate of change of the model wall pressures, C_{p_w} and C_{p_1} with spacing. On this basis

the above figures are then analysed as follows:

- (a) The isolated roughness flow regime corresponds to a spacing of $S/H > 3.3$ for the normal pattern in both smooth and rough flows, i.e. $\lambda < 9.2\%$. The corresponding values for the staggered pattern in the rough and smooth flows are $S/H > 3.37$ and 3.45 respectively, i.e. $\lambda < 17.6\%$ and 16.8% .
- (b) The skimming flow regime corresponds to an element spacing of $S/H < 2.5$ for all cases, i.e. $\lambda > 16\%$ and 32% for the normal and staggered patterns respectively in both incident flows.
- (c) The wake interference flow regime corresponds to an element spacing of $2.5 < S/H < 3.3$ for the normal pattern in both incident flows, i.e. $9.2\% < \lambda < 16\%$. The corresponding values for the staggered pattern in the rough and the smooth flows are $2.5 < S/H < 3.37$ and $2.5 < S/H < 3.45$ i.e. $17.6\% < \lambda < 32\%$ and $16.8\% < \lambda < 32\%$ respectively.

This classification of the flow regime by spacing, or density is supported by further evidence in later sections of the thesis.

7.3.4 From their investigations of the wake structure of an isolated cube in a turbulent boundary layer, Castro and Robins (1975) have shown that the reattachment distance for the downstream separation region occurs at a distance of $1.5H$ from the rear face. This is comparable with a distance of $1.53H$ and $1.59H$ determined from the present

investigation by the surface flow visualization of an isolated cube in a rough and a smooth flow respectively (Figures 7.15 and 7.16). If the upstream separation region lengths, which were similarly found to be $0.83H$ and $0.95H$ respectively, are added, then the total spacing between elements before flow interference occurs is $3.36H$ and $3.54H$ for the rough and smooth flows respectively. These values are in good agreement with the spacing of $3.3H$ and $3.37H$ (rough flow, Figures 7.11 and 7.12) and of $3.3H$ and $3.45H$ (smooth flow, Figures 7.13 and 7.14) at which the change of regime from isolated flow to wake interference flow was suggested. The change from the wake interference flow regime to the skimming flow regime may be explained as follows. In the work of Tani, Iuchi and Komoda (1961) for the flow over two-dimensional grooves, they were classified as deep or shallow grooves according to the flow behaviour. The deep groove behaviour is similar to the skimming flow over roughness in that a stable vortex within the groove was obtained. It was found that this behaviour occurs at a ratio of $b/H = 1.4$ where b is the groove breadth in the flow direction and H is the groove height. This value is equivalent to a value of $S/H = 2.4$ in the present work since b is equivalent to the clear spacing between cubes. Furthermore, the leeward groove - wall pressures reflected an increase when the vortex started to develop at $b/H = 1.4$ followed by gradual decrease. A replot of these results is given in Figure 7.17. On these grounds it is possible to explain the variation

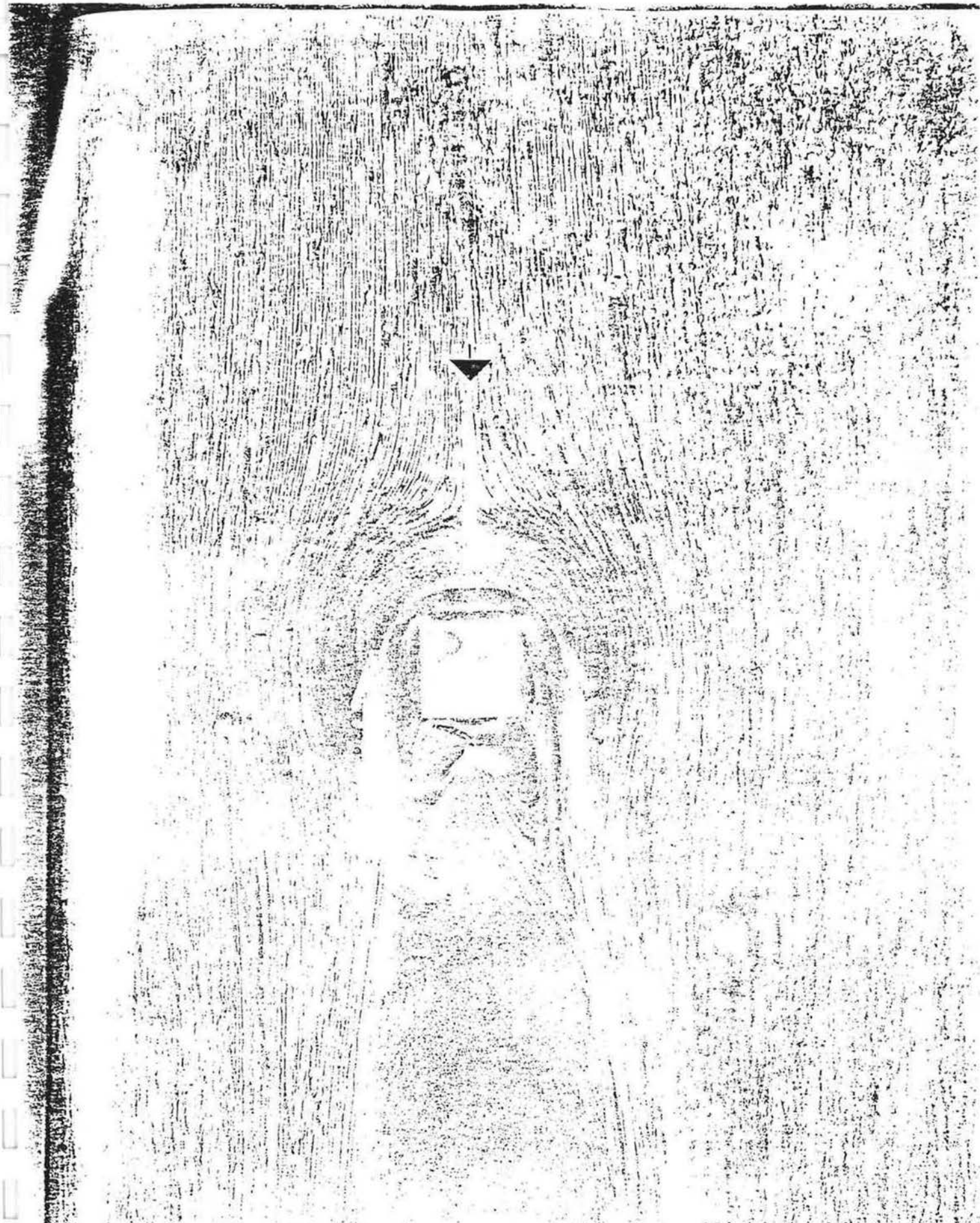


Figure 7.15 SURFACE FLOW VISUALIZATION OF THE
ISOLATED CUBE, (smooth flow).



Figure 7.16. SURFACE FLOW VISUALIZATION OF THE
ISOLATED CUBE, (rough flow).

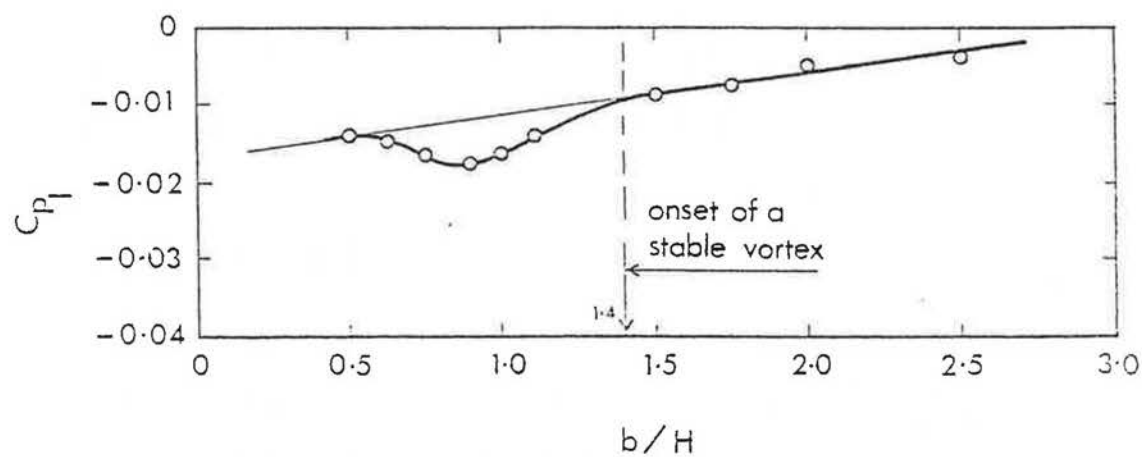


Figure 7.17 A REPLOT OF THE RESULTS OF TANI et. al. (1961) FOR THE LEEWARD GROOVE-WALL PRESSURE, C_{p1} .

of the leeward wall pressures C_{p_1} at $S/H < 2.5$ by the initiation of a stable vortex, a characteristic of the skimming flow regime. It is interesting to find that the values of b/H and S/H for the skimming flow over two-dimensional grooves and over cubes are in such good agreement i.e. 2.4 and 2.5 respectively. However, the maximum value of the negative pressure due to the vortex formation occurred at approximately $S/H = 2.25$ in the present work. These values differ from the value of $b/H = 0.875$ (which is equivalent to $S/H = 1.875$) given by Tani et. al. at which the negative pressures were maximum.

7.3.5 For an infinitely extending rough surface in which the model represents a typical roughness element then the effective local skin friction coefficient C'_{f_e} , may be calculated thus,

$$C'_{f_e} = C_{D_1}/A = C_{D_1} \cdot \lambda_f$$

assuming that the frictional drag on the intervening surface is negligible compared with the form drag of the elements themselves. The effective skin friction coefficient, C'_{f_e} , is shown plotted against the element density, λ_f , in Figure 7.18 for both normal and staggered patterns in the rough flow. The corresponding results for the same patterns in the smooth flow are also shown in Figure 7.19. The results of Koloseus and Davidian (1966) for the variation of K_s with λ_f , given in Figure 5.5 for an array of cubes, showed a similar variation. It is suggested that the interpretation of Wooding, Bradley

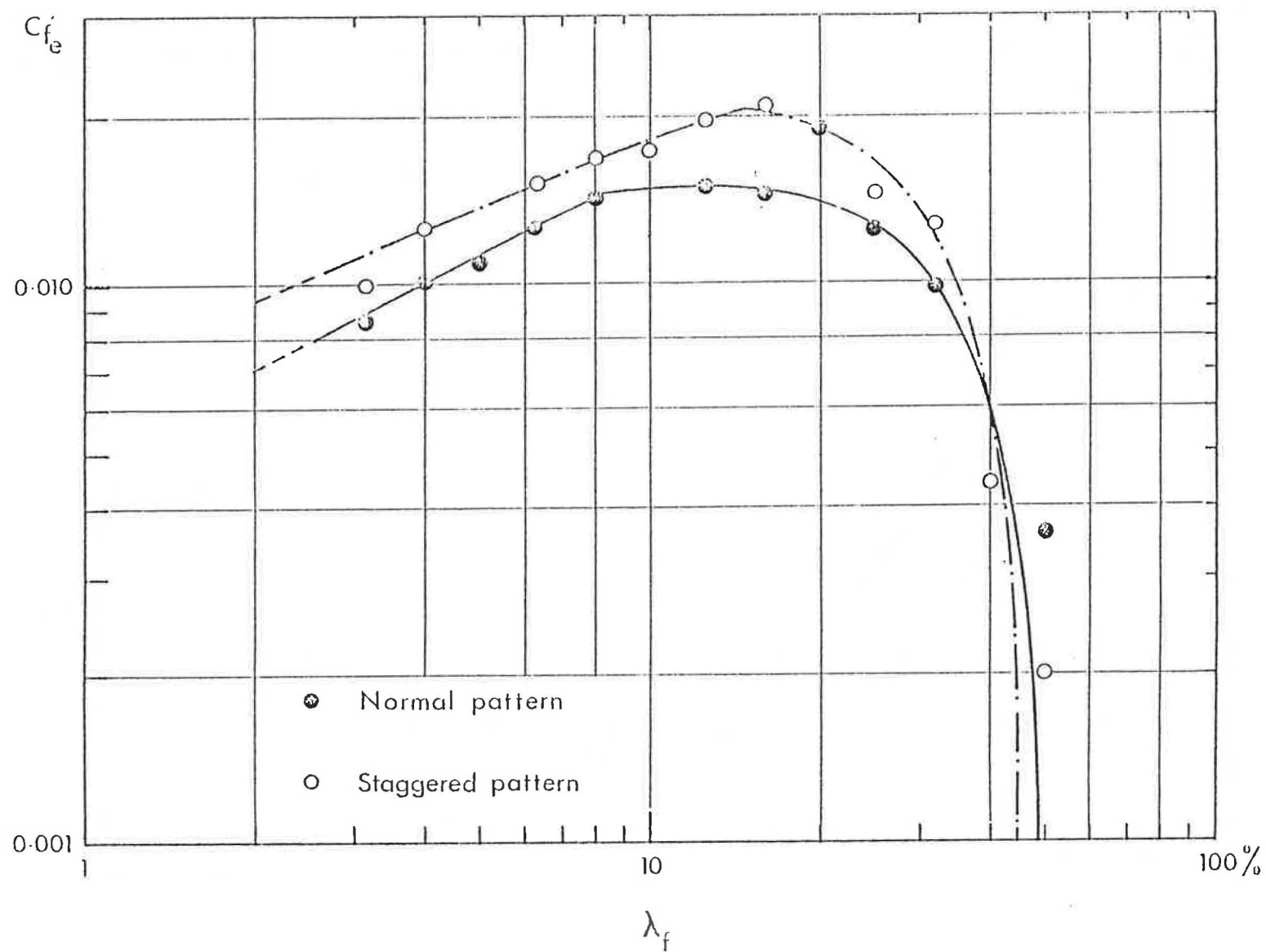


Figure 7.18 VARIATION OF THE EFFECTIVE SKIN FRICTION COEFFICIENT WITH DENSITY, (rough flow).

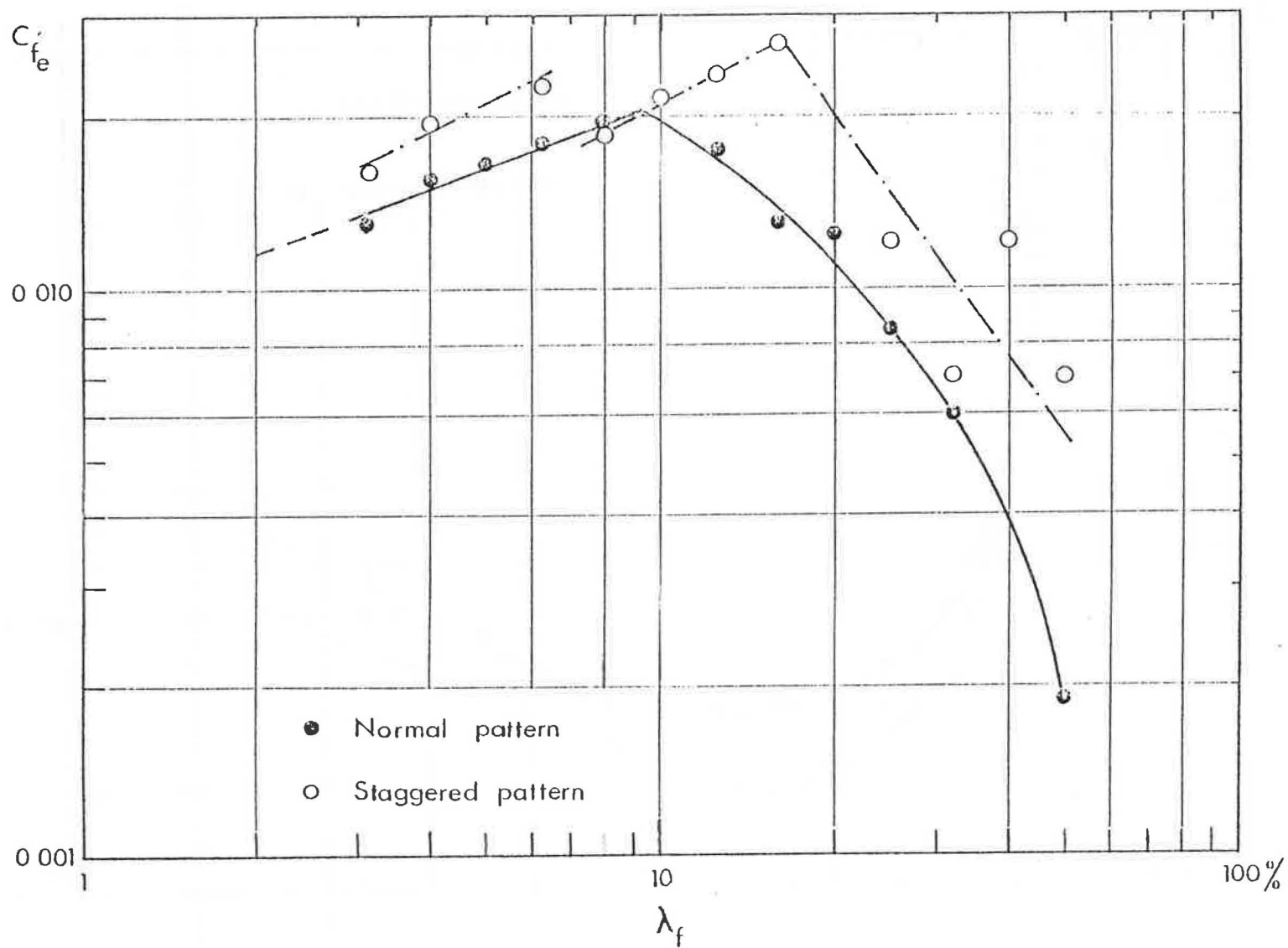


Figure 7.19 VARIATION OF THE EFFECTIVE SKIN FRICTION

and Marshall (1973) to this type of data presentation (see Chapter 5) indicates that the initial linear increase of $\log C'_{fe}$ with $\log \lambda_f$ represents the isolated roughness flow regime, the subsequent levelling off and slow decrease of the curve represents the wake interference flow regime and the final sharp cut-off represents the skimming flow regime. The values of the group density at which these changes of flow regime occur can be seen from Figures 7.18 and 7.19 to agree with those suggested by Figures 7.11 to 7.14. The results of Koloseus and Davidian postulate that the change of flow regime from isolated flow to wake interference flow for their staggered pattern would occur at $\lambda_f = 12.5\%$ compared with $\lambda_f = 17.6\%$ and 16.8% for the rough and smooth flows respectively in the present investigation.

7.3.6 The pressure distributions on the model shown in Figures 7.7 to 7.10 suggest that a grouping according to the variation of the mean wall pressure coefficients with S/H would result in a reasonable collapse of the data. This means that the windward wall pressures would be divided into two groups, i.e. the first corresponding to $S/H > 3.3$ (isolated roughness flow) and the second corresponding to $S/H < 3.3$ (wake interference and skimming flow). On the other hand, the leeward wall pressures would be divided into a group for $S/H > 2.5$ (isolated roughness flow and wake interference flow) and the other for $S/H < 2.5$ (for the skimming flow regime). When this grouping was performed by shifting the zeros, the

pressures collapsed as a family of self similar profiles within each group. This classification is shown in Figure 7.20 for the normal and staggered patterns in both flows. It may be noted that the pressure distributions of the windward wall at the highest densities in some cases (32% and 50% normal pattern, rough and smooth flows) showed a flattening pressure distribution at the lower part of the model. This type of distribution was also noted for the flow over slots, Roshko (1955), Tani et. al. (1961) and was explained by the existence of more than a single vortex in the narrow cavity though relatively weaker than the single vortex in the square cavity.

7.3.7 The similarity of shape and collapse of the data conform to the universal shape functions suggested by Schofield, Perry and Jonbert (1974) for the pressure distributions on the windward and leeward faces of two-dimensional square section roughness elements in the wake interference flow and skimming flow regimes. These shape functions were, however, for only one value of the roughness density in each of the two flow regimes. The present investigation enables this definition of a pressure profile shape function to be extended to the isolated flow regime. In this regime the windward face pressure distribution takes the form of an "S" shape, similar to the form found for an isolated rectangular body in a turbulent boundary layer.

7.3.8 The method of normalizing the windward pressures using the maximum pressure, suggested by Good and Joubert (1968) was also attempted. Although this

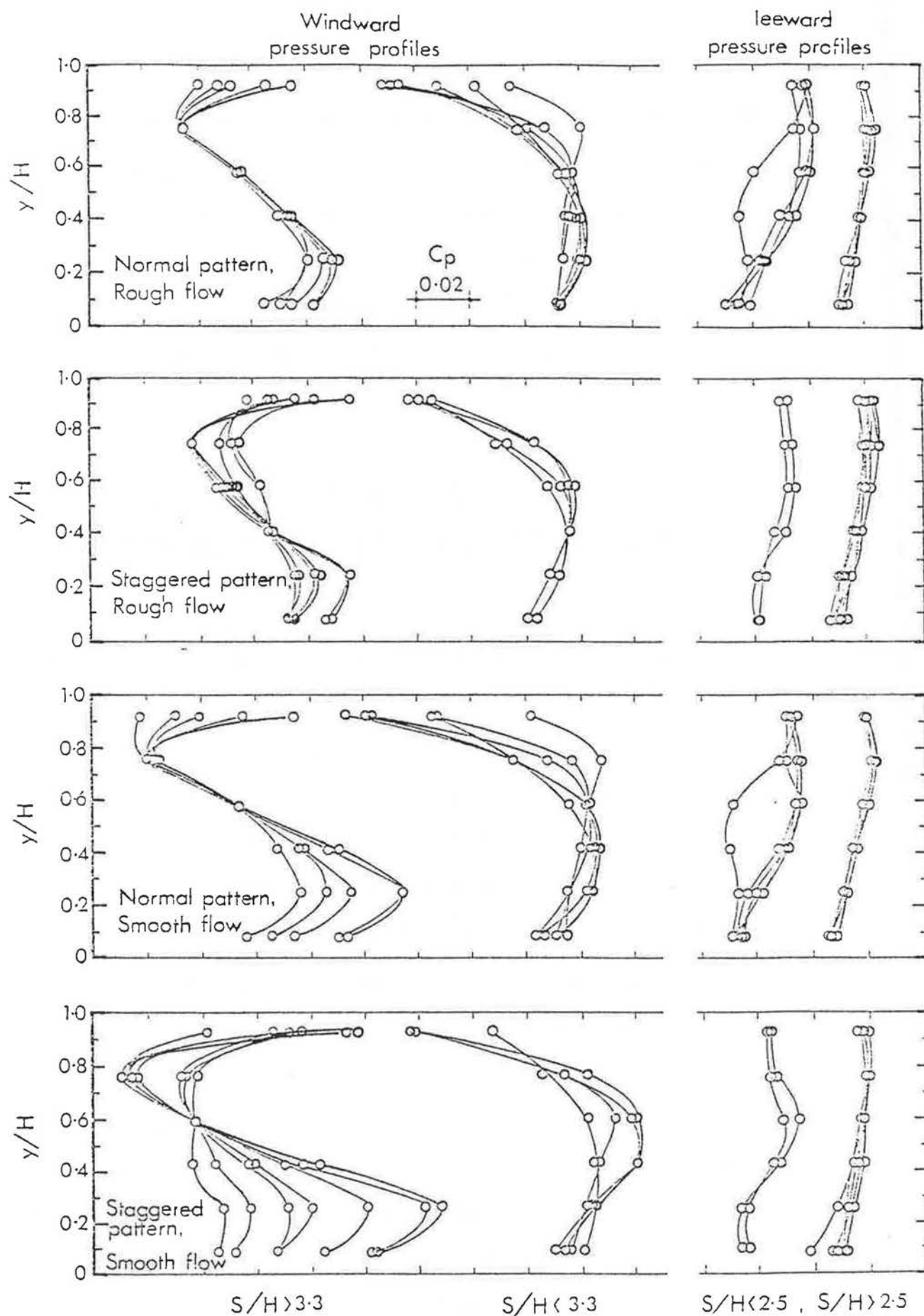


Figure 7.20 GROUPING OF THE WINDWARD AND LEEWARD PRESSURE DISTRIBUTIONS ACCORDING TO THE DIFFERENT FLOW REGIMES.

method proved to be successful in the isolated flow regime where an "S" distribution form prevailed it did not show any promise in collapsing the pressure profiles in the other flow regimes. A plot of the normalized pressure profiles on the windward walls of the normal and staggered patterns in the two flows investigated may be shown in Figures 7.21 and 7.22.

7.4 The effect of pattern and orientation on the pressure difference between two opposite faces, ΔC_p

7.4.1 The variation of ΔC_p with the model orientation, θ , is shown in Figure 7.23 for the two incident flow types, the two layout patterns and for three values of the group density. A comparison with the corresponding data for an isolated cube in both incident flows is also presented. The manner in which the results in Figure 7.23 have been obtained has an important effect on the conclusions which can be drawn from these data. Since each experimental point for a particular value of θ represents an average of 12 values for the variation of ϕ from $+90^\circ$ to -90° in 15° intervals, both the flow structure and the interpretation of the density value will differ from that applicable to the corresponding results for $\theta = 0^\circ$ where ϕ was not varied. Hence the density in Figure 7.23 cannot be represented by a single value of the cube spacing for a particular group layout. Instead, an effective spacing, \bar{S} , is used where \bar{S} is equal to the average value of the longitudinal axis cube spacing as the

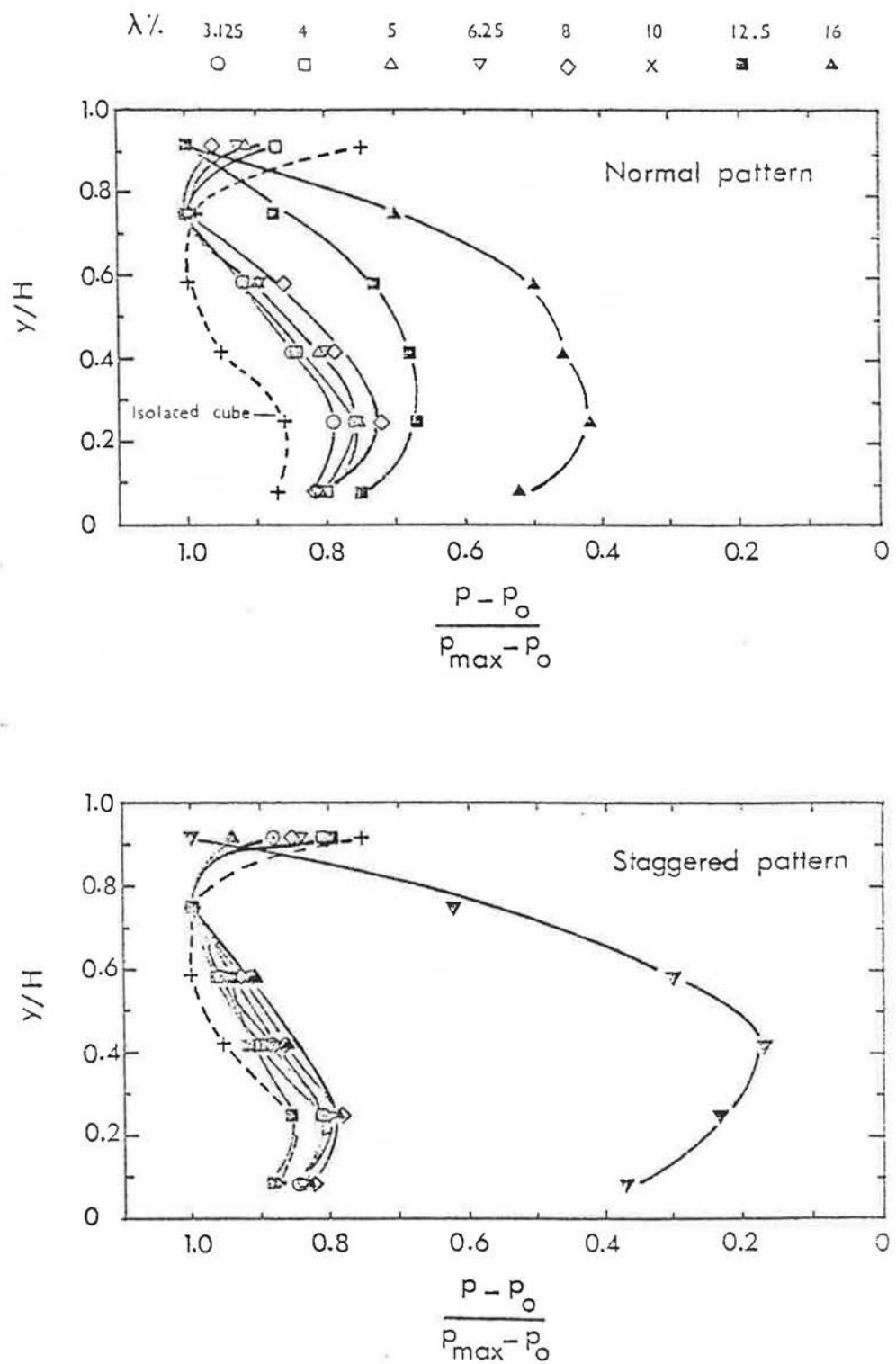


Figure 7.21 NORMALIZED WINDWARD PRESSURE PROFILES WITH RESPECT TO THE MAXIMUM PRESSURE, (rough flow).

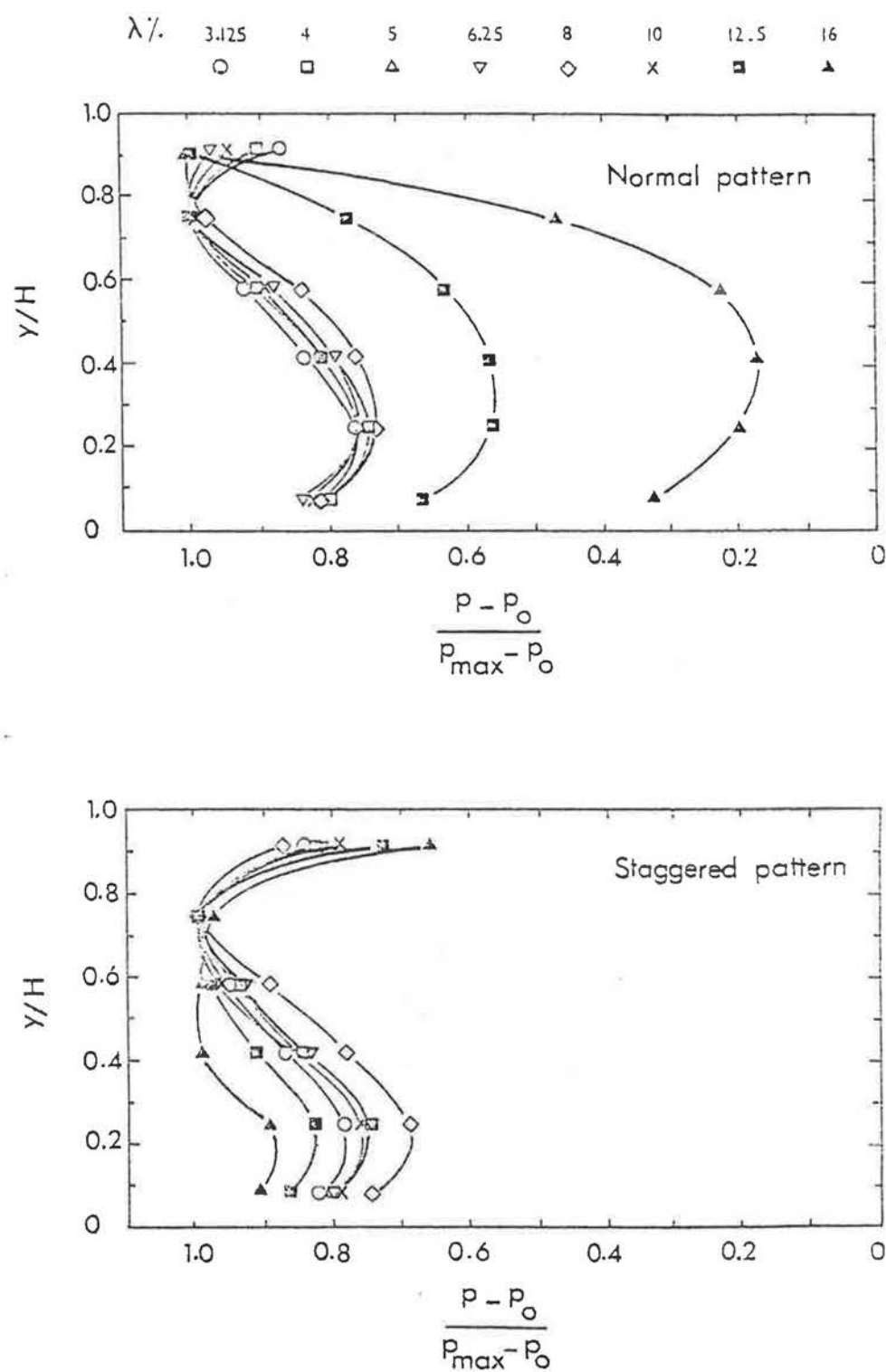


Figure 7.22 NORMALIZED WINDWARD PRESSURE PROFILES WITH RESPECT TO THE MAXIMUM PRESSURE, (smooth flow).

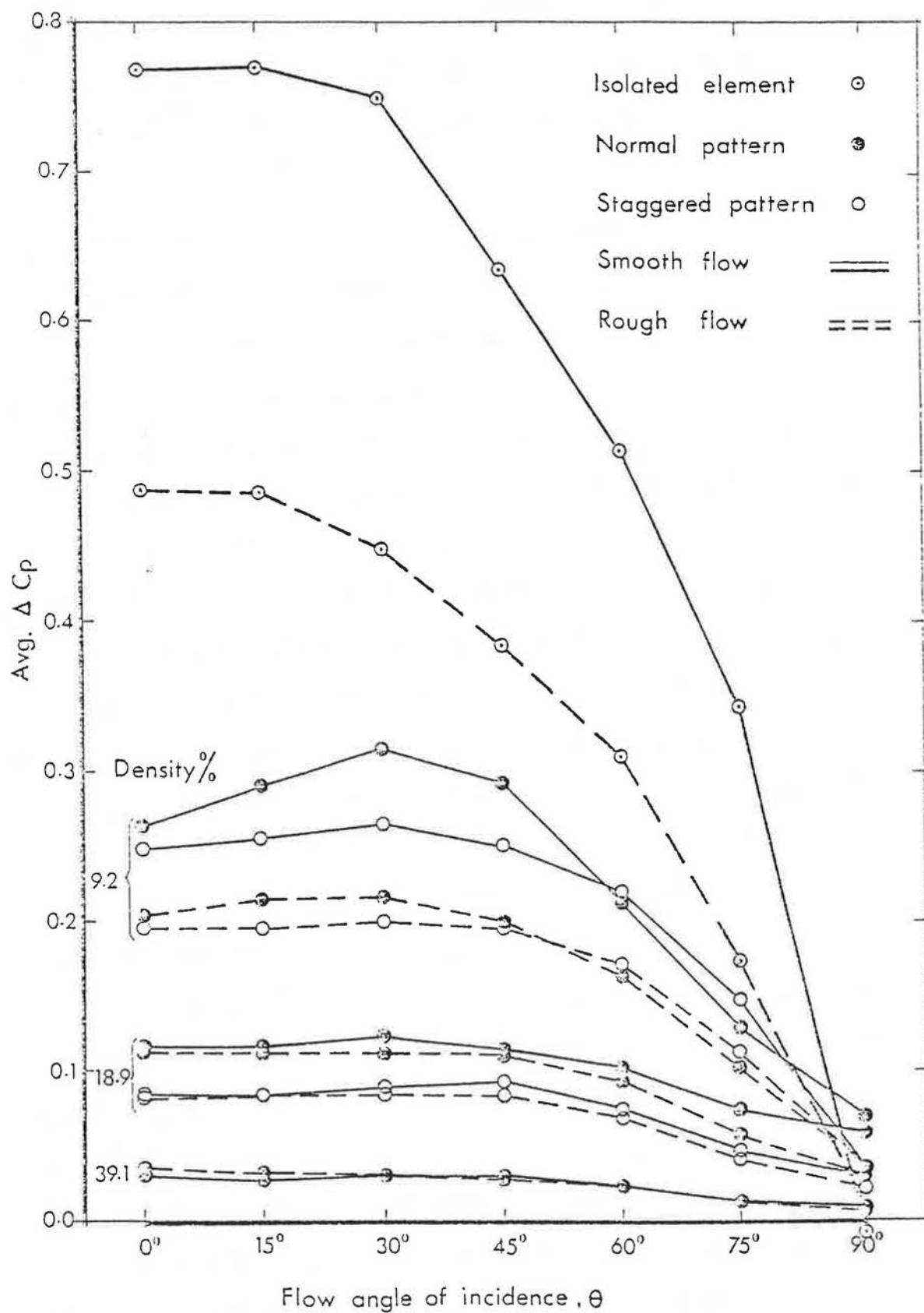


Figure 7.23 VARIATION OF ΔC_p WITH THE ORIENTATION ANGLE, θ , FOR VARIOUS DENSITIES.

model surroundings are rotated. In this manner effective spacings of \bar{S}/H equal to 4.0, 2.8 and 1.8 can be defined for the group densities 9.2%, 18.9% and 39.1% respectively, irrespective of whether the pattern is normal or staggered.

7.4.2 From Figure 7.23 it can be seen that the different incident flows have a large effect on the behaviour of the isolated model. This effect has been shown by Good and Joubert (1968) to be mainly due to the difference in the thickness of the two incident boundary layers. It can also be seen that the results for the 9.2% density layout are similarly grouped according to incident flow type and are not influenced by layout pattern. Conversely, for a layout density of 18.9% the resulting curves are grouped according to pattern whilst incident flow type no longer dominates. At 39.1% all the experimental points lie on a single line. The groupings of these curves may be explained, with reference to Figures 7.11 to 7.14, by classifying the flow regimes which correspond to the various values of \bar{S}/H . At a layout density of 9.2%, \bar{S}/H equals 4.0, and hence this is an isolated flow regime where the type of incident flow dominates the model behaviour. However, at a layout density of 18.9%, where $\bar{S}/H = 2.8$ the flow regime is wake interference flow. Here it is suggested that the model behaviour will be dominated by the wake of the blocks upstream which forms the boundary layer structure over the element layout itself, Perry et. al. (1969), and hence the results will be grouped now by layout pattern and not incident flow type.

Finally, at a layout density of 39.1%, \bar{S}/H equals 1.8, hence this is a skimming flow regime. Here the incident flow type is almost of no effect.

7.4.3 The effect of model orientation on the value of ΔC_p in the range $0^\circ < \theta < 60^\circ$ is shown to be negligible for the values of density considered. However, it might be expected that at smaller values of the layout density, i.e. larger values of \bar{S}/H , the effect of orientation in the isolated roughness flow regime would increase.

7.4.4 A comparison between the effect of model orientation on the value of ΔC_p in the normal and staggered patterns with that found for a random group layout is shown in Figure 7.24 for the rough flow case alone. The results for the 9.2% density confirm the assumption that this is an isolated roughness flow regime where the effect of pattern is not a major consideration and the approaching flow type is dominant. However, at 18.9% density in a wake interference flow regime the effect of layout pattern type is shown to be more important.

7.5 Conclusions

7.5.1 From the part of this study in which the effect of upstream fetch on the pressures experienced by the roughness elements, in order for the pressures to stabilize was investigated, it is concluded that longer fetches are required for lower densities, staggered patterns or thinner incident boundary layers (Figure 7.3).

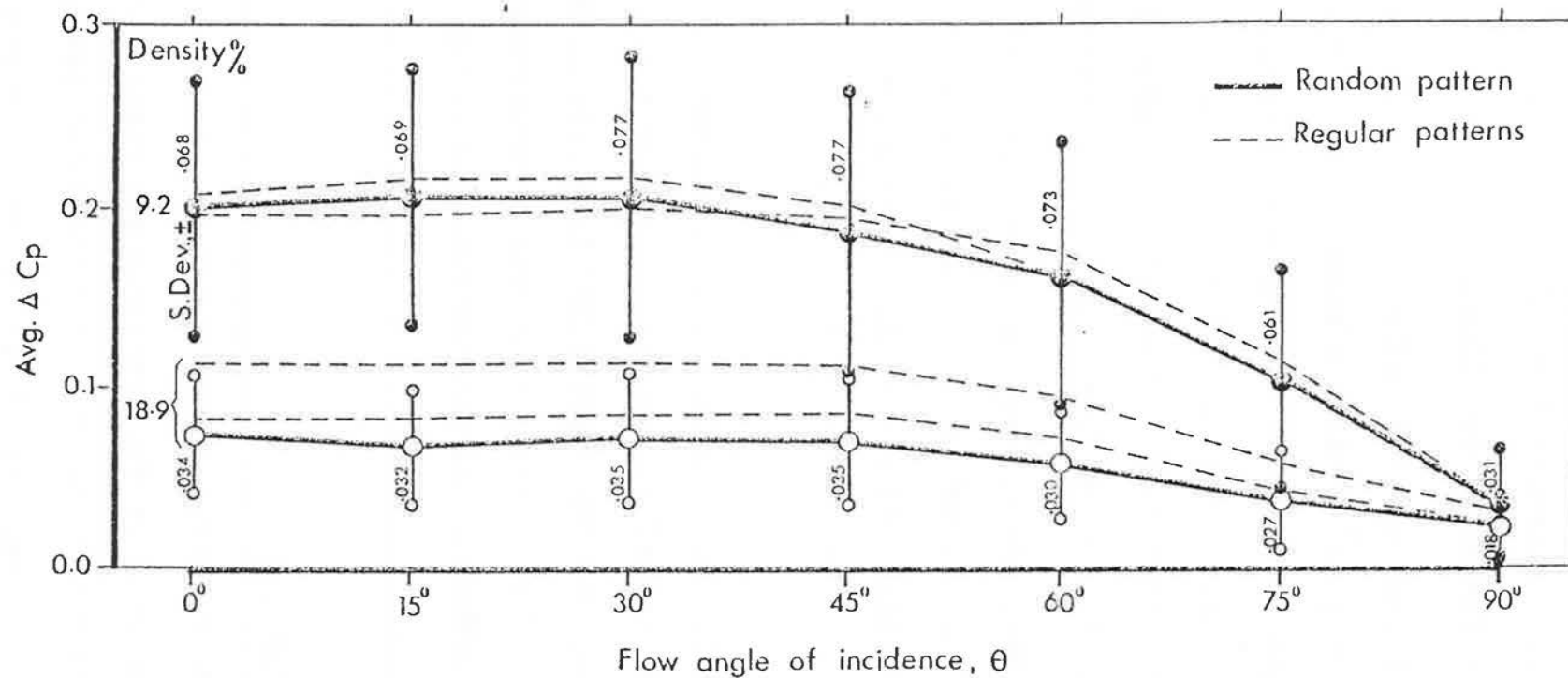


Figure 7.24 VARIATION OF ΔC_p WITH INCIDENT FLOW DIRECTION FOR THE REGULAR PATTERNS COMPARED WITH THE RANDOM PATTERN.

7.5.2 The size of the influence area round the model depends on the spacing in the flow direction, being larger for wider spacings. The limit of this area takes the form of a foot print shape rather than the assumed circular form. This new form emphasizes the effect of both the windward and leeward sectors, and suggests that the side sectors are less important, (Figure 7.5).

7.5.3 From the break point in the graph showing the variation of the mean windward pressure with spacing at a value of $S/H \approx 3.4$ and from the jump in the variation of the mean leeward pressure with spacing at a value of $S/H \approx 2.5$ in all cases, it is postulated that two changes of flow regime occur at these values of S/H . The first change from an isolated flow regime to a wake interference flow regime occurs at $S/H \approx 3.4$ while the second change at $S/H \approx 2.5$ corresponds to the change from the wake interference flow regime to the skimming flow regime, (Figures 7.11 - 7.14).

7.5.4 The explanation of these two changes, supported by previous work on isolated bodies and the flow over deep grooves (similar to the skimming flow regime), is given as follows. The isolated roughness flow regime is obtained if the spacing S/H is large enough so that the separation and reattachment zones of flow round the cube do not interfere with the next cube. The wake interference flow regime starts when these zones interfere with the next cubes. The skimming flow regime starts when a stable vortex begins to form in the space between the cubes.

7.5.5 The variation of the effective skin friction coefficient with density reflected a behaviour similar to the reported behaviour of the equivalent sand grain roughness with density. The variation of the layout pattern affected the values of the effective skin friction coefficient obtained in the three flow regimes with the exception of the high density values in the skimming flow regime, (Figures 7.18 and 7.19).

7.5.6 A collapse of the windward pressure distribution profiles was obtained when the profiles were classified by flow regime. A similar collapse was obtained for the leeward pressure profiles. The windward pressure profiles in the isolated flow regime took the form of an "S", while those in the wake interference and skimming flow regimes took the form of a reversed "C". The leeward pressure profiles in the isolated roughness flow regime and the wake interference flow regime reflected an approximately uniform distribution. In the skimming flow regime, the leeward pressure profiles were no longer uniform, and a minimum pressure at the cube mid-height indicated the existence of a stable strong vortex, (Figure 7.20).

7.5.7 The normalization scheme suggested by Good and Joubert (1968) for the isolated-body windward pressure profiles, applied only on the isolated flow regime pressure profiles, (Figures 7.21 and 7.22).

7.5.8 The effect of group layout pattern seems to be negligible in the isolated roughness flow regime, while the incident flow type is dominant. In the wake interference flow regime, the dominant effect is that of the layout pattern while the incident flow type becomes less important. In the skimming flow regime, neither the incident flow nor the layout pattern seem to affect the resulting pressure forces dominantly. Here the effect of the group layout density might be more important. (Figures 7.23 and 7.24).

7.5.9 In all densities, the effect of the group layout orientation angle, ϕ , becomes less important as the fetch increases. The effect of the model orientation angle, θ , was different in that, nearly similar effects were obtained at all densities, (Figures 7.23 and 7.24).

CHAPTER 8

EXPERIMENTAL RESULTS AND DISCUSSION:
Velocity Profile measurements.

8. EXPERIMENTAL RESULTS AND DISCUSSION

Velocity Profile Measurements

8.1 Introduction

8.1.1 An extensive series of velocity profile measurements have been undertaken with the aim of substantiating and extending the findings from the pressure measurement tests. The velocity measurements presented here are restricted to the rough flow case and the normal pattern of the group layout. The vertical origin of the measurements was the smooth surface between the cubes. Six values of the group density were chosen to cover the three flow regimes which emerged from the analysis of the pressure distribution measurements. These were 4% and 8% density in the isolated roughness flow regime, 12.5% density in the wake interference flow regime and 25%, 32% and 50% density in the skimming flow regime.

8.1.2 In most of the previously reported work where velocity profiles have been measured over roughness element arrays, the flow regimes considered have been the wake interference and skimming flows over two-dimensional elements. Hence, not only do the velocity profiles remain invariant in the transverse direction, but only negligibly small differences exist between adjacent elements in the streamwise direction for these element spacings. However, in the present investigation on flow over three dimensional elements, larger spacial variations in the velocity profiles will exist, particularly for the larger cube spacings of the isolated roughness flow regime. In view of this, two

sets of velocity profiles were taken at lines of symmetry where the greatest difference would be apparent, e.g. the longitudinal cube axis and the corresponding street axis. Each set of profiles consisted of measurements made at distances of 0, 1H, 2H and 3H upstream of the centre of the model, Figure 8.1. In the next part, the velocity profile analysis is presented starting with the incident velocity profiles.

8.2 Velocity Profile Analysis: the two incident flows

8.2.1 The smooth flow velocity profile measured at the turntable centre in the empty tunnel (before placing the pressure tapped model, the group layout or the rough sheet to obtain the rough flow) may be seen plotted in log-log form in Figure 8.2. From this type of plot the exponent of the power law, α , was found to be 0.15 and the boundary layer thickness, δ_s , was found to be 40 mm. Plotting the same profile as u/U_1 versus $\log y$, shown in Figure 8.3, gives the inner layer logarithmic line, the equation of which was found (by regression analysis) to be:

$$\frac{u}{U_1} = 0.220 \log y + 0.583 \quad \dots\dots\dots (8.1)$$

From the knowledge of U_1 and the slope of the log line, u_* , (the friction velocity) was found to be 0.822m/sec. and z_o (the roughness length) found to be 0.0022 mm,. Hence $\frac{u_* z_o}{\nu}$ takes the value of 0.124 which is in good agreement with the theoretical value of 0.11 - 0.13. The logarithmic part of the profile was also plotted in the

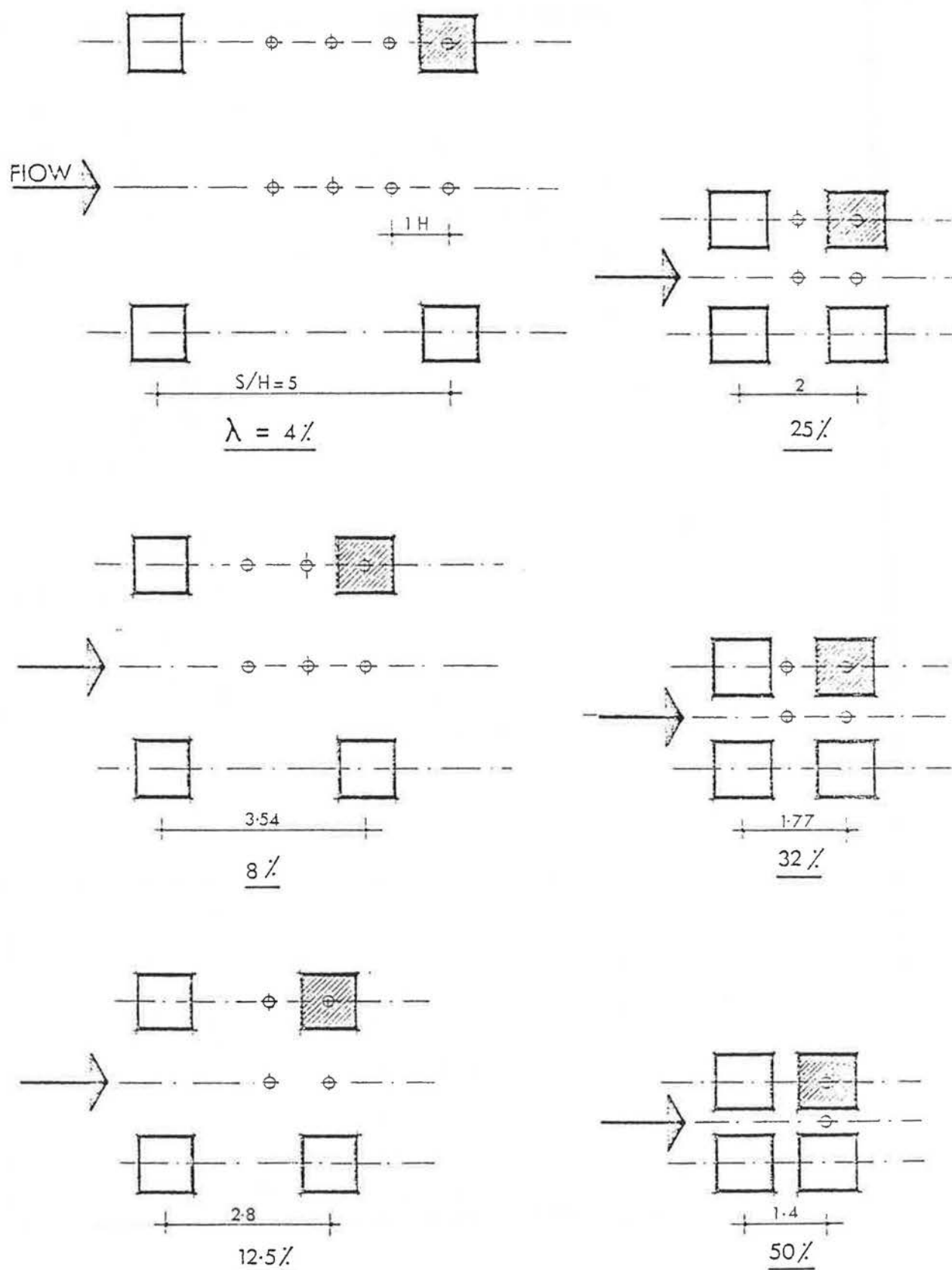


Figure 8.1 LOCATION OF THE VELOCITY PROFILES MEASURED AT DIFFERENT DENSITIES.

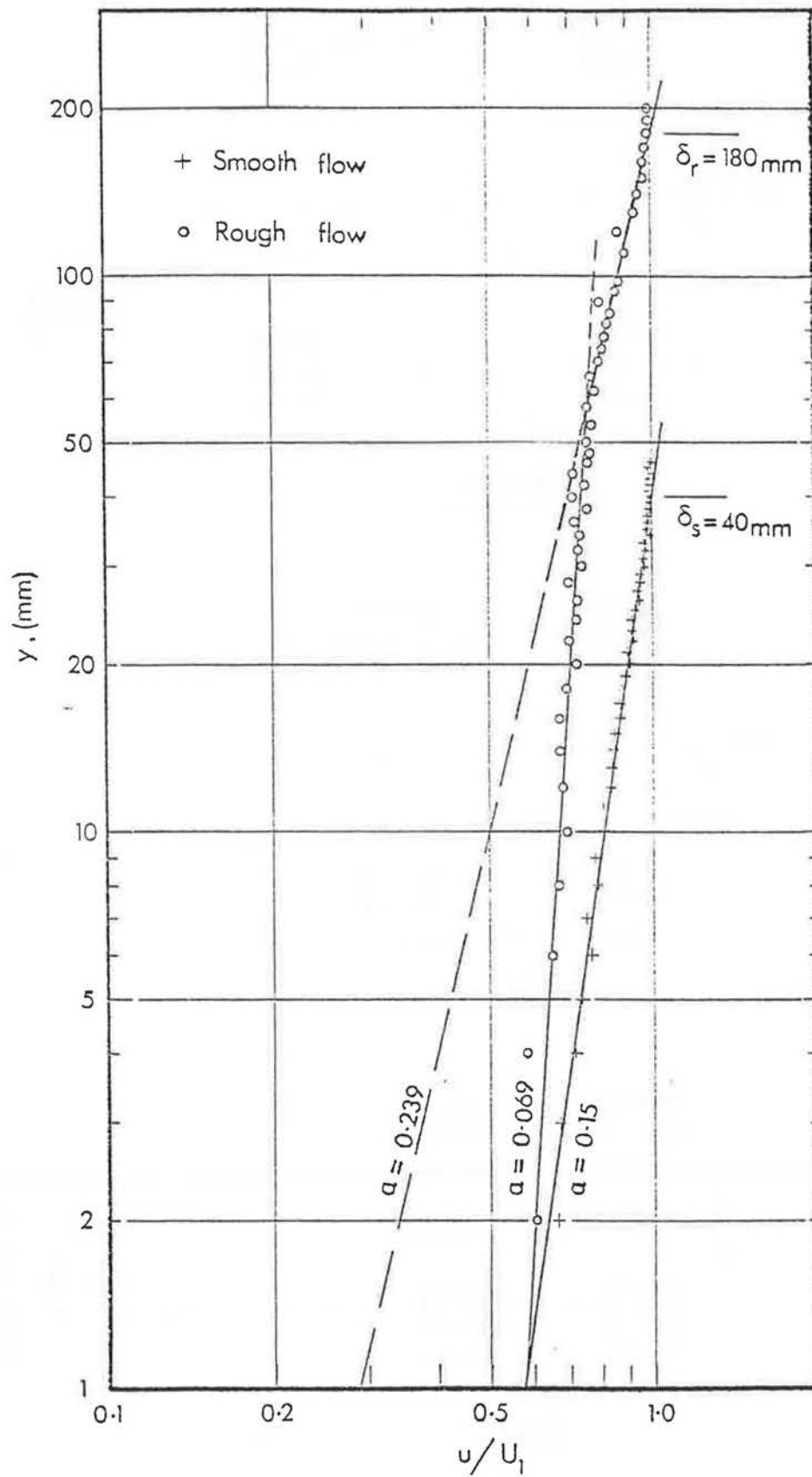


Figure 8.2 INCIDENT FLOW PROFILES, POWER LAW FORM.

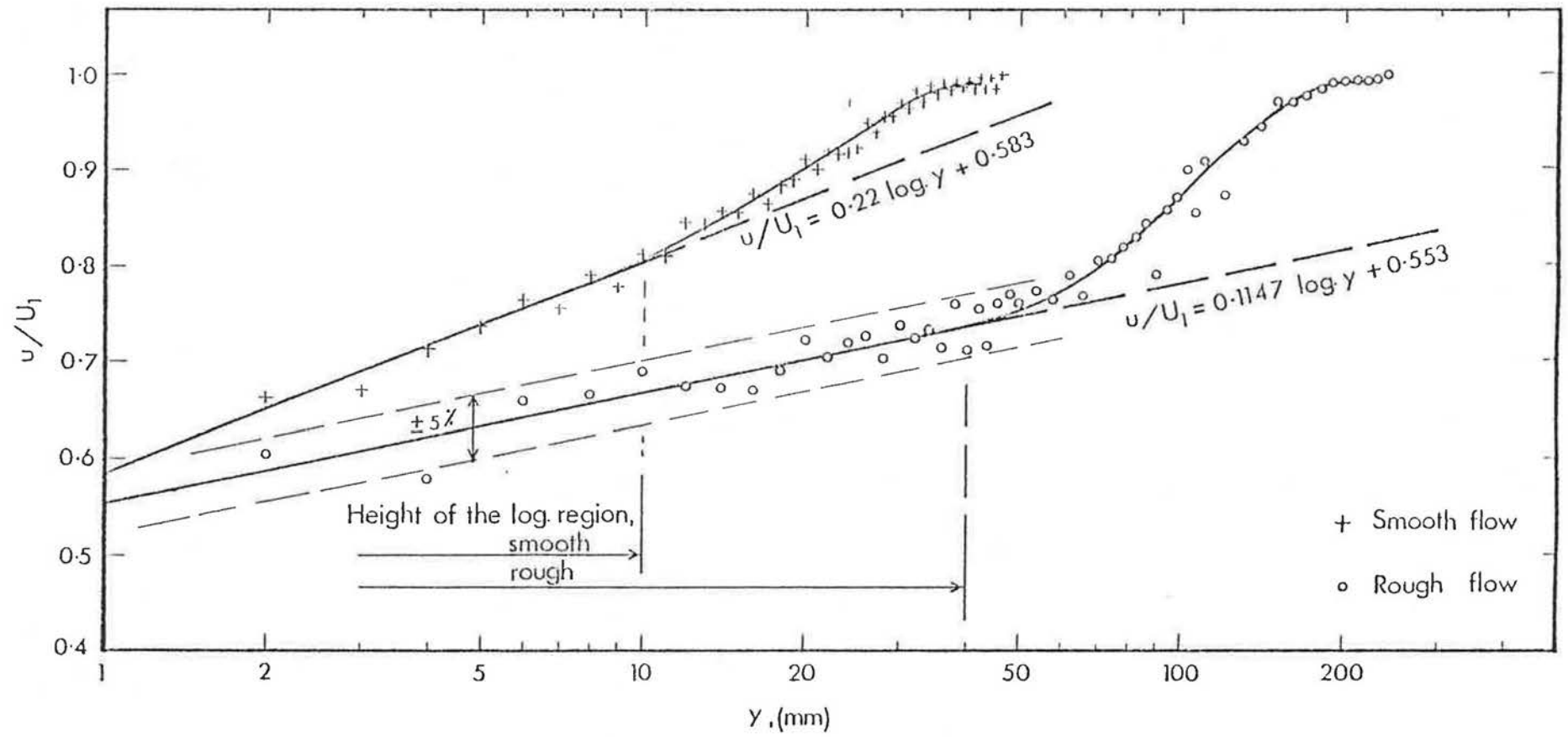


Figure 8.3 INCIDENT FLOW PROFILES, LOG-LAW FORM.

form of $\frac{u}{u_*}$ versus $\frac{yu_*}{v}$ in Figure 8.4 and compared with the theoretical line for smooth surfaces represented by:

$$\frac{u}{u_*} = 5.75 \frac{yu_*}{v} + 5.1 \quad \dots\dots (5.2)$$

8.2.2 The rough flow velocity profile, (measured at the turntable centre with the rough sheet in the tunnel, without either the model or the group layout) was also plotted and compared with the smooth flow profile in Figures 8.2, 8.3 and 8.4. From Figure 8.2 it can be seen that the boundary layer thickness $\delta_r = 180$ mm and there is an inflection in the profile at about $y = 55$ mm. Consequently two values of α were found, i.e. $\alpha = 0.069$ corresponding to the lower part of the profile and $\alpha = 0.239$ corresponding to the upper part of the profile.

This inflection is explained by the growth of an internal layer on the smooth surface between the end of the rough sheet and the measuring position. When the rough flow profile was plotted in the log Law form, the inflection shown in Figure 8.2 disappeared completely as shown in Figure 8.3. Here the logarithmic line of the inner layer may be represented by:

$$\frac{u}{U_1} = 0.1147 \log y + 0.5530 \quad \dots\dots (8.2)$$

from which u_* takes the value of 0.429 and Z_0 the value of 0.000015 mm. The height of the logarithmic region is shown to be approximately 40 mm in this flow, i.e. complete submerging of the model in this region. The presentation of the logarithmic region in the form of $\frac{u}{u_*}$ versus $\frac{yu_*}{v}$

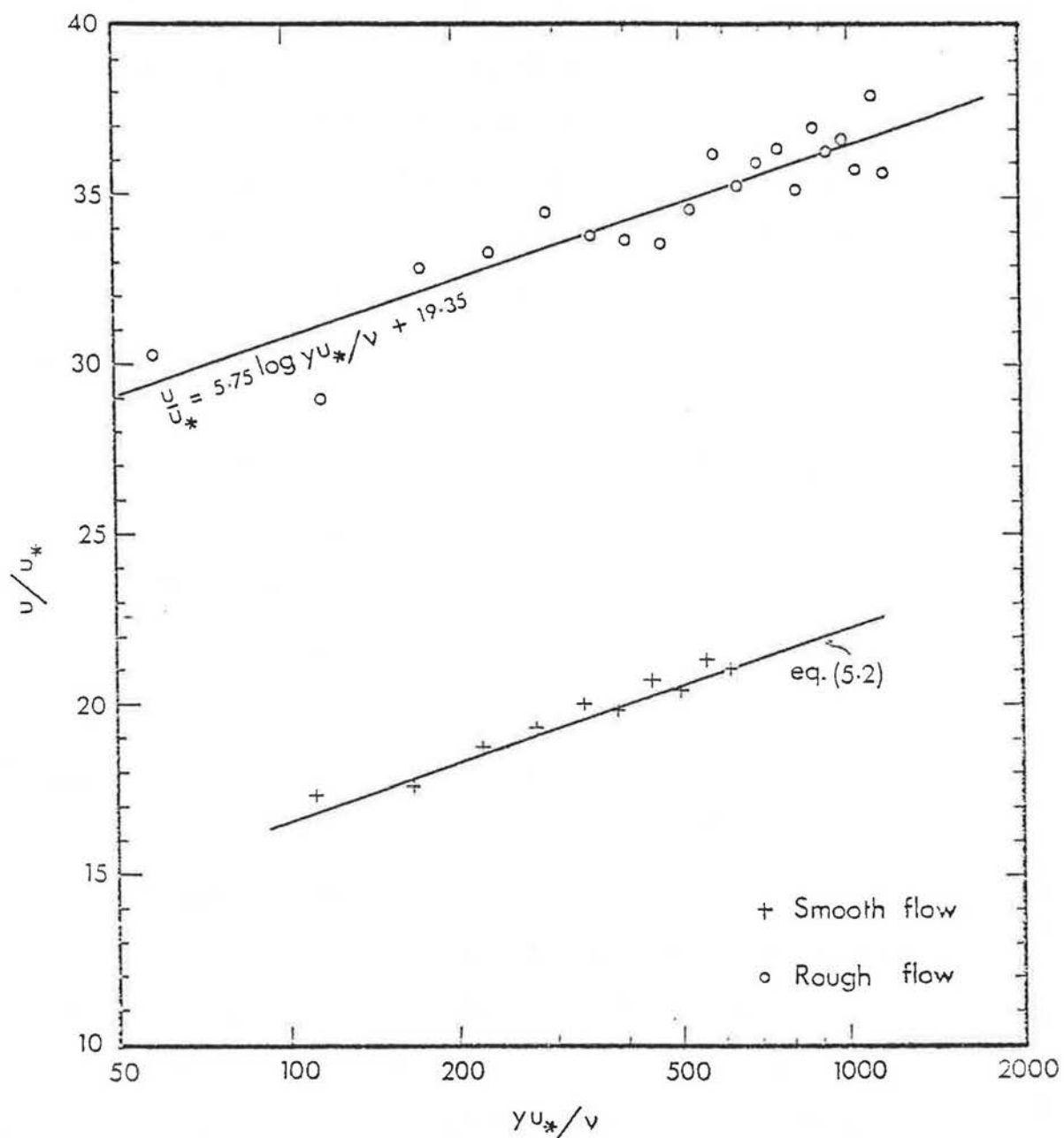


Figure 8.4 INCIDENT FLOW PROFILES IN THE FORM u/u_* VERSUS yu_*/ν .

shown in Figure 8.4 shows an upward shift of the line in contrast with the more usual characteristic for the flow over rough surfaces which result in downward shift equal to $\frac{\Delta u}{u_*}$. The value of B, the constant in equation 5.2, obtained from this line was 19.35. Similar large values for B were reported by Antonia and Luxton (1971) for a similar change of surface roughness, i.e. from rough to smooth at small fetches. They noted that B decreased gradually by increasing fetch but still had a large value, B = 6.9, at a fetch of 372H. They explained this behaviour by the incomplete adaptation of the logarithmic region of the profile in this type of surface roughness change, i.e. from rough to smooth.

8.3 Velocity profile analysis: flow within the group layout

8.3.1 At any change of surface roughness an internal layer is known to grow from the surface to eventually replace the old layer. In the present study, the incident rough flow underwent two subsequent changes of surface roughness before it reached the turntable on which the model group was placed. The first change was at the leading edge of the rough sheet, and the second change was at its trailing edge. A third change of surface then occurred at the leading edge of the model group layout. In the present case, the fetches between these changes were too small to allow for complete profile adaptation, though their effects will blend to give a resultant rough incident flow profile.

8.3.2 A careful study of the rough flow velocity profile shows that it is actually composed of four layers or zones arranged on top of each other in the same sequence as the changes occurred upstream, this is illustrated in Figure 8.5. The top of the profile, Zone I, is that corresponding to the flow on the smooth tunnel wall upstream the rough sheet. Next to this is zone II which corresponds to the flow on the rough sheet itself. In changing the surface roughness at the trailing edge of the rough sheet, adaptation to the new boundary conditions takes place in zone III after which an internal layer grows on the surface forming zone IV. A comparison between different profiles for different densities including the profile of the empty turntable before placing the model group is given in Figure 8.6 by shifting the origin. It can be seen that zones I, II and III are of approximately constant thickness and that their absolute position depends only on the thickness of zone IV. This internal layer, zone IV, either grows on the smooth turntable before the group is placed in position or on the new roughness composed by the layout group. It can also be seen from Figure 8.6 that the data points for all the corresponding zones collapse on each other apart from those of zone IV, this being the zone where the main differences occur. Therefore, in the rest of the velocity profile analysis, consideration will be confined to zone IV which is assumed to be most relevant to the model layout underneath.

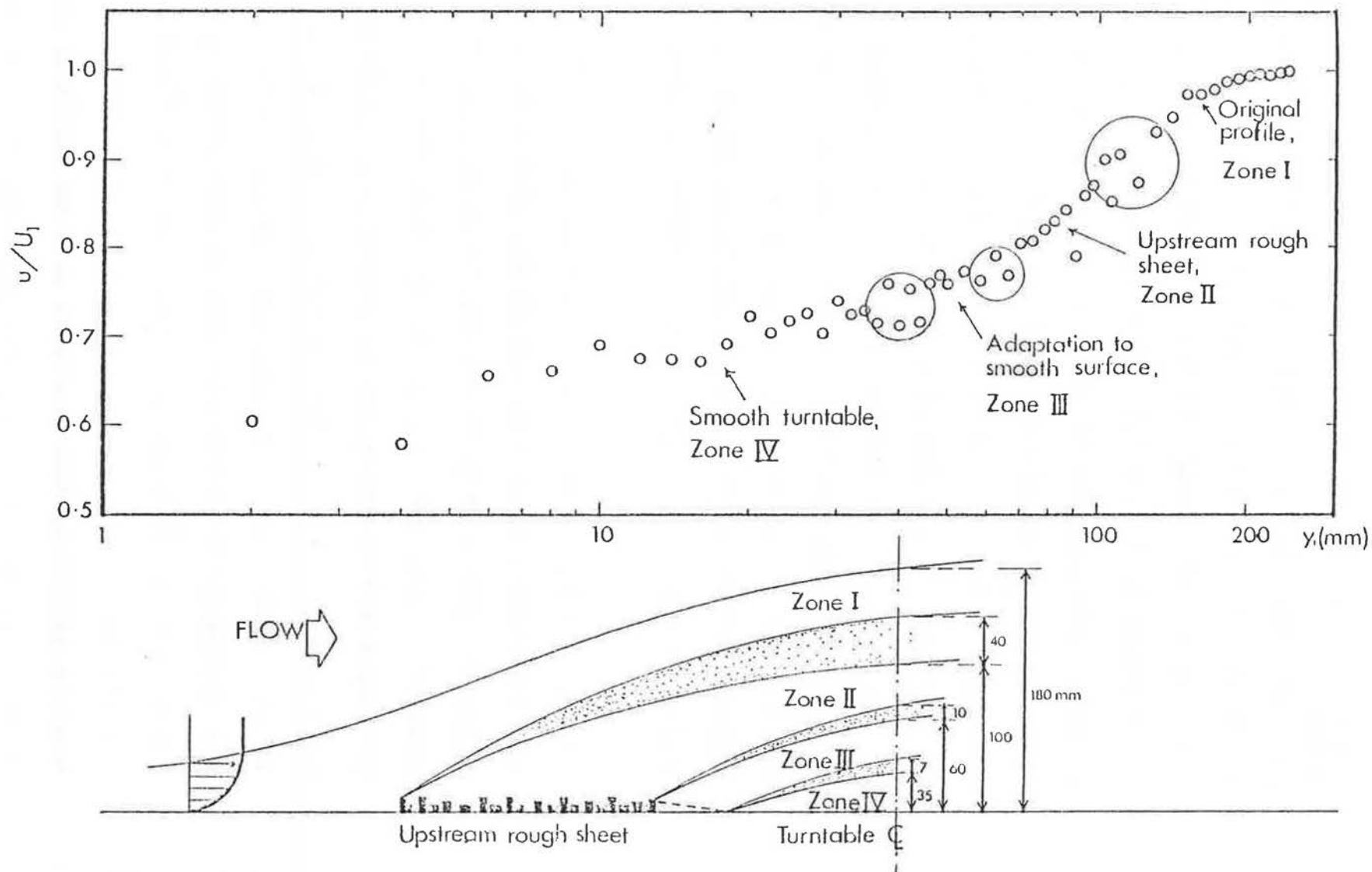


Figure 8.5 THE EFFECT OF THE SURFACE ROUGHNESS CHANGES ON THE INCIDENT ROUGH FLOW PROFILE.

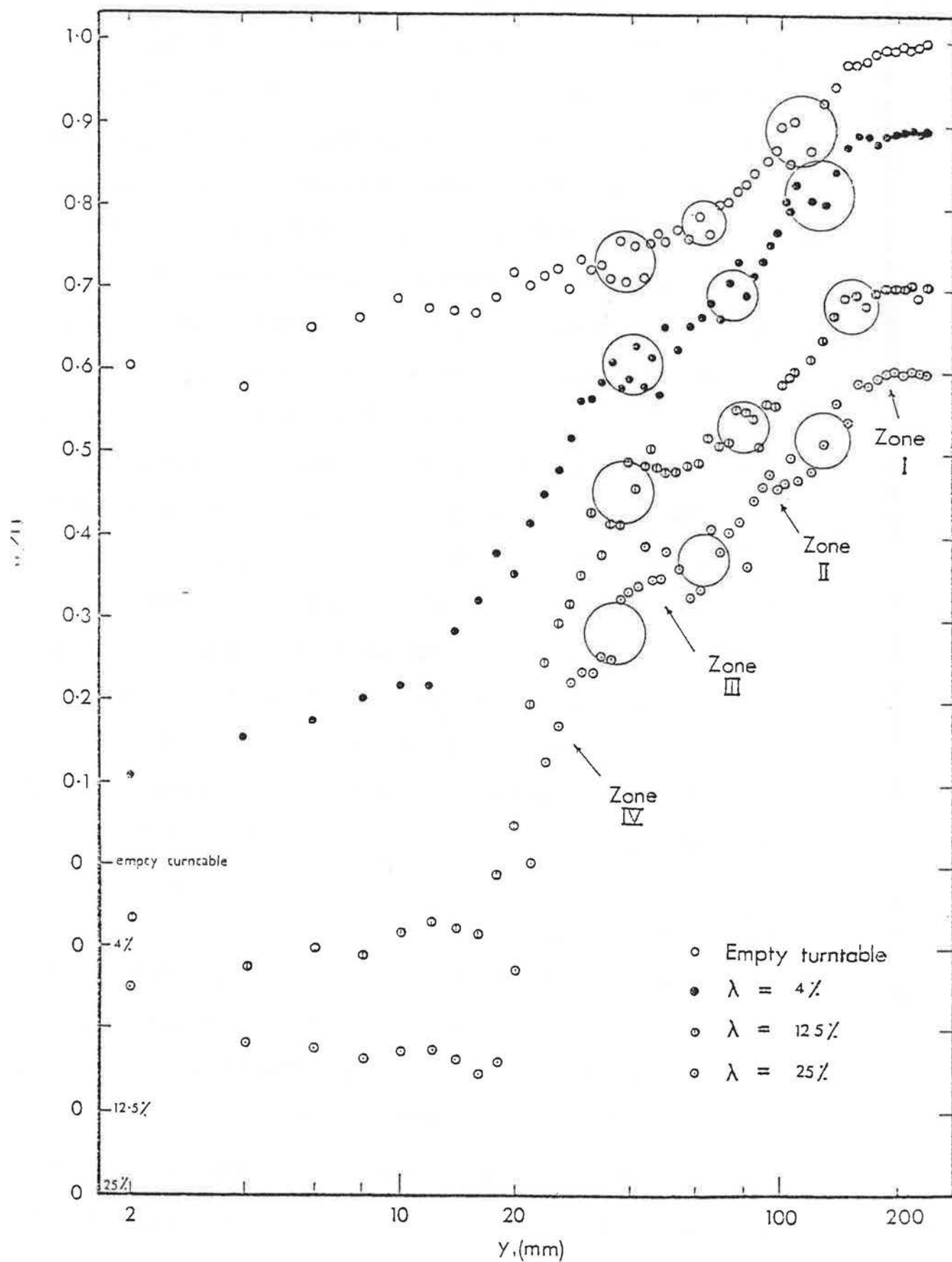


Figure 8.6 COMPARISON BETWEEN DIFFERENT PROFILES AT CUBE CENTRE LINES SHOWING THE EFFECT OF THE SUBSEQUENT CHANGES OF SURFACE ROUGHNESS.

8.3.3 Great variation in the velocity profiles were observed between those measured at the cube centre line and those corresponding to the street centre line. An example showing these variations from profiles taken at $\lambda = 4\%$, 12.5% and 32% is given in Figure 8.7. Conversely, relatively less variation in the velocity profiles was observed between those taken at different fetches in a particular density. This can be seen in the examples at $\lambda = 4\%$ given in Figures 8.8 and 8.9 for the street centre line and the cube centre line profiles respectively. The effect of increasing λ was to decrease the velocities, particularly those within the cube height. This effect was clearly observed in the street centre line profiles, Figure 8.10 and also in the cube centre line profiles, Figure 8.11. It may be noted from Figure 8.11 that the logarithmic region of the internal layer moves vertically upward as the density increases. At all densities this logarithmic part did not extend beyond the cube height and hence was not obtained from the profiles taken on top of the cube, illustrated in Figure 8.6. Since this logarithmic region is the back bone of the velocity profile analysis, only profiles taken at the cube centre line in between the cubes, at 1H upstream the model, in different densities will be considered further.

8.3.4 To obtain an estimate of the magnitude of d , the zero plane displacement, and also Z_0 , the roughness length, the graphical method of Perry and Joubert (1963) was used. In order to apply this method it is necessary to have a prior knowledge of the slope of the logarithmic region

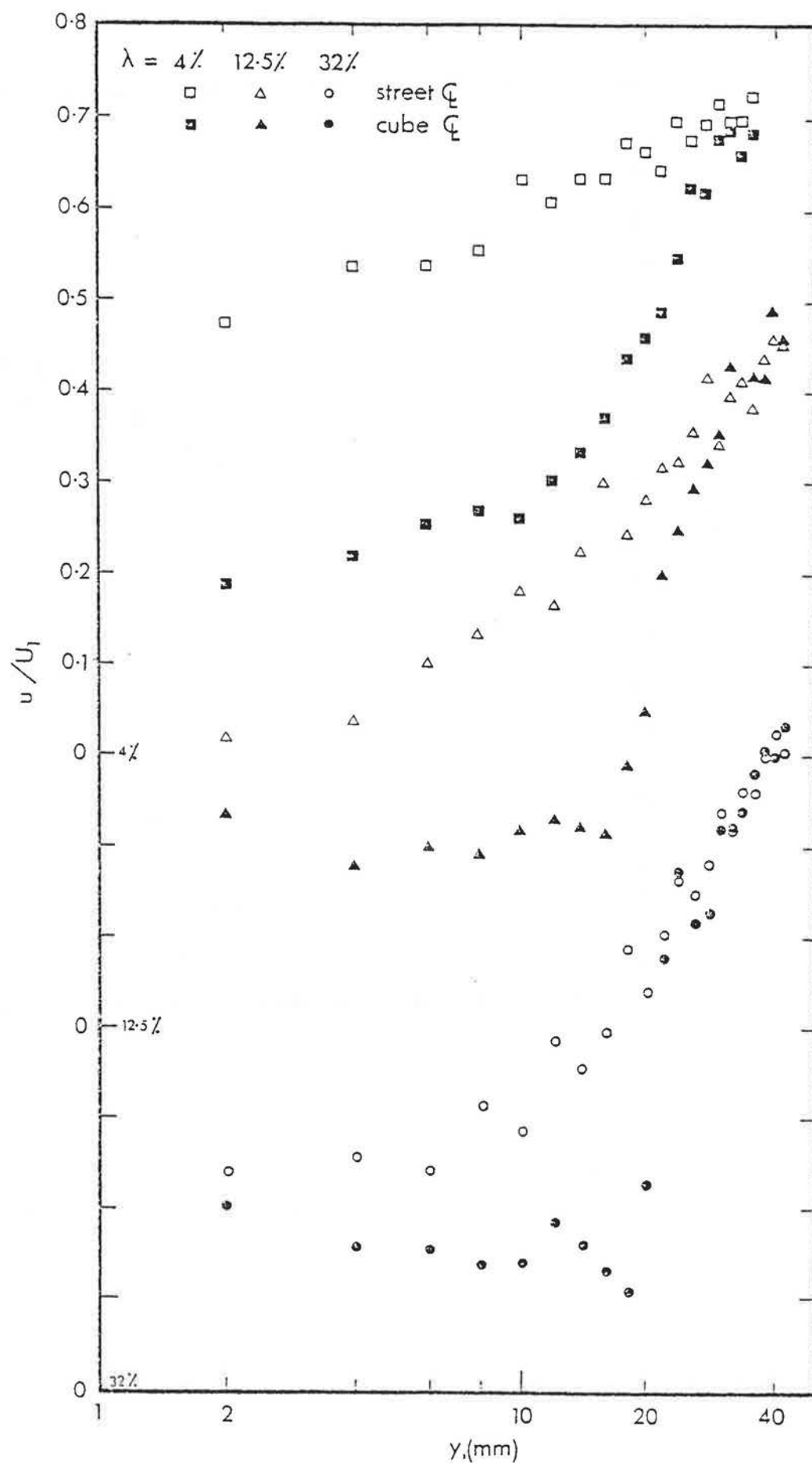


Figure 8.7 COMPARISON BETWEEN CUBE CENTRE LINE PROFILES AND STREET CENTRE LINE PROFILES AT $\lambda = 4\%$, 12.5% AND 32% .

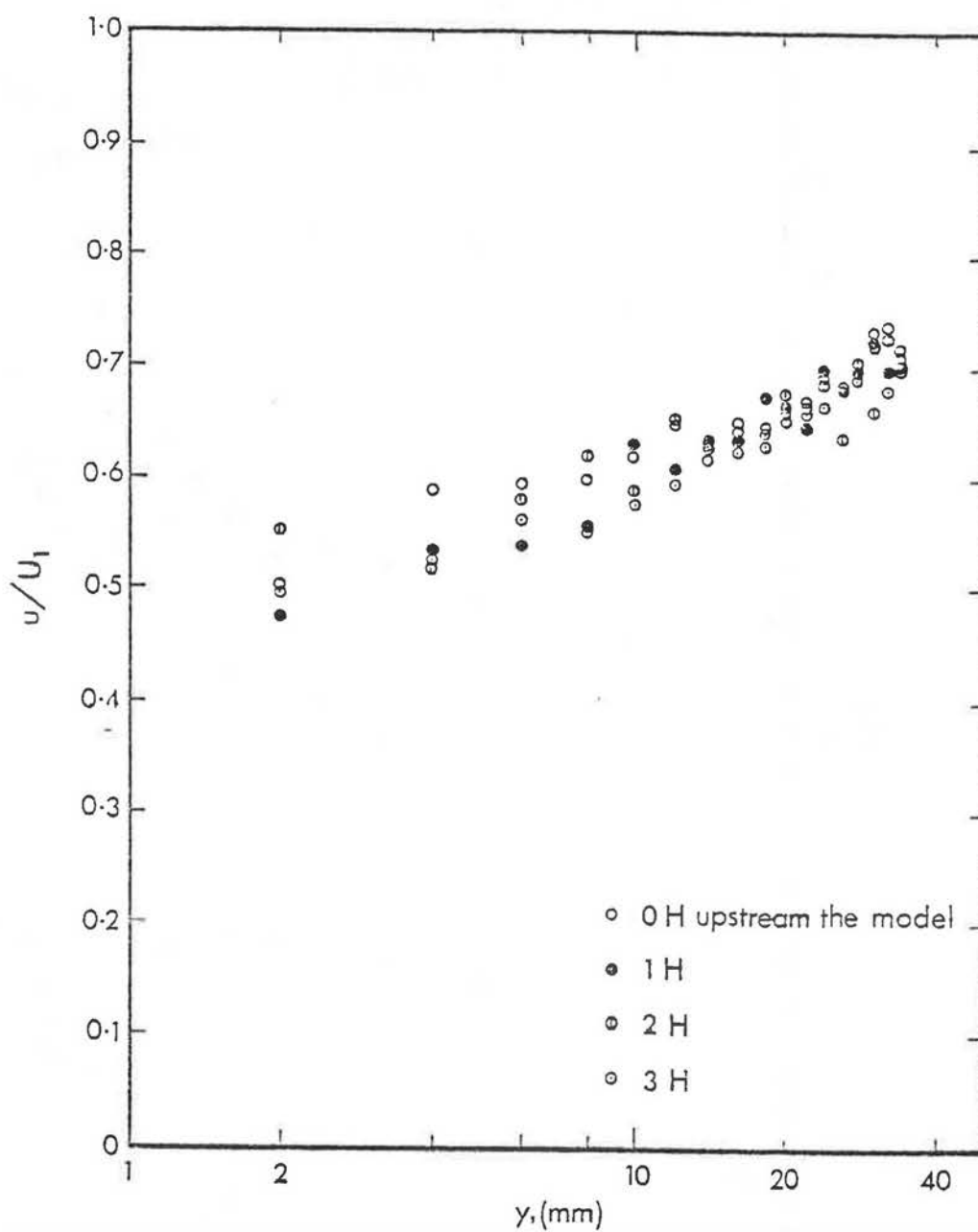


Figure 8.8 VARIATION OF VELOCITY PROFILES WITH FETCH, STREET CENTRE LINE PROFILES, $\lambda = 4\%$.

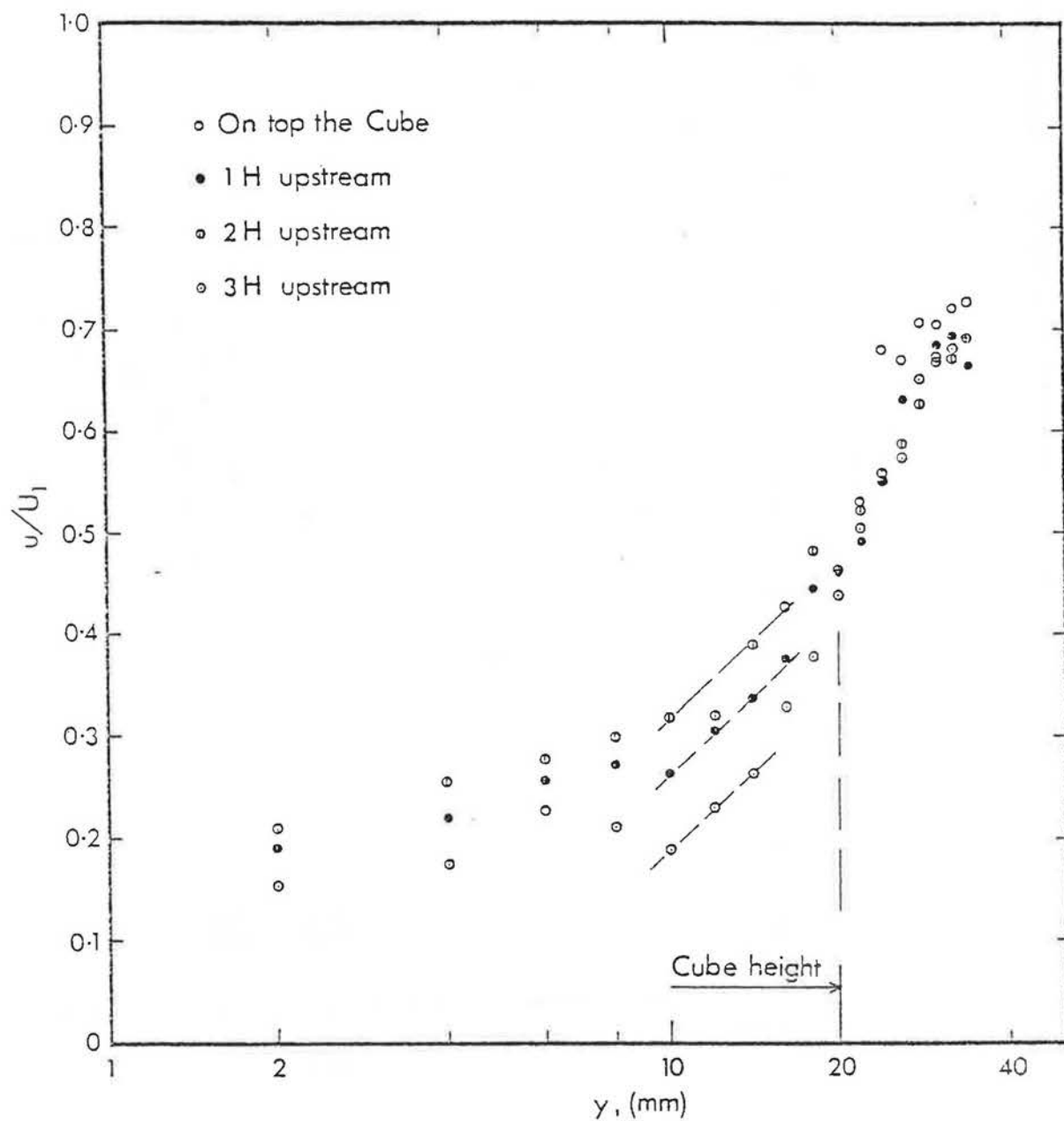


Figure 8.9 VARIATION OF VELOCITY PROFILES WITH
FETCH, CUBE CENTRE LINE PROFILES,
 $\lambda = 4\%$.

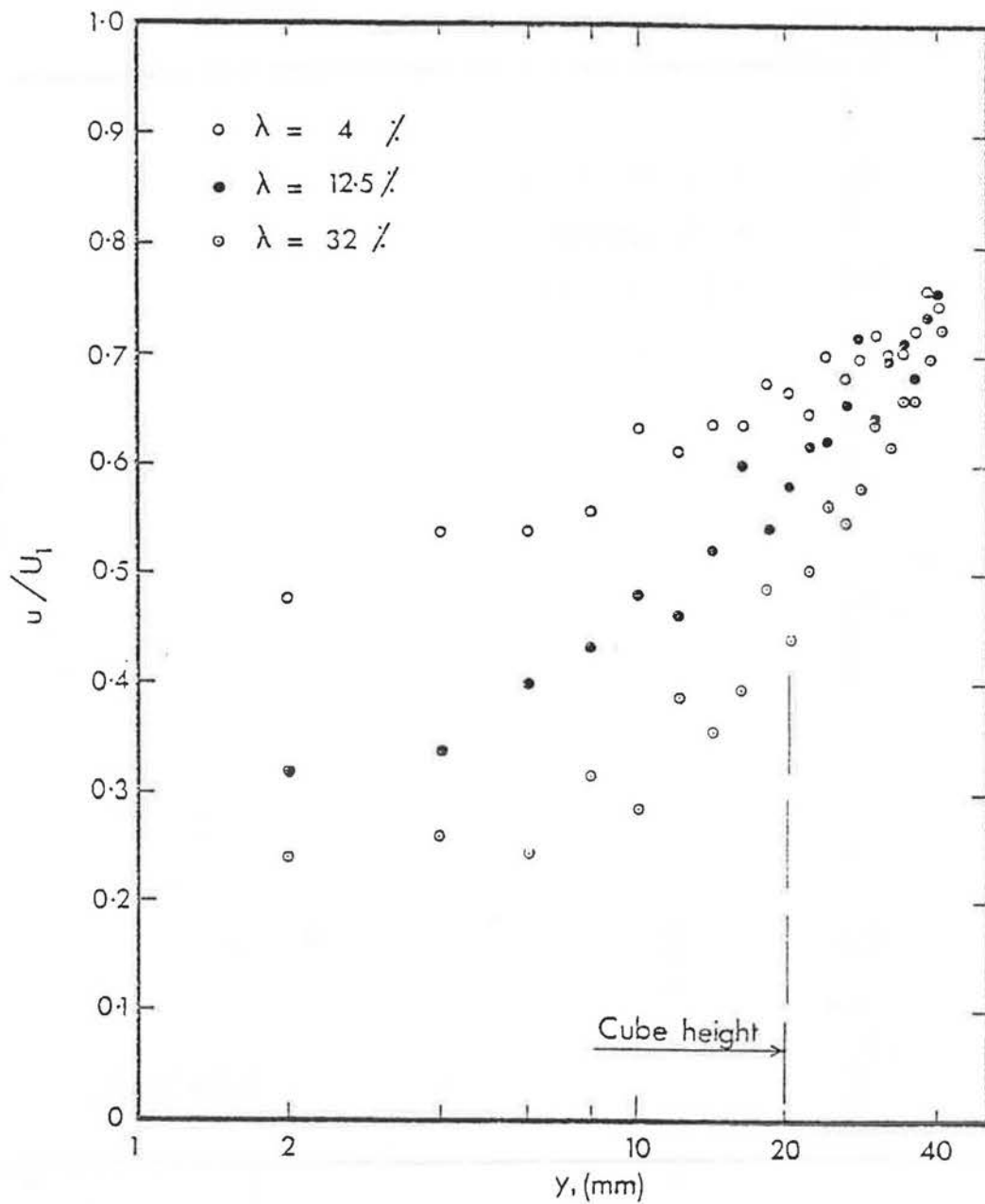


Figure 8.10 STREET CENTRE LINE PROFILES AT DIFFERENT DENSITIES.

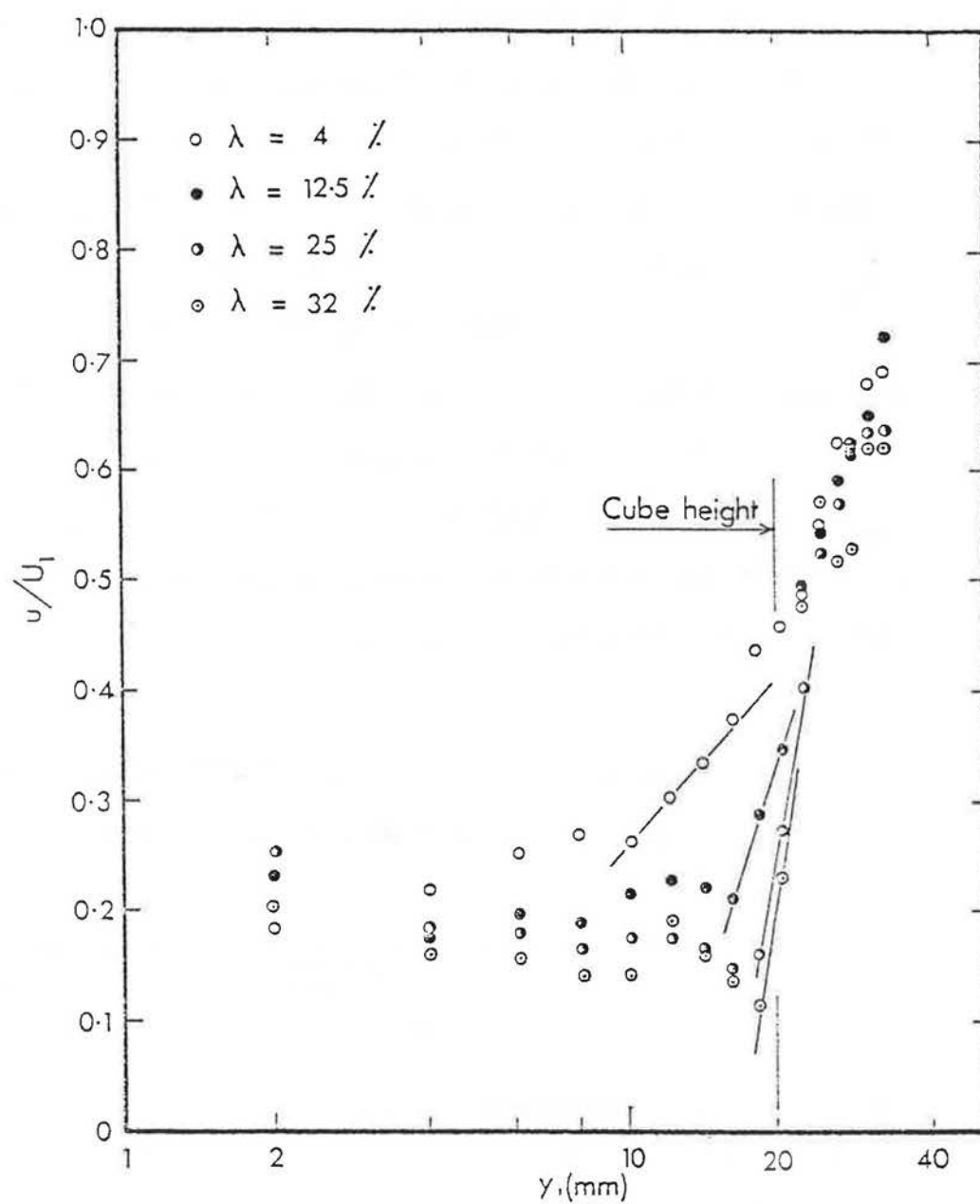


Figure 8.11 CUBE CENTRE LINE PROFILES AT VARIOUS DENSITIES.

of the internal layer profile. Hence it has been assumed that the value of C'_{fe} , obtained originally from the model pressure distributions, would make the log-region slope compatible with the profile nearest upstream to the model, measured on the cube centre line. In table 8.1, values of C_{D1} , C'_{fe} , u_* and the slope of the log-region are given for each density. The application of this graphical method of solution can be seen in Figures 8.12 to 8.16 for the five densities 4% to 32% respectively. Since the value of C'_{fe} for the street centre line is not known, no attempt has been made to determine the values of d from the street centre line velocity profiles.

Table 8.1 Velocity profile parameters determined from
the pressure measurement results

λ %	C_{D1}	C'_{fe}	$u_* (=U_1 \sqrt{C'_{fe}/2})$ (m/sec) ^e	Slope of log-region ($5.75 \frac{u_*}{U_1}$)
4	0.253	0.0101	1.559	0.409
8	0.178	0.0142	1.847	0.485
12.5	0.120	0.0150	1.897	0.498
25	0.050	0.0126	1.739	0.457
32	0.031	0.0098	1.535	0.403
50	0.007	0.0036	0.929	0.244

8.3.5 The cube centre line velocity profiles taken at the lower densities of 4% and 8% have also displayed a

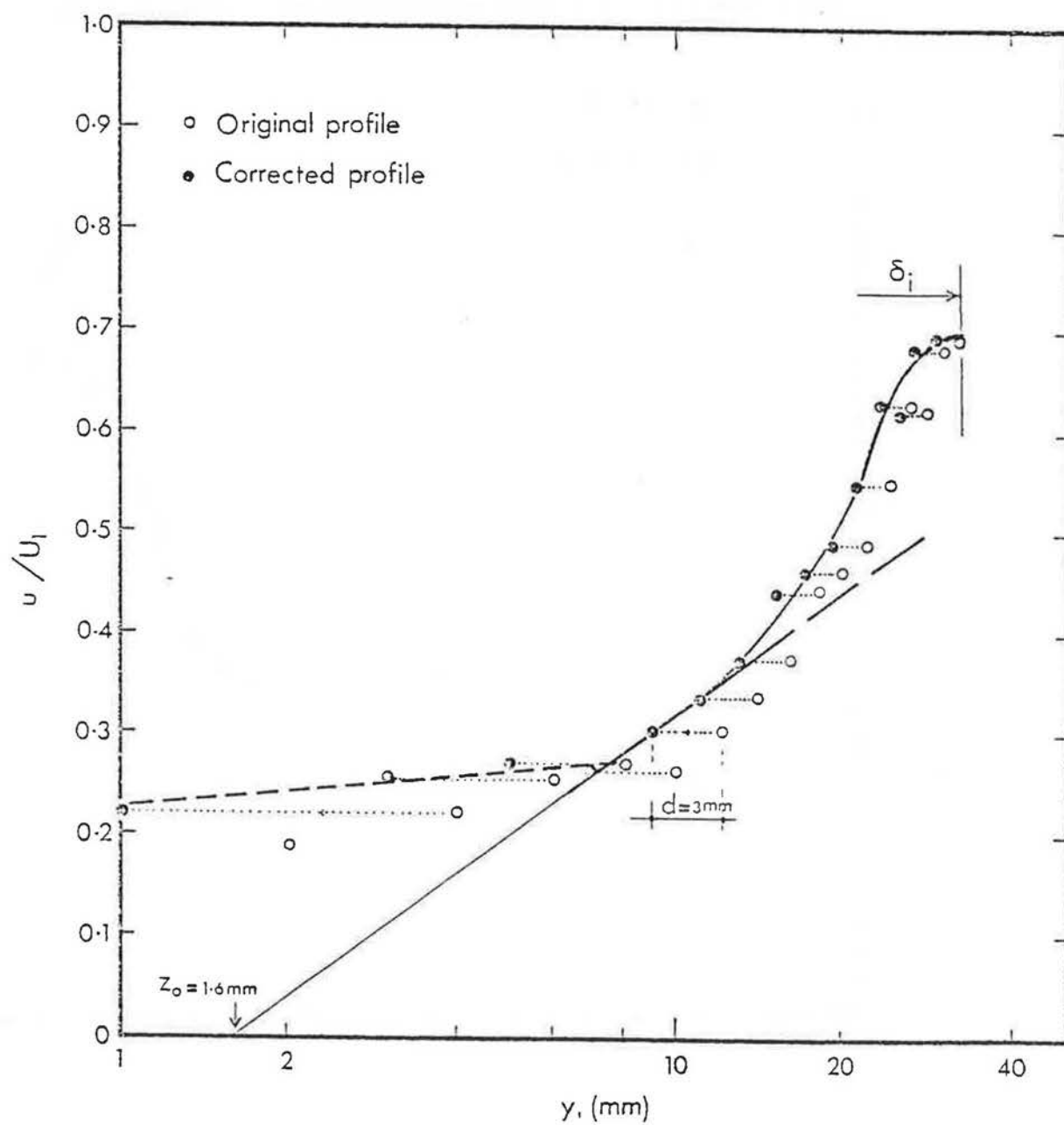


Figure 8.12 THE GRAPHICAL METHOD FOR DETERMINING THE ZERO PLANE DISPLACEMENT, d , ($\lambda = 43$).

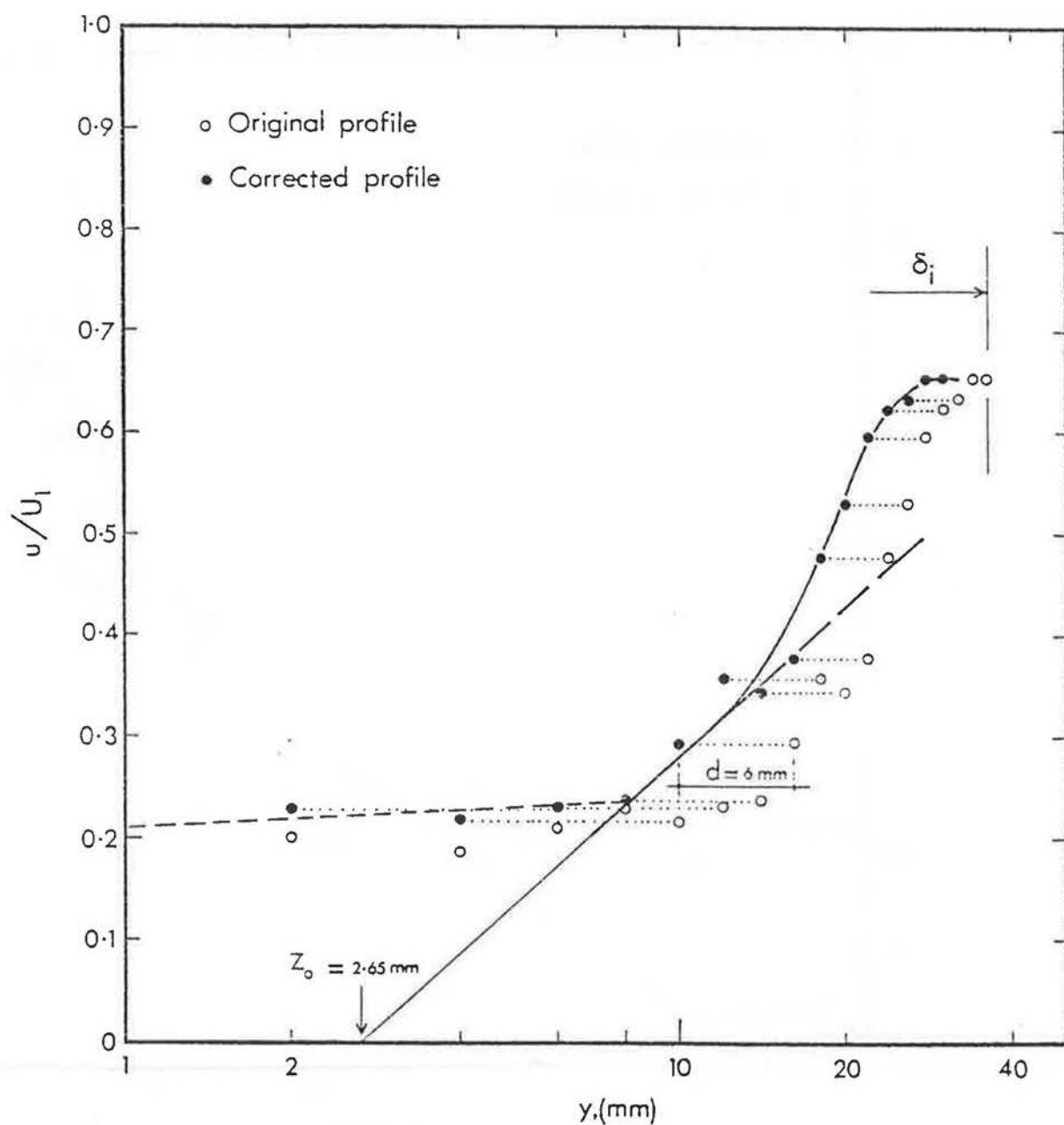


Figure 8.13 THE GRAPHICAL METHOD FOR DETERMINING THE ZERO PLANE DISPLACEMENT, d , ($\lambda = 8\%$).

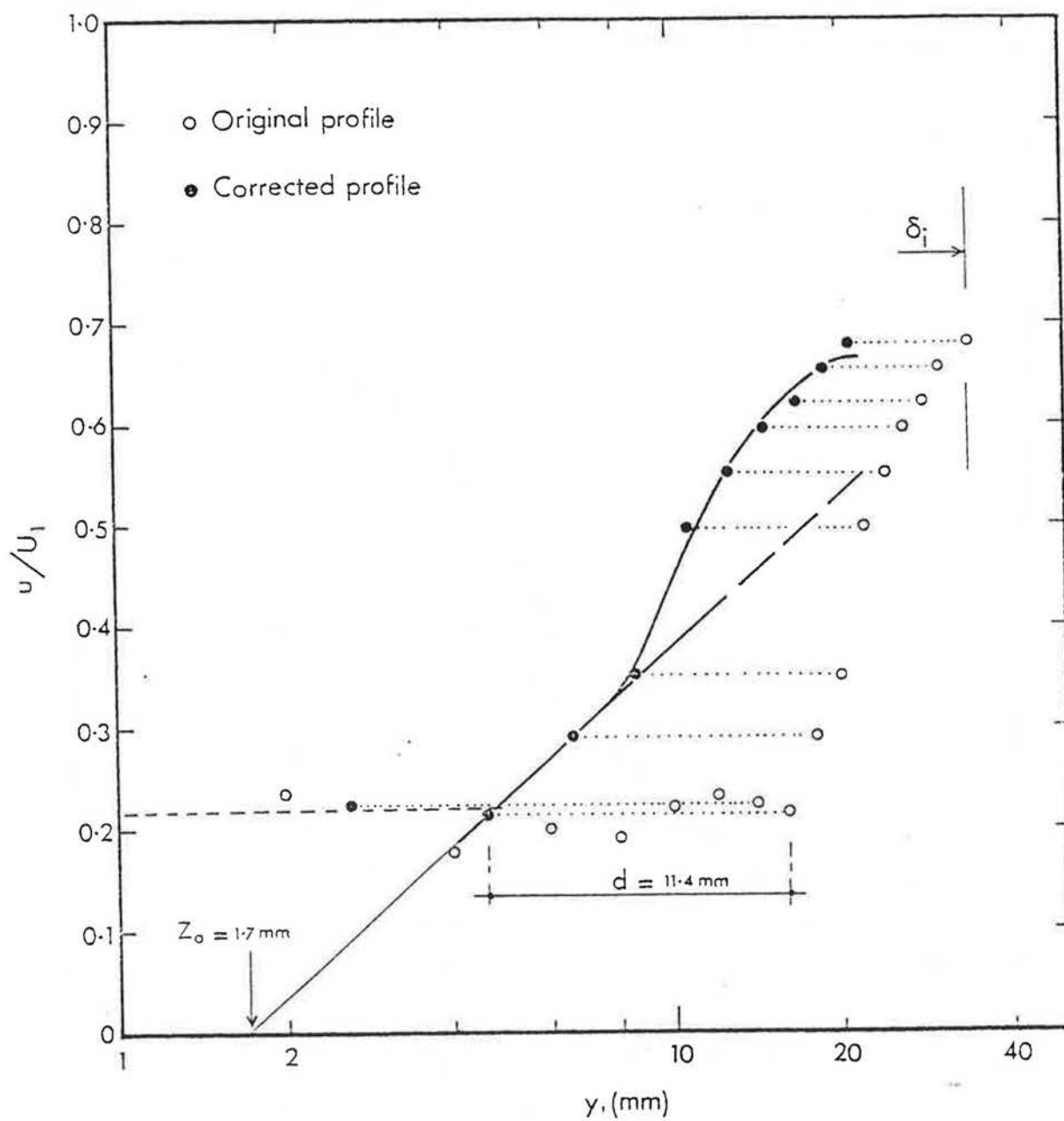


Figure 8.14 THE GRAPHICAL METHOD FOR DETERMINING THE ZERO PLANE DISPLACEMENT, d , ($\lambda = 12.5\%$).

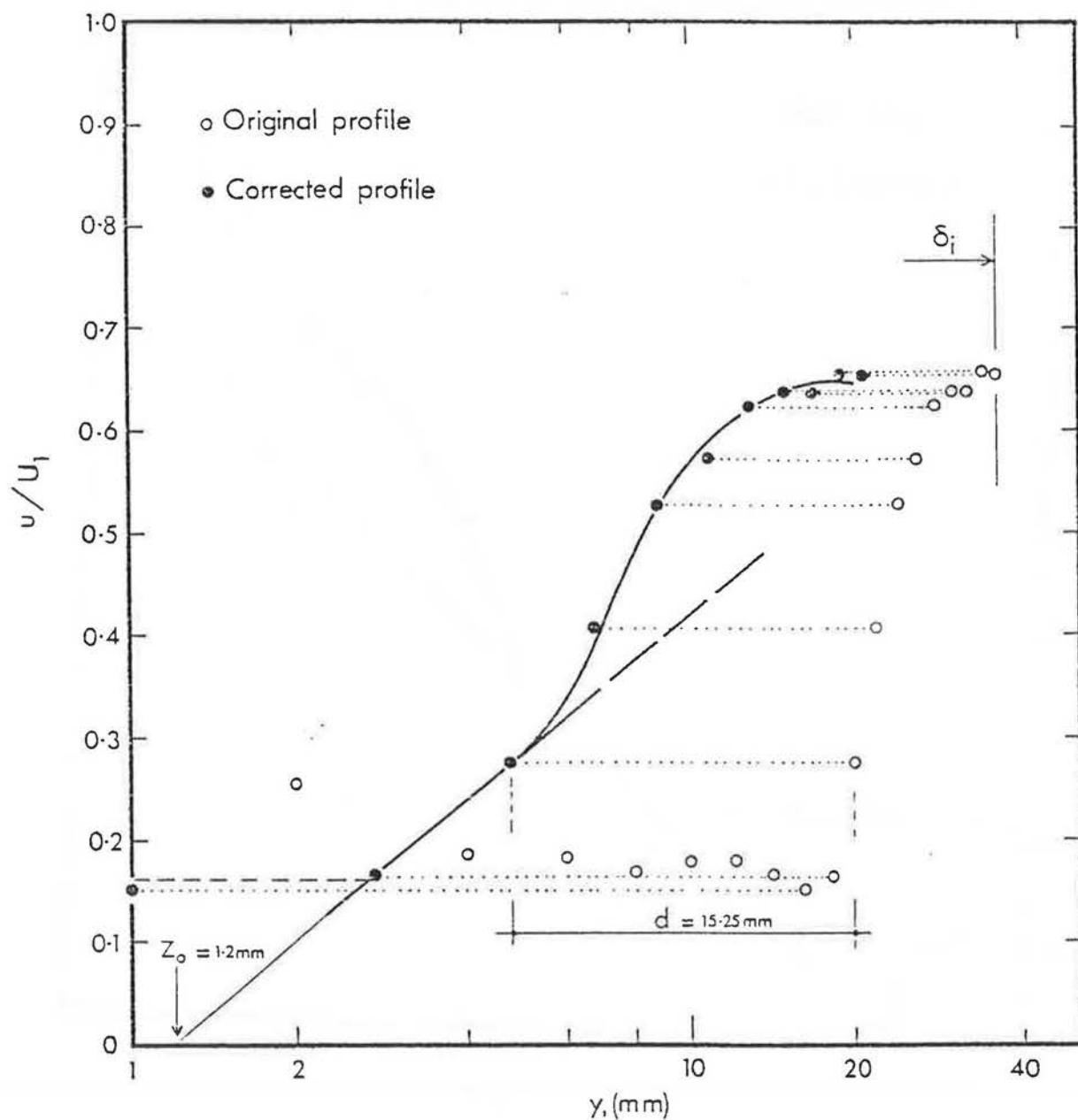


Figure 8.15 THE GRAPHICAL METHOD FOR DETERMINING THE ZERO PLANE DISPLACEMENT, d , ($\lambda = 25\%$).

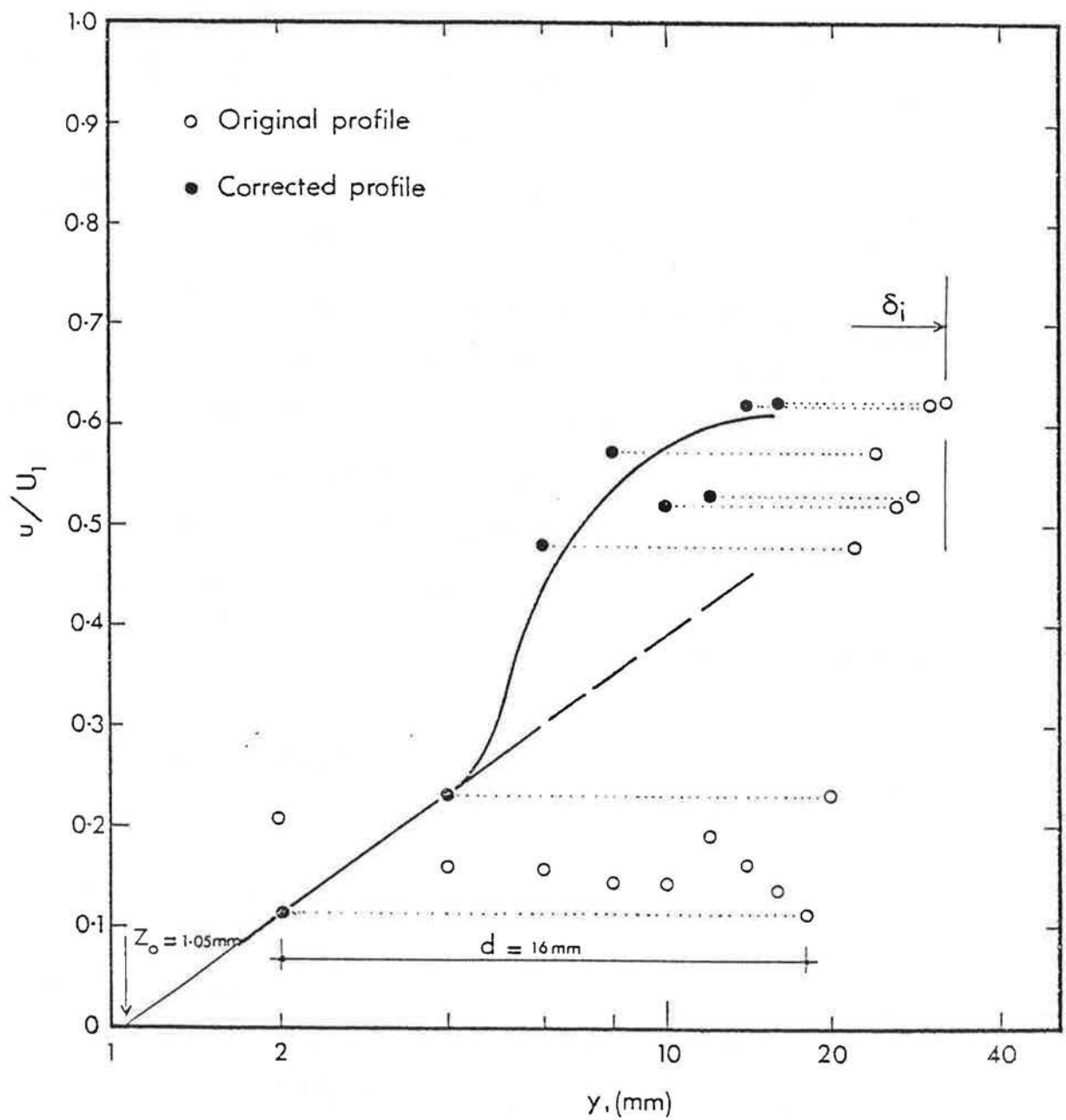


Figure 8.16 THE GRAPHICAL METHOD FOR DETERMINING THE ZERO PLANE DISPLACEMENT, d , ($\lambda = 32\%$).

logarithmic region below that of the internal layer due to the cube array, see Figure 8.12 and 8.13. Similar observations have been reported by O'Loughline and Annambhotla (1969) for flow over very low density arrays of cubical roughness elements, $\lambda_{\max} = 1.5\%$. They have attributed this lower logarithmic region to the flow over the smooth intervening surface between the roughness elements.

8.3.6 Three parameters are obtained from the analysis made in Figures 8.12 - 8.16, these being the zero plane displacement, d , the roughness length Z_0 and the internal layer thickness, δ_i . From the relations, $H = d + \epsilon$ and $K_s = 30 Z_0$, the error in origin, ϵ , and the equivalent sand grain roughness, K_s , were also obtained. These parameters are given in table 8.2.

Table 8.2 Velocity profile parameters for the various densities

λ (%)	d (m)	ϵ (m)	Z_0 (m)	K_s (m)	δ_i (m)
4	0.003	0.0170	0.0016	0.0480	0.032
8	0.006	0.0140	0.00265	0.0800	0.036
12.5	0.0114	0.0086	0.0017	0.0510	0.034
25	0.0153	0.0047	0.0012	0.0360	0.036
32	0.016	0.0040	0.00105	0.0315	0.032

Velocity profiles of the form u/u_* against $(y-d) u_*/\nu$ have been plotted in Figure 8.17 from which the roughness function $\frac{\Delta u}{u_*}$ has been obtained. The values of $\frac{Hu_*}{\nu}$ and

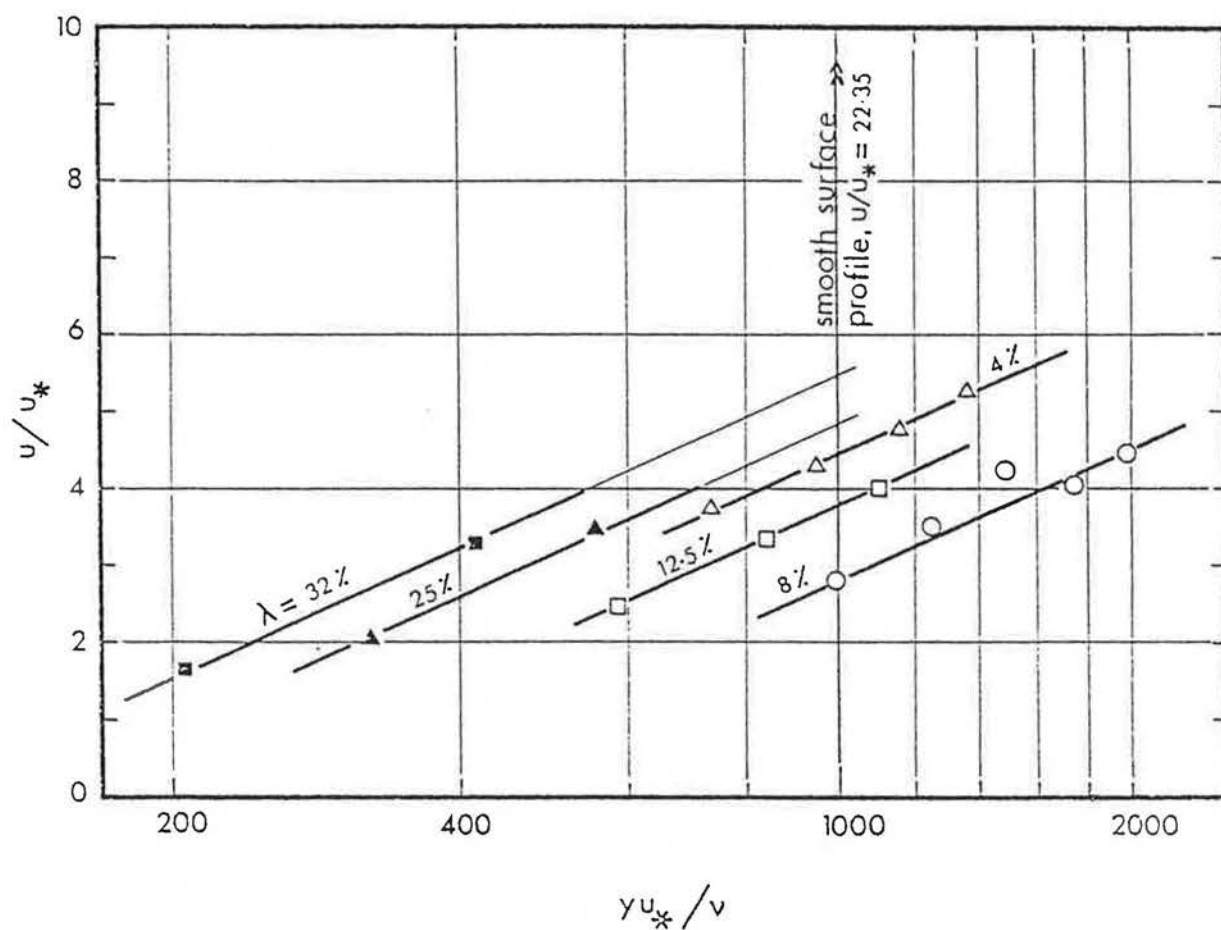


Figure 3.17 VELOCITY PROFILES IN THE FORM u/u_* VERSUS yu_*/ν .

$\frac{\epsilon u_*}{\nu}$ (the two correlation schemes with the roughness function to $\frac{\Delta u}{u_*}$) for the densities 4%, 8%, 12.5%, 25% and 32% are given in table 8.3. Neither $\frac{\Delta u}{u_*}$ nor ϵ were obtained for 50% density, since the only profile made was on top of the cube and did not show the logarithmic region.

Table 8.3 Roughness function parameters at various densities

$\lambda\%$	$\frac{\Delta u}{u_*}$	$\frac{Hu_*}{\nu}$	$\frac{\epsilon u_*}{\nu}$
4	17.91	2098	1888
8	19.59	2485	1740
12.5	18.60	2552	1098
25	17.55	2340	556
32	16.85	2065	413

The variation of $\Delta u/u_*$ with density, shown in Table 8.3, displays a similar trend to that of the effective skin friction coefficient C'_{f_e} , in which a maximum is obtained at the start of the wake interference flow regime. This is followed by a decrease in the skimming flow regime to a value of zero at 100% density, corresponding to flow over the smooth surface formed by the elements top surfaces.

8.4 Discussion of the velocity profile parameters

8.4.1 In the absence of a theoretical prediction technique to assess the validity of the present results, the only alternative is to compare them with previous comparable work in the field, the review of which is given in Chapter 5.

8.4.2 The roughness function $\frac{\Delta u}{u_*}$ obtained for the different densities, and hence different flow regimes, is checked against the two correlation schemes available, i.e. $\frac{Hu_*}{V}$ suggested by Clauser (1956) and $\frac{\epsilon u_*}{V}$ suggested by Perry, Schofield and Joubert (1969). In Figure 8.18 the results of Perry and Joubert (1963) and Perry, Schofield and Joubert (1969) for the wake interference flow regime are replotted together with the present results. The variation of density at a constant fetch in the present study resulted in small variation in the friction velocity u_* , hence the experimental data are covering smaller range than those by Perry et. al. (1963) and Perry et. al. (1969). Although their work was only for one density the large fetches considered, resulted in an appreciable change in u_* . Despite the limited range of roughness covered by the present experiments, there is a reasonable agreement for the isolated roughness flow regime and the wake interference flow regime. The deviation of the skimming flow regime results (i.e. for $\lambda = 25\%$ and 32%) is to be expected, since such a flow regime has been shown to yield poor correlation with $\frac{Hu_*}{V}$, Perry, Schofield and Joubert (1969). In the second correlation scheme, the present results are shown plotted in Figure 8.19 together with the line of best fit and the zone of experimental scatter obtained from the work of Perry, Schofield and Joubert (1969).

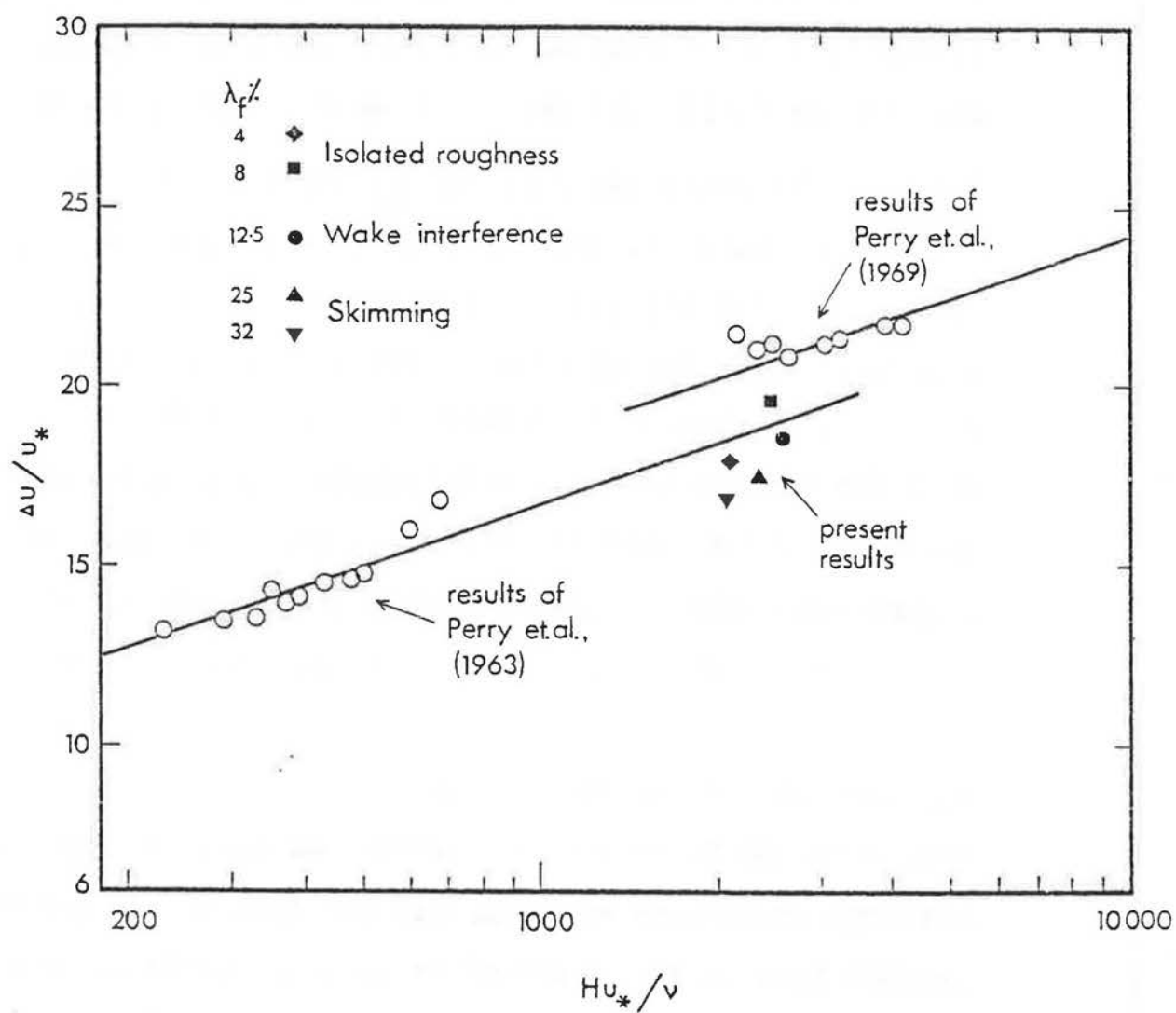


Figure 8.18 VARIATION OF THE ROUGHNESS FUNCTION WITH THE ROUGHNESS REYNOLDS NUMBER, Hu_*/ν .

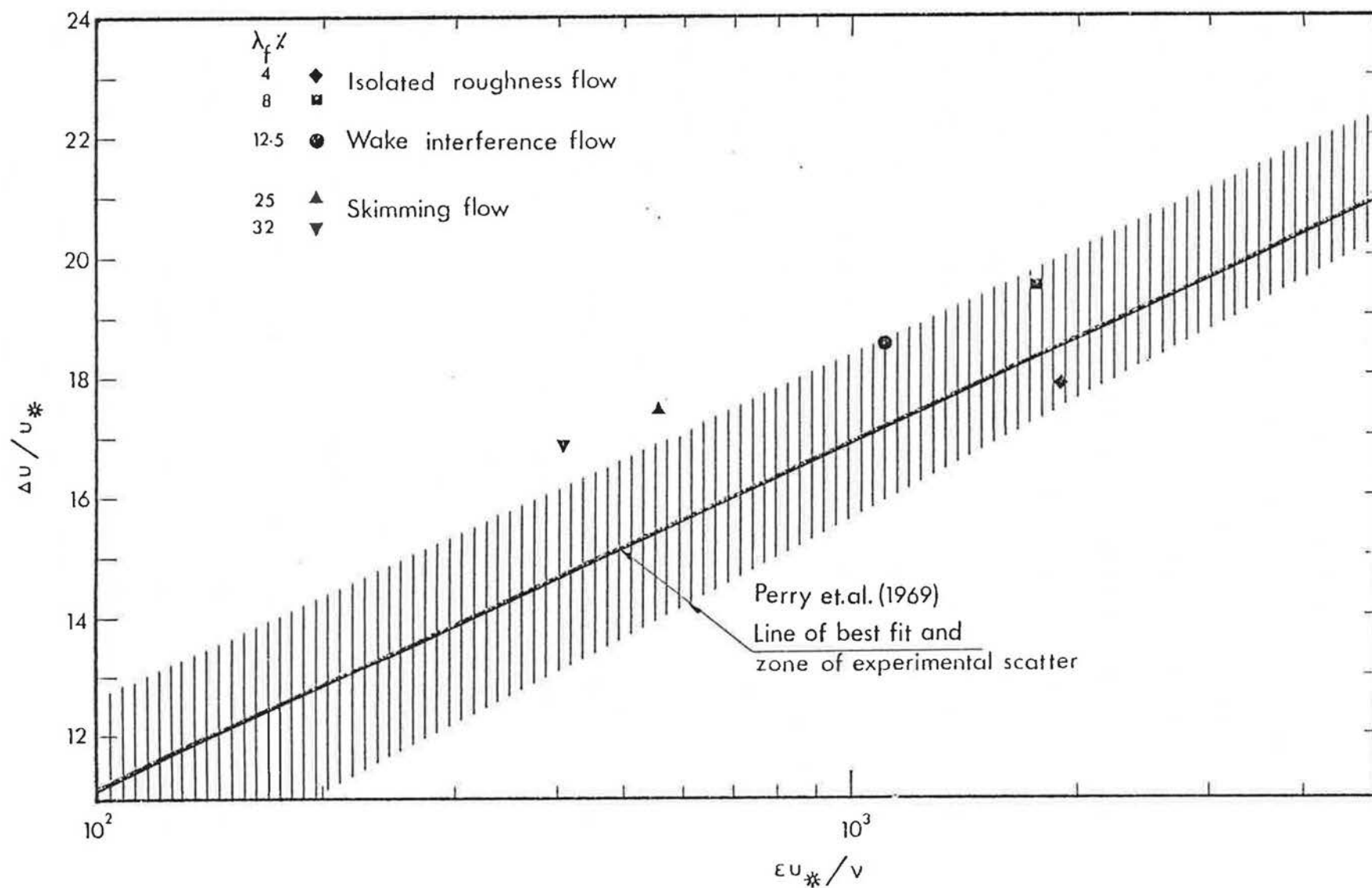


Figure 8.19 VARIATION OF THE ROUGHNESS FUNCTION WITH THE ROUGHNESS REYNOLDS NUMBER $\epsilon u^*/\nu$.

Reasonable agreement can be seen for this correlation scheme. From the good agreement obtained so far, it is suggested that the values of ϵ , the error in origin and Z_o , the roughness length, are sufficiently accurate to continue the investigation to see the effect of varying λ_p , the group density on the velocity profile parameters.

8.4.3 The variation of \bar{d}/H with λ_p has been previously investigated by Counihan (1971). A comparison between his results (in which λ_p has been replotted as λ_f) and the present results is shown in Figure 8.20. The values of \bar{d}/H obtained by Counihan are lower than the corresponding values in the present work. One reason for this difference is that the values of \bar{d}/H are an average of several locations normal to the flow between the block centre line and the street centre line. This figure indicates that a straight line relationship exists between the zero-plane displacement and the density in the isolated roughness and wake interference flow regimes. Further evidence for this linear relationship given from Cook's results, (1976) and obtained from rectangular blocks ($L = 100$ mm, $W = 50$ mm, $H = 50$ mm) in a staggered pattern is shown in this figure. A separate relationship for the skimming flow regime is suggested from both the present results and Counihan's extrapolated line.

8.4.4 The variation of Z_o/H , the roughness length, with λ has also been compared with the results obtained by Counihan (1971), shown in Figure 8.21. Both results show an increase in the roughness length with λ_f to reach a maximum then a subsequent decrease. This maximum in the value of Z_o/H occurs at the change of regime from isolated roughness flow to wake interference flow. It was shown in the

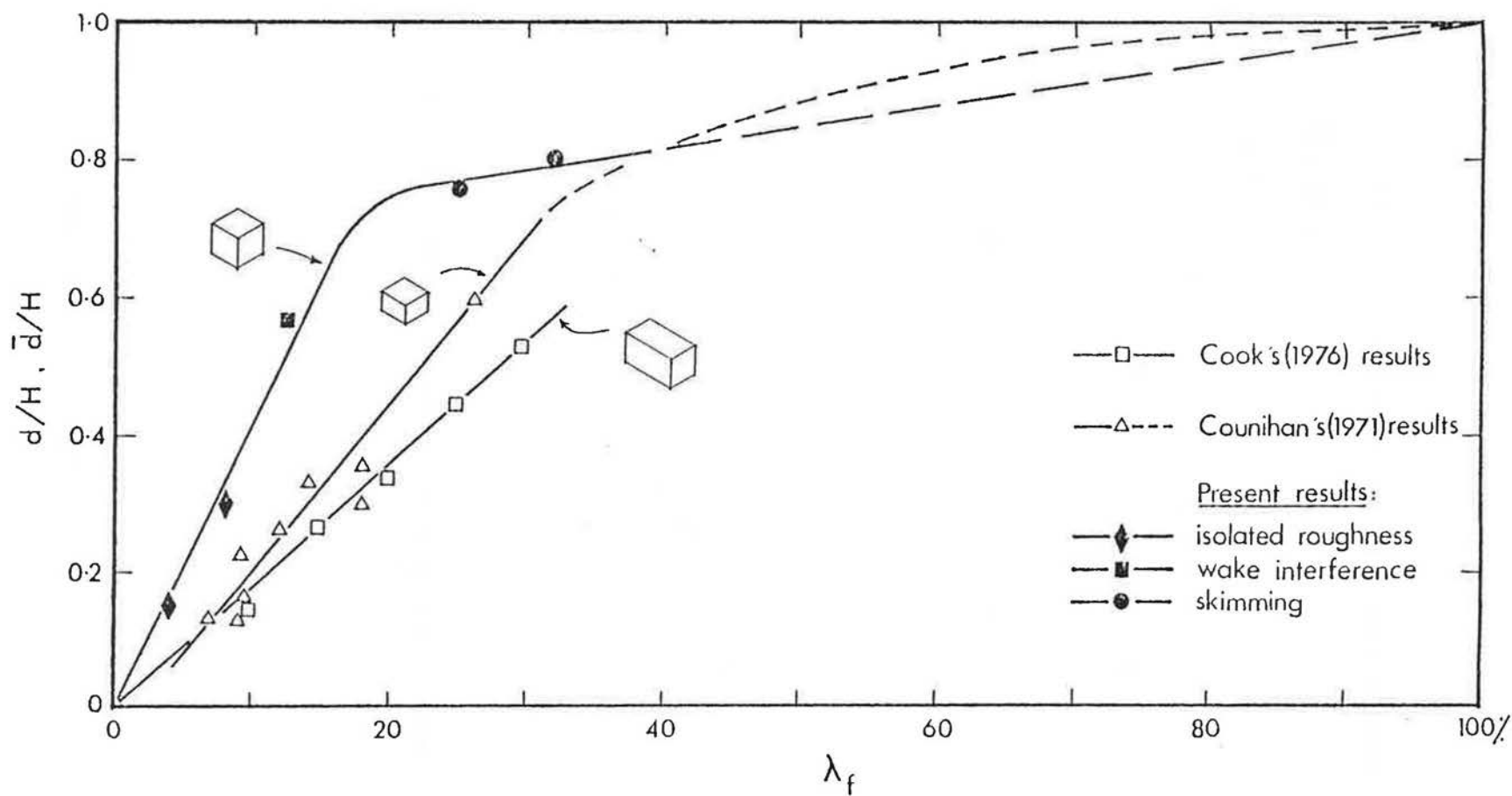


Figure 8.20 VARIATION OF THE ZERO PLANE DISPLACEMENT WITH DENSITY.

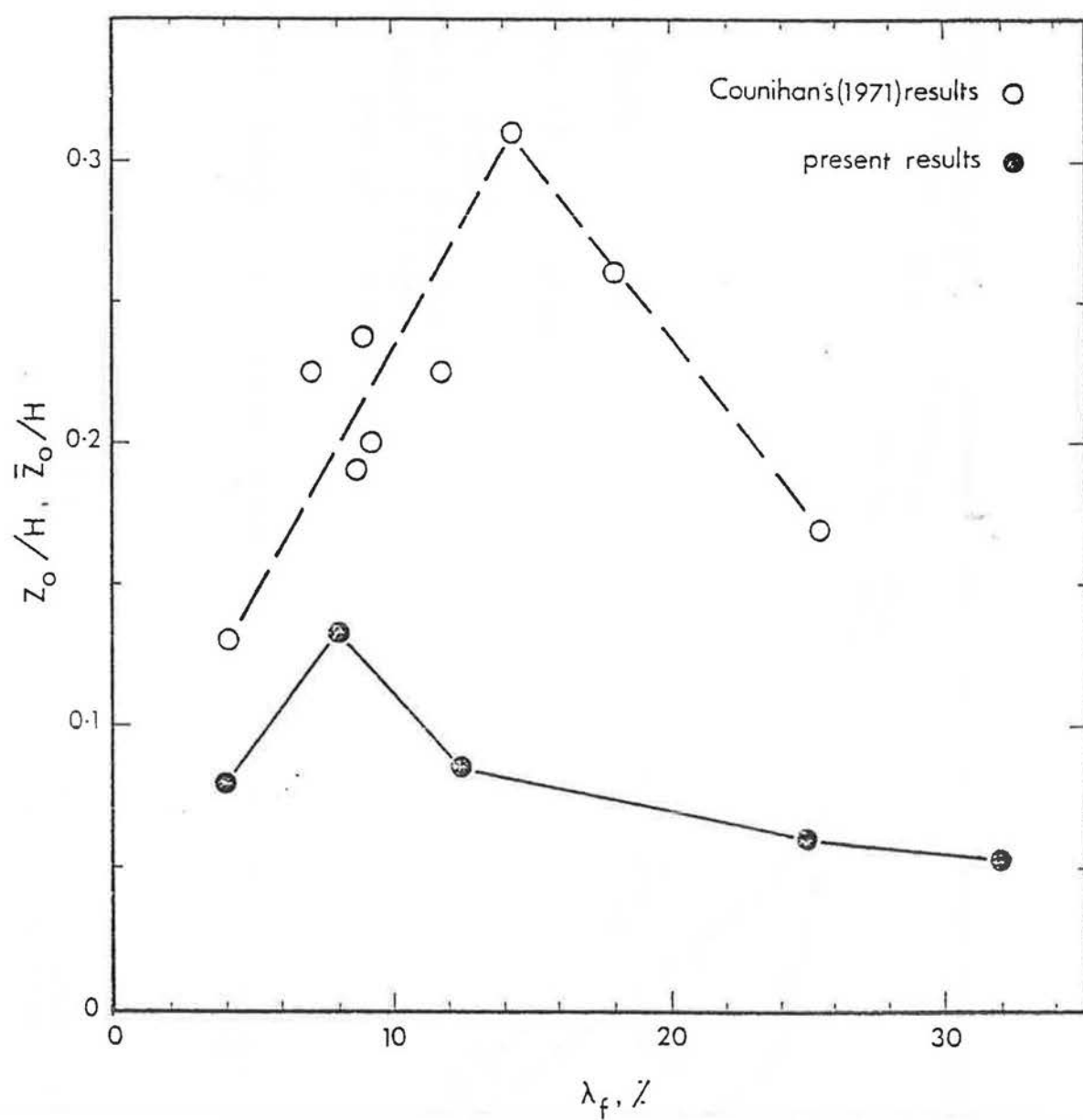


Figure 8.21 VARIATION OF z_o/H WITH λ_f .

previous chapter that such a change occurs at the same value of S/H and not λ_f for both the normal and the staggered pattern. Therefore the difference between the value of λ_f at which both Z_o/H and \bar{Z}_o/H reach their maximum is thought to be primarily due to the difference in layout patterns used by Counihan and that used in the present investigation, where different values of λ_f resulted from the same value of S/H . The values of \bar{d}/H obtained by Counihan were found by the graphical method of Perry and Joubert (1963) used in the present investigation but relied on a trial and error method which did not utilize C'_{fe} to determine the correct slope of the logarithmic line. It is thought that this may have resulted in an underestimate of the values of \bar{d}/H . Since lower values of d result in higher values of Z_o , this would explain the higher values of \bar{Z}_o/H in Figure 8.21 and the lower values of \bar{d}/H in Figure 8.20.

8.4.5 The present results have been compared in Figure 8.22 with the variation of K_s/H , the equivalent sand grain roughness with λ_f , reported by Koloseus and Davidian (1966) whose results were for roughness elements in the staggered pattern. In this pattern the value of λ_f obtained at a particular cube spacing S/H is double that obtained in a normal pattern. Therefore, in order to compare the present results for the normal pattern with those of Koloseus et. al. the results are plotted against λ_f and then shifted to correspond to double their original values, as shown in Figure 8.22. The agreement is satisfactory in the isolated roughness flow and wake interference flow regimes. In the skimming flow regime, it

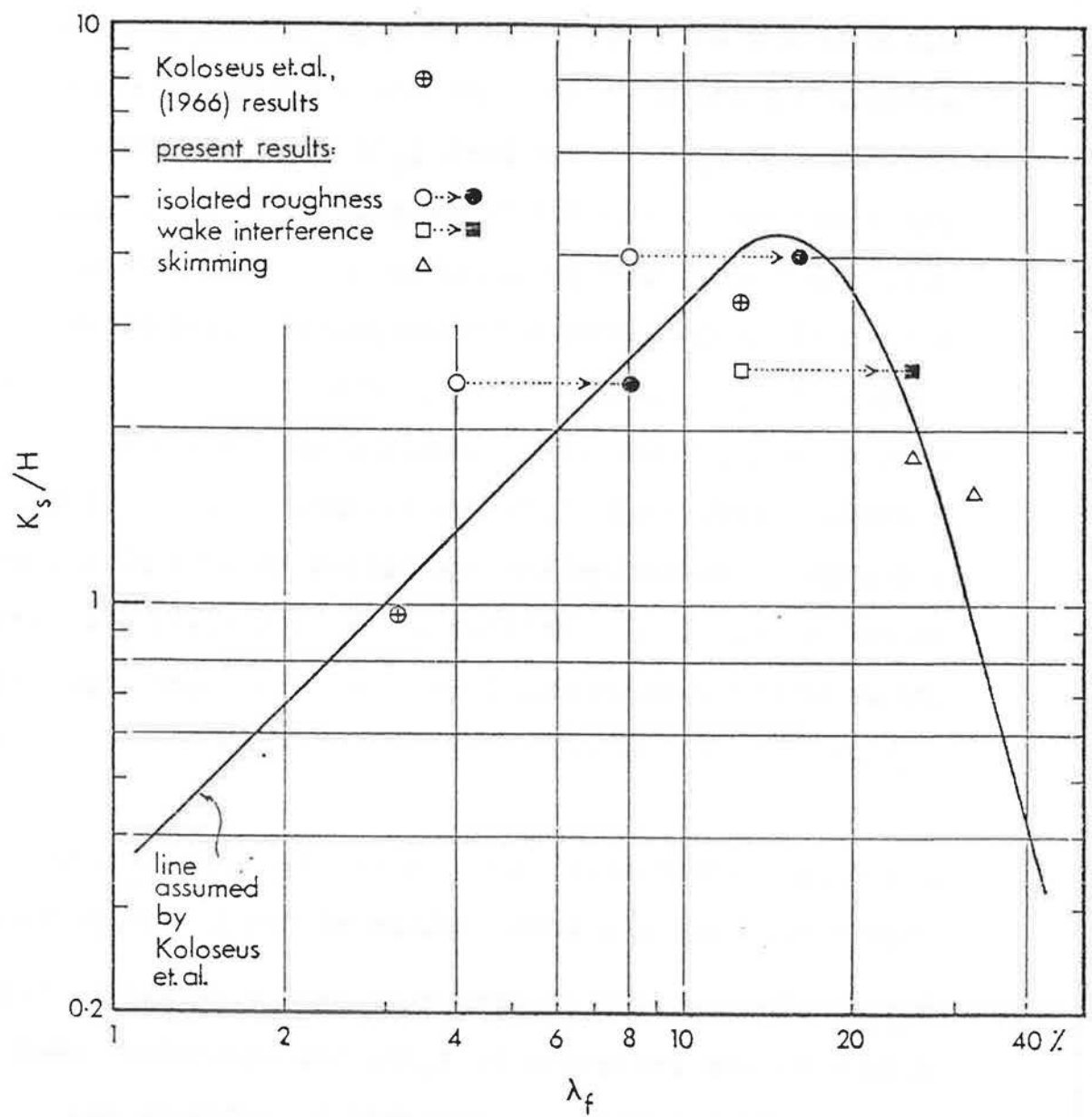


Figure 8.22 VARIATION OF k_s/H WITH λ_f .

appears that agreement between the present results and those of Koloseus et. al., does not depend on the shift of λ_f . This would imply that in this flow regime the dependency of K_s/H is primarily on the group density and not the spacing parameter S/H . This suggestion is supported by the variation of the effective skin friction with λ_f shown in Figure 7.18. 7.19.

8.4.6 The depth of the internal layer, δ_i , obtained in zone IV was also compared with the results of Schofield (1975) and Antonia and Luxton (1971). In Figure 8.23, $\frac{\delta_i - d}{Z_o}$ is shown plotted against R/Z_o where R is the group layout fetch. Good agreement is obtained not only with the experimental results of Schofield and Antonia et. al. but also with the theoretical prediction by Townsend's theory (1965) for the growth of an internal layer following a change in surface roughness. Consequently, it is concluded that the values of δ_i as well as Z_o are satisfactorily correct.

8.5 Correlations between group geometry, flow properties and the resulting pressure forces

8.5.1 The correlation between the group geometry parameters and the resulting pressures in terms of S/H versus C_{p_w} and C_{p_l} and C'_{f_e} versus λ_f are given in Chapter 7 in the discussion of the pressure measurements. In this chapter where flow measurement results are discussed, the correlations are given between the group geometry and the flow parameters in 8.3.3 to 8.3.5. In addition to

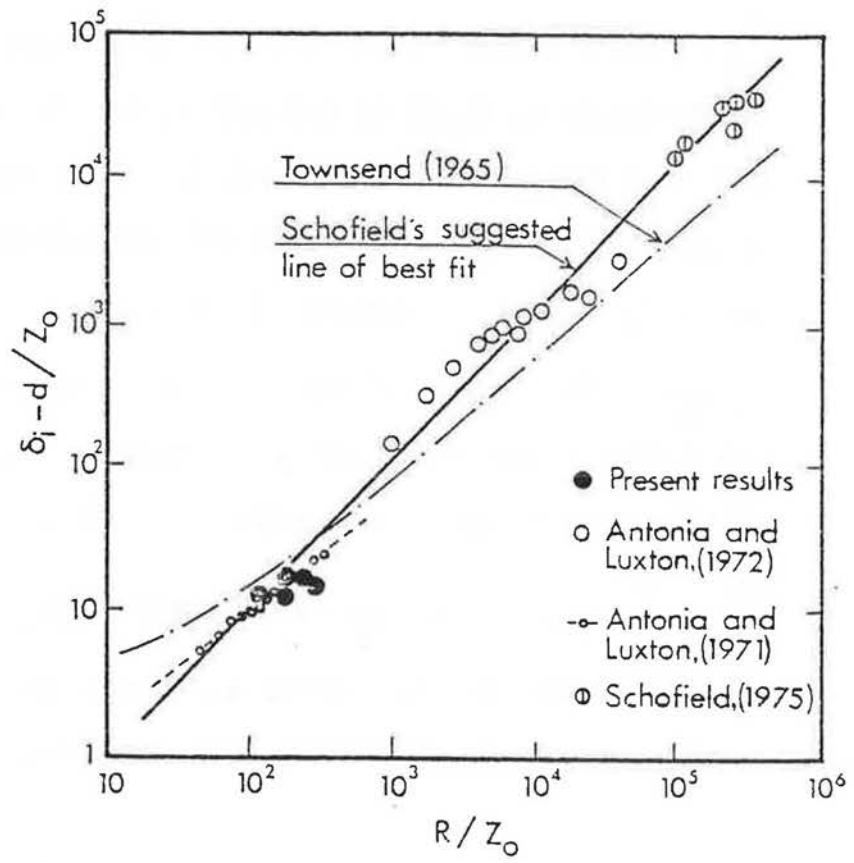


Figure 8.23 COMPARISON OF EXPERIMENTAL GROWTH OF INTERNAL LAYER WITH THEORY & PRESENT RESULTS.

these correlations, it is hypothesized that a relationship may exist between the element spacing, S , and the velocity at the cube height, U_H . A plot of U_H/U_1 against the clear spacing between the cubes, S_c/H is shown in Figure 8.24. A straight line was found to represent the experimental points and may be expressed by:

$$\frac{U_H}{U_1} = 0.27 \log \frac{S_c}{H} + 0.27$$

Extrapolation of the line indicates that $U_H \rightarrow 0$ as $S_c/H \rightarrow 0$. It should be noted that the values of U_H used are those measured at the cube height without any correction due to the zero plane displacement d .

8.5.2 The correlation between the flow properties and the resulting pressure, was suggested in Chapter 5 to take the form of equation (5.25) i.e.

$$C_{D*} = m_3 \log \frac{\epsilon}{Z_0} + B_3 \quad \dots\dots (5.25)$$

where m_3 and B_3 are constants dependent on the characteristics of the rough surfaces. Values of C_{D*} were calculated and plotted against $\frac{\epsilon}{Z_0}$ as shown in Figure 8.25. From this figure, the experimental points may be representing a straight line expressed by:-

$$C_{D*} = 98 \log \frac{\epsilon}{Z_0} - 50.3$$

Also shown in the figure is the corresponding line given by Good and Jobert from their work on a two dimensional plate in smooth surface flow.

8.5.3 For the case of flow over an isolated element the element pressure distributions are commonly normalized

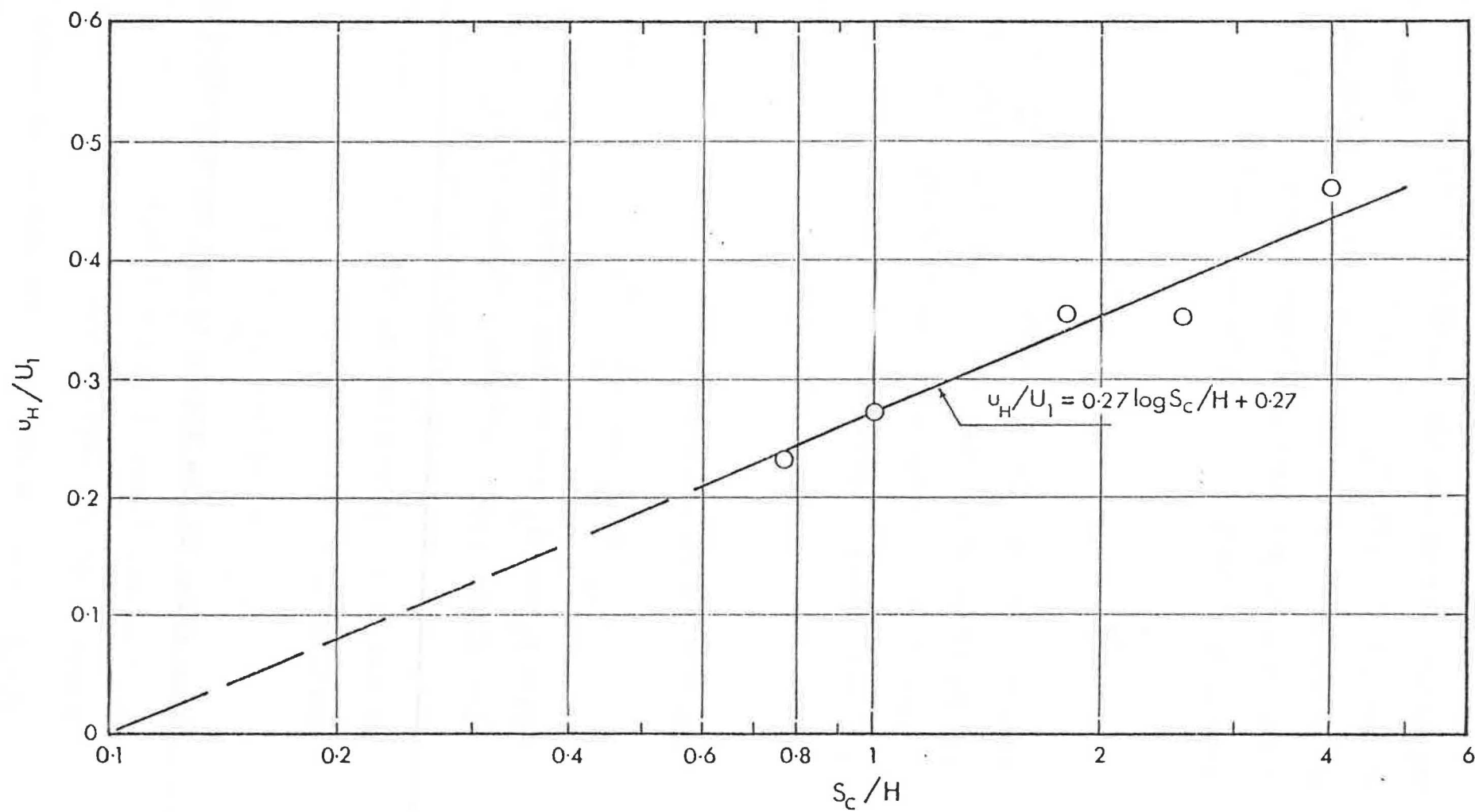


Figure 8.24 VARIATION OF $\frac{u_H}{U_1}$ WITH S_c/H .

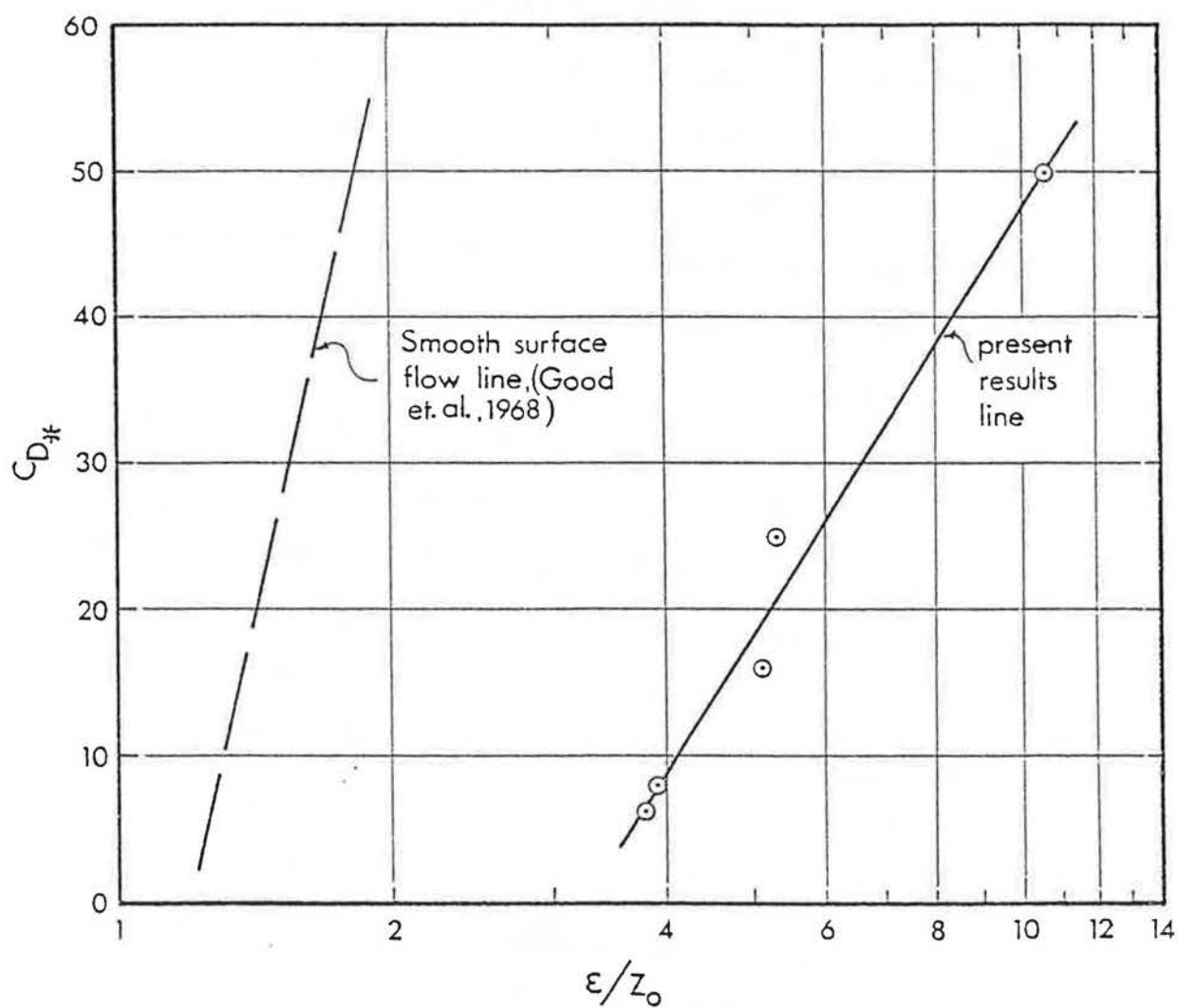


Figure 8.25 VARIATION OF C_{D*} WITH ϵ/z_0 .

with respect to the element height. However in the case of flow over groups of elements the boundary layer undergoes a zero plane displacement, d , which does not occur for the isolated element case. Hence it is suggested that a better correlation of the pressure distributions might be obtained if the effective height, ϵ , was used instead of H for normalizing the pressure tapping positions along the cube height. Since the maximum and minimum values of the pressure did not materially alter on the windward face of the cube at different densities, the pressure difference ($p_{\max} - p_{\min}$) on the face was used to normalize the different values of pressure. In order to have a pressure coefficient ranging from 0 to 1, the difference ($p - p_{\min}$) was used instead of the value of p . The values of ϵ determined from the different velocity profiles were used for the normalization of the corresponding pressure distributions previously obtained. Figure 8.26 shows a plot of $\frac{p - p_{\min}}{p_{\max} - p_{\min}}$ against $\frac{y - d}{\epsilon}$ in which the pressure distributions were approximately grouped around a single curve regardless of flow regime. It is considered that this collapse, though including some scatter is better than the previously suggested correlation in which only the isolated roughness flow was collapsed (see paragraph 7.3.8). It may also be noted that all the pressure profiles reached their maximum at a value of $0.6 - 0.7\epsilon$.

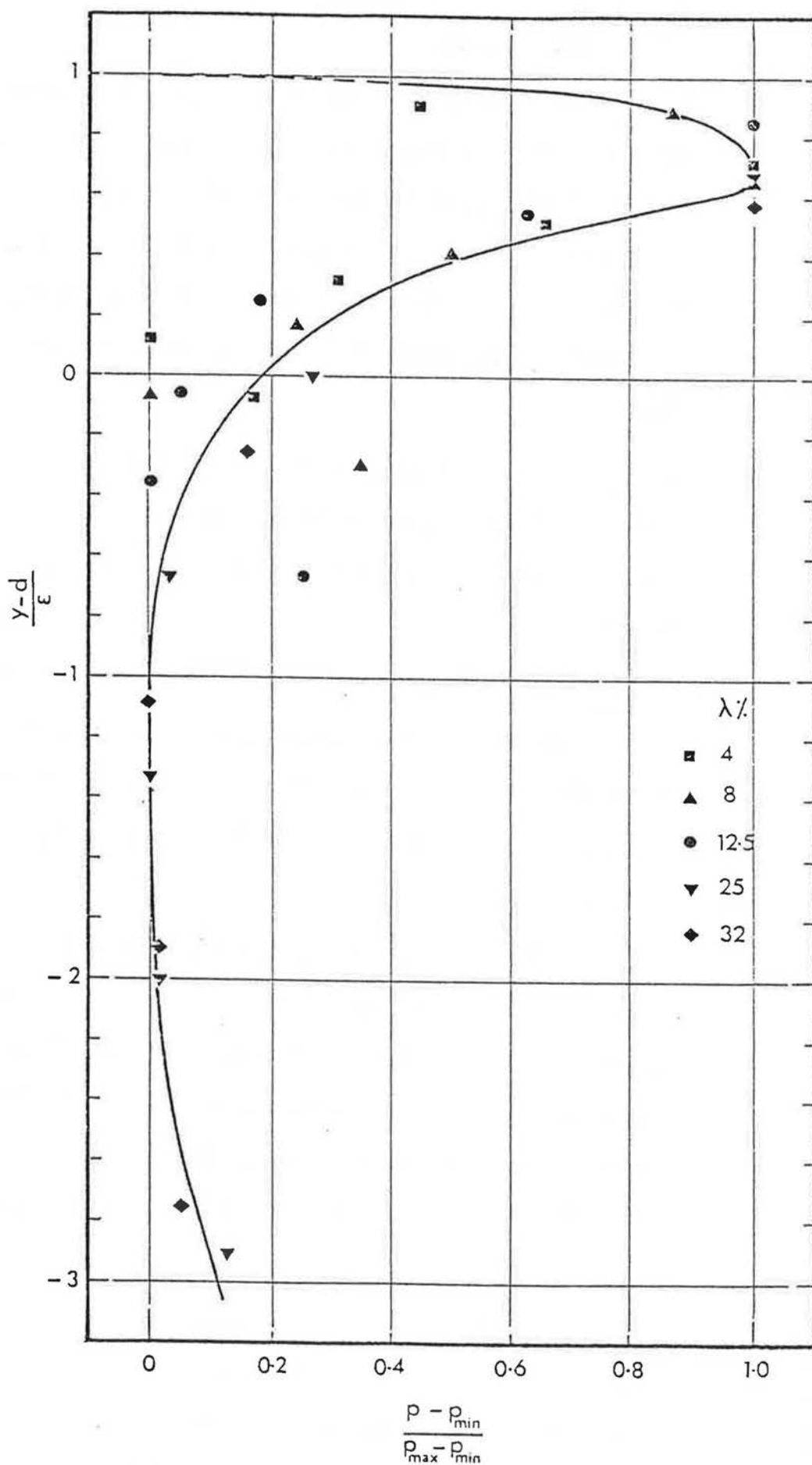


Figure 8.26 NORMALIZED PRESSURE PROFILES FOR THE THREE FLOW REGIMES.

8.6 Conclusions

8.6.1 The various changes of surface roughness experienced by the incident rough flow were reflected in all the velocity profiles in the form of different zones. The only change corresponding to group layout changes was noted to be in the lower zone of the profile, i.e. the internal layer growing over the group layout, (Figures 8.5 and 8.6).

8.6.2 The logarithmic region of the internal layer of the cube centre line profiles did not extend above the cube height in any case at the fetch considered (Figure 8.11)

8.6.3 In the isolated flow regime, the roughness function was shown to increase with increasing group layout density and reached a maximum at the change to the wake interference flow regime after which it decreased, (Table 8.3)

8.6.4 The Clauser type correlation scheme for the roughness function and the roughness Reynolds number based on the friction velocity and the element height (the cube height) was shown to yield good correlation for the present experimental results in the isolated flow and wake interference flow regimes, (Figure 8.18).

8.6.5 The alternative correlation scheme suggested by Perry, Schofield and Joubert (1969) for the roughness function and the Reynolds number based on the friction velocity and the error in origin was also shown to yield reasonable agreement, (Figure 8.19).

8.6.6 A linear relationship was shown to exist between the zero plane displacement and the group layout density for both the isolated flow and wake interference flow regimes. Another relationship is suggested to exist for the skimming flow regime, (Figure 8.20).

8.6.7 The variation of the roughness length with increasing group layout density was shown to increase to reach a maximum at the change from the isolated roughness flow regime to the wake interference flow regime and to decrease subsequently (Figure 8.21).

8.6.8 The variation of the equivalent sand grain roughness with increasing density showed good agreement between the present results and the results of Koloseus and Davidian (1966) (Figure 8.22).

8.6.9 The depth of the internal layer obtained indicated good agreement with both previous results and the theoretical prediction by Townsend, (Figure 8.23).

8.6.10 A relationship was suggested to exist between the velocity at the cube height and the clear spacing between cubes, (Figures 8.24).

8.6.11 A relationship between the drag coefficient based on the friction velocity and the error in origin normalized with respect to the roughness length was also shown to exist, (Figure 8.25).

8.6.12 A normalization scheme for the pressure distribution profiles which takes into account the zero plane displacement and the effective height (error in origin) has been suggested. In this scheme there was an approximate

collapse of all the pressure distribution profiles on a single curve, (Figure 8.26).

CHAPTER 9

EXPERIMENTAL RESULTS AND DISCUSSION:
Surface Flow Visualization.

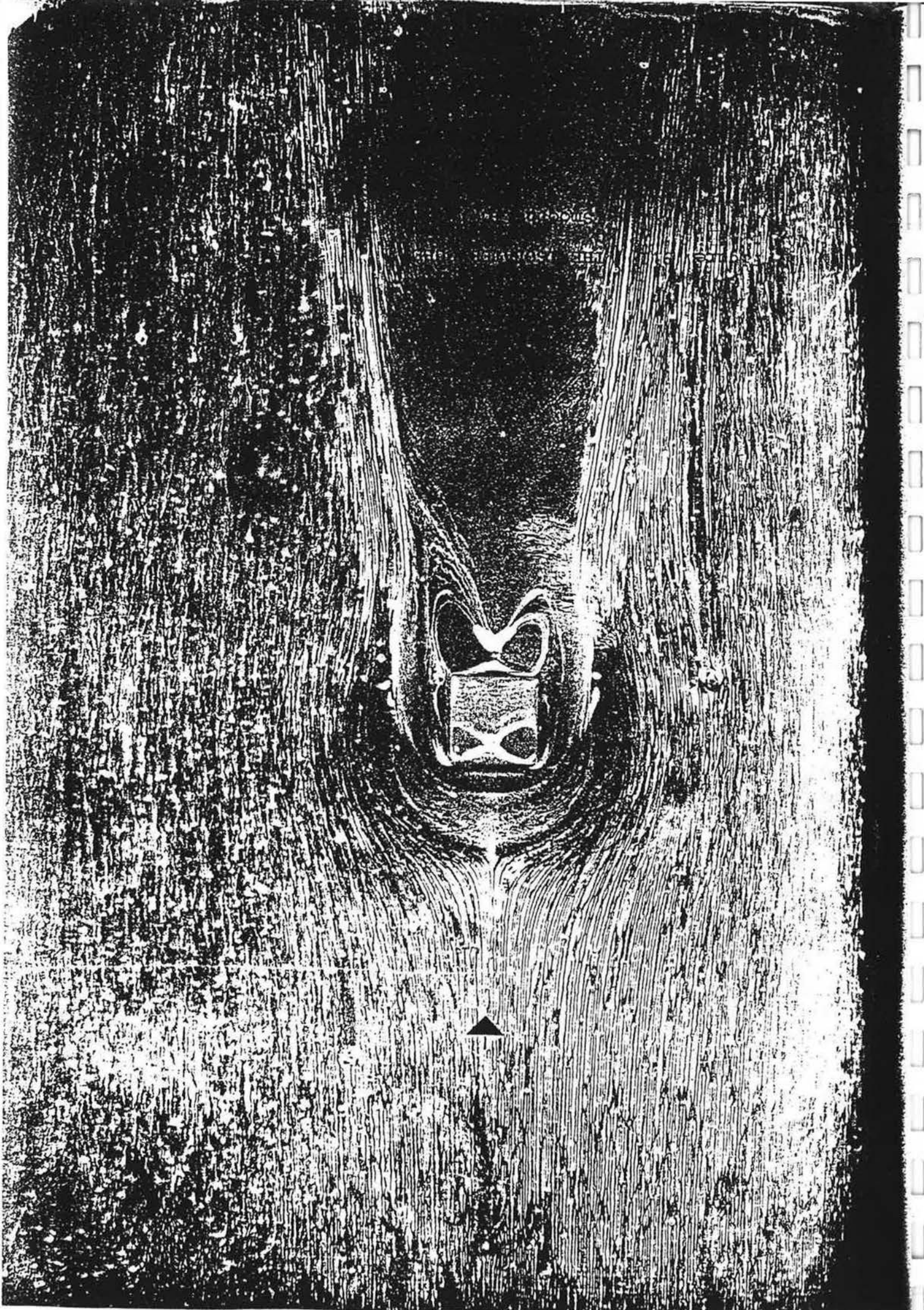
9. EXPERIMENTAL RESULTS AND DISCUSSION:
Surface Flow Visualization.

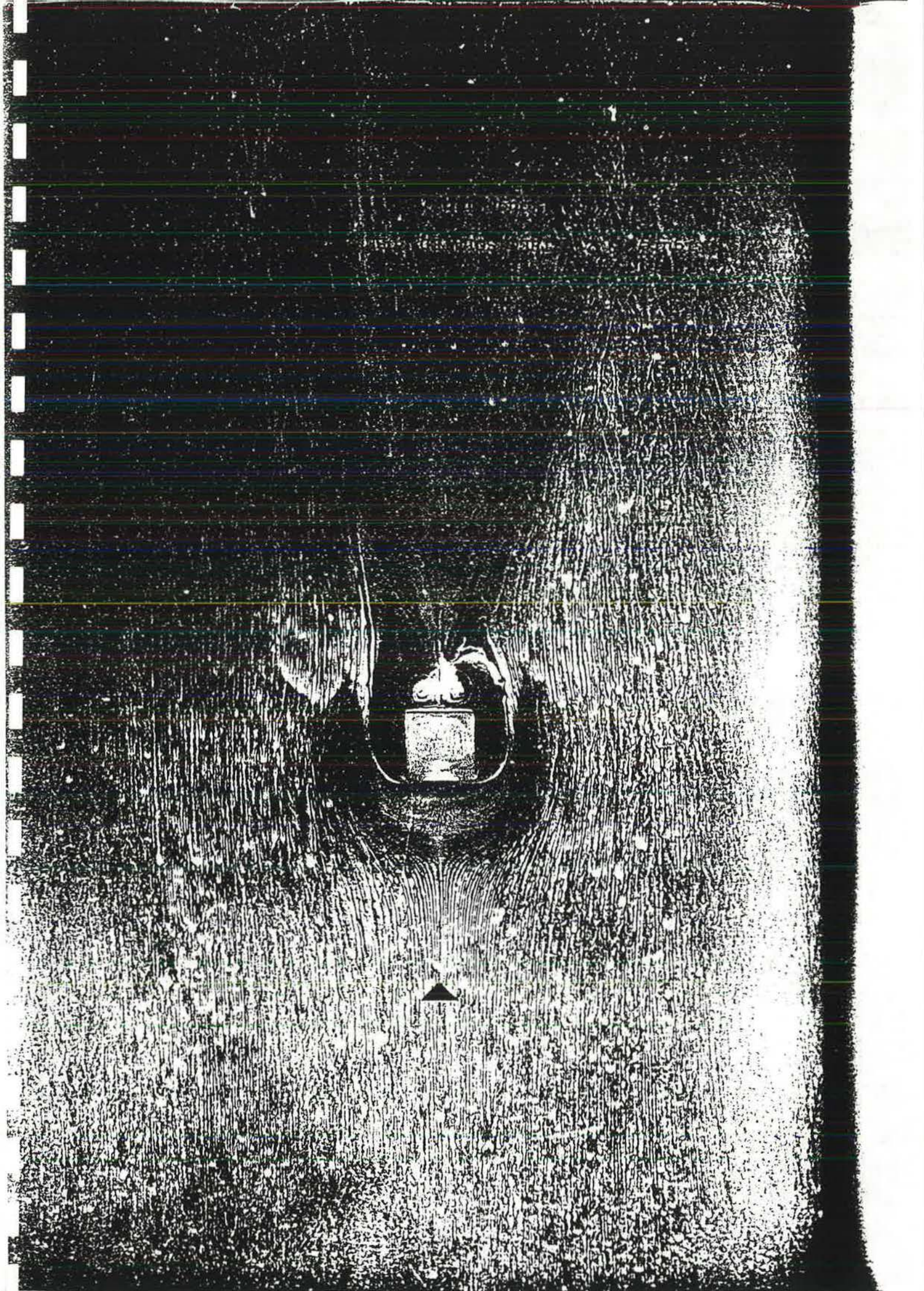
9.1 Introduction

9.1.1 In the flow visualization experiments, only a small selection of the many possible combinations of flow and form parameters were examined. This selection was composed of one value of the density in each of the flow regimes for each of the two layout patterns under investigation. The density parameter was given the following values, $\lambda = 4\%$ (isolated roughness flow regime), 16% (wake interference flow regime) and 50% (skimming flow regime) in the case of the normal pattern. The corresponding density values investigated for the staggered pattern were 8% , 32% and 50% . Two results were obtained for each density and pattern, one for the rough incident flow and the other for the smooth incident flow.

9.2 Discussion of the isolated cube case

9.2.1 The flow pattern obtained from the isolated cube in both the smooth and rough flows are shown in Figures 9.1 and 9.2. The similarity of flow pattern is apparent in the two figures, though the smooth flow resulted in a clearer display, this possibly resulting from the higher velocities close to the surface. These two surface flow patterns have been used to build up a three-dimensional picture of the flow around the cube, Figures 9.3 and 9.4. From these the main features of the





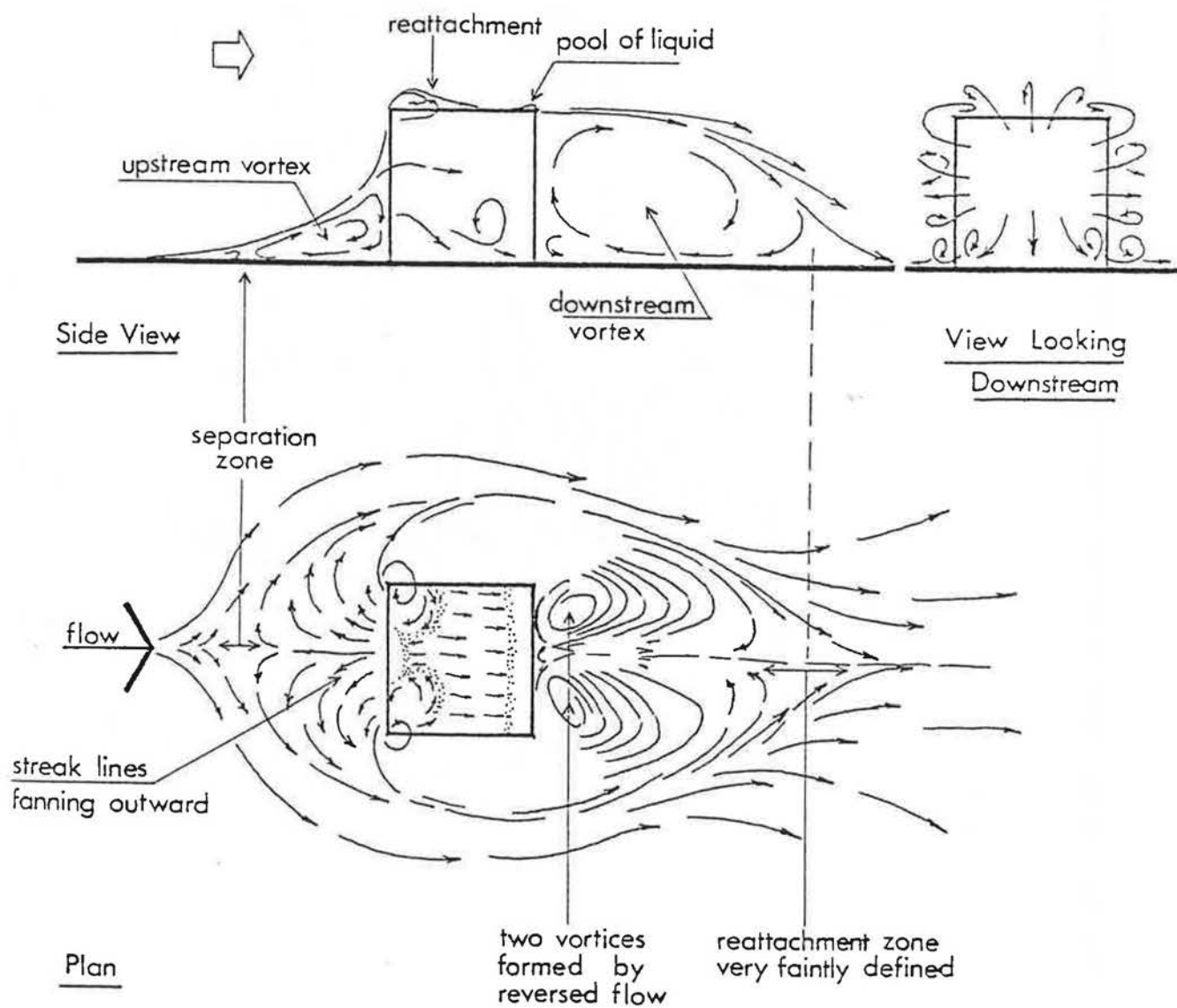


Figure 9.3 THE FLOW PATTERN ROUND AN ISOLATED CUBE.

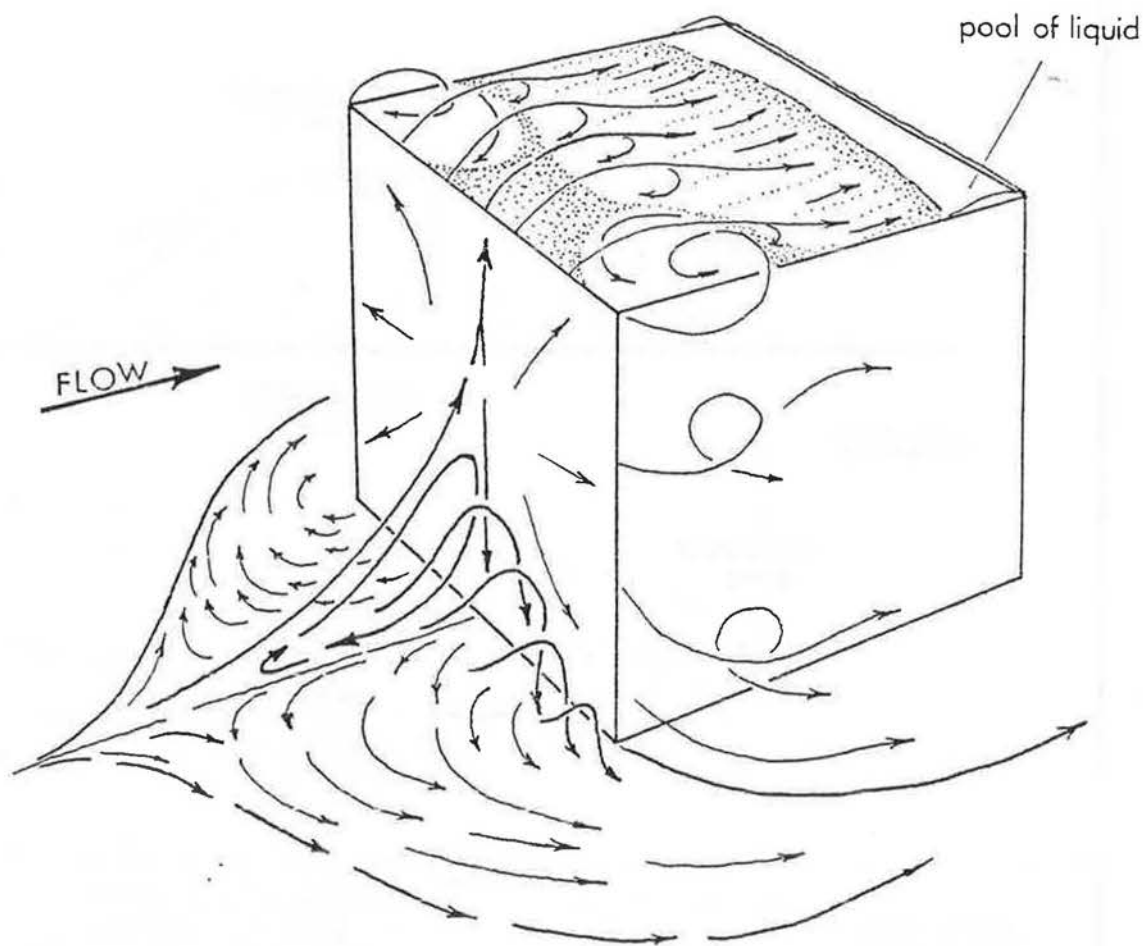


Figure 9.4 SUGGESTED THREE-DIMENSIONAL DIAGRAM
FOR THE FLOW PATTERN ROUND THE
ISOLATED CUBE.

flow may be summarized as follows:

- (i) The existence of an upstream vortex which is identified by the streaklines fanning outward from the windward cube face.
- (ii) The existence of a downstream eddy bubble formed by the reversed flow. The separation originating at the windward edge of the vertical cube sides seems to divide the bubble into two vortices forming at the leeward cube wall. Although the flow reattaches on the ground plane leeward of the cube, the reattachment zone is very faintly defined. This is probably due to the zero velocity of the flow in that zone.
- (iii) The flow separation which occurs at the cube top windward edge is followed on the upper surface by a reattachment at about $H/3$ from the windward edge. Two small vortices were noted to exist at the leading top surface corners. Therefore the pigment collected round the edge of these vortices and may be seen as a white zone in Figures 9.1 and 9.2. The suggested flow pattern in these zones may be seen in the 3-dimensional diagram of Figure 9.4.

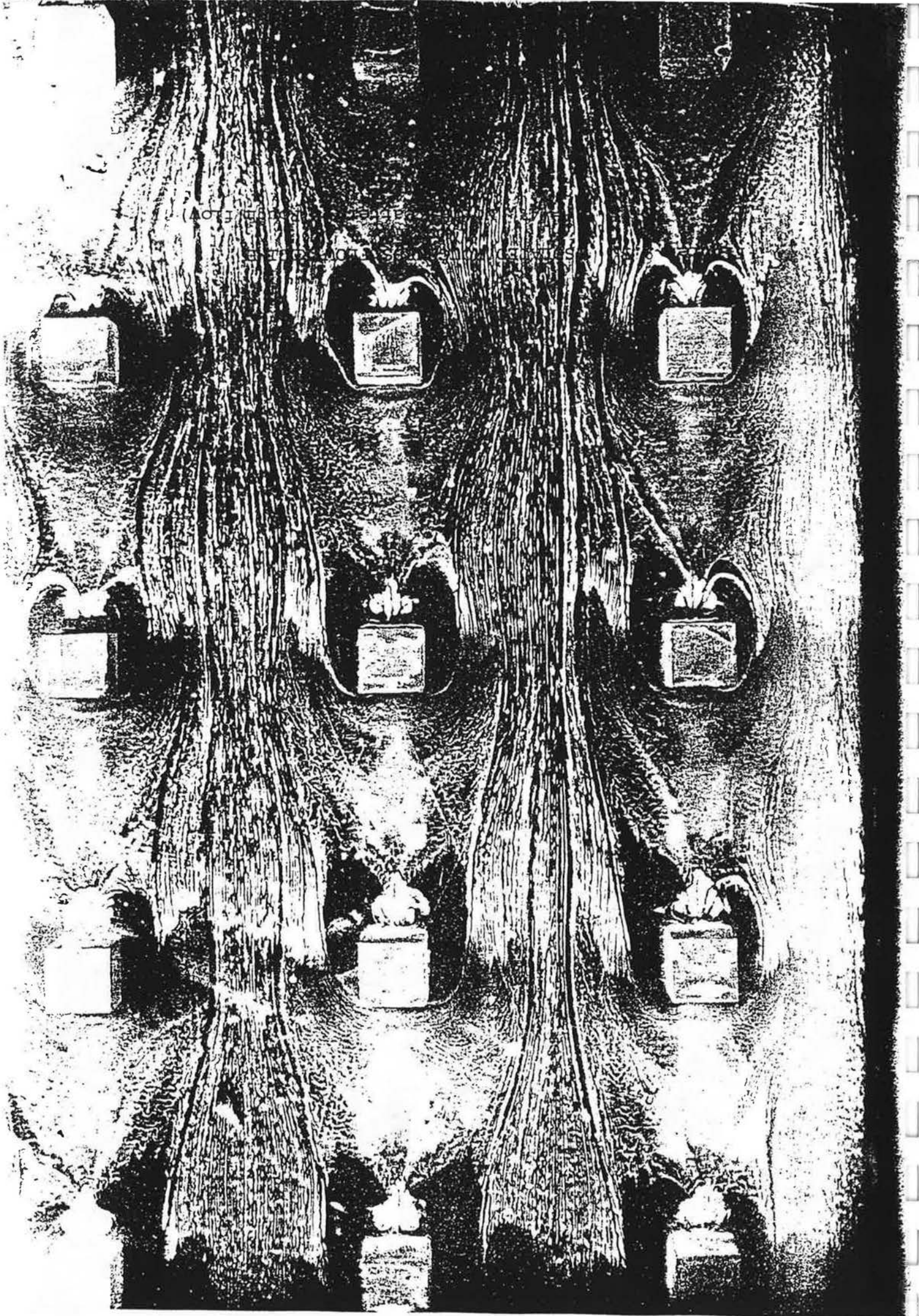
9.2.2 When the top of the cube was sprayed with an ample amount of paint mixture, the liquid was pushed to the leeward edge of the cube top by the reattached flow

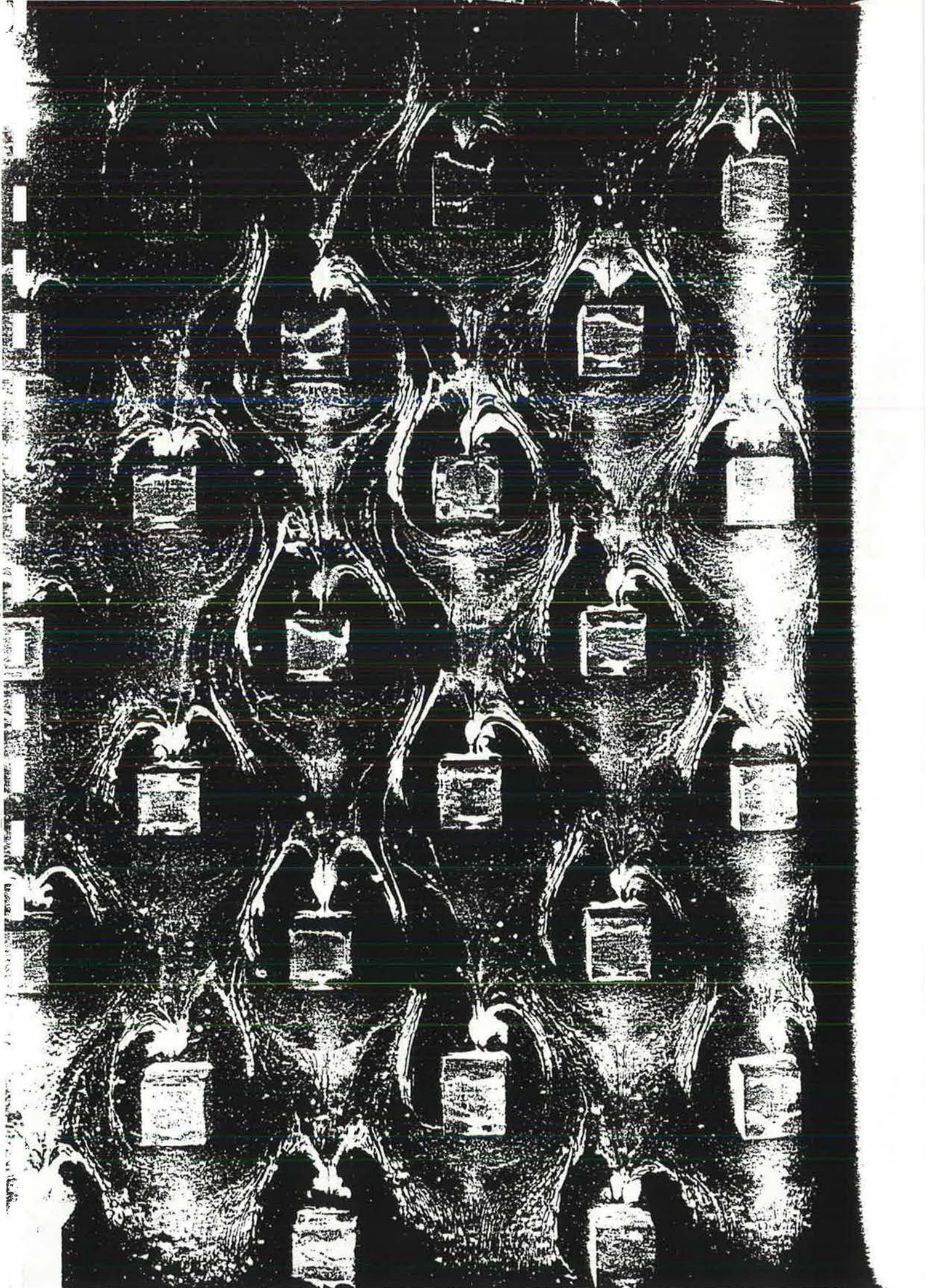
to form a pool (see Figures 9.3 and 9.4). Therefore, the pigment particles collecting at this pool edge showed as a white zone, (see Figure 9.1). A similar observation may be noted in the subsequent cases for the flow over the different group layouts, in the smooth as well as the rough flow.

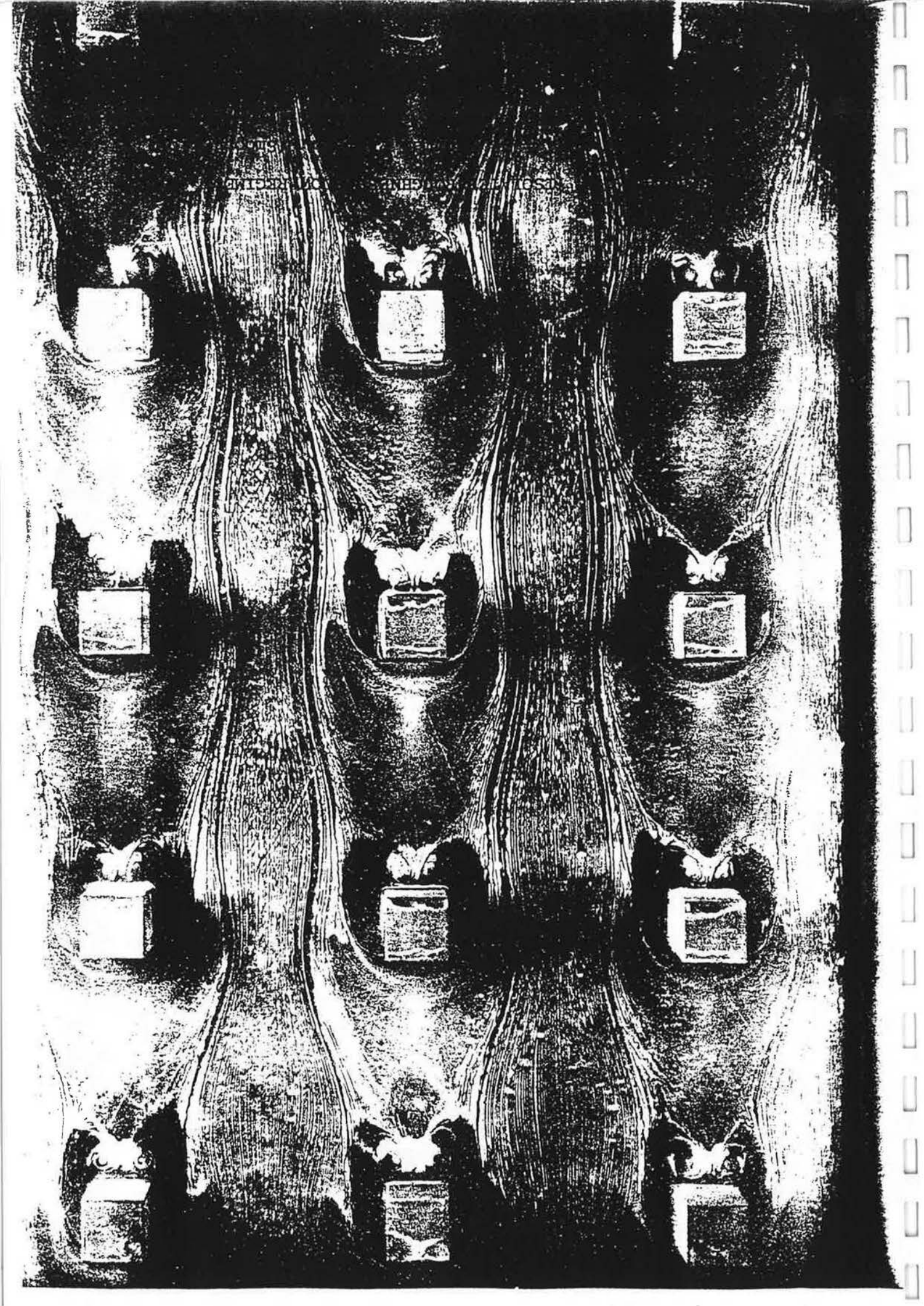
9.3 Discussion of the isolated flow regime results

9.3.1 It is postulated that the isolated roughness flow regime is characterized by a complete development of the wake and separation bubble behind each element, thus allowing the flow reattachment to occur before the next element is reached. An examination of the results of this flow regime either for the normal pattern, ($\lambda = 4\%$) or the staggered pattern, ($\lambda = 8\%$) in the rough flow, shown in Figures 9.5 and 9.6 indicates that the flow did reattach between subsequent cubes. A comparison between these figures and the isolated cube flow pattern case, given in Figure 9.1 indicates that the separation bubble behind each cube is approximately equal in size to that of the isolated cube case.

9.3.2 The observations made regarding the rough flow cases discussed above are also substantially applicable to the smooth flow cases of the normal and staggered patterns shown in Figures 9.7 and 9.8. Here the appropriate comparison to be made is that with the isolated cube case shown in Figure 9.2.





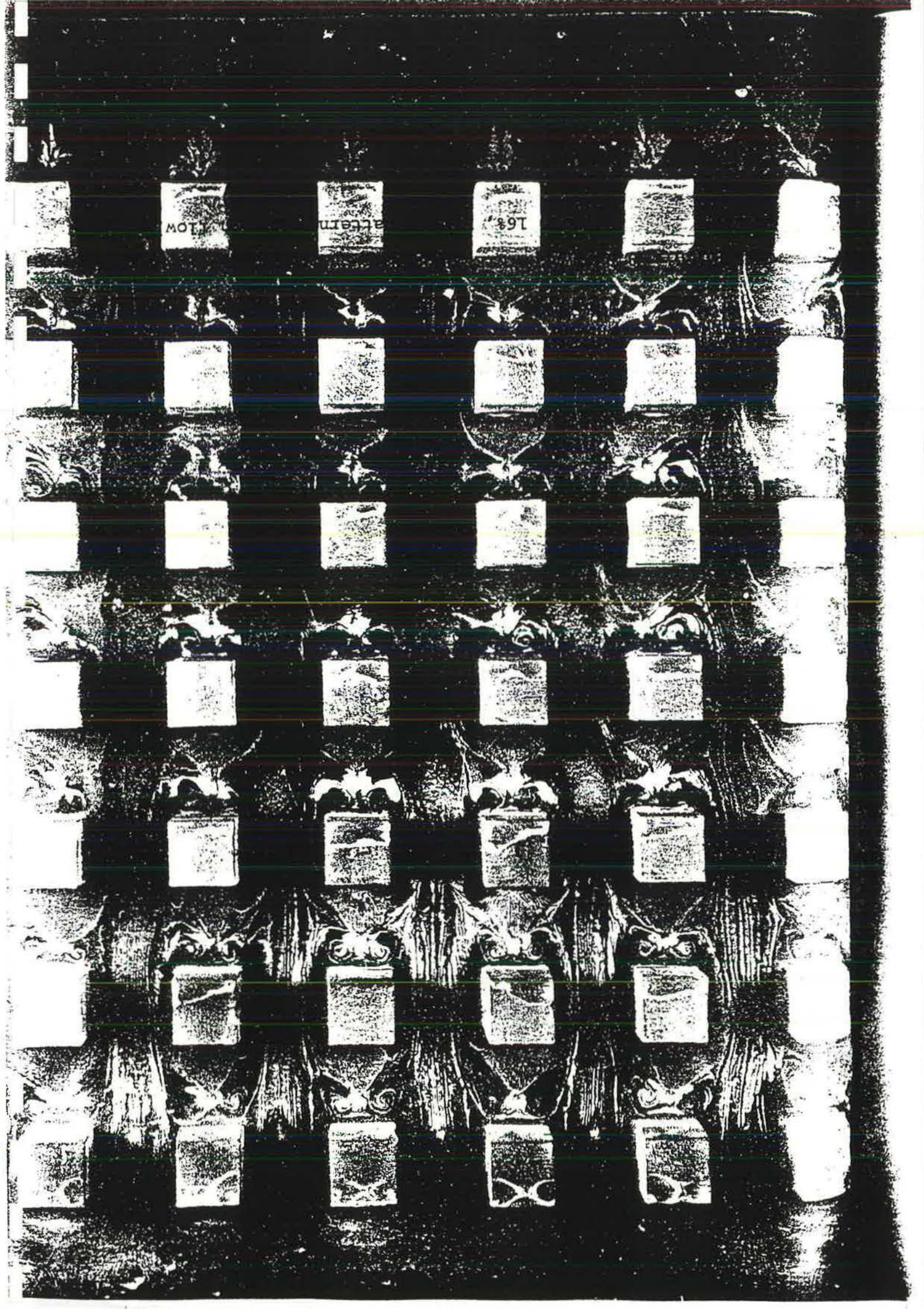




9.4 Discussion of the wake interference flow regime results

9.4.1 In Figure 9.9 the normal pattern group layout at $\lambda = 16\%$ is shown as an example of the wake interference flow regime in the smooth flow. The higher flow velocities round the second and third rows of the array arising from a shorter fetch, resulted in the clearest streak marks in this flow regime. It was then possible to draw a three dimensional diagram flow, given in Figure 9.10, which would explain the surface paint pattern. The streak marks in front of each cube do not exhibit the fanning out pattern, shown in the previous figures. Instead, they indicate two stagnation lines corresponding to the two shear layers separating from the vertical sides of the upstream cube. The clarity of these streak lines even at the back rows suggest that the windward face of each cube deflected the flow downward and resulted in higher velocities near the ground plane, see Figure 9.10. Thus, this interpretation of the flow pattern suggests that it is a wake interference flow regime where each cube face interfered with the separation bubble of the upstream cube, confirming the pressure and velocity measurements.

9.4.2 The results obtained in the rough flow for the same density and pattern (16%, normal), Figure 9.11, indicates that the general flow pattern is similar to that discussed above. However, the lower flow speeds



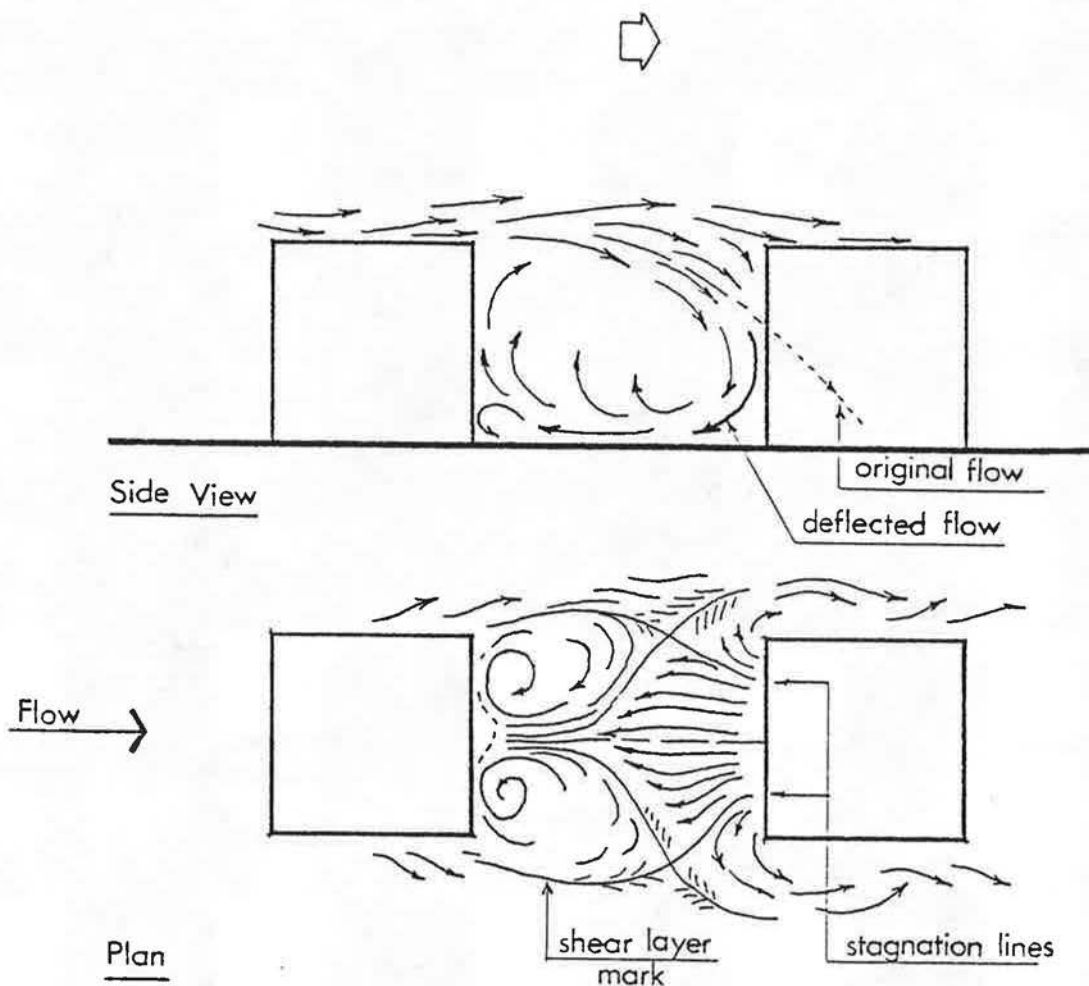
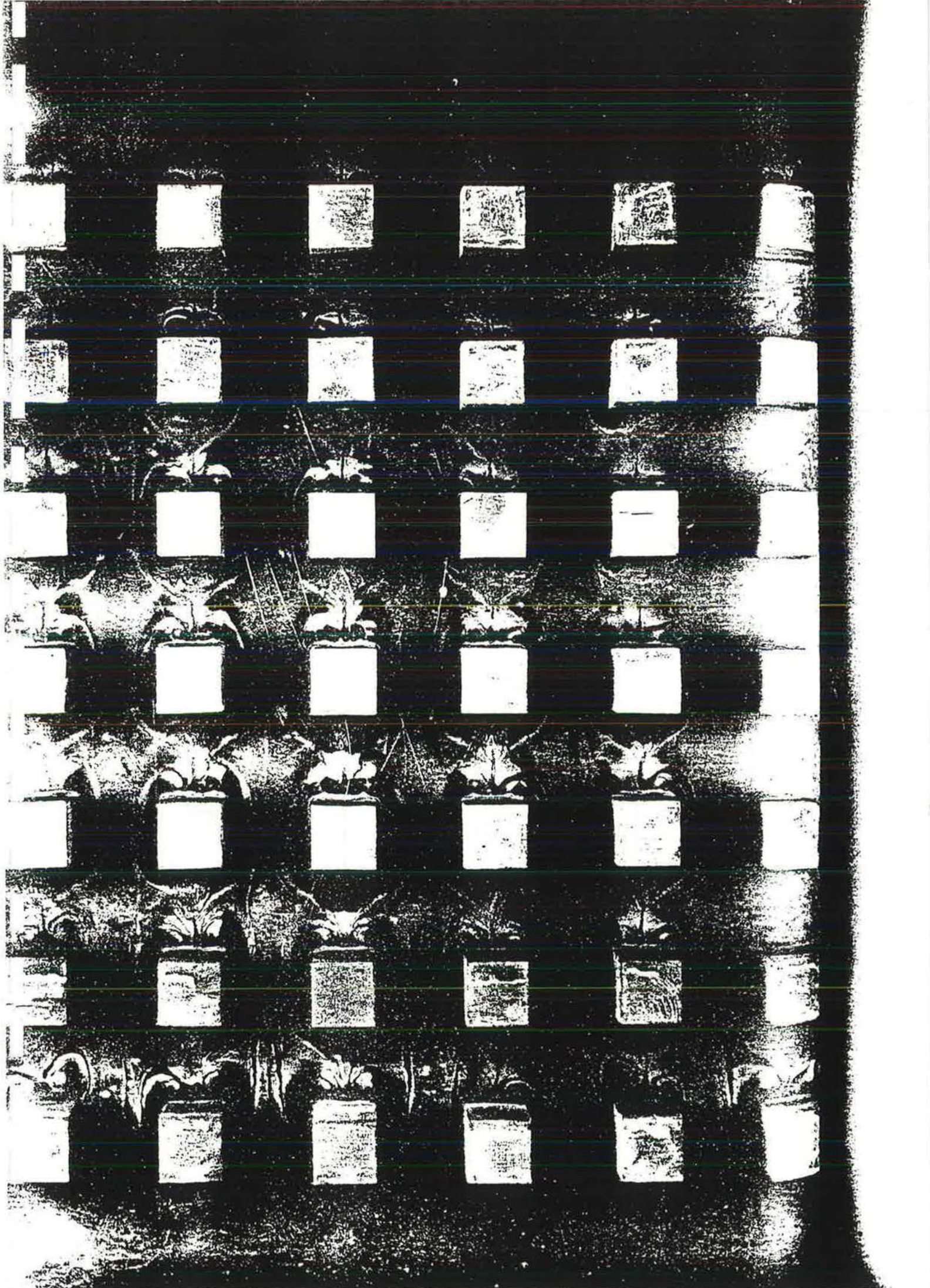


Figure 9.10 FLOW PATTERN IN THE WAKE INTERFERENCE FLOW REGIME, BASED ON FIGURE 9.9.



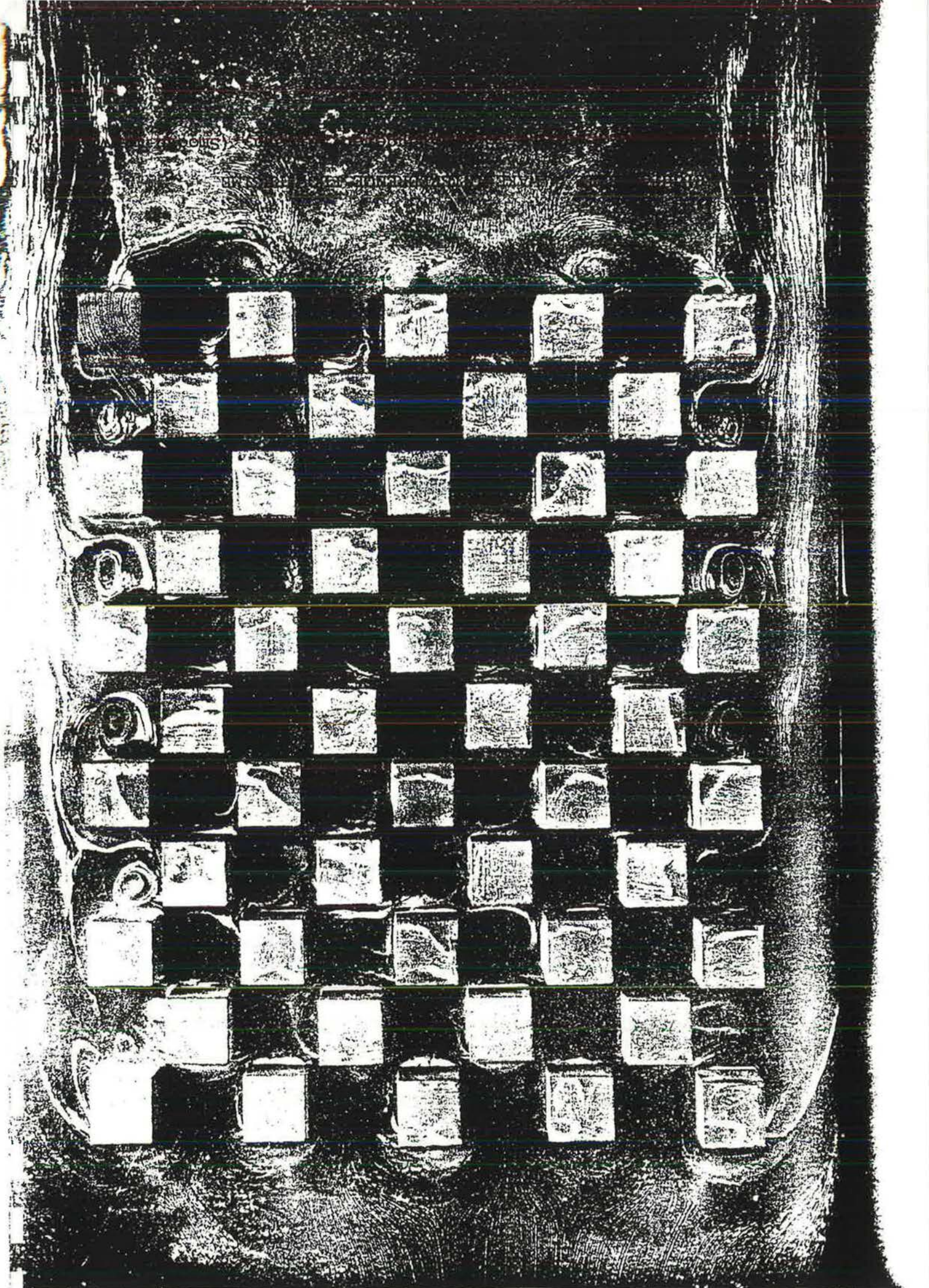
resulted in a less well-defined streak line pattern.

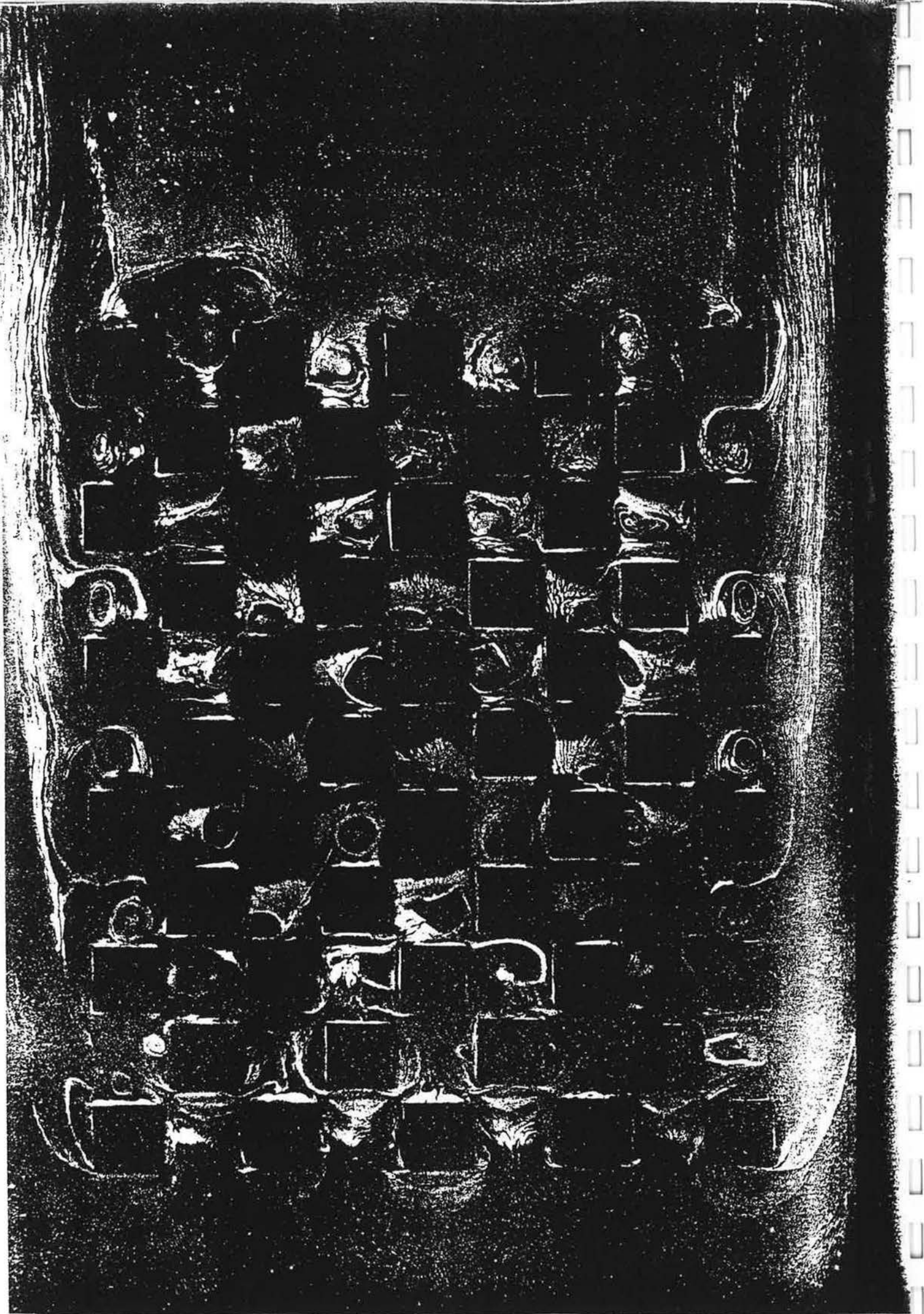
9.4.3 The staggered pattern results ($\lambda = 32\%$) in either the smooth flow, Figures 9.12 and 9.13, or the rough flow, Figure 9.14 did not give a defined streak line pattern. However, the smooth flow results of Figure 9.13 indicate the existence of vortices in between some of the cubes.

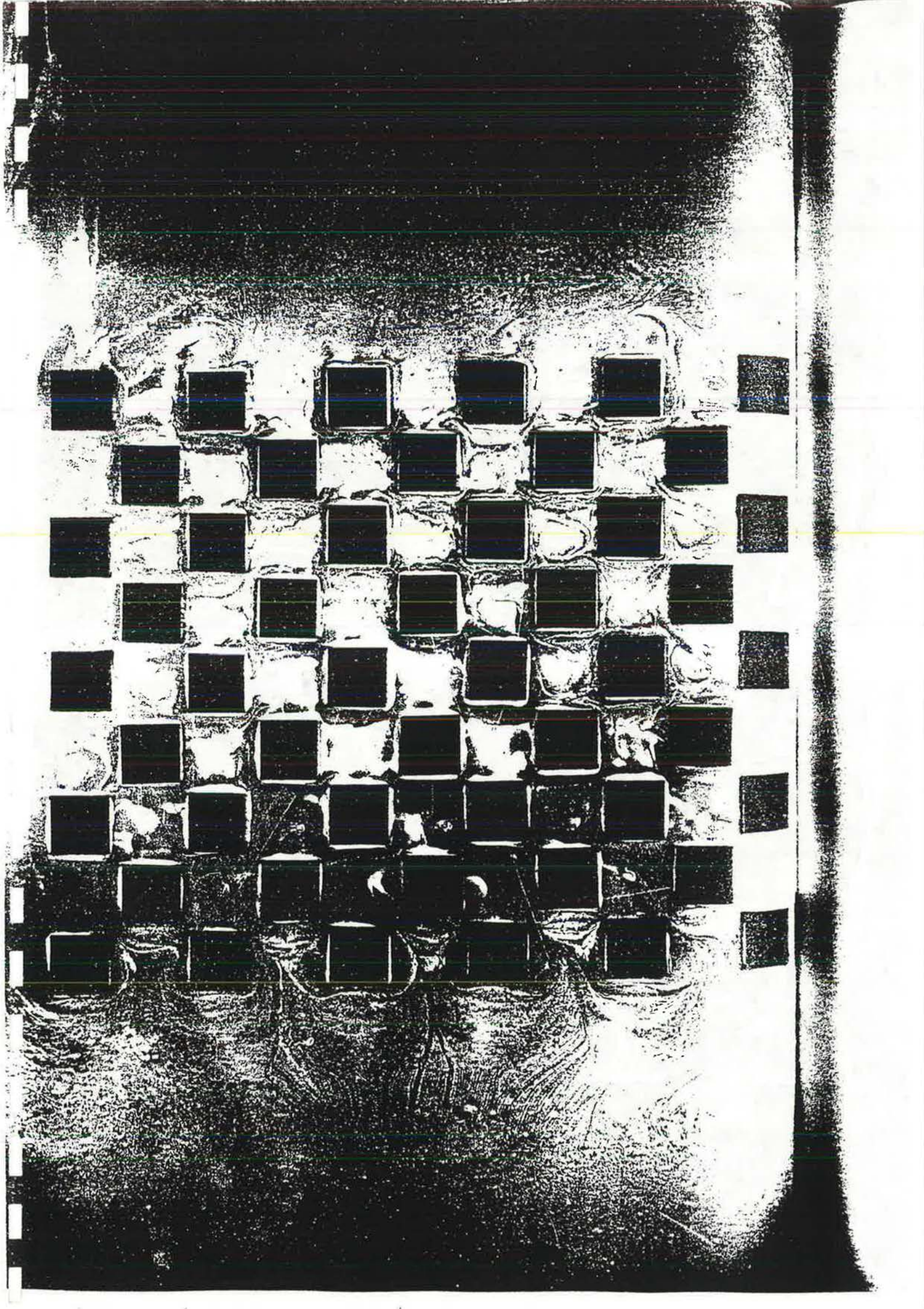
9.5 Discussion of the skimming flow regime results

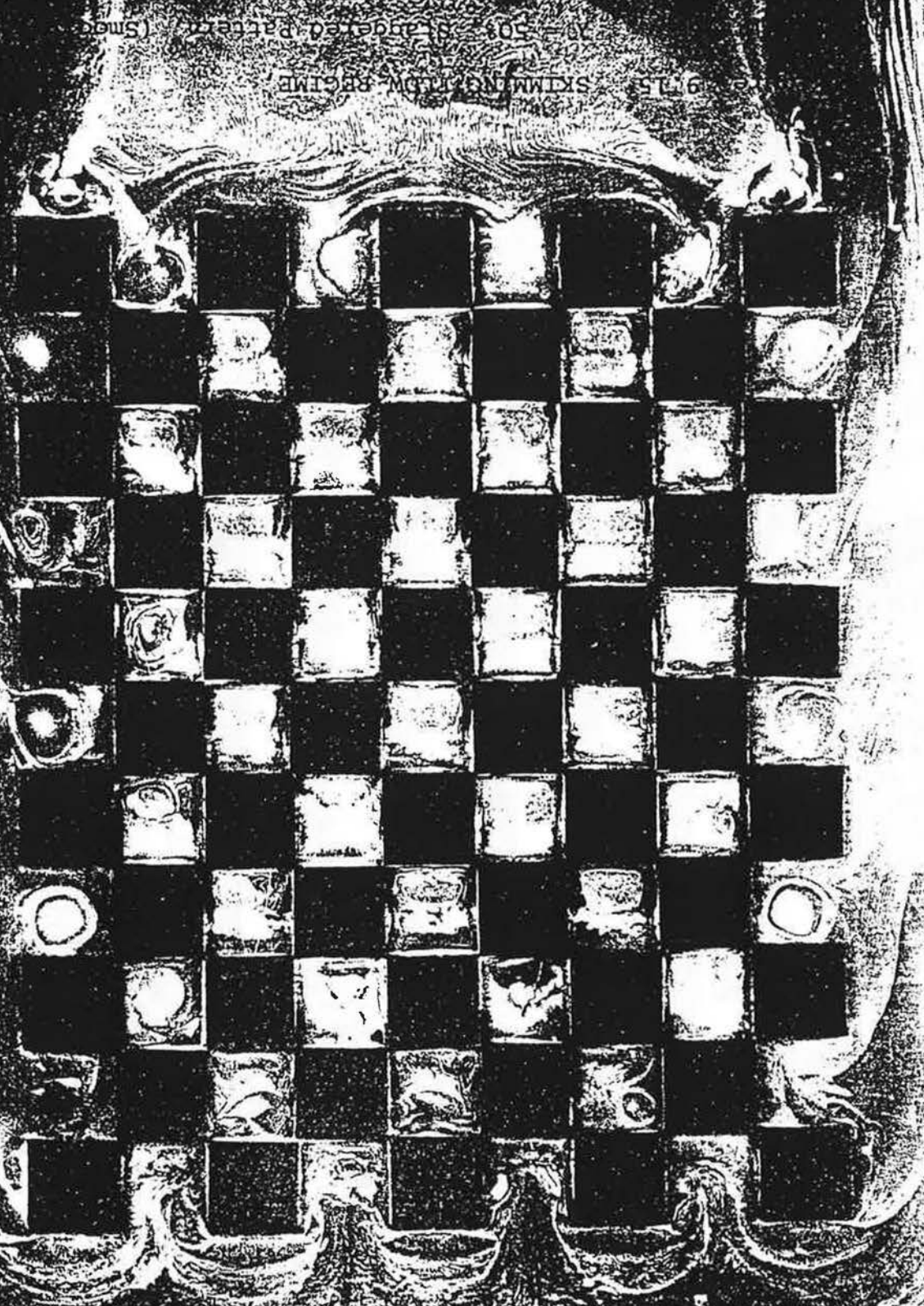
9.5.1 In this type of flow regime, a stable vortex is known to occupy the space between the roughness elements, whilst the flow rides relatively undisturbed on top of the elements. In the present study, the best flow visualization results obtained for this flow regime were for the staggered pattern ($\lambda = 50\%$) in both the smooth flow, Figure 9.15, and the rough flow, Figure 9.16. In this layout pattern, the space between the cubes became a cubical void in isolation. As a result, a strong stable vortex existed in these spaces and was indicated by the streak lines shown on the floor between cubes. A sketch representing this type of flow may be seen in Figure 9.17.

9.5.2 The results obtained from the normal pattern in this flow regime either in the smooth flow, Figure 9.18, or the rough flow, Figures 9.19 and 9.20 seems to give little information. This might be attributed to the existence of only a weak vortex in the space between the cubes which resulted in lower velocities near the floor.



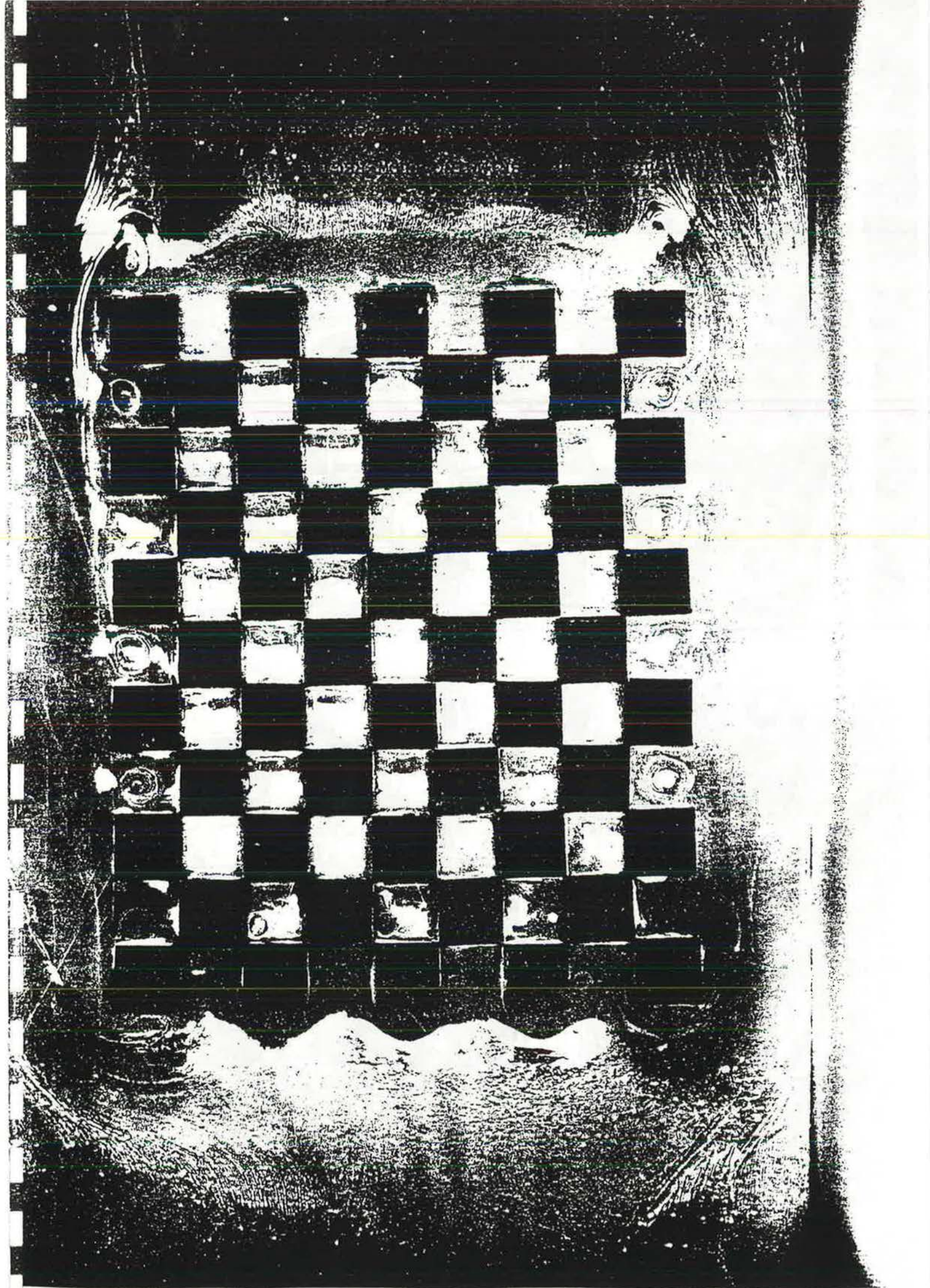






9115 SKIMMING TIDM-BRIGME

101-501 St. Anged. Patte (Smeg)



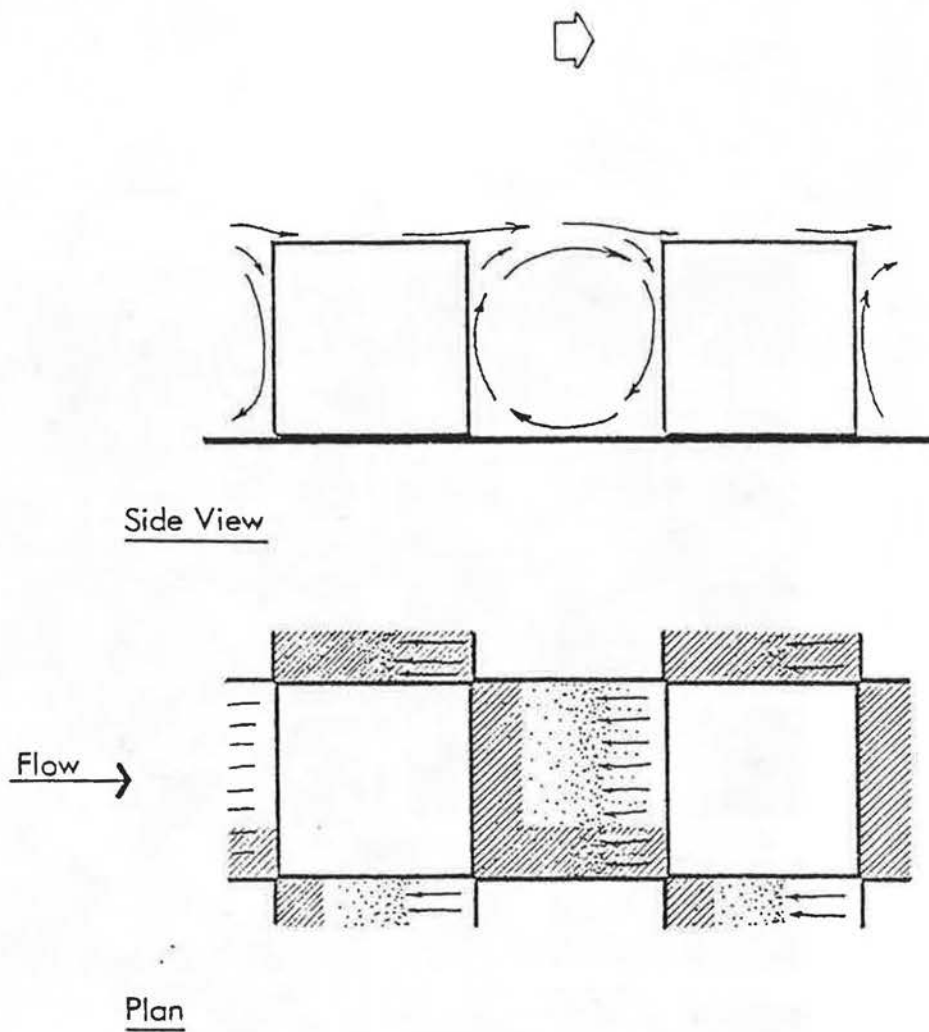
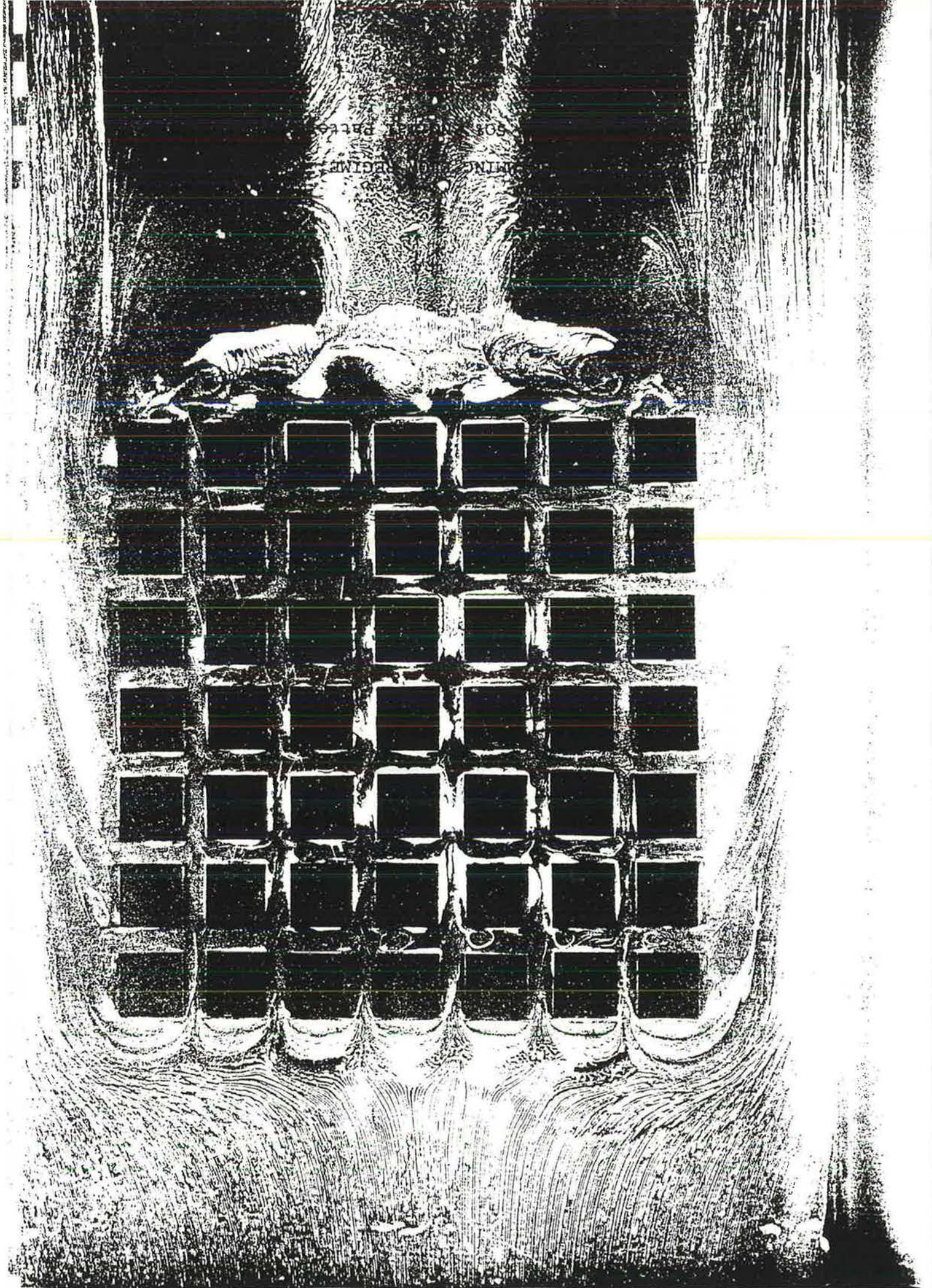
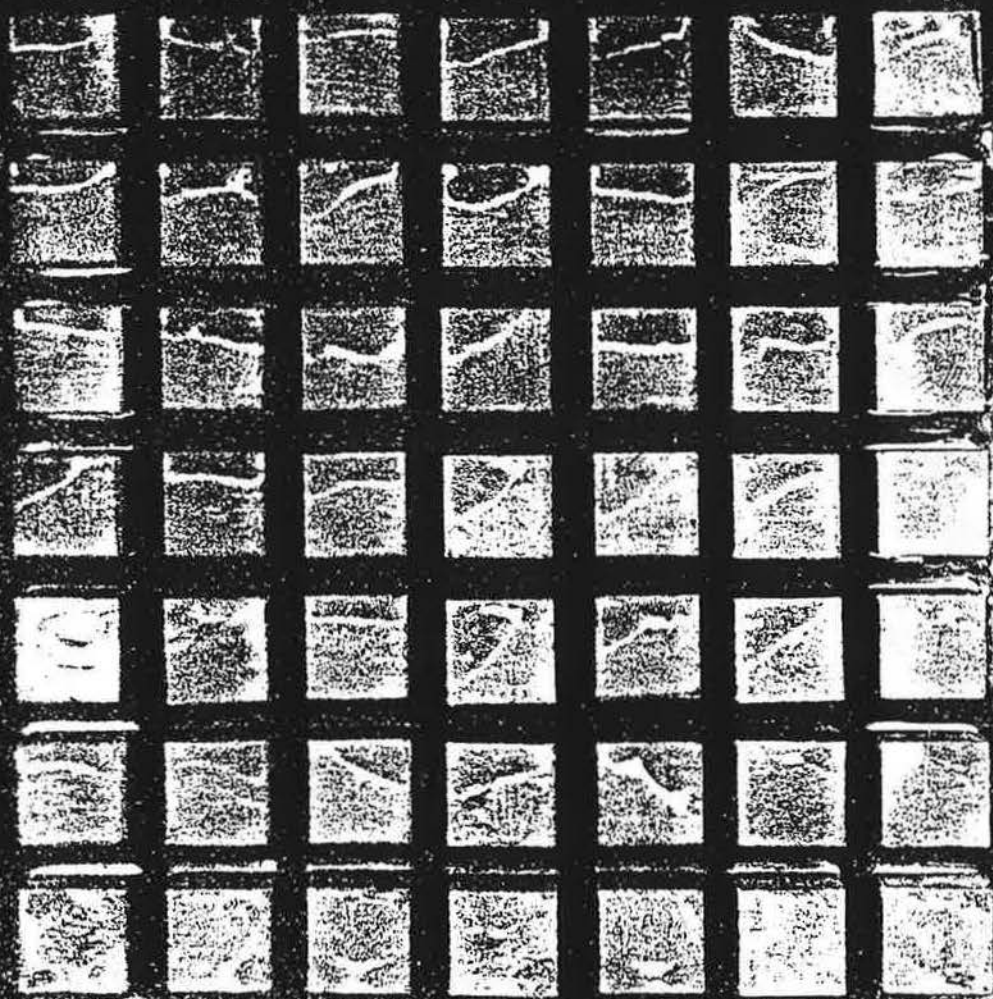
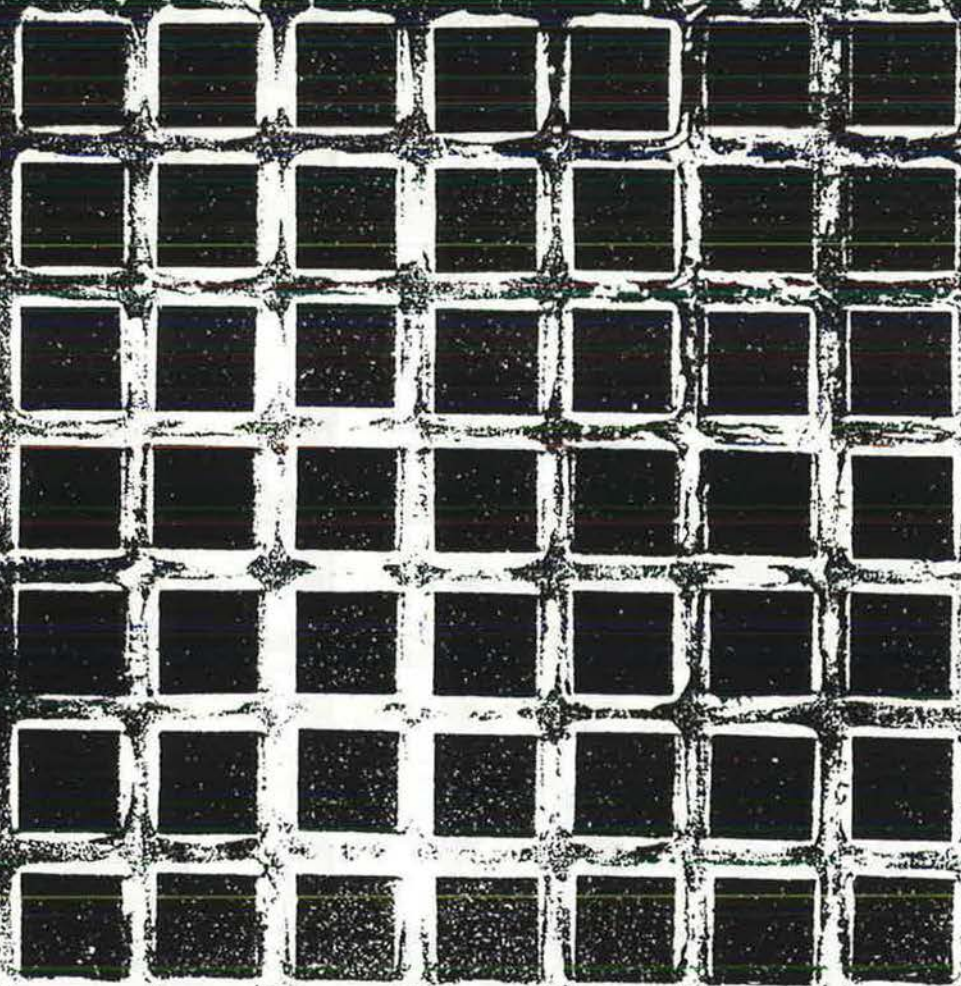


Figure 9.17 FLOW PATTERN IN THE SKIMMING FLOW REGIME.







9.6 Conclusions

9.6.1 The three regimes which have been indicated to exist for the flow over various rough surfaces are shown to give different flow pattern round the cubes (representing roughness elements).

9.6.2 For the cubes investigated, the effect of changing the incident flow type and thus the parameter H/δ from $0.5 \rightarrow 0.05$ did not result in an appreciably different flow pattern. The main difference in this comparison were clearer streak lines in the smooth flow ($H/\delta = 0.5$). This is thought to be mainly due to the higher velocities occurring at lower levels.

9.6.3 The isolated roughness flow regime is characterised by a flow pattern round each cube similar to the flow pattern round a cube in isolation. The separation and reattachment of the flow is indicated to occur for each cube in the group with the associated vortices upstream and downstream. A small separation region was noted on the leading part of each cube top surface. The group pattern was of little effect on the flow behaviour round the cubes.

9.6.4 In the wake interference flow regime, the flow pattern showed a strengthened upstream vortex coupled with a restricted downstream vortex for each cube. This is explained by the interaction between the cube windward face and the separated flow from the preceeding cube.

9.6.5 The flow pattern between the cubes in the skimming flow regime was thought to indicate traces of a stable vortex in the staggered pattern. In the normal pattern no indication of a particular flow was apparent.

CHAPTER 10

GENERAL APPLICATION FOR BUILDINGS.

10. GENERAL APPLICATION FOR BUILDINGS

10.1 Introduction

10.1.1 In Chapter 1, the Crack Method for natural ventilation calculations, as described in the I.H.V.E Guide, was discussed (see paragraph 1.2.2). It was explained how an infiltration chart, shown in Figure 10.1, is utilized to determine the infiltration rate. It was noted that some of the relevant factors affecting the pressure difference across buildings, ΔC_p , are neglected. The major omissions in this category are building form and flow properties. An attempt is made in this chapter to present an alternative method of determining ΔC_p , in which these factors are now included.

10.1.2 In explaining this alternative method, the generalized effect of these other factors is presented. Any quantitative estimate of the likely values of ΔC_p requires detailed experimental data which includes both an accurate simulation of the natural wind properties as well as a wide range of different building forms. Such requirements are considered to be outside the scope of the present work.

10.2 The three flow regimes and their generalized parameters

10.2.1 The different behaviour in each of the flow regimes is reflected in the pressure forces, the velocity profile parameters and flow pattern given in Chapters 7, 8 and 9 respectively. These results indicate that the flow regime

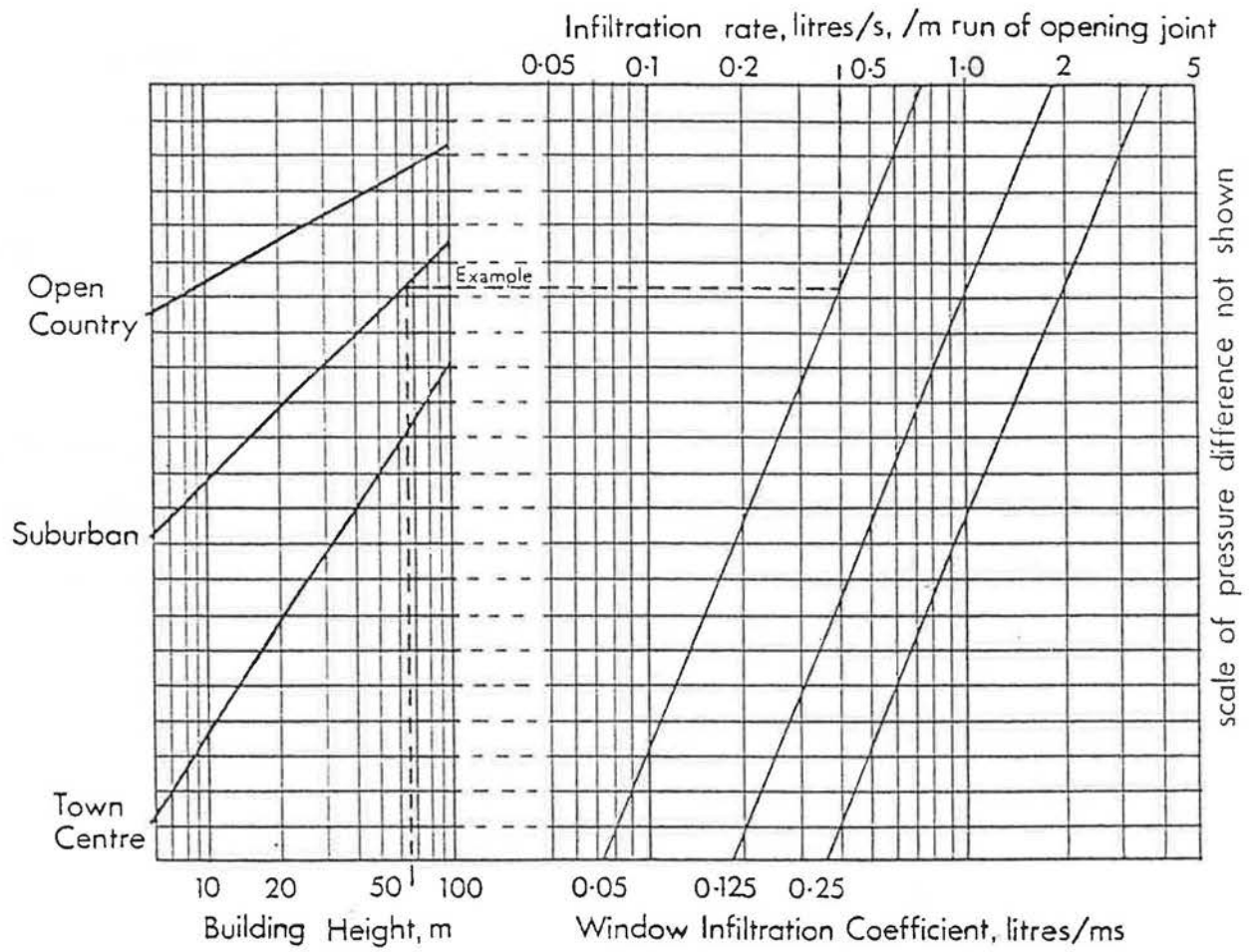


Figure 10.1 THE IHVE GUIDE INFILTRATION CHART

for any building group must first be defined if any estimate of the pressure forces on buildings are to be made.

10.2.2 From the present work, it has been clearly demonstrated that the first change of regime from isolated roughness flow to wake interference flow, is dependent on the distances of separation and reattachment around the cubes. In the second change of regime from wake interference to skimming flow the condition of maintaining at least one stable vortex in the space between the cubes was also indicated. The governing condition for each flow regime may then be expressed as follows:-
for the isolated roughness flow regime

$$S_c/H > E_t/H,$$

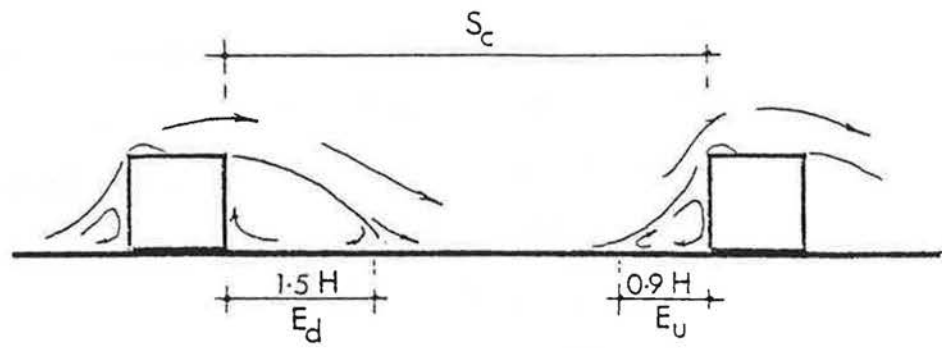
for the wake interference flow regime

$$\frac{E_v}{H} < S_c/H < E_t/H$$

and for the skimming flow regime

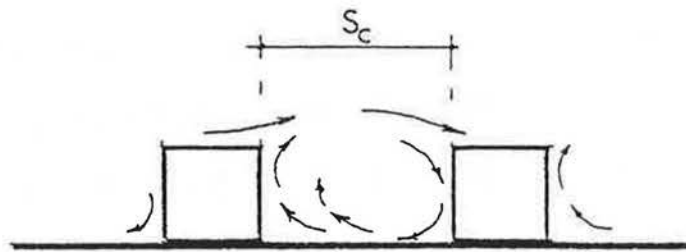
$$S_c/H < E_v/H$$

where S_c is the clear spacing between buildings, E_t is the sum of the separation and reattachment distances E_u and E_d around the isolated cube respectively and E_v is the stable vortex dimension in the flow direction, see Figure 10.2. From these conditions, it follows that the different flow regimes may also be estimated for other building forms if the corresponding dimensions of E_t/H and E_v are known.



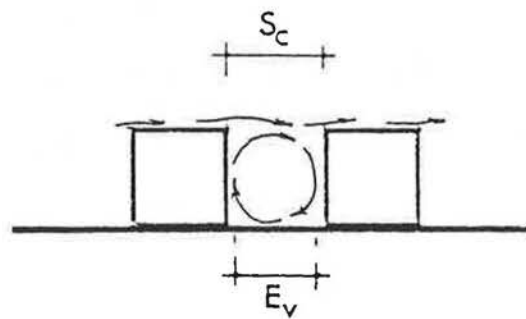
Isolated Roughness Flow Regime

$$S_c > E_t$$



Wake Interference Flow Regime

$$E_v < S_c < E_t$$



Skimming Flow Regime

$$S_c \lesssim E_v$$

Figure 10.2 THE GOVERNING CONDITIONS FOR THE THREE FLOW REGIMES.

10.2.3 From previous studies reported on the flow over rectangular cutouts and grooves, Roshko (1955), Tani, Iuchi and Komoda (1961) and Maull and East (1963), it appears that the vortex dimension E_v is directly related to the groove height, and not the groove length normal to the flow. This is explained by the breakdown of the flow into cellular three dimensional vortices (Maull and East). In the tests by Tani et. al it was found that the vortex flow was initiated at a value of $S_c/H = 1.4$. Since this is similar to the value of 1.5 determined in the present study, for the stable vortex dimension behind cubes it lends further support to the suggestion that E_v is related to the roughness element height. Hence it follows from this similarity between groove flow and flow over cubes at high densities, that the skimming flow regime will occur at $S_c/H = 1.5$ for buildings with a wide range of values of the frontal width, L/H .

10.2.4 The dependence of the downstream reattachment distances, E_d , on the frontal aspect ratio L/H has been reported by Evans (1957) for different building roof shapes and side aspect ratios. Evans's results which will be analysed later in this chapter indicate that E_d increases as L/H increases. Conversely, the upstream separation distance E_u seems to be of the same order of the building height H_1 for a wide range of values of L/H .

10.2.5 From this discussion, it may be concluded that the frontal aspect ratio is the dominant parameter and may alter the flow from the isolated flow regime to

the wake interference flow regime. The role of the frontal aspect ratio may then be considered similar to the role of the frontal area density or the plan area density. It also follows that any of the three flow regimes is not a sole function of the plan area density, λ_p , the frontal area density, λ_f or the frontal aspect ratio, A_f . In Figure 10.3 three examples are given for the different flow regimes obtained when only one of the three parameters, λ_p , λ_f , and A_f is varied while the other two were constant.

10.3 The relationship between the building form, its relative height and the downstream eddy size

10.3.1 In the above discussion, information about the downstream eddy size was shown to be required if the transition from the isolated roughness flow regime to wake interference flow regime is to be identified for different building forms. Therefore, in an attempt to extend the applicability of the present results to forms other than the cube, a series of flow visualization experiments were carried out to measure the downstream reattachment distance, E_d , behind different building shapes. Variation of form parameters included L/H in the range 1 to 15 and W/H in the range 0.5 to 1.5. The effect of the incident boundary layer thickness was also investigated i.e. using both the smooth and rough incident flows described in Chapter 8. The wind tunnel used was that described in Chapter 6, while the model height was 32 mm.

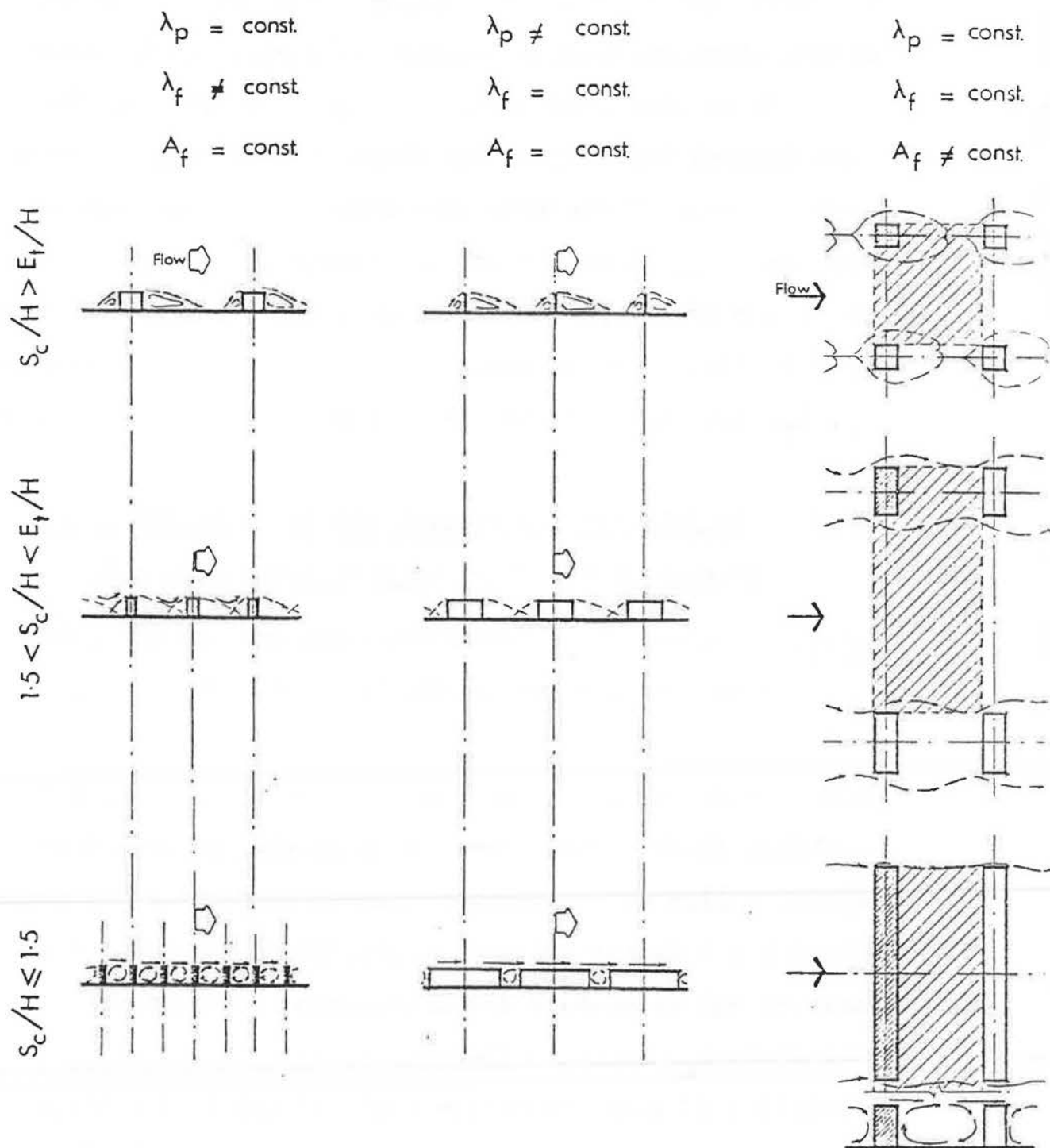


Figure 10.3 EXAMPLES SHOWING THAT THE THREE FLOW REGIMES ARE NOT A SOLE FUNCTION OF λ_p , λ_f OR A_f .

10.3.2 The results obtained for the variation of E_d/H with L/H is shown plotted in Figure 10.4 for the different values of W/H . From this figure it may be concluded that larger values of E_d/H are obtained with increasing L/H , H/δ or decreasing W/H . It may also be noted that E_d/H tends to a constant value after a certain size of L/H . This value of L/H is larger for thinner boundary layers or smaller building thickness. The range of E_d/H corresponding to any particular value of L/H (due to change of H/δ or W/H) is minimum at $L/H = 1$ (cubes), and increases as L/H increases. This would imply that as longer buildings are considered, the spacing at which a change of regime would occur will be increasingly affected by the ratio H/δ or W/H .

10.3.3 When the work reported by Evans (1957) on the variation of E_d with rectangular building forms were plotted in the same way as shown in Figure 10.4, not only was the same trend reflected, but also good agreement was obtained, see Figure 10.5(a). Furthermore, when Evans's results for other building forms were normalized with respect to the total building height in each case, the data points collapsed on single line Figure 10.5(b). The range of variation of W/H covered in Figure 10.5(b) was $0.75 < W/H < 2.0$. Figure 10.5(b) would seem to indicate that the effect of changing either the roof shape, or W/H is not of prime importance.

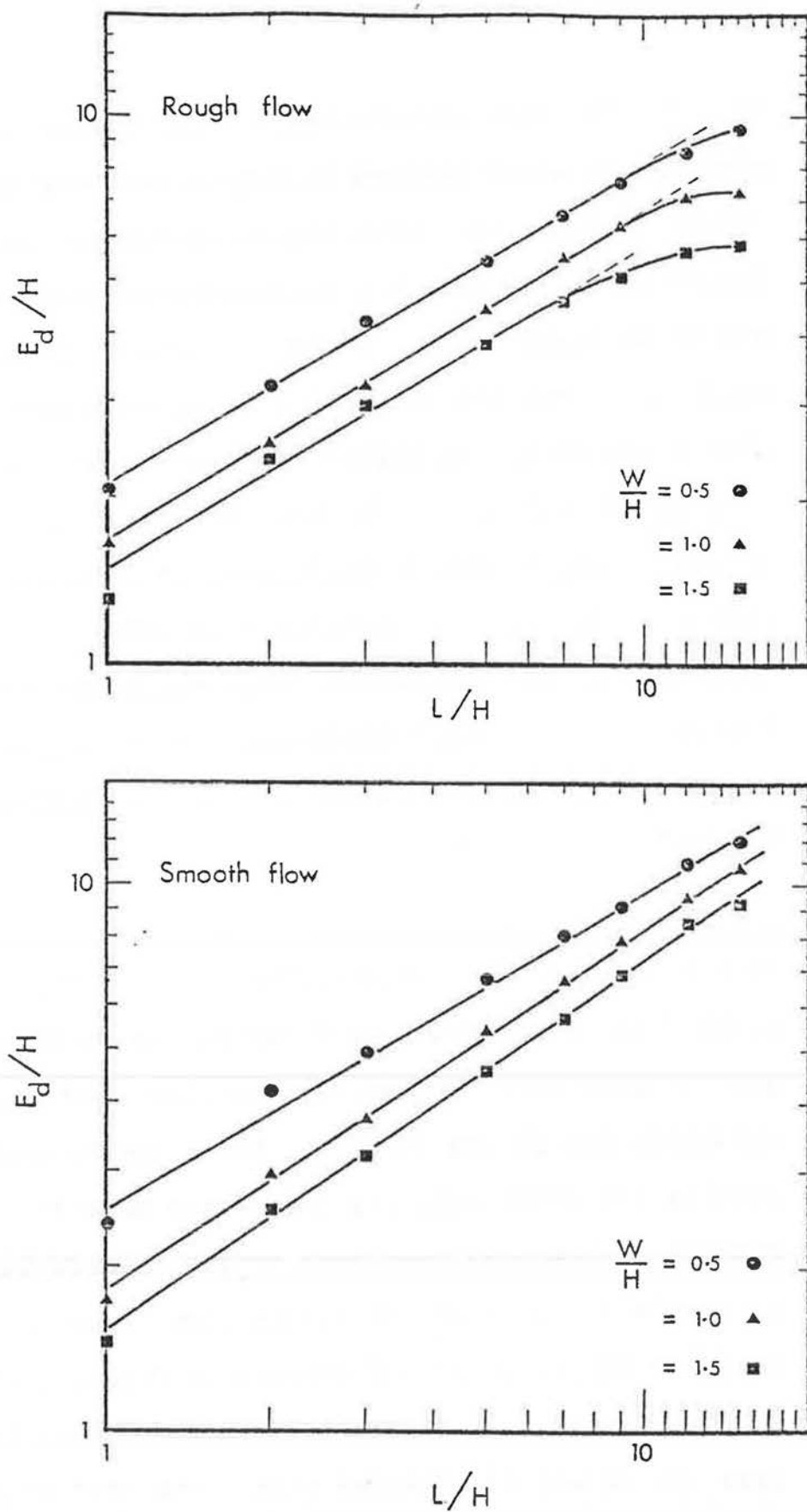


Figure 10.4 VARIATIONS OF E_d/H WITH L/H .

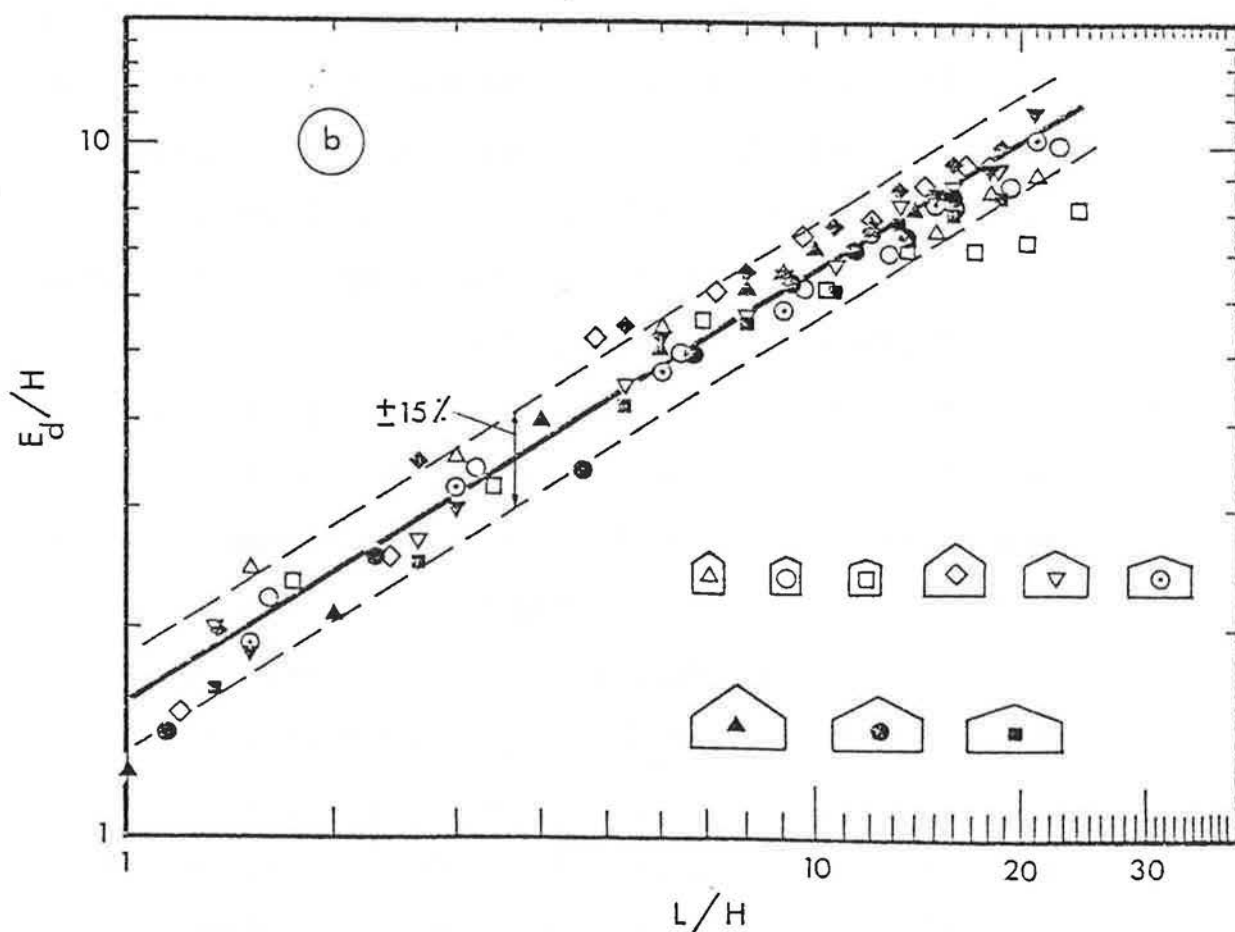
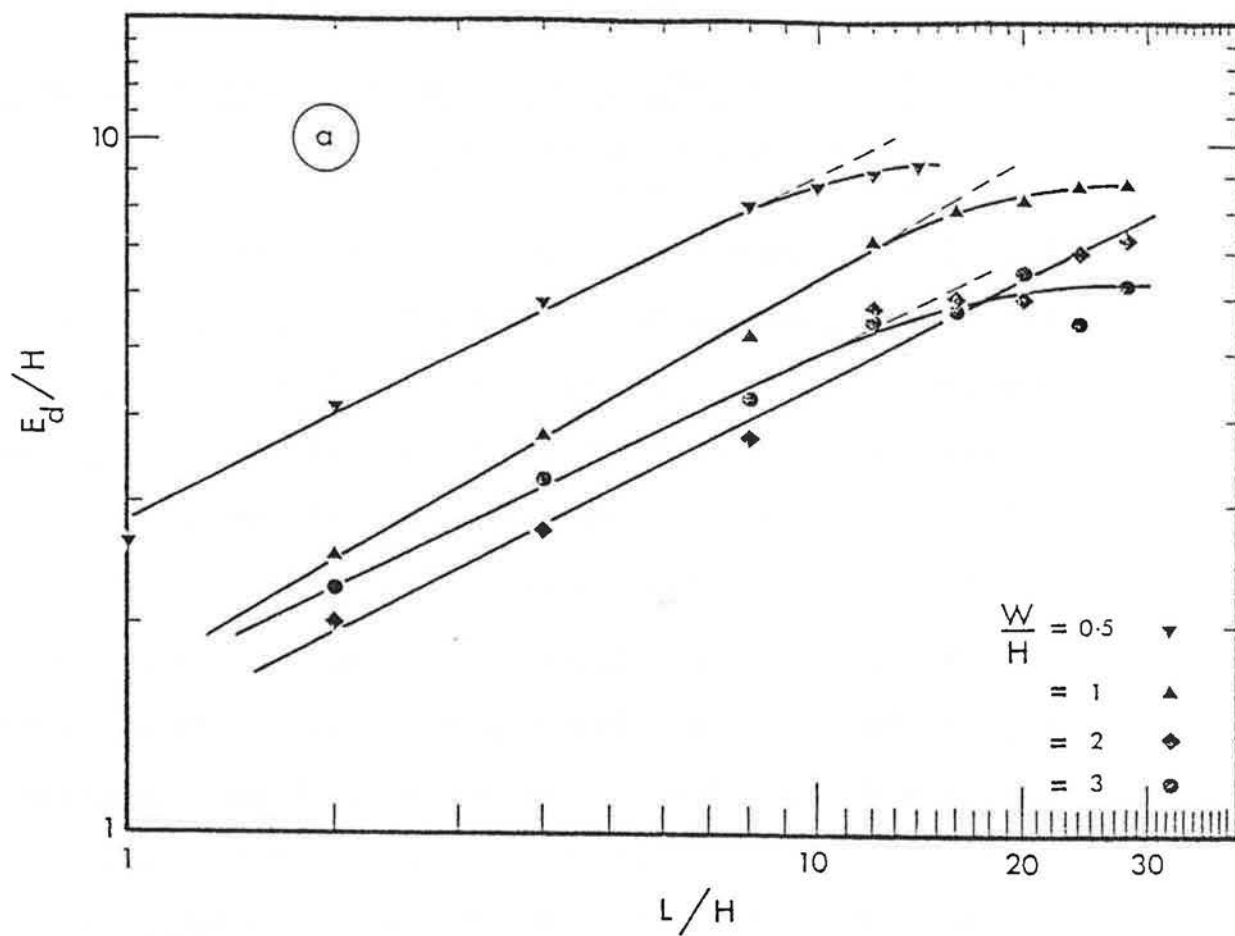


Figure 10.5 ANALYSIS OF EVANS'S (1957) RESULTS.

10.4 The suggested method for determining the natural ventilation potential, ΔC_p

10.4.1 In order to make an estimate of the probable value of ΔC_p across the opposite faces of a building within a group of similar form and height information will be required about the individual form, the group form, the building fetch and the building orientation with respect to the oncoming wind.

10.4.2 In order to identify the type of flow regime applicable to a given layout pattern of buildings it is possible to plot the separation and reattachment distances against the frontal aspect ratio L/H . In Figure 10.6 the left hand ordinate represents both the total separation distance E_t for the isolated building case as well as the minimum vortex size E_v for the onset of skimming flow. Using the same units of distance, the clear space length S_c may be represented by the right hand ordinate. The criteria by which different values of S_c/H are divided into different flow regimes given in paragraph 10.2.2 may now be applied to Figure 10.6. In this way the lines in the figure may now be seen to divide the geometrical parameter into their different flow regimes where zone A represents the isolated roughness flow regime i.e. $S_c/H > E_t/H$, zone B represents the wake interference flow regime i.e. $1.5 < S_c/H < E_t/H$ and zone C represents the skimming flow regime, i.e. $S_c/H < 1.5$. Thus for any pair of values of S_c/H and L/H the flow regime may be defined. The effect of variation of W/H from 0.5 to 1.5 is indicated by the dotted lines dividing zone A

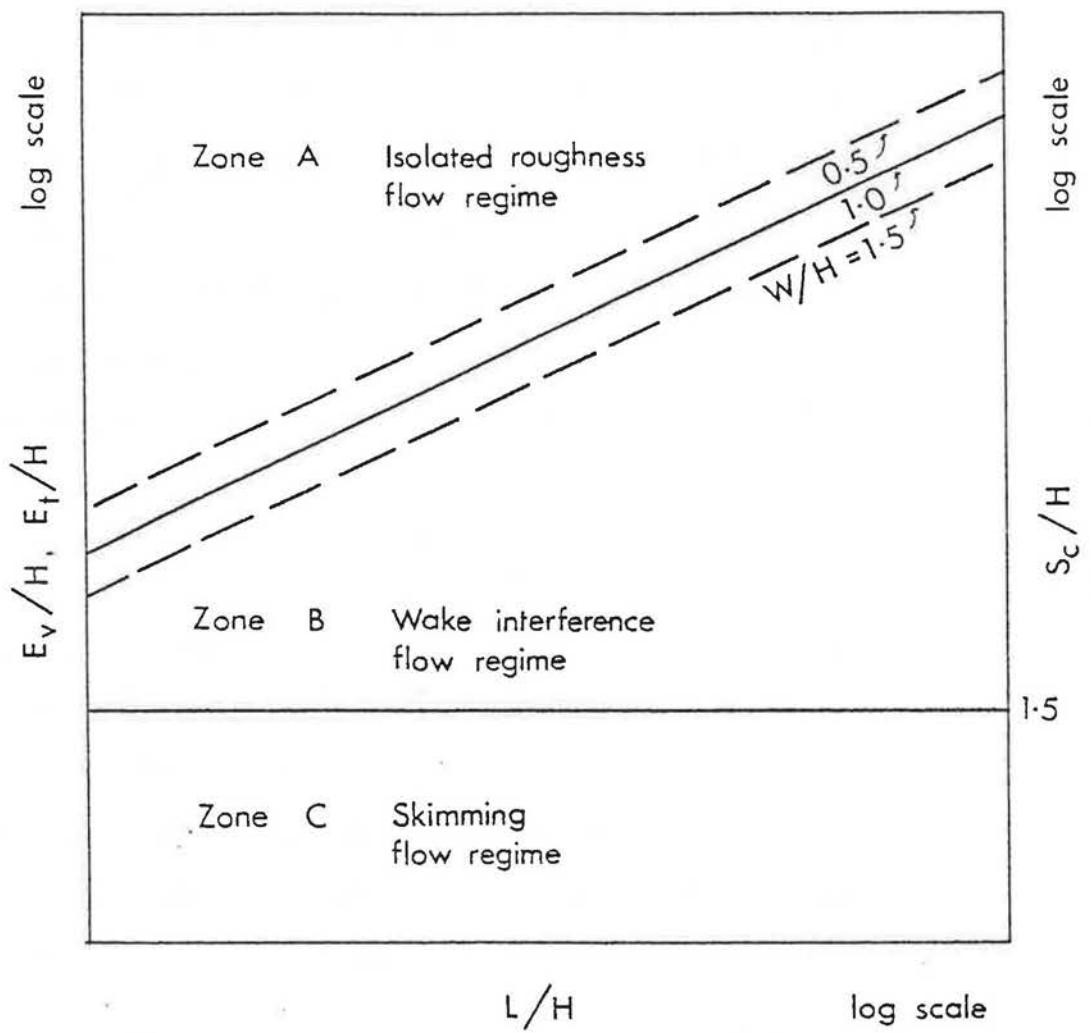


Figure 10.6 IDENTIFICATION OF THE THREE FLOW REGIMES FROM THE LAYOUT PATTERN.

from zone B. By definition of E_v variation in W/H will not affect the onset of the skimming flow regime, zone c.

10.4.3 For ventilation purposes, building surface pressures are usually normalized with respect to the velocity pressure at the building roof level, giving C_{D_H} . The correlation between the roof height velocity, u_H/U_1 , and S_c/H obtained from the velocity profile measurements and given in Figure 8.24 was then used to convert the experimental values of C_{D_1} into C_{D_H} using the following relationship.

$$C_{D_H} = C_{D_1} \left(\frac{U_1}{u_H} \right)^2$$

When the results of C_{D_H} obtained were plotted against S_c/H a broken line relationship was obtained as may be seen in Figure 10.7. It may be noted that not only do the inflections of the graph correspond to the changes of flow regime, but also the line corresponding to the skimming flow regime gives C_{D_H} a value of 0 at $S_c/H = 0$.

10.4.4 Since the data given in Figure 10.7 are for cubes, i.e. $L/H = 1$, it is necessary to extend the range by considering the information given in Figure 10.6. It is suggested that as L/H increases the break point between the isolated roughness and wake interference flow regime at $S_c/H = 2.5$ will move towards higher values of S_c/H while the value of C_{D_H} remains constant. Conversely, the break point at $S_c/H = 1.5$ denoting the start of the skimming flow regime, will remain in the same position. The data extrapolated for other values of L/H is shown in Figure 10.8.

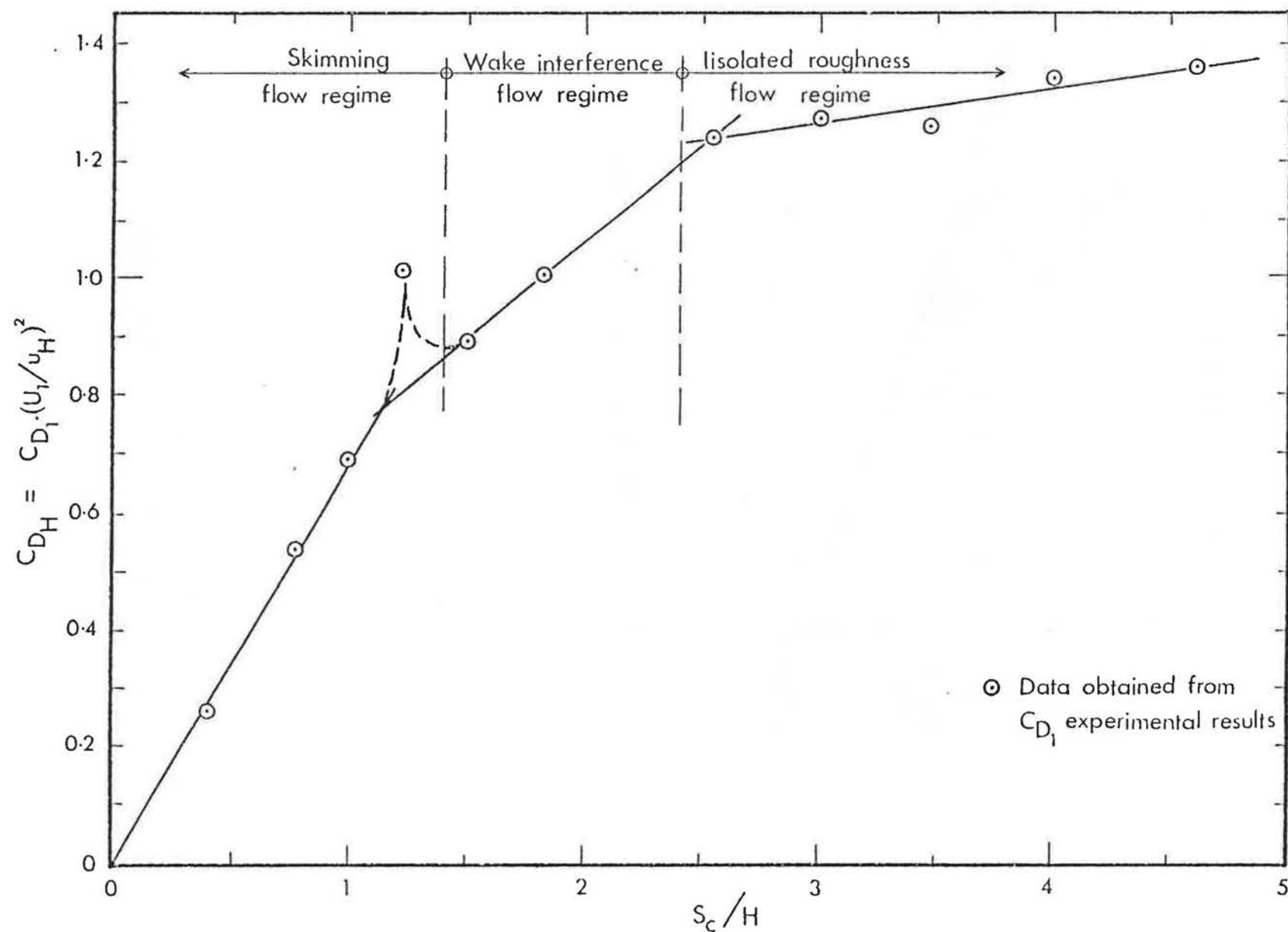


Figure 10. 7 VARIATION OF C_{DH} WITH S_c/H

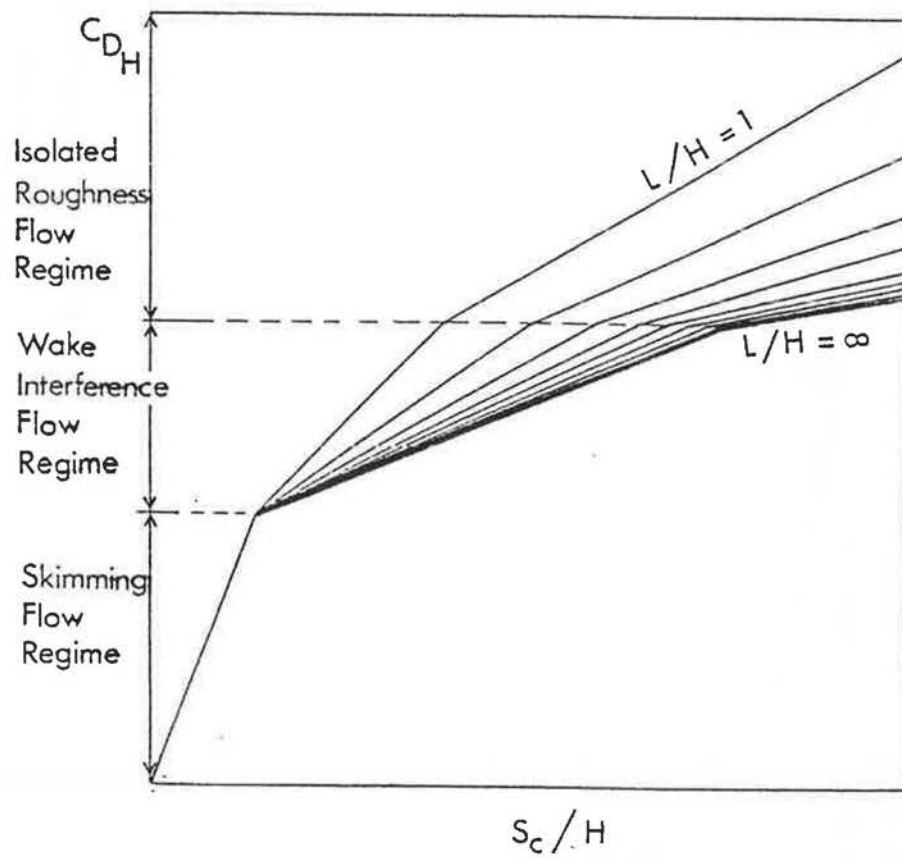


Figure 10.8 SUGGESTED VARIATION OF C_{DH} WITH S_c/H FOR DIFFERENT BUILDING FORMS.

10.4.5 It was shown earlier in Chapter 7 that the effect of decreasing the upstream fetch was to increase the pressure forces on the model. It was also shown that the change of the pressure forces increased as the density decreased particularly for small fetches. It is, therefore, suggested that the effect of decreasing the fetch would be to produce a family of curves in each of the three flow regimes, Figure 10.9. Because of the disturbance which usually occurs at the first and second blocks in the flow direction in the wake interference and skimming flow regimes, it is assumed that the fetch, x/H , represented in Figure 10.9 starts at the third block, provided that the array size is not very small. Furthermore the effect of a small array size would result in an increase in C_{DH} due to the proximity to the leeward edge of the group.

10.4.6 To allow for the effect of the building orientation angle, θ , the results obtained for ΔC_p at different values of θ and group density in the rough flow, given in Figure 7.23, were normalized with respect to the value at $\theta = 0$. A plot of these normalized values for the two patterns in three flow regimes is given in Figure 10.10. It seems from this figure that all the results, regardless of pattern or flow regime fall in a single curve. On the basis of this figure, a reduction factor for C_{DH} may be used at each value of θ .

10.4.7 Having now arrived at a means of determining the value of C_{DH} for systematic variations in the important parameters which influence its value, it is now possible to specify the alternative prediction procedure. Assuming

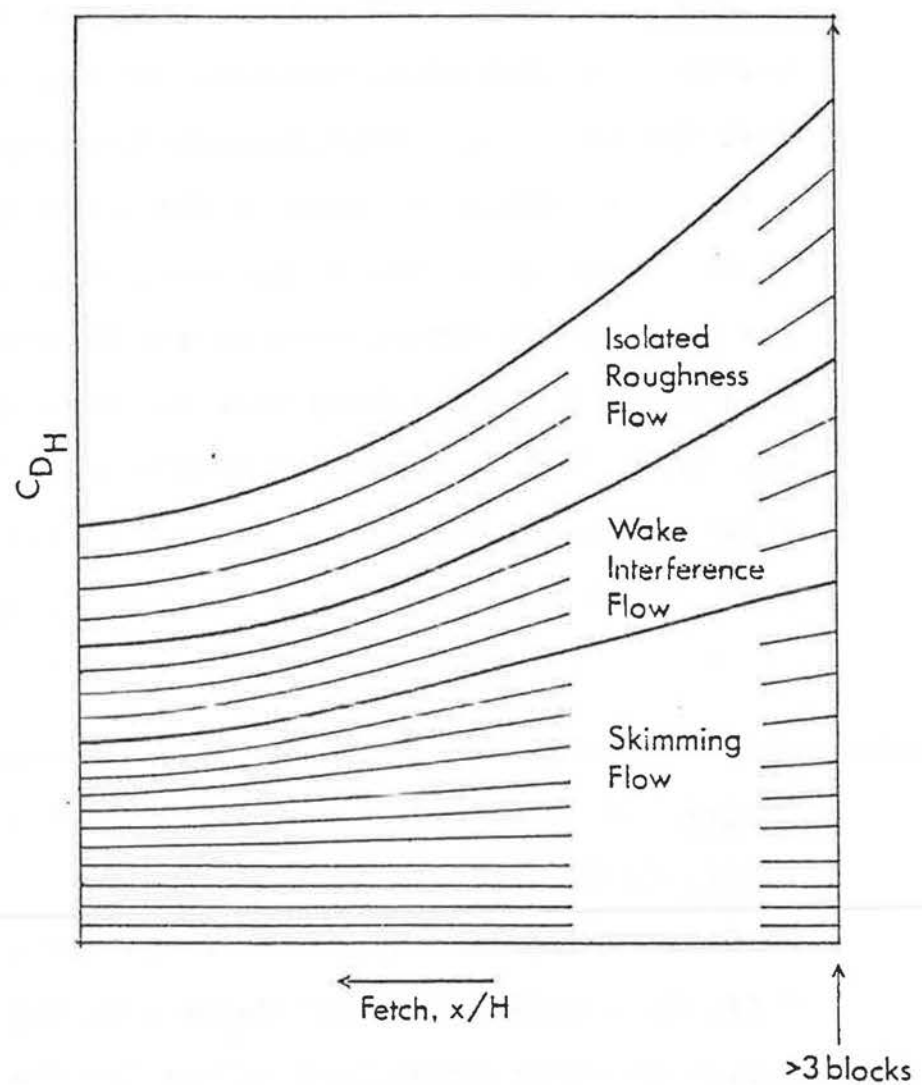


Figure 10.9 SUGGESTED VARIATION OF C_{DH} WITH FETCH IN THE THREE C_{DH} FLOW REGIMES.

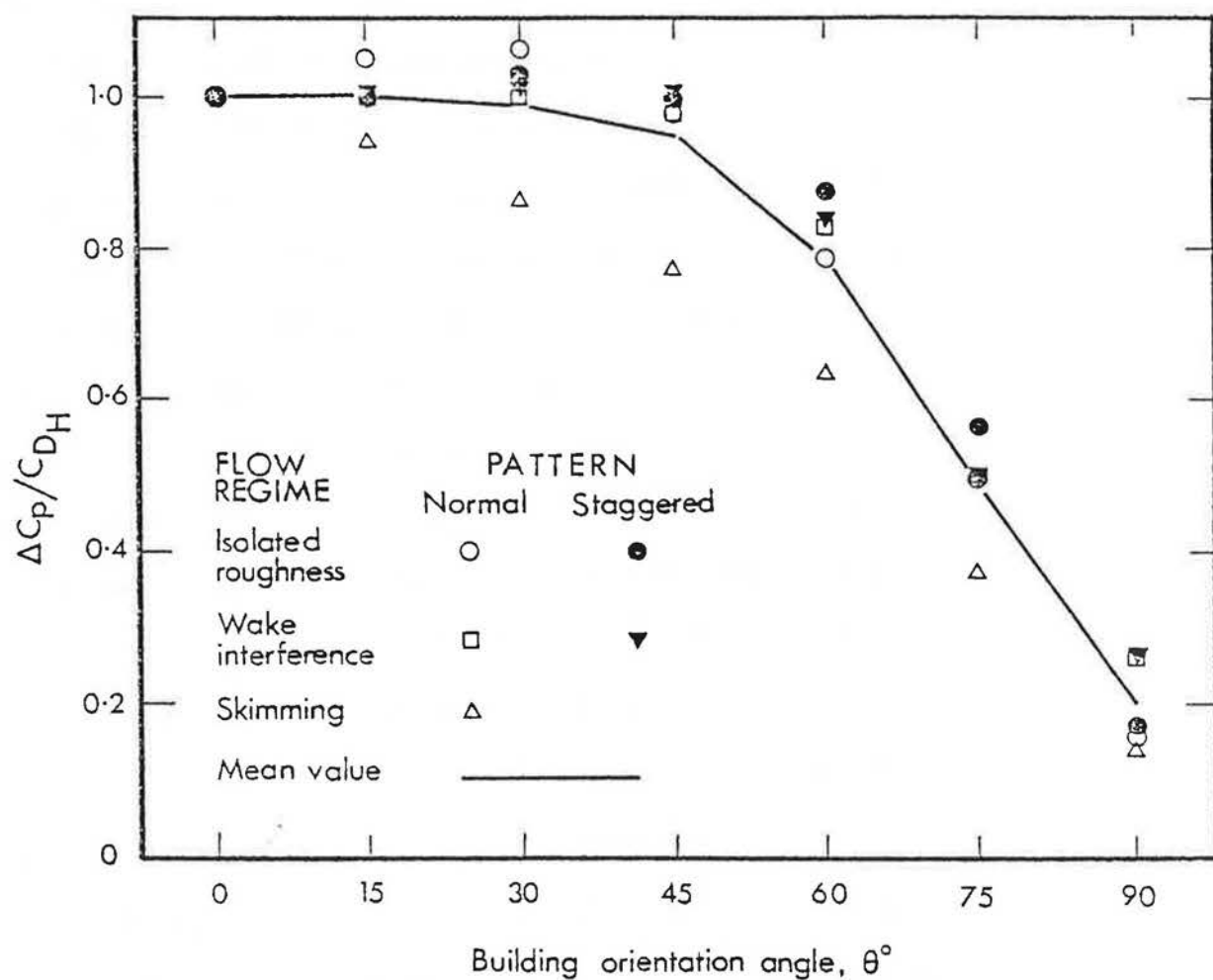


Figure 10.10 VARIATION OF THE NORMALIZED PRESSURE DIFFERENCE WITH THE BUILDING ANGLE OF ORIENTATION θ .

a group of buildings of constant height, a chart may be constructed as shown in Figure 10.11, simply by placing Figures 10.8. 10.9 and 10.10 side by side. For one value of W/H ($=1$) and a constant ratio of H/δ . the value of C_{D_H} may be determined from the first part of the chart given the building form (L/H) and the group clear spacing in the flow direction S_c/H . Knowing the building fetch would then enable a correction in the value of C_{D_H} to be made by means of the second part of the chart. Finally, the required value of ΔC_p across the building may be obtained from the third part of the chart where the line indicating the value of C_{D_H} intercepts any one of the lines representing the building orientation angle θ . An example showing the sequence of these steps is given on the chart Figure 10.11.

10.4.8 The chart described above utilized one value of W/H and one ratio of H/δ . To take into account the effect of both these parameters, different charts might be used. The effect of increasing the ratio H/δ will be to increase the resulting C_{D_H} values while increasing W/H will result in; lower C_{D_H} values. However, since the total boundary layer thickness δ in nature varies from 300m in open country to 600m in city centres, it is most likely that the effect of such a change will be relatively small on C_{D_H} . Similarly, since the range of W/H from 0.5 - 1.5 would cover a wide range of building forms, for which the corresponding effect on E_t/H is relatively small, it is suggested that a chart based on $W/H = 1$ and $H/\delta = 0.025$ (assuming $H = 12m$ and $\delta = 480m$) would be suitable for most practical purposes.

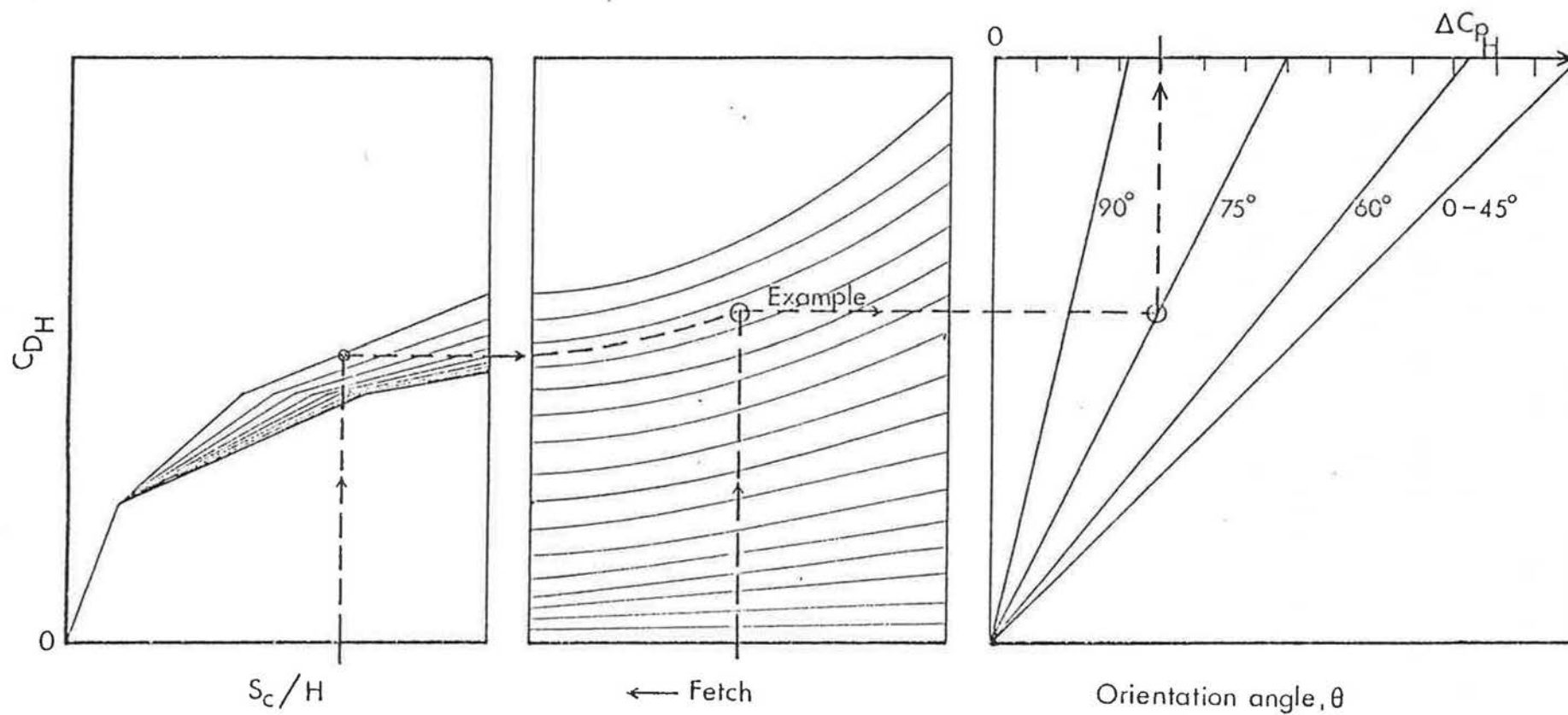


Figure 10.11 THE SUGGESTED CHART FOR THE PREDICTION OF ΔC_{DH} .

10.5 Conclusions

10.5.1 From the analysis and discussion made in this chapter it is concluded that the suggested chart Figure 10.11 shows how the different parameters are taken into account to yield the required pressure difference across buildings. This chart may then replace the left hand side of the infiltration chart given in the IHVE Guide, once the values of C_{D_H} are obtained from a simulated natural velocity profile. In general any prediction procedures based on these lines can only lead to a substantial improvement in the present technique.

CHAPTER 11

CONCLUSIONS.

11. CONCLUSIONS

11.1 The level of accuracy of natural ventilation calculations using the Crack Method depends on the accuracy of determining the pressure difference across the building.

11.2 The main assumptions made in the IHVE Guide by which the pressure difference across buildings are estimated may result in considerable error since important factors affecting the pressure forces, i.e. the building form and the properties of the natural wind, are over simplified.

11.3 From the review made of the relevant literature on natural ventilation, wind loading and external wind flows, no general relationship was found to be available which related the group geometry of built form to the resulting flow and the pressure forces on the elements of the group. However, it was evident that the flow and the pressure forces on groups of buildings are dependent on both the individual building form and the building group form.

11.4 From the investigation made of the planning and geometric parameters of housing groups it was concluded that for a matrix of similar buildings, the usual planning parameters alone are not sufficient to define the group form. A complete definition of the group form required a knowledge of both the individual building form (frontal and side aspect ratios) and the building site proportions (ratios of building length to site length and the clear

spacing between buildings in both directions). Equations representing the general relationship between these parameters have been formulated.

11.5 Since buildings may be considered as roughness elements on the earth's surface, an investigation was made of the flow over idealized rough surfaces. The main effect of changing the roughness geometry and the pattern of distribution of the elements is to produce different flow regimes. The velocity profile parameters and the pressure forces are dependent on the flow regime and hence the roughness geometry.

11.6 The analysis made of the flow velocity and pressure measurements on a building model (a cube) within a group of similar form showed that it is possible to apply the boundary layer theory for flow over rough surfaces to building model groups. The concept of the three regimes of flow over roughness elements has been substantiated by the experimental measurement of pressure forces, velocity profiles and flow visualization.

11.7 For small values of the upstream fetch the building model experienced a high drag which was shown to be dependent on the incident boundary layer thickness. As the fetch was increased the model drag decreased until a stable value was attained, longer fetches being required for lower values of the layout density or thinner incident boundary layers, (Figure 7.3).

11.8 The size of the influence area round the model was found to depend on the element spacing in the flow

direction, this area being larger for wider spacings. The limit of this area takes the form of a foot print rather than the circular form previously adopted, (Figure 7.5).

11.9 The different flow regimes were shown to be characterized by a change of behaviour in the mean windward and leeward wall pressures as the spacing between the buildings in the flow direction is increased, (Figures 7.11 - 7.14).

11.10 The governing conditions of these changes of behaviour in the pressure forces, supported both by previous work and the current flow visualization results may be given as follows:-

- (a) In the isolated roughness flow regime, the clear spacing between blocks is greater than the sum of the distances of separation and reattachment round the block obtained in the isolated element case.
- (b) In the skimming flow regime, the space between the blocks contains a stable vortex. The onset of formation of the vortex appears to be entirely dependent on the ratio between the clear spacing and the block height. This ratio was found to be 1.5 for the present study of flow over cubes, a value which is in good agreement with figures given previously for flow over two dimensional grooves.

- (c) The wake interference flow regime occurs if the clear spacing between the blocks takes any value between the previous two cases.

11.11 The variation of the effective skin friction coefficient with density reflected a behaviour similar to the reported behaviour of the equivalent sand grain roughness with density, (Figures 7.18 and 7.19).

11.12 A collapse of both the windward and leeward pressure distribution profiles was obtained when the profiles were classified by flow regime. The windward pressure profiles in the isolated flow regime took the form of an "S", while those in the wake interference and skimming flow regimes took the form of a reversed "C". In the skimming flow regime the leeward pressure profiles were no longer uniform with height as they had been for the other two regimes, (Figure 7.20).

11.13 The effect of group layout pattern on the surface pressures seems to be negligible in the isolated roughness flow regime, while the incident flow type is dominant. In the wake interference flow regime, the dominant effect is that of the layout pattern while the incident flow type becomes less important. In the skimming flow regime neither the incident flow nor the layout pattern seem to affect the resulting pressure forces dominantly, (Figures 7.23 and 7.24).

11.14 In all densities, the effect of the group layout orientation angle ϕ , becomes less important as the fetch increases. The effect of the model orientation angle, θ ,

was approximately similar for all densities and patterns (Figures 7.23 and 7.24).

11.15 From the velocity profile measurements, it was shown that the various changes of surface roughness experienced by the incident rough flow were reflected in all the velocity profiles in the form of different zones (Figures 8.5 and 8.6).

11.16 In the isolated flow regime, the roughness function was shown to increase with increasing group layout density and reached a maximum at the change to the wake interference flow regime after which it decreased, (Table 8.3).

11.17 The Clauser type correlation scheme for the roughness function and the roughness Reynolds number based on the friction velocity and the element height (the cube height) was shown to yield good correlation for the results of the isolated flow and wake interference flow regimes, (Figure 8.18).

11.18 The alternative correlation scheme suggested by Perry, Schofield and Joubert (1969) for the roughness function and the Reynolds number based on the friction velocity and the error in origin was also shown to yield reasonable agreement, (Figure 8.19).

11.19 A linear relationship was shown to exist between the zero plane displacement and the group layout density for both the isolated flow and wake interference flow regimes. Another relationship is suggested to exist for the skimming flow regime, (Figure 8.20).

11.20 The variation obtained of both the roughness length and the equivalent sand grain roughness with density showed good agreement with previous work, (Figures 8.21 and 8.22). Similarly, good agreement with the theoretical prediction of the internal layer depth was also demonstrated, (Figure 8.23).

11.21 A relationship was suggested to exist between the velocity at the cube height and the clear spacing between cubes, (Figure 8.24).

11.22 A relationship between the drag coefficient based on the friction velocity and the error in origin normalized with respect to the roughness length was also shown to exist, (Figure 8.25).

11.23 A normalization scheme for the pressure distribution profiles which takes into account the zero plane displacement and the effective height (error in origin) has been suggested. In this scheme there was an approximate collapse of all the pressure distribution profiles on a single curve, (Figure 8.26).

11.24 For the purpose of general application on buildings a chart has been produced in which the different parameters affecting the pressure difference across buildings are included. This chart may then replace the left hand side of the infiltration nomogram given in the IHVE Guide, once the values of the pressure coefficient are obtained from a simulated natural velocity profile. It is considered that any prediction procedures based on these lines can only lead to a substantial improvement in the present technique.

1. The first part of the paper discusses the importance of the study of the history of the United States. It is argued that a knowledge of the past is essential for a full understanding of the present and for the development of a sound policy for the future.

2. The second part of the paper discusses the importance of the study of the history of the United States. It is argued that a knowledge of the past is essential for a full understanding of the present and for the development of a sound policy for the future.

3. The third part of the paper discusses the importance of the study of the history of the United States. It is argued that a knowledge of the past is essential for a full understanding of the present and for the development of a sound policy for the future.

4. The fourth part of the paper discusses the importance of the study of the history of the United States. It is argued that a knowledge of the past is essential for a full understanding of the present and for the development of a sound policy for the future.

5. The fifth part of the paper discusses the importance of the study of the history of the United States. It is argued that a knowledge of the past is essential for a full understanding of the present and for the development of a sound policy for the future.

REFERENCES

6. The sixth part of the paper discusses the importance of the study of the history of the United States. It is argued that a knowledge of the past is essential for a full understanding of the present and for the development of a sound policy for the future.

References

- Antonia, R. A. &
Luxton, R. E.
1971
The Response of a Turbulent Boundary Layer to a Step Change in Surface Roughness, Part 1. Smooth to Rough. Jnl. Fl. Mech., Vol. 48, Part 4, pp. 721 - 726.
- Antonia, R. A. &
Luxton, R. E.
1972
The Response of a Turbulent Boundary Layer to a Step Change in Surface Roughness, Part 2. Rough-to-Smooth. Jnl. Fl. Mech., Vol. 53, Part 4, pp. 737 - 757.
- Armitt, J.
1974
Wind Loading on a Rectangular Block. Central Electricity Generating Board, Report No. RD/L/N 59/74.
- ASHRAE
1972
Handbook of Fundamentals. American Society of Heating, Refrigerating and Air Conditioning Engineers, New York, 1972.
- Beckett, H. E.
1942
Population Density and the Heights of Buildings, Transactions of the Illuminating Engineers Society (London), July, 1942).
- Bilsborrow, R. E.
1973
Natural Ventilation of Buildings. Ph.D. Thesis, Sheffield University.
- Blom, J. &
Warner, L.
1969
The Influence of Change in Surface Roughness on the Development of the Turbulent Boundary Layer in the Lower Layers of the Atmosphere. Jnl. of the Atmos. Sciences, Vol. 26, March 1969.
- Bradley, E. F.
1968
A Micrometeorological Study of Velocity Profiles and Surface Drag in the region Modified by a Change in Surface Roughness, Quart. Jnl. Roy. Meteorol. Soc., 94, 361 - 79.
- B.R.S. Digest 119.
1970
The Assessment of Wind Loads. Building Research Station, Digest 119, 1970.

- Castro, I. P. &
Robins, A. G.
1975
- The Effect of a Thick Incident Boundary Layer on the Flow Around a Small Surface Mounted Cube.
Central Electricity Generating Board, Report No. R/H/N795, Jan. 1975, Research Dept. Marchwood Eng. Labs.
- Caton, P.G.F.
1975
- "Standardised Maps of Hourly Mean Wind Speed Over the United Kingdom"
Fourth International Conference on Wind Effects on Buildings and Structures, Heathrow, London, 8 - 12 Sept. 1975.
- Clauser, F. H.
1956
- The Turbulent Boundary Layer
Advances in Applied Mechanics
Vol. 4, pp. 1 - 51.
- Code of Practice
1972
- Code of Practice, CP3, Basic Data for the Design of Buildings, Chapter V, Loading, Part II, Wind Loads.
B.S.I.
- Cook, N. J.
1972
- Effect of Scale of Turbulence on the Flow Around Buildings.
Ph.D Thesis, Dept. of Aeronautical Engineering, University of Bristol.
- Cook, N. J.
- Private Communication.
- Counihan, J.
1971
- Wind Tunnel Determination of the Roughness Length as a Function of the Fetch and the Roughness Density of Three Dimensional Roughness Elements.
Atmos. Envir., Vol. 5, pp.637 - 642.
- Counihan, J.
1972
- The Structure and the Wind Tunnel Simulation of Rural and Urban Adiabatic Boundary Layers Symposium on External Flows, University of Bristol.
- Counihan, J.
1975
- Adiabatic Atmospheric Boundary Layers. Atmos. Envir., Vol. 9, pp. 871 - 905.
- Davenport, A. G.
1965
- The Relationship of Wind Structure to Wind Loading.
Div. of Building Research. Ottawa, Canada, Technical Paper No. 88.

- Dean, R. B.
1974
An Investigation of Shear Layer Interaction In Ducts & Diffusers. Ph.D. Thesis, Imp. Coll. London.
- Dick, J. B.
1949
Experimental Studies in the Natural Ventilation of Houses. J.I.H.V.E., Vol. 17.
- Dvorak, F. A.
1969
Calculation of Turbulent Boundary Layers on Rough Surfaces in Pressure Gradient, A.I.A.A.J., Vol. 7, No. 9, Sept. 1969, pp. 1752 - 1759.
- Elliott, W. P.
1958
The Growth of the Atmospheric Internal Boundary Layer. Trans. am. Geophys. Union, Vol. 39, No. 6, 1958, pp. 1048 - 1054.
- Evans, B. H.
1957
Natural Air flow Around Buildings. Texas Engineering Experimental Station, Research report No. 59, March 1957.
- Givoni, B.
1968
Ventilation Problems in Hot Countries. Technion - Isreal Institute of Technology, Building Research Station, Dept. of Building Climatology.
- Good, M. C. & Joubert, P. N.
1968
The Form Drag of Two Dimensional Bluff Plates Immersed in Turbulent Boundary Layers. Jnl. Fl. Mech., Vol. 31, pp. 547 - 582.
- Grigg, P. F. & Sexton, D. E.,
1974
Experimental Techniques for Wind Tunnel Tests on Model Buildings. B.R.S. Current Paper 43/74.
- Gropius, W.
1956
Scope of Total Architecture, Allen and Unwin.
- Hama, F. R.
1954
Boundary Layer Characteristics for Smooth and Rough Surfaces. Transactions of the Society of Naval Architects and Marine Engineers, Vol. 62, 1954, pp. 333-358.
- Harris, R. I.
1972
Measurements of Wind Structure, Proceedings of Symposium on External Flows, University of Bristol, July 1972.

I.H.V.E., Guide
1970

Jensen, M. &
Franck, N.
1965

Joubert, P. V.,
Perry, A. E. &
Stevens, L. K.
1971

Klatt, F.
1969

Koenigsberger, O. H.,
Ingersoll, T. G.,
Mayhew, A &
Scokolay, S. V.
1973

Koloseus, H. J. &
Davidian, J.
1966

Lee, B. E.
1975(a)

Lee, B. E.
1975(b)

Lee, B. E.
1975(c)

Liu, C. K.,
Kline, S. J. &
Johnston, J. P.
1966

Institution of Heating and
Ventilating Engineers,
Book A; Design Data. London
1971.

Model Scale Tests in Turbulent
Wind. Danish Technical Press,
Copenhagen, 1965.

Drag of Bluff Body Immersed in
a Rough Wall Boundary Layer.
Wind Effects on Buildings and
Structures. Tokyo, 1971.

The X Hot-wire Probe in a
Plane Flow Field.
DISA Information, No. 8
July 1969, pp 3 - 12

Manual of Tropical Housing
and Building.
Climate Design, Part 1.
Longman Group Ltd. London,
1973.

Free Surface Instability
Correlations and Roughness
Concentration Effects on
Flow over Hydrodynamically
Rough Surfaces.
Geol. Surv. Water Supply
paper 1592 - CD., U.S. Govt.
Printing Office.

An investigation of the Effects
of Turbulent Scale on the
Mean Forces on Two Dimensional
Square Prisms. BS. 24,
Sheffield University,
Department of Building Science,
June 1975.

The Effect of Turbulence on the
Surface Pressure Field of a
Square Prism.
Jnl. Fl. Mech. (1975), Vol.69,
Part 2, pp. 263-282.

The Wind Climate of Sheffield.
BS. 27, Sheffield University,
Department of Building Science,
December 1975.

An Experimental Study of
Turbulent Boundary Layers on
Rough Walls, Stanford
University Report MD-15.

- Marshall, J. K.
1971
Drag Measurements in Roughness
arrays of Varying Density and
Distribution.
Agric. Meteorol., Vol. 8,
pp. 269 - 292.
- Martin, L. &
March, L. (Eds).
1972
Urban Space and Structures,
Cambridge University Press,
1972.
- Mauill, D. J. &
East, L. F.
1963
Three-Dimensional Flow in
Cavities, Jnl. Fl. Mech. Vol.
16., p. 620.
- Morris, H. M.
1955
Flow in Rough Conduits.
Trans. A.S.C.E., Vol. 120,
pp. 373 - 398.
- Munn, R. E.
1966
Descriptive Micrometeorology
Academic Press, New York
& London.
- Nelson, L.
(Lokmanhekim, Ed.)
1971
An Algorithm for Infiltration
Rate Calculations.
A.S.H.R.A.E. Task Group on
Energy Requirements for
Heating and Cooling.
- Newberry, C. W.,
Eaton, K. J. &
Mayne, J. R.
1973
Wind Loading on Tall Buildings -
Further Results from Royex House.
B.R.S. Current Paper 29/73.
- Olgyay, V. &
Olgyay, A.
1963
Design With Climate.
Princiton Univ. Press,
Princiton 1963.
- O'Loughlin, E. M. &
Annambhotla, V. S.
1969
Flow Phenomena Near Rough
Boundaries, Jnl. Hyd. Res.,
Vol. 7, pp 231 - 250.
- Panofsky, H. A. &
Townsend, A. A.
1964
Change of Terrain Roughness
and the Wind Profile.
Quart. J. Roy. Meteorol. Soc.,
Vol. 90. pp 147 - 155.
- Pasquill, F.
1970
Wind Structure in the Atmospheric
Boundary Layer.
Phil. Trans. Roy. Soc. Lond. A.,
Vol. 269, pp. 321 - 554.
- Perry, A. E. &
Joubert, P. N.
1963
Rough Wall Boundary Layers
in Adverse Pressure Gradients.
Jnl. Fl. Mech., Vol. 17,
pp. 193 - 211.

- Perry, A. E.,
Schofield, W. H. &
Joubert, P. N.
1969
- Rough Wall Turbulent Boundary
Layers.
Jnl. Fl. Mech., Vol. 37,
pp. 383 - 413.
- Roshko, A.
1955
- On the Wake and Drag of Bluff
Bodies. Jnl. Aero. Sci.,
Vol. 22, pp. 124 - 132.
- Schlichting, H.
1968
- Boundary Layer Theory. (6th-
Edition) McGraw-Hill.
- Schofield, W. H.,
Perry, A. E. &
Joubert, P. N.
1974
- Similarity Relations for
Pressure Distributions on Slot
Type Rough Walls under
Turbulent Boundary Layers.
Trans. A.S.M.E., Jnl. Fl.
Eng., pp. 185 - 188, June
1974.
- Schofield, W. H.
1975
- Measurements in Adverse Pressure
Gradient Turbulent Boundary
Layer with Step Change in
Surface Roughness. Jnl. Fl.
Mech. Vol. 70., pp. 573 - 593.
- Segal, W.
1965
- The Use of Land in Relation to
Building Height, Coverage and
Housing Density.
Ekistics, Vol. 19, No. 110.,
pp. 66 - 70.
- Simpson, R. L.
1973
- A Generalised Correlation of
Roughness Density Effects
on the Turbulent Boundary
Layer.
A.I.A.A.J., Vol. 11., No. 2,
pp. 242 - 244.
- Stevens, P. H. M.
1960
- Densities in Housing Areas.
Tropical Buiding Studies No. 1,
BRS Dept. of Scientific and
Industrial Research.
- Svennar, E.
1972
- Density of Residential Areas,
Commonwealth Scientific and
Industrial Research Organisation,
Division of Building Research,
Trans. No. 4, Australia, 1972.
- Sundaram, T. R.,
Ludwig, G.R. &
Skinner, G. T.
1972
- Modelling of the Turbulence
Structure of the Atmospheric
Surface Layer. A.I.A.A.J., Vol.
10, No. 6. pp. 743 - 750.

- Sutton, O. G.
1953
Micrometeorology.
McGraw - Hill
- Tani, I.,
Iuchi, M. &
Komoda, H.
1961
Experimental Investigation of
Flow Separation Associated with
a Step or a Groove.
Aeronautical Research Institute,
University of Tokyo, Report No.
364.
- Townsend, A. A.
1951
The Structure of the Turbulent
Boundary Layer. Proc. Camb.
Phil. Soc. Trans. Vol. 47.
- Townsend, A. A.
1965
The Response of a Turbulent
Boundary Layer to Abrupt
Changes in Surface Conditions.
Jnl. Fl. Mech., Vol. 22, Part 4,
1965, pp. 799 - 822.
- Turner, J.
1973
A comparative Study of the Land
Use and Built Form of 110
Schemes. Technical Study,
A.J. Vol. 158, 1st Aug. 1973,
pp. 265 - 280.
- Van den Hoven, I.
1957
"Power Spectrum of Horizontal
Wind Speed"
Jnl. Meteorology, Vol. 14.
- Vincent, N. D. G. &
Bailey, A.
1943
Wind Pressure on Buildings
Including Effects of Adjacent
buildings. Jnl. Inst. C.E.,
Vol. 20 (8), Paper No. 5367.
pp. 243 - 275.
- Weston, E. T.
1956
Air Movement in Industrial
Buildings: Effect of Nearby
Buildings. Special Report
No. 19. Commonwealth
Experimental Building Station.
Sydney, 1956.
- Wise, A.F.E.,
Sexton, D.E. &
Lillywhite, M. S.
1969
Air Flow Round Buildings.
Urban Planning Research
Symposium, Jan. 1965. Min.
Technology, B.R.S. pp. 71 - 91.
- Wise, A.F.E.
1970
Wind Effects Due to Groups of
Buildings B.R.S. Current Paper
23/70., Jul. 1970.
- Wooding, R. A.,
Bradley, E.F. &
Marshall, J. K.
1973
Drag Due to Regular Arrays of
Roughness Elements of Varying
Geometry.
Boundary Layer Meteorol., Vol.
5., pp. 285 - 308.

Wood, D. H. &
Antonia, R. A.
1975

Measurements in a Turbulent
Boundary Layer over a D-type
Surface Roughness.
Transactions A.S.M.E., Jnl.
of App. Mech.

Soliman B.F. A Study of the Wind Pressure Forces Acting on Groups
of Buildings.
AD 176.

THESIS No. 61093

I undertake that neither the whole nor any part of this thesis shall be copied, quoted or published without the consent of the Author and of the University of Sheffield.

Date

Thesis No. 4093.